

BASIN AND PALEOCLIMATE EVOLUTION OF THE PAMPA DEL
TAMARGUAL FOREARC VALLEY, ATACAMA DESERT, NORTHERN
CHILE

A Dissertation

Presented to the Faculty of the Graduate School
of Cornell University

In Partial Fulfillment of the Requirements for the Degree of
Doctor of Philosophy

by

Peter Nester

May 2008

© 2008 Peter Nester

BASIN AND PALEOCLIMATE EVOLUTION OF THE PAMPA DEL
TAMARGUAL FOREARC VALLEY, ATACAMA DESERT, NORTHERN
CHILE

Peter Nester, Ph. D.

Cornell University 2008

This work details the Neogene to Recent evolution of the Pampa del Tamarugal (20°30' - 21°45'S), a northward-trending forearc basin located between the Coastal Cordillera to the west and the Precordillera to the east in the hyper-arid core of the Atacama Desert of northern Chile. Tectonic, sedimentary, and paleoclimatic implications, and their relationships to one another, are considered.

Deformation structures within the Upper Oligocene and Miocene lithologies reveal a complex and long lived tectonic history. Fault mapping reveals north-, and northwest-trending reverse faults, east-trending reverse faults, as well as north-trending normal faults ubiquitous within the basin during the Lower and Middle Miocene, and concentrated during the Upper Miocene in the southwestern sector of the study area. Surface stratigraphy and seismic facies analysis indicate a short Middle Miocene humid interval, resulting in lacustrine and playa deposits over extensive regions. Increased aridity after ~15 Ma is here related to a global desiccation and after ~11 Ma is tied to orographic blocking of precipitation.

Long-wavelength rotation of surfaces at the eastern limit of the

basin accompanied uplift of the Altiplano plateau to its east. Conservative estimates place the magnitude of uplift at 1155 ± 475 m between 11 and the present, with highest rates between 11-5.3 Ma. This rotation is not accompanied by any significant surface-breaking faults over this same distance. Our preferred mechanism of uplift is lower or middle crustal ductile flow related to the underthrusting of the Brazilian Shield beneath the Altiplano from the east, although delamination of dense lower crust is also considered.

Despite long-lasting hyperaridity during Pleistocene, there was perennial stream flow within the hyperarid core of the desert, which does not exist under modern climate conditions. Nineteen radiocarbon dates from deposits on terraced fluvial deposits indicate ages from 16,380 to 13,740 cal yr BP, synchronous with other regional evidence for wetter conditions. The stream flow responsible for these deposits likely represents the most important groundwater recharge event of the last 18,000 years. Sea surface temperature gradient changes in the equatorial Pacific was perhaps the major driver of hydrologic change in the Atacama on both centennial and millennial timescales.

BIOGRAPHICAL SKETCH

Peter Lee Nester was born on January 1, 1973 in Johnson City, New York. He graduated from Johnson City Senior High School ('90), obtained his A.A. in Liberal Arts from Broome Community College ('93) and his B.S. from the State University of New York at Cortland ('95) in Geological Sciences. He then spent 3 years studying Quaternary paleoclimate and sedimentology at the University of Tennessee, Knoxville, where he received his M.S. in Geological Sciences ('99). Upon graduation, he began work with Exxon Exploration Corporation in New Orleans and Houston as a production and exploration geologist, but left after one year to return to Upstate New York, accepting a position with the Paleontological Research Institution as Webmaster and Petroleum Geology Educator. During this time, he married Sara Elizabeth Humbert in July 2002. In fall of 2003, he began work towards his Ph.D. at Cornell University, and in May 2006, Peter and Elizabeth welcomed their first child, Nora Errett Nester into the world. Peter is currently employed by Chevron Energy Technology Company as a geoscientist in their Reservoir Characterization division. As you read this, he is somewhere wondering how it all turned out this well.

This work is dedicated to my wife, Sara Elizabeth Humbert, and daughter, Nora Errett Nester, who have always provided me with the love and inspiration to persevere.

ACKNOWLEDGMENTS

From the top, thanks need to go to my committee members Teresa Jordan, Larry Brown and Jed Sparks. If not for Terry's reputation as an outstanding researcher and advisor, I would not have chosen to re-enter the world of academia. She seemingly was always able to read my ever-changing situation, and knew when to push me, and also when to allow me space to struggle through challenges on my own. She became more than just an advisor, and I trust that she will remain a lifelong friend. Larry Brown helped lead me through many geophysical hoops and never let me forget that I had "a lot of good stuff rattling around inside that head of [mine] up there". Thanks also to Jed for agreeing to be a part of this project. I regret that my studies here did not evolve into something leading to more direct interactions between the two of us. It is my hope that some of the loose ends will benefit his research or that of his future students.

I am grateful to my mother and father back in Johnson City, NY for being supportive of my move back to academia, and for being such loving and extremely helpful grandparents.

Thanks also go to members of the Cornell faculty, especially those associated with the Cornell Andes Project. Muawia Barazangi allowed the use of his scanner for transferring of seismic lines into their initial digital format, and Melissa Stephenson and Carrie Brindisi assisted me in this procedure. Bryan Isacks assisted in data manipulation as it applied to ER Mapper. Sue Kay, Matt Pritchard, Robert Kay, Rick Allmendinger, Art Bloom, Chris

Andronicos, Larry Cathles and Jason Phipps-Morgan sat through numerous talks and seminars, always with an eye to make my research better and an interest in discussing the finer points of the science and techniques. Rick Allmendinger provided for me structural guidance, through the relearning of many forgotten principals of the trade, as well as help with my seismic interpretation and many discussions of structural domains in the Atacama Desert as it related to my field area. It has been a pleasure to learn from him, as he is one of the best teachers I have come across during my years as a geologist. Warren Allmon has inspired me to be a more effective communicator of the science, and he, along with Rob Ross (of the Paleontological Research Institution/Museum of the Earth), has been a consistent source of encouragement. Thanks to Lou Derry for use of his fourth-floor lab facilities and for seemingly free reign to graze through his chemicals. Jack Oliver helped provide inspiration by reminding me that, in science, sometimes the difference between “good” and “lucky” doesn’t really make that much difference in the end, as long as you take advantage of both. Bill White provided me with tools necessary for subsampling of organic material. Thanks to Art Bloom for being Art Bloom. Those who know him know what I’m talking about.

The Snee Hall front office support staff: Elena Welch, Linda Hall, Lynda Swafford, Amy Colvin, Nadine Porter, Jeanne Boodley-Buchanan, Judy Starr, and Brenda Leonard (to name but a few of the unfortunately highly-changeable cast of characters) struggled to

meet my every request, and allowed me to persevere when the red tape threatened to trip me from around the ankles.

Steve Gallow deserves his own page in this section of thanks. Endlessly patient and kind, Steve shattered any preconception that I might have had concerning computer technology support staff as being condescending or intolerant, even if my questions about “the RAM on my hard-drive, or processor, or whatever” caused him to giggle on the inside. Computer support staff members Aaron Wade and Mike Brodsky were also available, usually at a moment’s notice, to quickly solve whatever computer crisis I was having at the time.

Thanks to Cornell researcher Michelle Goman for use of her lab space, chemicals and equipment, as well as for discussions of Quaternary climate and geochemical processes. Guaciara dos Santos at the Keck-CCAMS lab, University of California, Irvine, provided me with ^{14}C dates on plant organic matter, and I am indebted to Terry Spell and Kathleen Zanetti of the Nevada Isotope Geochronology Laboratory for some of the geochronological analyses reported here, with the rest conducted by Sernageomin of Chile.

Maria Gandolfo helped me with early stages of plant identification. Cornell post-doc Noah Finnegan was always interested in my project and willing and supremely able to talk science on a wide range of topics. Art Kasson and Kim Sparks helped me with data collection of stable isotopes on plant organic matter. Carol Griggs spent valuable hours with me explaining the

science of dendrochronology, and provided me with tree-coring equipment for the field. Alex Wiedenhoeft of the Forest Products Laboratory in Madison, WI succeeded in identifying the mystery tree sample when there seemed nowhere else to turn.

Claudia Mora at the University of Tennessee, Knoxville, provided the lab for me to have my carbonate samples analyzed for stable isotopic data, and Zheng-Hua Li analyzed these samples. Claudia has offered words of advice and support since she signed on as a committee member during my M.S. program at Tennessee, and her 13 years of encouragement and friendship have gone a long way in helping me through periods of self-doubt. Paul and Hazel Delcourt of the University of Tennessee, Knoxville, served as excellent mentors in my formative years (it turns out) as a researcher, and provided me the blueprint and confidence to tackle the challenges ahead. Robert Darling, professor of metamorphic petrology at the State University of New York, Cortland, has served as a mentor in geology and life for the better part of 15 years, and has always helped me to find the confidence within myself to continue towards whatever goal I have been striving for at particular periods of my professional and academic careers. He also assisted with heavy mineral separations for geochronological analyses, taking an entire afternoon to help me with this task.

I am indebted to Fred and Donna Digert of International Exploration Associates who provided data, without which there would have been no research project, in addition to providing generous hospitality during its transfer. Robert Anderson of

INSTAAR, University of Colorado, Boulder, was generous in allowing me use of his office space during initial data analysis. David Mohrig of MIT provided the blueprint (generated by his student Kyle Straub) that was critical in converting these data into a workable digital format.

Kim Whipple of Seismic Micro made a strong case for being included on my committee by the many phone calls and emails she endured during the eleventh hour, as I struggled with understanding both new software and the geophysical parameters of my data. Her patience won't be forgotten. Kevin Wright of Fairfield Industries was kind enough to entertain an entirely random phone call, which provided me information about the original processing of the data and helped me move forward.

Jason Rech and Brian Currie (University of Miami, Ohio) imparted much wisdom centered about the stratigraphy and recognition of paleoclimate from the identification of desert soils during portions of two field seasons. In doing so, they made it obvious that the University of Miami, Ohio, is an excellent place to gain an advanced degree in geology. Karen Gotter also provided field assistance and friendship, although we both are saddened by the fact that we were never able to sneak over the border and into Peru.

Thanks also to Carmala Garzione of the University of Rochester for engaging conversations concerning Altiplano uplift, and for last minute data and discussions on the subject that

supplemented the content presented here.

Interactions with our Chilean colleagues were constantly rewarding from both a personal and academic perspective, and were without fail a pleasure to work with. Claudio Latorre (Departamento de Ecología, Pontificia Universidad Católica de Chile) acted as my *de facto* fourth committee member during the preparation of my chapter on Pleistocene fluvial terraces, and was a joy to work with and learn from in the field. Thanks also to Claudio's student Eugenia (Kena) Gayó for discussions on Atacama Desert ecology both in the field and here at Cornell, and for being able to commiserate as we both progressed through our respective programs.

To colleagues working with Chile's geological survey (Sernageomin): Antonio (Tuco) Díaz was a trusted guide for all or part of three field campaigns, leading me through terrain that was not meant for automobile traffic. Tuco was kind enough to almost never speak English to me (even though his English was better than my Spanish) in hopes that I would actually learn to communicate with the local population when I really needed to. No longer getting the opportunity to spend time with him each summer is quite possibly the single aspect of fieldwork that I will miss the most. Nicolás Blanco has been a friend, patient educator, and collaborator from day-one, and he, along with Tuco, was able to overlook my first few tentative days in the field and still agree to carry on with me in tow. Nico also provided valuable data and maps and helped with their interpretation. Thanks also to Andy

Tomlinson for scientific discussions over lunch, and for the “only real cup of coffee” in all of Santiago, and Paula Cornejo for helping me feel at home in the Sernageomin offices.

Constantino Mpodozis of Sipetrol (international subsidiary of Chile’s state oil company ENAP) secured for me clearance and allowed me access to well cuttings from ENAP’s core warehouse outside of Santiago, spending an entire day with me to make sure that the process went smoothly. Arturo Jensen and Rodrigo Riquelme of the Universidad Católica del Norte in Antofagasta de Chile both taught me everything they could during our time together in the field, sometimes in fact teaching me the same thing two or three times without annoyance.

Thanks to officemates in the various offices I occupied while I was at Cornell, including Katie Tamulonis, Gabriela Depine, Stephanie Devlin, Louise McGarry, Tiffany Tchakirides, Chen Chen and José (Joey) Rosario. Discussions with Stephanie and Katie, in particular, on anything from the Colbert Report to the Philadelphia Eagles may not have helped me earn my degree, but sure were a pleasant diversion. In addition, both were valued confidants as we struggled through the program together. Joey also accompanied me in the field, with nights spent talking about life over a fire. Last but not least, Louise’s ability to listen and provide insight and perspective that cuts right to the heart of the matter has truly been a gift. My time at Cornell has been infinitely richer because of her friendship and trust, and I owe her my immense gratitude just knowing that she had faith that I would persevere. I am lucky to

have had the opportunity to share this experience with her, and can only hope I have given back half of what she has given me.

Brian Ruskin earned my immense respect for his knowledge of both nonmarine sedimentary systems and Genesis. His ability to stay calm, at least outwardly, in the eye of the storm was an excellent example that I tried to follow when my time finally came. He also became an invaluable confidant, and I am not sure I would have gotten this far without his friendship. Holly Caprio was a pleasure to work with in the field and I want to thank her for showing me that it is possible to fit 20 pounds of rocks (*sic*) into a 10 pound bag.

Jack Loveless has been invaluable from the day I arrived as someone who knows twice as much as he lets on. It is this characteristic which will serve him best as a mentor to countless advisees as his career moves forward. Jack was always willing, no matter how busy he may have been, to sit and discuss any and every aspect of my work. He was also key in providing me with ER Mapper and ArcInfo solutions to problems that otherwise would have stopped me dead in my tracks. I look forward to watching his scientific discoveries unfold in the many journal articles undoubtedly already in preparation. In the same vein, Adam Goss also deserves special gratitude for sharing with me his seemingly endless knowledge of geology. His passion for the discipline is infectious.

Jacob Moore, Herdis Schopka, Meghan Herz and Julie Pett-Ridge provided chemical supplies and help with other odd pieces of

chemical equipment that always seemed to be required. Neil McGlashan helped me to understand some of the complexities and variations of lower crustal thicknesses to the east of my field area. Greg Hoke provided essential field assistance during my first field campaign, and planted many of the seeds from which this dissertation has grown. He also assisted me with ER Mapper and swath profile generation, some of which he accomplished while in Germany(!). My biggest quarrel with Greg was that he obtained his degree at just the moment when I finally understood what he was talking about. Thanks to Dave Wolf for helping keep the Cornell University of the AAPG up and running when I could no longer dedicate any time to the matter.

And to those Cornell graduate students come and gone whom I have not mentioned individually, Greg Kirkpatrick, Danielle Glasgow, Phoebe Judge, Stephen Romaniello, Stephen Holtkamp, Adrienne Long, Amanda Baker, Chris Garvin, Christina Patricola, Emily Riddle, Chao Shi, Melissa Stephenson, Helen Jones, Mary Kosloski, Rachel Shannon, Ursula Smith, thanks for making Snee Hall an interesting and stimulating environment that I will always remember fondly.

Mike Brown conducted lab work on plant organic matter, and Ben Haravich and Mike Brown provided a creative outlet as the Snee and the Blue Lemons, musical collaborations that I am sure will someday plant themselves securely into the cultural underground. For help with lab work as well as map preparation (which provided me with a sense that I really was *somewhere* when

standing in the middle of absolute desert), thanks go to Lindsey Trachtenberg. Linea Koons answered questions during my initial ER Mapper days. I also want to thank Patrick Brennan for introducing me to Facebook.

And of course, thanks to my wife, Elizabeth, and daughter Nora, for always helping me to keep my research in its proper perspective, and creating the most wonderful environment to return to every evening.

And finally, thanks to that chicken salad sandwich purchased at the Quillagua *aduana* for teaching me humility, and to never order anything containing mayonnaise from a customs office.

Portions of this research were funded by the National Geographic Society (project 800006), Geological Society of America's Harold T. Stearns Fellowship Award, the National Science Foundation (EAR 0609621 and 0208130 to Teresa Jordan), the Cornell University College of Engineering, and the Bender Family.

TABLE OF CONTENTS

Biographical Sketch.....	iii
Dedication.....	iv
Acknowledgements.....	v
Table of Contents.....	xv
List of Figures.....	xvi
List of Tables.....	xviii
1. Introduction	1
2. Neogene deformation and sedimentary history of the Pampa del Tamarugal, northern Chile	12
3. Evidence for long-wavelength westward rotation of the western Andean slope (20°45' - 21°40'S) from Miocene to Recent	159
4. Perennial stream discharge in the hyperarid Atacama Desert of northern Chile during the latest Pleistocene	217
Appendix	249

LIST OF FIGURES

Figure 2.1	90 m resolution digital elevation model of study area.....	15
Figure 2.2	East-west topographic profile at 21°S	17
Figure 2.3	Chronostratigraphic diagram between 19° and 22°S.....	21
Figure 2.4	Thematic Mapper image of the Pampa del Tamarugal	28
Figure 2.5	Stratigraphic columns of Neogene deposits.....	31
Figure 2.6	Sections of Pintados #1 and Pintados #2 well logs	37
Figure 2.7	Well ties for the Pintados #1 and Soledad #1 wells.....	45
Figure 2.8	Line 99-07 used to develop seismic facies relationships.	58
Figure 2.9	Photograph of Guatacondo, showing fluvial incision	66
Figure 2.10	Side-by-side comparison of lines 99-03 and 99-13.....	70
Figure 2.11	Line z1f-004 showing deposition within channels	76
Figure 2.12	Cenozoic sediment thickness and fault map	79
Figure 2.13	Sediment distribution cross-section at 21°S	83
Figure 2.14	Generalized facies distribution across the study area.....	85
Figure 2.15	Unit thickness maps for AdP and generalized facies.....	87
Figure 2.16	TM image of hills corresponding to N-trending faults	92
Figure 2.17	Seismic line 99-04	95
Figure 2.18	Seismic line 99-03 showing north trending faults	98
Figure 2.19	East-vergent faults at west end of seismic line z1f-003	100
Figure 2.20	Seismic line 99-07 revealing Challacollo uplift history .	103
Figure 2.21	Comparison between line z1f-004 and Challacollo topographic profile	105
Figure 2.22	Seismic line 99-09 showing fault patterns	109
Figure 2.23	Seismic line 99-06 revealing Challacollo uplift history .	114
Figure 2.24	Photograph showing Middle Miocene timing of faults ...	118

Figure 2.25 TM image and line 99-10 showing young faulting	120
Figure 2.26 Seismic line 99-08 illustrating young deformation	123
Figure 2.27 Photograph, schematic diagram and air photo showing evidence of Late Miocene-Pliocene (?) deformation	126
Figure 2.28 Shaded DEM showing surface disruptions.....	128
Figure 2.29 DEM of the Lomas de Sal showing E-W fault scarps	131
Figure 3.1 Regional 90 m SRTM image of the study area	162
Figure 3.2 Local 90 m SRTM image of the study area	165
Figure 3.3 Schematic diagram showing idealized rotational uplift.	167
Figure 3.4 Geologic map with topographic contours	172
Figure 3.5 Landsat TM image showing seismic line locations.....	175
Figure 3.6 Photograph of upper Quebrada de Sama catchment	178
Figure 3.7 Schematic showing idealized Altos de Pica rotation.....	183
Figure 3.8 Longitudinal channel profiles	187
Figure 3.9 Graphs showing Altos de Pica and Arcas Unit surfaces in cross section at the surface and extending to the subsurface.....	191
Figure 3.10 Schematic showing surface rotations through time....	193
Figure 3.11 Surface topography transect for the Arcas Fan	195
Figure 3.12 Seismic line 99-11 with AdP member 3 surface	197
Figure 3.13 Surface topography showing the break in slope ("rollover") at the crest of the western Andean slope.....	200
Figure 4.1 Shaded DEM of northern Chile study area with field photos of organic deposits and topographic transect.....	221
Figure 4.2 Map of drainages and reported organic deposits	228
Figure 4.3 Generalized stratigraphy of studied fluvial deposits	233
Figure 4.4 Correspondence of data and Lake Tauca highstand	240

LIST OF TABLES

Table 2.1	Radiogenic ages for Neogene volcanic deposits	22
Table 2.2	Reflection characteristics for seismic sequences	56
Table 3.1	Summary of uplift estimates along the western Andean slope from late Miocene to Recent.....	170
Table 3.2	Modern depositional angles for stream channels	188
Table 3.3	Modern slopes for ancient surfaces summarized	192
Table 3.4	Magnitudes and rates of uplift based on this study	201
Table 4.1	Sample Locations and Conventional or AMS ¹⁴ C dates of organic material	223
Table 4.2	North-south relationship between catchment area and stream type	229

CHAPTER 1

INTRODUCTION

The Atacama Desert of northern Chile has long been of interest to the international community of geologists because of its natural resources and the unique geologic consequences of its extreme climate. Aridity has more-or-less been an ongoing condition since the Triassic (Clarke, 2006) in extreme northern Chile and southern Peru, with the modern hyper-arid regime dominant since at least 3 million years ago (Hartley and Chong, 2002), and possibly as far back as the Oligocene-Miocene transition (Dunai *et al.*, 2005). Evidence of this paleoclimate history is recorded in Mesozoic and Cenozoic sedimentary rocks, in which evaporites are repeatedly a component in the nonmarine sediments. Especially since the Miocene, episodically deposited alluvial clastic sedimentary rocks predominate, and indicate that precipitation events were sporadic.

Climate and sedimentation are intricately tied to one another, as climate is one of the most important factors in delivery of sediment to a basin (Broecker *et al.*, 1958; Perlmutter and Matthews, 1989; Summerfield, 1991). It is now known, however, that climate in some cases may also play a role in tectonic processes (Beaumont *et al.*, 2001; Lamb and Davis, 2003; Wobus *et al.*, 2003). Specifically in the case of northern Chile, aridity during the Cenozoic is thought to have restricted the amount of sediment that has been delivered to the mountain-parallel subduction trench (Galli-Olivier, 1969; Schweller *et al.*, 1981). This in turn may have increased the shear stresses along the plate interface, and

contributed to the rise of the Andes (Lamb and Davis, 2003). There is still much to be learned about the interplay between climate and tectonics, and the Central Andean orogenic belt is a likely candidate for providing information necessary to resolve fundamental questions.

Embedded within the many tens-of-millions of years of aridity of this region of northern Chile have been repeated fluctuations in the degree of aridity (Houston and Hartley, 2003). Climatic conditions and sediments that are produced as a result of oscillations within the climate system should be predictable. Therefore, one method for discerning climate oscillations is by investigating the types of sediments that are deposited through space and time. Fluctuations will affect both sediment delivery (via erosion) and facies (via transport). More or less arid conditions will result in changes in power of drainages to deliver sediment not only to the Pacific Ocean and Peru-Chile trench, but also to other nonmarine basins in the forearc. This power of sediment delivery will also be manifested in the rate of stream incision and evolution of drainage systems through the area (Hoke *et al.*, 2007; Kober *et al.*, 2006; Schlunegger *et al.*, 2006). All of this will then influence types of sediments that are deposited. The distribution of sedimentary facies should be predictable if enough is known about conditions of sedimentation and erosion at any given point in time. However, it is not only climate, but also deformation and evolution of the sedimentary basin and adjacent mountainous regions as morphotectonic features that will have an impact on their distribution. Recognition of changing sedimentary environments in conjunction with an understanding of the

tectonic history within and adjacent to a basin affords us the opportunity to separate the relative importance of these two aspects of the basin evolution which are acting in tandem.

The forearc sedimentary basins, or “central depression” or “longitudinal valley” of Chile provide sedimentary histories which record earlier climate states and changes, and which have been shaped by tectonic activity. The eastern flank of these forearc basins is the western slope of the Andes Mountains. While other studies have documented the sedimentary history of portions of the 100-km-long Pampa del Tamarugal forearc basin (Dingman and Galli, 1965; Hartley *et al.*, 2000; Sáez *et al.*, 1999; Victor *et al.*, 2004), this work is the first basin-scale treatment on the subject, and the first to consider sedimentation history throughout the entire Neogene. Because this region has thus far received relatively little attention due to its lack of surface exposure of the underlying strata, this work fills an important knowledge gap in the central Andean forearc.

Based on the synthesis of information about the sedimentary fill of the Pampa del Tamarugal basin presented here, there are a variety of products. First, we demonstrate the relationships of sedimentary facies to the coeval deformation of the valley, with consequences to groundwater flow. Second, we interpret the history of long-wavelength deformation of the western Andes. Third, we describe outcomes in the basin of paleoclimate change over both relatively short (thousands of years) and very long (many million years) time spans. The understanding of the complete Neogene basin history is vital to the future of the region

in terms of water resource management (which impacts the region's prolific copper industry as well as the growing population of the coastal communities), agriculture (including the current reforestation program by Chile's Corporación Nacional Forestal [CONAF]) and the newly energized efforts towards discoveries of natural gas in Mesozoic backarc sediments which lie beneath the modern forearc, with drilling now underway near the town of Pica. Although the specifics of these Mesozoic deposits are not discussed as a part of this work, knowledge of the Cenozoic deformation history throughout the basin will provide an understanding of reservoir connectivity, hydrocarbon migration and hydrocarbon maturation, which should allow for a more informed guidance of future drilling programs should the play prove to be viable.

Neogene sedimentation within the basin has responded to both climatic as well as tectonic forcing. To a first order, while sedimentation has responded to deformation within the basin, climate appears to be the primary factor in determining lithofacies deposited and preserved. While aridity has been the dominant climatic regime during the time spanning our study, large lakes were a major feature of the landscape during at least two stages within the last 20 Ma, the early Miocene and at the Miocene-Pliocene boundary. Also, we illustrate that, hidden beneath the relatively smooth modern topographic surface, the Pampa del Tamarugal has a complex structural history, with deformation occurring throughout the entire Neogene. We also tie the changes in facies to global climate changes as well as semi-regional impacts brought about by the uplifting Altiplano-Puna plateau at the eastern margin of the basin.

One of the major research aims of the past 10 years in northern Chile has been to detail the uplift of the Altiplano-Puna plateau of the central Andes (Fariás *et al.*, 2005; Garzione *et al.*, 2006; Garzione *et al.*, 2008; Ghosh *et al.*, 2006; Hoke *et al.*, 2007, Muñoz and Charrier, 1996; Schildgen *et al.*, 2007; Thouret *et al.*, 2007; Victor *et al.*, 2004), and to then determine a mechanism for the uplift (Gubbels *et al.*, 1993; Isacks, 1988; Kay and Kay, 1993; Molnar and Garzione, 2007) of this, the second-highest broad plateau on Earth, and the highest in a non-collisional setting. Estimates of plateau uplift relative to the forearc basins are on the order of 2 to 3 kilometers since 10 Ma (Garzione *et al.*, 2006; Gregory-Wodzicki, 2002). While portions of the western slope were uplifted across surface-breaking reverse faults (Charrier *et al.*, 2005; Fariás *et al.*, 2005; Muñoz and Charrier, 1996; Pinto *et al.*, 2004; Victor *et al.*, 2004) of uplift, much of that faulting occurred earlier than 10 Ma. While deformation has clearly been active since 10 Ma for portions of the northern Chilean forearc (*e.g.*, Allmendinger *et al.*, 2005; Riquelme *et al.*, 2003; Soto *et al.*, 2005), the magnitude of vertical throw on upper crustal structures is insufficient to explain the ~2,000 m of relief that is believed to have been generated between the Central Depression and Altiplano during this time interval. This naturally leads to the question of crustal mechanisms for uplift when faulting is almost certainly not the entire answer. Included in this body of work is a study of relict surfaces as well as time-constrained horizons in the subsurface. We document magnitudes of large-scale westward rotation of this part of the mountain belt through time, with an eye toward shedding some light on other

mechanisms which may be acting to create the modern relief seen today between the plateau and the forearc.

But the Atacama Desert is not only valuable in terms of answering geologic questions. Because it is clearly a climatic end member, it is a region that is particularly sensitive to changes in air mass variations that inevitably occur as part of Earth's dynamic weather systems. Relatively minor fluctuations in factors affecting climate have served to bring more moisture into the region. This work illustrates that a generalization such as "The Atacama Desert has been hyper-arid for millions of years" can be over simplified, and that in the relatively recent past (latest Pleistocene), water was more abundant during discrete time intervals at some locations in what is today the hyperarid core of the Atacama Desert. This holds great importance for a variety of reasons. An understanding of the climatic perturbation which caused this dramatic increase in fresh water supply will allow climate modelers to more accurately ascertain the likelihood of a return to these conditions. A quantification of stream discharge rates during times of increased surface flow and subsequent infiltration and aquifer recharge is critical in assessing the sustainability of current extraction rates since ground water, be it modern or "fossil", is a significant source of freshwater in this parched environment. As such, an understanding of freshwater stores in increasingly exploited underground aquifers holds great importance to the burgeoning populations of the coastal communities in this portion of northern Chile, namely the towns of Arica, Iquique, Tocopilla and Antofagasta. This problem becomes even more acute when one considers that the use of

potable water is often in direct competition with other industrial activities such as iodine processing as well as nitrate and, most importantly, copper mining. As the world's leading copper exporter, copper is at the heart of Chile's national economy.

What follows are three studies which detail the paleoenvironments and deformational history of the Pampa del Tamarugal from the Oligocene to Recent, and the sedimentary responses resulting from these conditions. This work demonstrates that in this sedimentary basin, often a seemingly straight forward and simple story turns out to be much more complex, and initial impressions of "dry" and "undeformed" for the region can often turn out to be misleading. By studying the finer details of responses to climatic and tectonic forcing within the sedimentary and hydrologic system of the Pampa del Tamarugal, it is hoped that a greater understanding will be gained not only for this basin, but in other regions that may have been similar in the past, or will become similar given the current unpredictability of global climate change.

REFERENCES

- Allmendinger, R. W., Gonzalez, G., Yu, J., Hoke, G., and Isacks, B., 2005, Trench-parallel shortening in the Northern Chilean Forearc: Tectonic and climatic implications: Geological Society of America Bulletin, v. 117, no. 1-2, p. 89-104.
- Beaumont, C., Jamieson, R. A., Nguyen, M. H., and Lee, B., 2001, Himalayan tectonics explained by extrusion of a low-viscosity crustal channel coupled to focused surface denudation: Nature, v. 414, no. 6865, p. 738-742.
- Broecker, W. S., Turekian, K. K., and Heezen, B. C., 1958, The Relation of Deep Sea Sedimentation Rates to Variations in Climate: American Journal of Science, v. 256, no. 7, p. 503-517.
- Charrier, R., Chavez, A. N., Elgueta, S., Hérail, G., Flynn, J. J., Croft, D. A., Wyss, A. R., Riquelme, R., and Garcia, M., 2005, Rapid tectonic and paleogeographic evolution associated with the development of the Chucal anticline and the Chucal-Lauca Basin in the Altiplano of Arica, northern Chile: Journal of South American Earth Sciences, v. 19, no. 1, p. 35-54.
- Clarke, J. D. A., 2006, Antiquity of aridity in the Chilean Atacama Desert: Geomorphology, v. 73, no. 1-2, p. 101-114.
- Dingman, R. J., and Galli O, C., 1965, Geology and ground-water resources of the Pica area, Tarapaca Province, Chile, U. S. Geological Survey Bulletin: Reston, VA, USGS, 1-113 p.
- Dunai, T. J., Lopez, G. A. G., and Juez-Larre, J., 2005, Oligocene-Miocene age of aridity in the Atacama Desert revealed by exposure dating of erosion-sensitive landforms: Geology, v. 33, no. 4, p. 321-324.
- Fariás, M., Charrier, R., Comte, D., Martinod, J., and Hérail, G., 2005, Late Cenozoic deformation and uplift of the western flank of the Altiplano: Evidence from the depositional, tectonic, and geomorphologic evolution and shallow seismic activity (northern Chile at 19 degrees 30 ' S): Tectonics, v. 24, no. 4.
- Galli-Olivier, C., 1969, Climate - a Primary Control of Sedimentation in Peru-Chile Trench: Geological Society of America Bulletin, v. 80, no. 9, p. 1849-1852.

- Garzione, C. N., Hoke, G. D., Libarkin, J. C., Withers, S., MacFadden, B. J., Eiler, J. M., and Mulch, (in press), Rise of the Andes: Science.
- Garzione, C. N., Molnar, P., Libarkin, J. C., and MacFadden, B. J., 2006, Rapid late Miocene rise of the Bolivian Altiplano: Evidence for removal of mantle lithosphere: Earth and Planetary Science Letters, v. 241, no. 3-4, p. 543-556.
- Ghosh, P., Garzione, C. N., and Eiler, J. M., 2006, Rapid uplift of the Altiplano revealed through C-13-O-18 bonds in paleosol carbonates: Science, v. 311, no. 5760, p. 511-515.
- Gregory-Wodzicki, K. M., 2002, A late Miocene subtropical-dry flora from the northern Altiplano, Bolivia: Palaeogeography Palaeoclimatology Palaeoecology, v. 180, no. 4, p. 331-348.
- Gubbels, T., Isacks, B., and Farrar, E., 1993, High-level surfaces, plateau uplift, and foreland development, Bolivian central Andes: Geology, v. 21, p. 695-698.
- Hartley, A. J., and Chong, G., 2002, Late Pliocene age for the Atacama Desert: Implications for the desertification of western South America: Geology, v. 30, no. 1, p. 43-46.
- Hartley, A. J., May, G., Chong, G., Turner, P., Kape, S. J., and Jolley, E. J., 2000, Development of a continental forearc: A Cenozoic example from the Central Andes, northern Chile: Geology, v. 28, no. 4, p. 321-324.
- Hoke, G. D., Isacks, B. L., Jordan, T. E., Blanco, N., Tomlinson, A. J., and Ramezani, J., 2007, Geomorphic evidence for post-10 Ma uplift of the western flank of the central Andes 18 degrees 30'-22 degrees S: Tectonics, v. 26, no. 5.
- Houston, J., and Hartley, A. J., 2003, The central andean west-slope rainshadow and its potential contribution to the origin of hyper-aridity in the Atacama desert: International Journal of Climatology, v. 23, no. 12, p. 1453-1464.
- Isacks, B. L., 1988, Uplift of the central Andean plateau and bending of the Bolivian orocline: Journal of Geophysical Research, v. 93, p. 3211-3231.

- Kay, R. W., and Kay, S. M., 1993, Delamination and delamination magmatism: *Tectonophysics*, v. 219, p. 177-189.
- Kay, S. M., Coira, B., and Viramonte, J., 1994, Young mafic back-arc volcanic rocks as indicators of continental lithospheric delamination beneath the Argentine Puna plateau, Central Andes: *Journal of Geophysical Research*, v. 99, no. B12, p. 24323-24339.
- Kober, F., Schlunegger, F., Zeilinger, G., Schneider, H., Willett, S. D., Hovius, N., Brandon, M. T., and Fisher, D. M., 2006, Surface uplift and climate change; the geomorphic evolution of the western escarpment of the Andes of northern Chile between the Miocene and present, Geological Society of America (GSA), Boulder, CO, p. 75-86.
- Lamb, S., and Davis, P., 2003, Cenozoic climate change as a possible cause for the rise of the Andes: *Nature*, v. 425, p. 792-797.
- Molnar, P., and Garzzone, C. N., 2007, Bounds on the viscosity coefficient of continental lithosphere from removal of mantle lithosphere beneath the Altiplano and Eastern Cordillera: *Tectonics*, v. 26, no. 2.
- Muñoz, N., and Charrier, R., 1996, Uplift of the western border of the Altiplano on a west vergent thrust system, Northern Chile: *Journal of South American Earth Sciences*, v. 9, no. 3/4, p. 171-181.
- Perlmutter, M. A., and Matthews, M. D., 1989, Global cyclostratigraphy - A model, *in* Cross, T. A., ed., *Quantitative Dynamic Stratigraphy*: Englewood Cliffs, NJ, Prentice-Hall, p. 233-260.
- Pinto, L., Hérail, G., and Charrier, R., 2004, Sedimentación sintectónica asociada a las estructuras neógenas en la Precordillera de la zona de Moquella, Tarapacá (19°15'S, norte de Chile): *Revista Geologica de Chile*, v. 31, no. 1, p. 19-44.
- Riquelme, R., Martinod, J., Hérail, G., Darrozes, J., and Charrier, R., 2003, A geomorphological approach to determining the Neogene to Recent tectonic deformation in the Coastal Cordillera of northern Chile (Atacama): *Tectonophysics*, v. 361, no. 3-4, p. 255-275.
- Saez, A., Cabrera, L., Jensen, A., and Chong, G., 1999, Late Neogene lacustrine record and palaeogeography in the Quillagua-Llamara basin, Central Andean fore-arc (northern Chile): *Palaeogeography*

Palaeoclimatology Palaeoecology, v. 151, no. 1-3, p. 5-37.

Schildgen, T. F., Hodges, K. V., Whipple, K. X., Reiners, P. W., and Pringle, M. S., 2007, Uplift of the western margin of the Andean Plateau revealed from canyon incision history, southern Peru: *Geology (Boulder)*, v. 35, no. 6, p. 523-526.

Schlunegger, F., Zeilinger, G., Kounov, A., Kober, F., and Husser, B., 2006, Scale of relief growth in the forearc of the Andes of Northern Chile (Arica latitude, 18 degrees S): *Terra Nova*, v. 18, no. 3, p. 217-223.

Schweller, W. J., Kulm, L. D., and Prince, R. A., 1981, Tectonics, structure, and sedimentary framework of the Peru-Chile Trench: *Memior*, Geological Society of America, p. 323-349.

Soto, R., Martinod, J., Riquelme, R., Hérail, G., and Audin, L., 2005, Using geomorphological markers to discriminate Neogene tectonic activity in the Precordillera of North Chilean forearc (24-25 degrees S): *Tectonophysics*, v. 411, no. 1-4, p. 41-55.

Summerfield, M. A., 1991, *Global geomorphology*: New York, John Wiley and Sons, Inc., 537 p.

Thouret, J. C., Wörner, G., Gunnell, Y., Singer, B., Zhang, X., and Souriot, T., 2007, Geochronologic and stratigraphic constraints on canyon incision and Miocene uplift of the Central Andes in Peru: *Earth and Planetary Science Letters*, v. 263, p. 151-166.

Victor, P., Oncken, O., and Glodny, J., 2004, Uplift of the western Altiplano plateau: Evidence from the Precordillera between 20 degrees and 21 degrees S (northern Chile): *Tectonics*, v. 23, no. 4.

Wobus, C. W., Hodges, K. V., and Whipple, K. X., 2003, Has focused denudation sustained active thrusting at the Himalayan topographic front?: *Geology*, c. 31, no. 10, p. 861-864

CHAPTER 2

NEOGENE DEFORMATION AND SEDIMENTARY HISTORY OF THE PAMPA DEL TAMARUGAL, NORTHERN CHILE¹

Introduction

Due to prolonged aridity, the Cenozoic tectonic history of the forearc of northern Chile is in many places easily visible in surface geology and landforms, and is especially visible on remote sensed data. However, the sedimentary deposits of the Central Depression (or forearc basin) associated with this uplift have in some places nearly completely concealed evidence of this deformation. In addition, the sediments themselves are only sporadically exposed, leading to a paucity of information related both to deformation history as well as sedimentary response.

Recently, considerable attention has focused on magnitude and mechanisms of Neogene surface uplift in this region of the central Andes. Consistently, only a moderate amount of compression-related deformation (maximum 10's of meters) has been reported since 10 Ma within and at the eastern boundary of the Central Depression (Muñoz and Charrier, 2006; Fariás *et al.*, 2005; Pinto *et al.*, 2004; Soto *et al.*, 2005; Victor *et al.*, 2004) when the principal shortening of the central Andean Cordillera had shifted to the eastern foothills (Allmendinger and Gubbels, 1996). Although the forearc displays little deformation, evidence

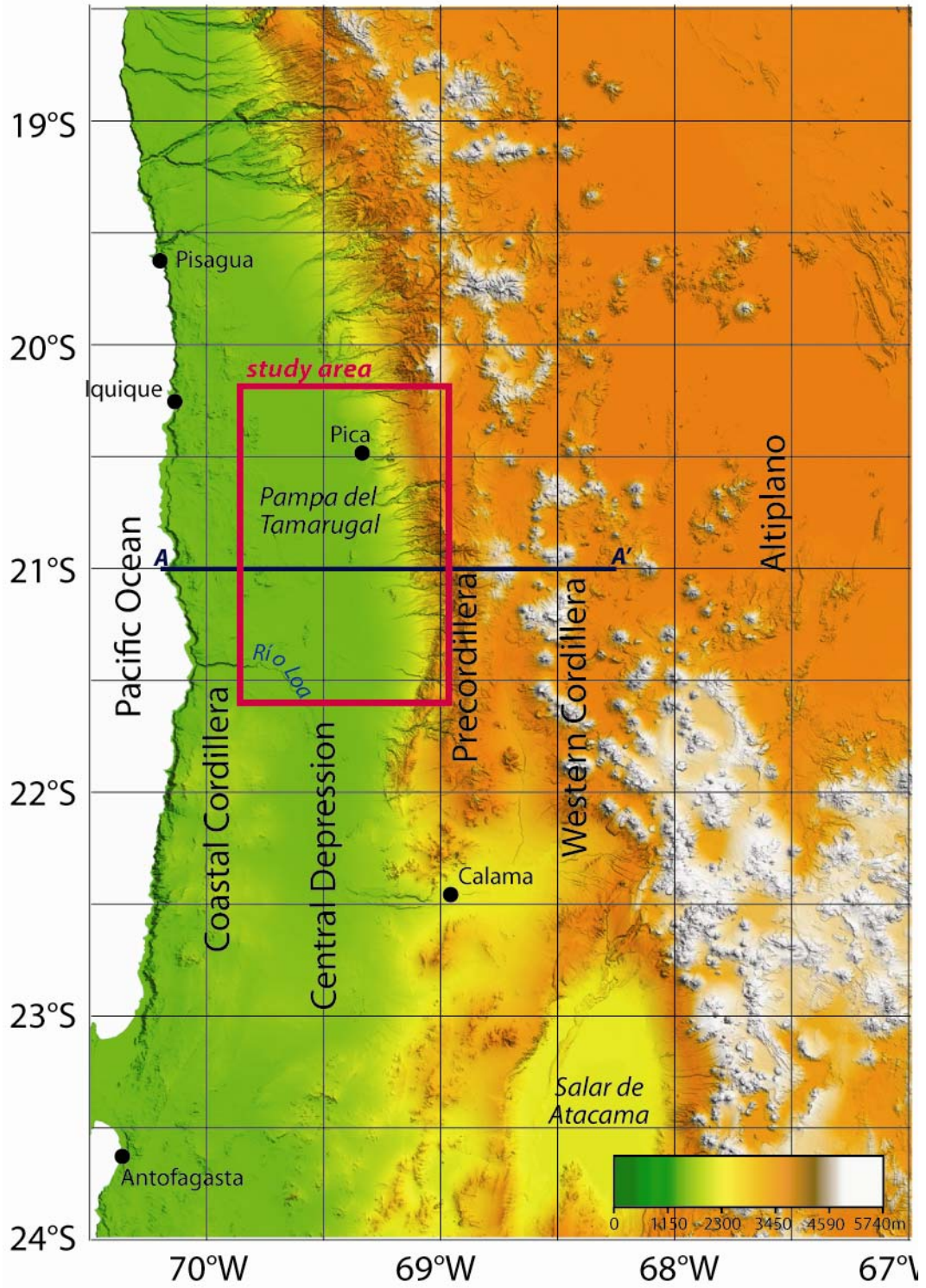
¹Portions of the following chapter to be published with collaborators Blanco, N., Jordan, T., Jensen, A., and Tomlinson, A.

continues to mount that uplift of the Altiplano-Puna plateau immediately to the east of the Central Depression was rapid during the late Miocene (Gregory-Wodzicki 2000, 2002; Garziona *et al.*, 2006; Hoke *et al.*, 2007; Chapter 3). An understanding of the concealed forearc structure may be of great importance in the refinement of models which attempt to attach a mechanism to this rapid ascent.

In addition, this region is globally unique in its degree and duration of aridity. It acts as an end member illustration of sedimentary processes within a hyperarid climate regime in a zone of active tectonic activity (Hoke, 2006). Sedimentation in this region during the Cenozoic is highly unusual, as similar relief generated under any other climate regime would have lead to much greater volumes of siliciclastic detritus supplied as well as dissolved species from chemical weathering.

Seismic reflection data between the latitudes of 20°30' and 21°30'S reveal the tectonic and sedimentary evolution of the Pampa del Tamarugal, an endorheic, nonmarine forearc sedimentary basin, immediately adjacent the western Andean slope (Figure 2.1). Structures in the Pampa del Tamarugal have not been studied in any great detail. Because of uppermost Cenozoic and Quaternary alluvial cover in the basin, as well as the timing and magnitude of the deformation history, almost all structure is concealed beneath the surface. For the same reasons, data concerning Neogene sediment distribution is also virtually nonexistent. However, seismic data image a complex and long-lived structural history, and one that dovetails with structural studies of adjacent areas. Here, we provide for the first time a comprehensive report on the Neogene tectonic history within the Pampa del Tamarugal and the

Figure 2.1: 90 m resolution digital elevation model showing the main morphotectonic provinces of the study area. Red box indicates study area. A-A' represents location of topographic cross section shown in Figure 2.2.



adjacent western Andean slope, and we report on the associated sedimentary response. This information is then put into the larger context of central Andean uplift and aridification of the Atacama Desert.

Geologic background

The study area is categorized as an intramassif forearc basin in the sense of Dickinson and Seely (1979). Thin sedimentary cover rests atop strata of a former Mesozoic backarc basin and the arc massif (Figure 2.2). Morphologically, the Pampa del Tamarugal basin can be considered a segment of an underfilled bench forearc basin (Dickinson, 1995) with the modern volcanic arc to the east and the emergent ridge of the Coastal Cordillera to the west, with sediments “benched” between these two topographic highs (Figure 2.2).

While the Andes have existed as a convergence-related orogenic belt since at least the Jurassic, the current chain was born in the Paleocene (Lamb *et al.*, 1997). At the latitude of the study area, the volcanic arc migrated to near its current position approximately 23 Ma (Reutter *et al.*, 1996; Allmendinger *et al.*, 1997). The Altiplano-Puna plateau began to deform (Isacks, 1988) and rise (Naranjo and Paskoff, 1985) at around 30 Ma, at which time sediment deposition was initiated to the west in the forearc basin beginning 30-25 Ma (Salas *et al.*, 1966; Naranjo and Paskoff, 1985; García and Hérail 2005; Victor *et al.*, 2004).

Today, in the onshore forearc to the west of the Altiplano at the latitudes of 20-22°S, four morphotectonic units are recognized, all trending N-S. From west to east, these are the Coastal Cordillera, Central Depression, Precordillera (Sierra Moreno) and Western Cordillera (Figures

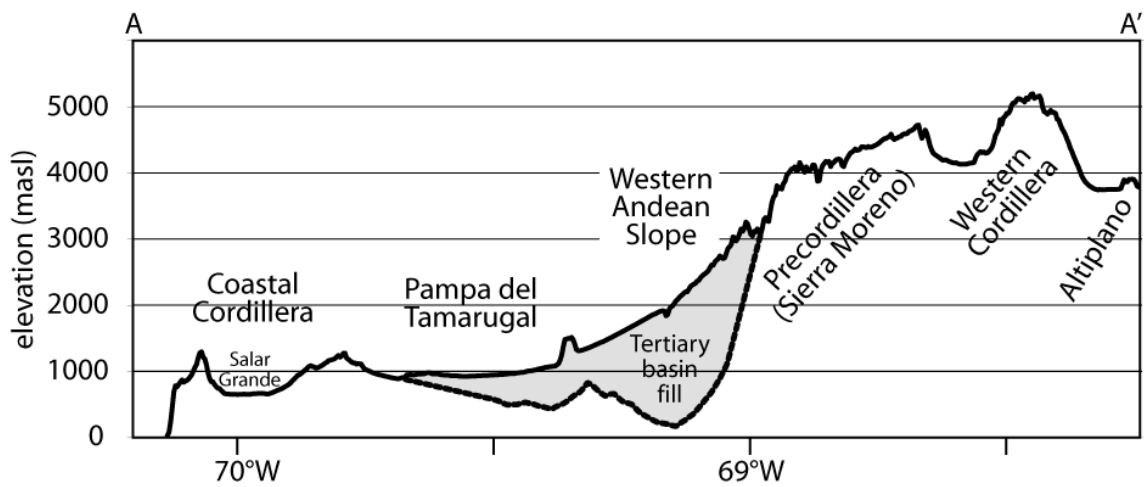


Figure 2.2: East-west topographic profile at 21°S, illustrating Tertiary forearc basin fill above mostly Mesozoic basement. Tertiary sediment thickness is based on interpretations of seismic lines.

2.1 and 2.2), with the Peru-Chile Trench located offshore, parallel to the coastline. Mostly ephemeral and low-discharge perennial streams are directed to the west within canyons incised into the Precordillera and eastern edge of the Central Depression, with their headwaters generally at between 3000 and 4000 m elevation in the Mesozoic rocks of the Precordillera. The Coastal Cordillera averages approximately 40 km in width at this latitude, and effectively acts as a barrier, not allowing any appreciable volume of sediment from the western Andean slope to reach the Pacific Ocean.

Stratigraphic Background

The Pampa del Tamarugal basin trends north between the Coastal Cordillera to the west and the Precordillera and Sierra Moreno (the western foothills of the Andes) to the east (Figure 2.1), with a mean modern elevation of approximately 1000 meters (Figure 2.2). The sedimentary basin includes all of the Central Depression and the western flank of the Precordillera to a modern elevation of ~3500 m (Figure 2.2), where outcrop of Oligo-Miocene strata meet deformed Mesozoic sedimentary rocks atop an angular unconformity. The eastern ~20 km of the Cenozoic basin fill crop out in the westward-draining canyons of the Precordillera and Sierra Moreno. Western sectors of the basin fill are only very sparsely exposed. The well-imaged upper part of the reflection seismic data and boreholes utilized in this study reveal that the sedimentary basin contains a maximum of ~1700 m of nonmarine Oligocene to Recent clastic sediments intercalated with extrusive volcanic deposits. The more poorly-imaged basement rocks to the Cenozoic basin are strongly folded Mesozoic shallow and marginal marine sedimentary

units, other siliciclastic and evaporite strata of uncertain age, and rhyodacitic intrusive units. Surface and borehole data indicate that the entire Cenozoic package is composed of facies formed under semi-arid to hyperarid conditions.

The general chronology and stratigraphic relationships of the Central Depression have been defined further to the north between 18-20°S (Fariás *et al.*, 2005; Mortimer and Saric, 1975; Naranjo and Paskoff, 1972; Parraguez, 1998; Pinto *et al.*, 2004; Salas *et al.*, 1966; von Rotz *et al.*, 2005; Wörner *et al.*, 2000, Figure 2.3), where outcrop is especially accessible in the spectacularly-entrenched canyons that extend from the western limit of the Altiplano to the Pacific Ocean, and where volcanism yields a wealth of dateable material (summarized by Wörner *et al.*, 2000). Here, perennial streams have discharged to the Pacific Ocean since before at least ~6.4 Ma (Hoke *et al.*, 2007) and possibly earlier than 7.5 Ma (Kober *et al.*, 2006). Erosional stream capacity and late-Miocene to Recent uplift have created incised canyons, providing excellent exposure of, in many cases, >1 km depth into the basin fill (Kober *et al.*, 2006; Hoke *et al.*, 2007).

It was not possible to construct a synthesis diagram which satisfies all of the published data. In spite of excellent exposures in the canyons, inconsistencies between different studies still exist, as correlations over long distances in this part of the Atacama Desert have been wrought with difficulty due to the often patchy nature of the nonmarine sediments and volcanic deposits, structural complications and different geochronological dating methods which have been employed to ascertain ages on the volcanic units. More work is necessary

Figure 2.3: Chronostratigraphic chart located at an elevation of approximately 2000 m above sea level parallel to the mountain front, using information from published studies in conjunction with this work. References and dating methods for radiometric dates used in its construction can be found in Table 2.1.

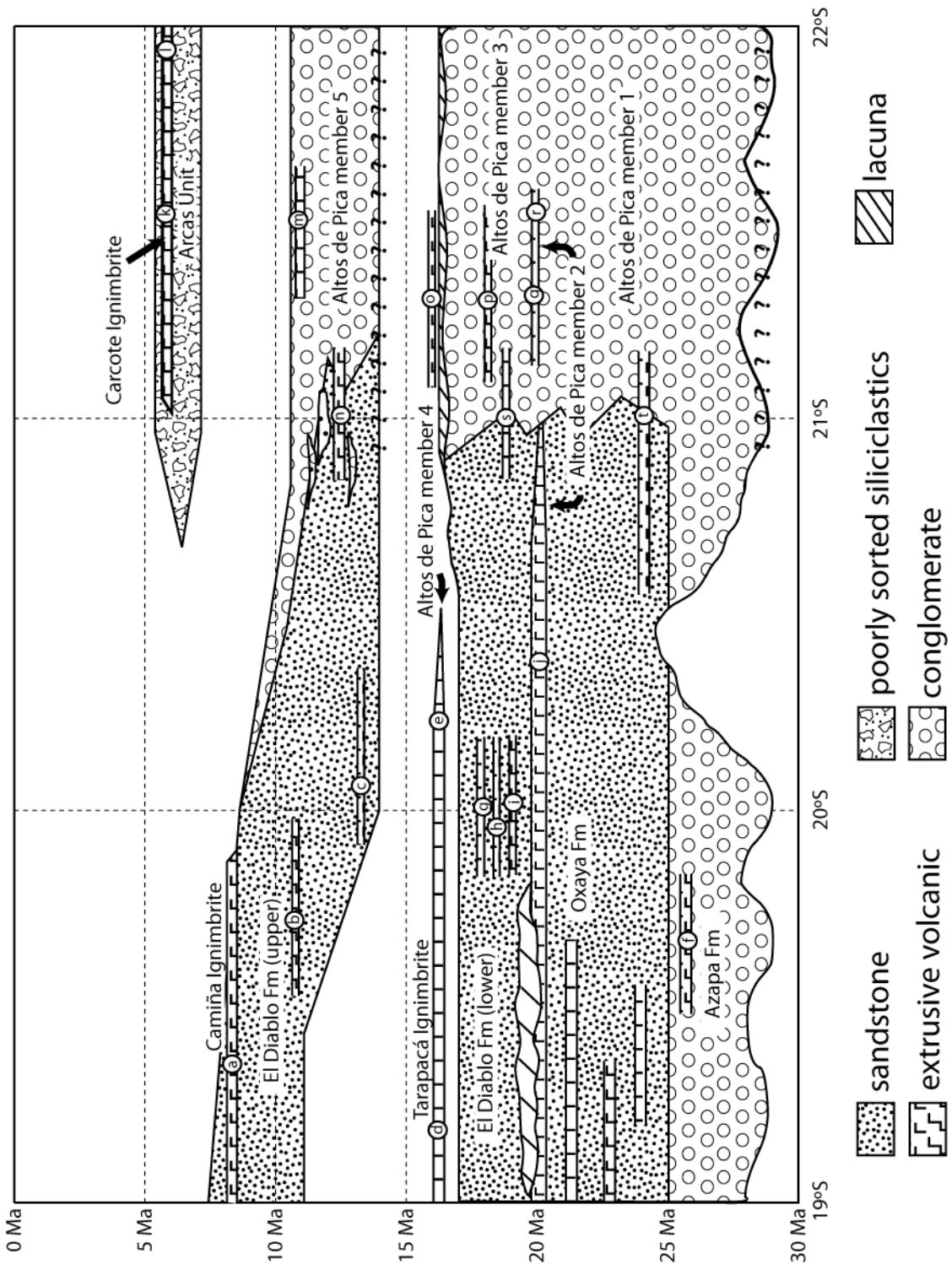


Table 2.1. Radiogenic ages for the Neogene volcanic deposits located along the western Andean slope. Letters refer to labels in Figure 2.3

	date	error	AdP member	reference	sample # (this study)	method of dating	lat (°S)/long (°W)
a	8.2	±0.5		Muñoz and Charrier 1996		K-Ar whole rock	~19°20' / ~69°31'30"
b	11.7	±0.4		Farias <i>et al.</i> , 2005		K-Ar whole rock	19°38' / 69°13'
c	13.7	±0.6		Muñoz 2007		Ar-Ar biotite	19°51'01" / ~69°27'13"
d	16.2	±0.7		Muñoz and Sepúlveda 1992		K-Ar whole rock	19°13' / 69°37'
e	16.27	±0.16		Victor <i>et al.</i> , 2004		Bi-hbl isochrons (Rb/Sr)	20°12'52" / 68°59'13"
f	26.0	±0.4		Farias <i>et al.</i> , 2005		Ar-Ar biotite	19°32' / 69°20'
g	17.3	±0.5		Vergara <i>et al.</i> , 1986		K-Ar rutile	20°10' / 69°20'
h	18.6	±0.3		Vergara <i>et al.</i> , 1986		K-Ar rutile	20°10' / 69°20'
i	19.25	±0.43		Bouzari and Clark, 2002		Ar-Ar biotite	20°03' / 69°15'
j	20.90; 20.61	±0.21; ±0.21		Victor <i>et al.</i> , 2004		Bi-hbl isochrons (Rb/Sr)	20°29'07" / 69°21'18"; 20°18'58" / 69°00'49"
k	5.26	±0.02	Mio-Plio	this study	IB-17	Ar / Ar biotite total gas	21°26'10" / 69°13'29"
l	5.38	±0.09	Mio-Plio	Hoke <i>et al.</i> , 2007	IB-09a	Ar / Ar biotite	20°58'29" / 69°11'58"
m	11.62	±0.05	5	this study	IB-20	Ar / Ar biotite total gas	21°27'03" / 69°10'39"
n	13.03	±0.17	5	this study	IB-07	Ar / Ar biotite plateau	20°57'50" / 69°10'19"
o	15.83	±0.04	5	this study	IB-24	Ar / Ar single crystal sanidine weighted mean	21°13'33" / 69°09'22"
p	17.86	±0.12	3	this study	IB-21	Ar / Ar biotite isochron	21°13'00" / 69°08'33"
q	19.69	±0.03	3	this study	IB-22	Ar / Ar single crystal sanidine isochron	21°12'34" / 69°05'57"
r	19.77	±0.1	3	this study	IB-18	Ar / Ar Single crystal sanidine weighted mean	21°28'55" / 69°05'24"
s	18.89	±0.24	3	this study	IB-11	Ar / Ar biotite isochron	20°59'23" / 69°18'25"
t	24.4	±0.3	1	this study	IB-8	Ar / Ar plagioclase ("integrated")	20°59'23" / 69°18'25"

*=date on reworked volcanic clast
#=biotites altered; either date possible

Table 2.1. (continued)

date	error	AdP member	reference	sample # (this study)	method of dating	lat (°S)/long (°W)
12.94	±0.08	5	Blanco <i>et al.</i> (in prep)	IB-34	Ar/Ar biotite plateau	20°42'42"/69°12'28"
5.6*	±0.03	Mio-Plio	this study	GH-04-01	Ar/Ar biotite isochron	21°22'57"/69°16'26"
5.53‡	±0.21	Mio-Plio	this study	N04-20	Ar/Ar biotite total gas	21°22'01"/69°03'35"
3.43‡	±0.47				Ar/Ar biotite plateau	
18.2*	±0.8	4	this study	IB-01	K-Ar biotite	Quebrada Chacarilla
16.4*	±0.5	4	this study	IB-02	K-Ar	Quebrada Chintagua
19.65*	±0.2	2	this study	IB-03	K-Ar	Quebrada Chintagua
5.56	±0.09	Mio-Plio	this study	IB-05	Ar/Ar Biotite	20°57'23"/69°09'47"

*=date on reworked volcanic clast

‡=biotites altered; either date possible

in order to standardize the chronostratigraphic relationships within the northern Chilean forearc.

It is observed that the majority of the sedimentary infill was delivered to the basin between the Oligocene and end of the Miocene (~30 and ~5 Ma). The oldest widely recognized unit is the Azapa Formation, a fluvial conglomerate consisting of well-rounded, well-imbricated clasts derived from volcanic and sedimentary rocks of mostly Cenozoic age (Salas *et al.*, 1966). At the western edge of the basin, these rocks in many places grade into fluvio-lacustrine and salar sediments, often onlapping to the west the Jurassic and Paleozoic rocks of the Coastal Cordillera (von Rotz *et al.*, 2005; García and Hérail 2005; Kober *et al.*, 2006). Above the Azapa Formation are several thick and extensive volcanic rhyolitic ignimbrites and associated tuffs with interbedded fluvial and lacustrine sediments, known as the Oxaya Ignimbrites. This unit reaches a cumulative thickness of up to 1100 m at 18°S (Wörner *et al.*, 2002), but thins to less than 200 m at 19°S (von Rotz *et al.*, 2005). Extensive dating places the age of this unit at between approximately 23 and 19 Ma (Wörner *et al.*, 2002). Discordantly overlying the Oxaya Ignimbrites is the El Diablo Formation. This unit displays predominantly fluvial facies near the mountain front, grading into braidplain and fluvio-lacustrine sandstones and mudstones in the central and western portion of the basin. It has been differentiated into two distinct units (Parraguez, 1998; Farías *et al.*, 2005). At the center of the basin, the lower El Diablo is composed of fine-grained sands and silicified limestone with silicified plant fragments, interpreted as a lacustrine facies. At this same central position within the basin, the energy of deposition increases during the

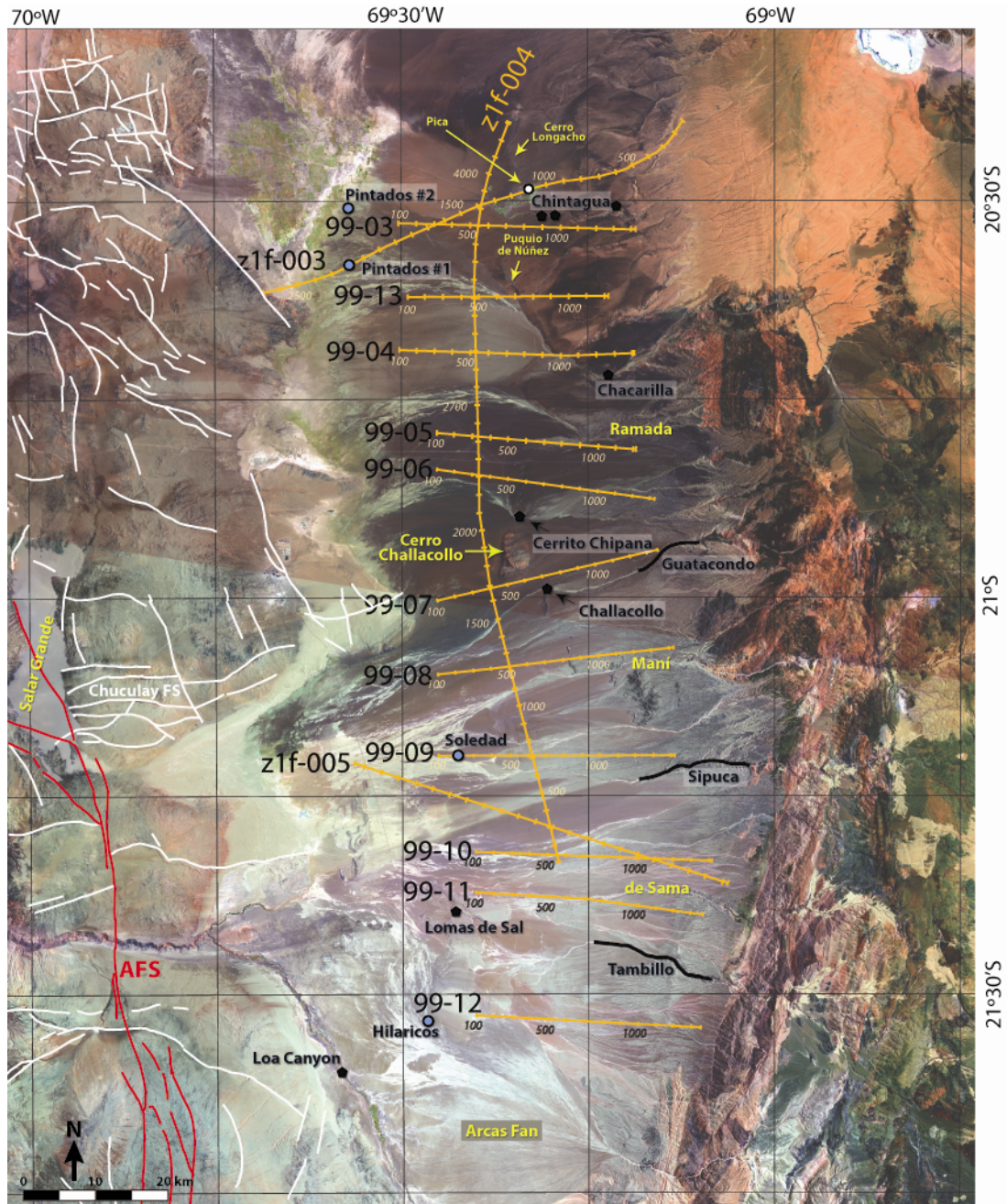
time of the upper El Diablo Formation, which consists of sands and gravels which in places are rounded and well sorted, suggesting a fluvial depositional environment, and in others are more poorly sorted and alluvial in nature. Thickness is highly variable between 18° and 20°S. Magnetostratigraphy suggests that the youngest El Diablo deposits are in places as young as 7.5 Ma (von Rotz *et al.*, 2005, Figure 2.3), although a review of the literature suggests that the age of termination of El Diablo deposition occurred earlier, prior to the Camiña Ignimbrite (Pinto *et al.*, 2004) which is dated to 8.2 ± 0.5 Ma (K-Ar whole rock, Muñoz and Charrier, 1996) and which covers the El Diablo Formation in the eastern part of the basin. An andesite clast within the El Diablo Formation which dated to 11.9 ± 0.6 Ma (K-Ar, whole rock) gives a maximum age for the termination of El Diablo deposition (Garcia and Hérail, 2005). The maximum age of the El Diablo Formation is younger than the top of the Oxaya Ignimbrites at 19.3 ± 0.8 Ma (von Rotz *et al.*, 2005).

As a consequence of downcutting due to a relative baselevel change since its deposition ceased in the late Miocene (Hoke *et al.*, 2007; Kober *et al.*, 2006), the upper El Diablo Formation ceased to accumulate sediment and ignimbrites and in many places today forms a regional pediplain. Gypsic soils which have developed atop this surface are evidence of the long exposure history of this pediplain. These soils of the Central Depression are different than the gypcrete soils of the Coastal Cordillera. The Coastal Cordillera gypcretes are an accumulation of minerals draping the surface which have been largely sourced from moisture originating from the coastal fog, or *camanchaca* (Rech *et al.*, 2003), whereas the soils in the Central Depression are the result of slow

dry atmospheric deposition in the form of aerosols which impregnate the ground surface (Rech *et al.*, 2003; Michalski *et al.*, 2004; Ewing *et al.*, 2006). These arid paleosols have been interpreted as evidence of long (100,000's to 1,000,000's of years) periods of exposure and landscape stability (Ewing *et al.*, 2006; Owen *et al.*, 2006; Rech *et al.*, 2006)

Within the study area, the basement to the Cenozoic basin at its eastern margin is comprised of Jurassic to Cretaceous sandstones, mudstones and carbonates deposited within a marginal marine backarc basin, intercalated with and crosscut by largely granitic to andesitic igneous intrusions and rhyolitic tuffs (Dingman and Galli, 1965; Digert *et al.*, 2003). Within the basin center occur elongate hills which individually trend north-south, and exist at most latitudes within the basin, while being especially concentrated at latitudes between 20°50'-21°10'S, between Quebradas Ramada and Maní (Figure 2.4). These hills are conspicuous above the valley, standing up to 300 m above the plain, and can be broken into two broad categories. Hills with a high degree of macroscopic physical weathering are mostly composed of a variety of intrusive volcanic rocks of generally intermediate composition (Wörner *et al.*, 2000), in addition to Jurassic sandstones and limestones (SERNAGEOMIN, 2002). A second class of hills in the center of the basin is composed of Oligocene-Pliocene (?) sedimentary and volcanic rocks which are sharper landforms than their Mesozoic and early Tertiary counterparts. Given the differences in erosion of their surfaces, the more weathered hills were likely exposed for a significantly longer interval.

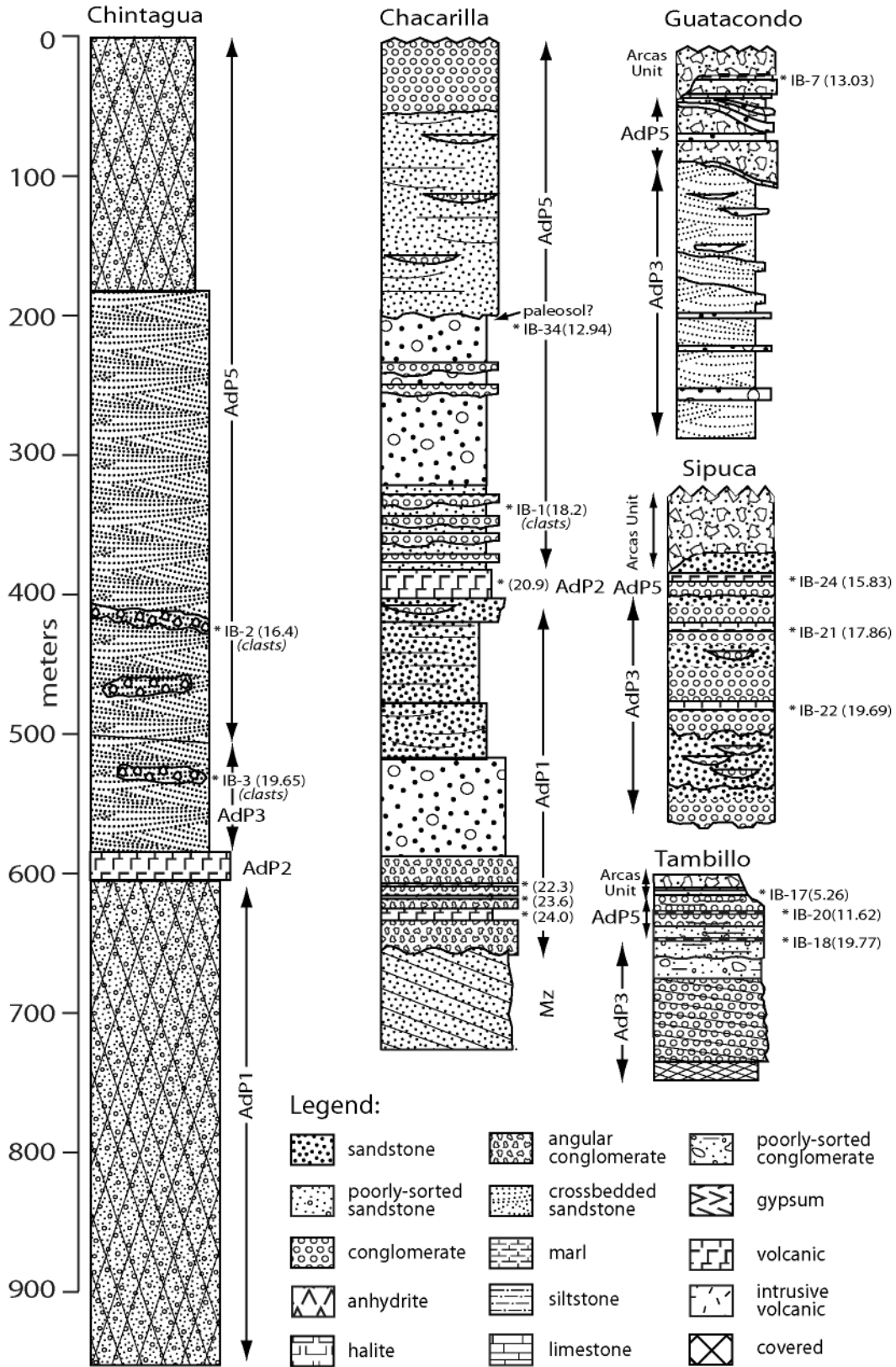
Figure 2.4: Thematic Mapper image of the Pampa del Tamarugal showing location of the seismic grid (and selected shotpoints) used in this study, as well as wells (blue dots), stratigraphic columns (black pentagons) and locations mentioned in the text (yellow). Faults of the Coastal Cordillera are represented by white and red lines, and have been modified from the 1:1,000,000 scale map produced by SERNAGEOMIN (2002). The location of the labeled, predominantly east-west trending Chuculay Fault System, recently identified as composed primarily of reverse faults, was modified from data presented in Allmendinger *et al.* (2005). “AFS” = Atacama Fault System.

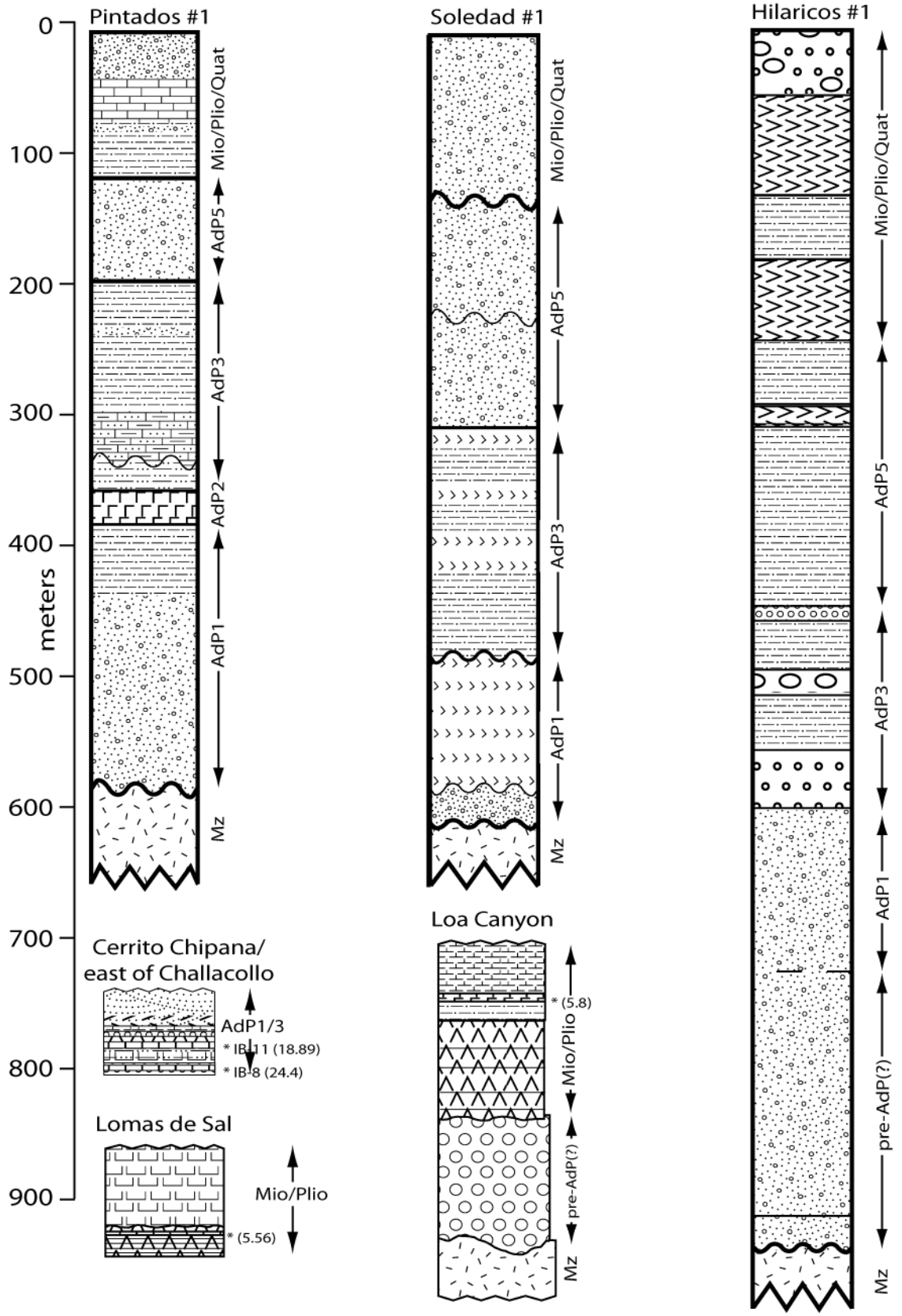


The stratigraphic type section for our study area (20°15'-21°30'S) was defined by Dingman and Galli (1965) in the eastern sector of the basin near Pica (20°30'S, 69°15'W, Figure 2.4). The principal Cenozoic (Upper Oligocene to Middle Miocene) deposits are known as the Altos de Pica (AdP) Formation and consists of five members. The AdP rests atop an angular unconformity above the basement. The AdP member 1 is interpreted as the beginning of the uplift of the Altiplano (Naranjo and Paskoff, 1985), and can broadly be correlated to the Azapa Formation to the north (Figure 2.3).

The AdP member 1 is a light-colored, dominantly conglomeratic unit consisting of reworked tuffs and other igneous clasts originating from the east, interbedded with pyroclastic deposits, especially near the base. Its average reported thickness at the northern end of our study area is ~325 m (Figure 2.5, Chintagua column). It pinches out at the eastern margin of the basin along the western Andean slope at approximately 3200-3250 m (Dingman and Galli, 1965; Victor *et al.*, 2004). Conformably resting atop this unit is the AdP member 2, a rhyolitic welded tuff (ignimbrite) (Dingman and Galli, 1965), which has been dated at 20.90±0.21 and 20.61±0.21 Ma (biotite-hornblende isochrons, Victor *et al.*, 2004). The AdP member 3 is a sandy aeolian and fluvial deposit with alluvial conglomeratic interbeds, conformably overlying the AdP member 2. With an average thickness of ~175 m (Dingman and Galli, 1965), the AdP member 3 pinches out to the east at an elevation of 2300 m along the western Andean slope near Pica (Victor *et al.*, 2004). The AdP member 4 is a locally-welded rhyolitic tuff (Dingman and Galli, 1965), resting nonconformably atop the AdP

Figure 2.5: Stratigraphic columns of the Neogene deposits from within the Pampa del Tamarugal. All columns are at the same scale. Supporting information regarding geochronological dates is located in Table 2.1. Location of columns can be found on Figure 2.4.





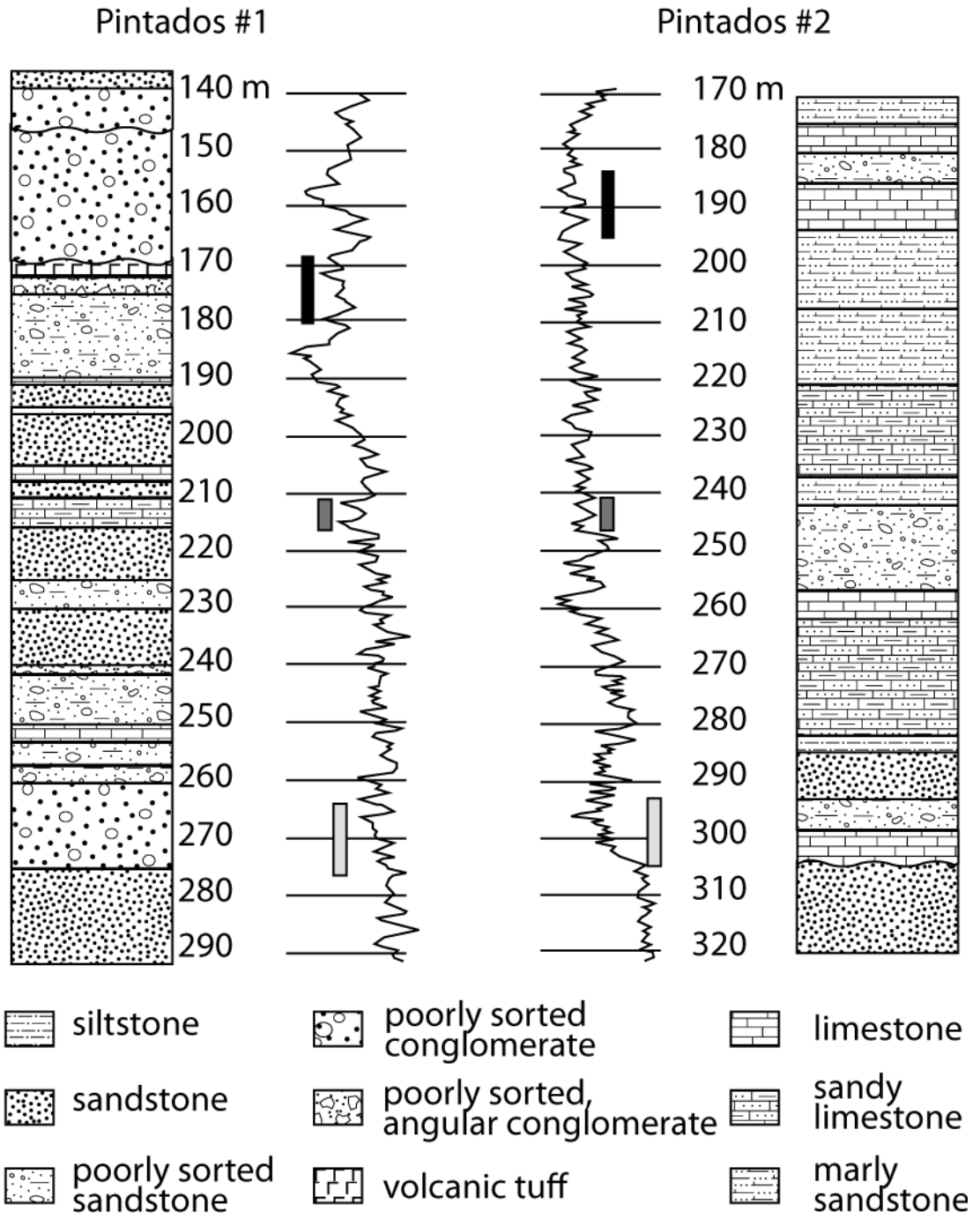
member 3. It is up to 150 m thick, but as it was sourced from an eruptive center located to the east, it thins westward to a feather edge at ~2000 m elevation (Dingman and Galli, 1965) and is not known to be a unit of any consequence much further south than 21°S (this study). AdP member 4 is dated at 16.2 ± 0.7 Ma (K-Ar whole rock, Muñoz and Sepúlveda, 1992). The AdP member 5 rests disconformably atop the AdP members 1 and 3 towards the basin center and nonconformably over the AdP member 4 higher in altitude on the western Andean slope. Member 5 pinches out at an altitude of 3100 m (Dingman and Galli, 1965; Victor *et al.*, 2004). This unit is sandy in the north at 20°30', but becomes increasingly more conglomeratic southward (this study), reflecting a more alluvial environment of deposition. Ash layers south of 21°S indicate that the youngest deposits within the AdP member 5 are at least as young as 11.62 ± 0.5 Ma.

The Azapa and Oxaya Formations are considered to be time-equivalent to the AdP member 1 (Figure 2.3). Based on the limited outcrop of AdP member 1, it is inferred that the proportion of ignimbrites, tuffs and reworked ashes in these units of ~26 – 20 Ma diminishes from 20°S to the study area sector of the Pampa del Tamarugal, where siliciclastic strata predominate. AdP member 3 appears to be age equivalent to the lower part of the El Diablo Formation. The AdP member 4 is age-equivalent to the Tarapacá Ignimbrite further north (Pinto *et al.*, 2004, Figure 2.3) and is referred to as the Huasco ignimbrite further east. The youngest horizons of AdP member 5, 11.62 ± 0.05 Ma, are likely to be several million years older than the youngest deposits within El Diablo Formation further north (Figure 2.3).

For the study area, 20°15'-21°30'S, the best exposure of uppermost Miocene and Lower Pliocene (?) sediments (post ~7(?) Ma) is observed along the Río Loa canyon and its tributaries near their intersection with the Coastal Cordillera at 69°30'W (Figure 2.4). In this western portion of the basin, Upper Miocene-Pliocene (?) lacustrine and salar facies of the Soledad Formation accumulated in areas of paleorelief generated by local tectonics (Sáez *et al.*, 1999). Outcrops reveal a combination of siliciclastic and evaporite deposits (Figure 2.5, Loa Canyon) which are in places highly variable in both thickness and lateral facies extent (Sáez *et al.*, 1999). In addition to those outcrops, uppermost Miocene (7.2 – 5.3 Ma, Kiefer *et al.*, 1997; Hoke *et al.*, 2007; SERNAGEOMIN, 2002) alluvial sheetflood deposits are inset into the westward-draining canyons and form relict bajadas and relict alluvial fans that are highly conspicuous geomorphological features, including the Arcas alluvial fan centered at 21°40'S (Figure 2.4, Kiefer *et al.*, 1997). These deposits are here given the designation of the “Arcas Unit”, and will be referred to in this manner throughout the rest of the text. The deposits of the Arcas Unit rest atop and onlap the Altos de Pica Formation in a subtle angular unconformity. They reach a maximum thickness of ~150 m (Kiefer *et al.*, 1997) in the southern portion of the study area, thinning to 20 m or less at the western limit of the sedimentary basin (Sáez *et al.*, 1999). Evidence for an extensive equivalent of this unit north of the study area in the Central Depression is lacking (Figure 2.3). After this time, deposition in the basin ceased entirely, with only a thin veneer of late Pleistocene to Recent fluvial and alluvial facies present in the center of the basin (Houston, 2002; Nester *et al.*, 2007).

Four petroleum exploration wells help to inform us about the western side of the sedimentary basin, where exposure of the basin fill is practically nonexistent. Hilaricos #1 well (21°31'S, 69°28'W; Figure 2.4) is distinguished by the comparatively large thickness of strata and by the dominance of a thick evaporite unit in the upper part of the borehole. It displays nearly 1 km (925 m) of basin fill (Figure 2.5) resting atop rhyodacites of Mesozoic age. This southernmost well log differs from Soledad #1, 35 kilometers to the north (21°12'S, 69°25'W; Figure 2.4), at which thick evaporites characterize much of the lower part of the column rather than the upper part. The Soledad #1 well encountered 602 m of Cenozoic fill before entering Mesozoic basement (Figure 2.5). In the northernmost sector of our study area, the Pintados #1 well (20°34'30"S, 69°34'00"W; Figure 2.4) is most noticeably different in the complete lack of evaporite deposits. Here, the thinnest sedimentary sequence is observed, with only 577 meters of Cenozoic fill (Figure 2.5). An ignimbrite is seen in borehole cuttings at 352-378 m depth, which very likely correlates with the Altos de Pica member 2 seen outcropping in the canyons at higher elevations to the east based on the characteristics of these cuttings (color, hardness, and stratigraphic position). Pintados #2 (21°30'30"S, 69°34'00"W; Figure 2.4), located less than 8 km to the north of Pintados #1, displays essentially the same stratigraphic succession, although between approximately 175 and 280 m depth in Pintados #2, there is a more significant proportion of limestone relative to Pintados #1, which predominantly reveals sandstone with thin limestone interbeds (Figure 2.6). In addition, depth to Mesozoic basement rocks increases to 704 m within Pintados #2. This increase in thickness between the two Pintados wells is mostly a function of an 85 m sequence of breccias

Figure 2.6: Comparison of a segment of well logs Pintados #1 and Pintados #2, showing stratigraphic interpretation, true vertical depth for each well, gamma ray curves used in the correlation, and correlative sections (black-gray bars) identified by curve-matching in conjunction with lithologic comparisons observed within the boreholes themselves.



composed of igneous clasts present above the basement rocks in Pintados #1. The Altos de Pica member 2 was present at 342-382 m depth in the Pintados #2 borehole. It should be noted that the Pintados #1 and #2, and the Soledad #1 wells were drilled at locations of interpreted structural highs, whereas in fact they were located at the crests of volcanic knobs (F. Digert, pers. comm., 2004). Therefore, stratigraphic thicknesses of the sedimentary fill at these locations can be assumed to be a minimum representation of the regional thickness, with some units potentially missing altogether.

Structural Background

The Pampa del Tamarugal basin is just one of a series of north-trending basins which exist between the uplifting Andes to the east (Precordillera and Altiplano-Puna plateau) and the emergent Coastal Cordillera to the west. Many mechanisms have been presented in an attempt to explain its origin. Two hypotheses involve a graben-like configuration: normal faulting at both margins (Mortimer, 1973), or local to regional extension in a stress field with lateral motions along major regional strike-slip faults (Flint *et al.*, 1991; Cabrera *et al.*, 1995; Jensen *et al.*, 1995). Other contrasting hypotheses involve creation of the basin as a passive topographic feature. One half of the proposed passive origin of the Pampa del Tamarugal is by long-wavelength rotation (between 50-100 km) (see Chapter 3) or by basement-involved faulting (Victor *et al.*, 2004) of the western Andean slope. The other half of a potential passive origin of the Pampa del Tamarugal is by uplift of the west flank of the basin, the Coastal Cordillera, due to tectonic underplating (Delouis *et al.*, 1998). However, its exact origin remains unclear, and may be a

combination of these mechanisms, which may also vary along strike. Within and immediately adjacent to the basin are shorter wavelength structures that are the primary focus of this study, which may be related to the longer wavelength and higher amplitude structures associated with the formation of the basin. Of relevance are primarily reverse faults trending generally parallel to the mountain front along the western Andean slope and within the Central Depression, as well as both normal and reverse faults of various orientations located within the Coastal Cordillera.

Between 18° and 20°30'S, largely north of our study area, the dominant structural trend of faults and folds along the western Andean slope and in the western ranges of the Andes is NW to NNW (Muñoz and Charrier, 1996; García and Hérail, 2005; Farías *et al.*, 2005; Pinto *et al.*, 2004; Muñoz, 2007). Those studies have reported Andean uplift commencing in the latest Oligocene, largely controlled by the Western Thrust System (WTS) as defined by Muñoz and Charrier (1996). The WTS is a series of thick-skinned, high-angle, basement-involved west-vergent reverse faults striking roughly parallel to the current topographic expression of the Andean mountain front. Where faults do not break the surface, fault-bend folds are observed as broad flexures at the surface (Muñoz and Charrier, 1996) or as growth strata in the subsurface as revealed by seismic data (Victor *et al.*, 2004). In their study of seismic line z1f-003 at 20°30'S, Victor *et al.* (2004) proposed that movement along faults that they associate with the southern extremity of the WTS may have accommodated as much as 2600 m of Andean uplift during the Miocene. These faults, and those associated with the WTS further north in and along the eastern margin of the Central Depression, largely ceased

activity by the latest Miocene (Muñoz and Charrier, 1996; Victor *et al.*, 2004; Fariás *et al.*, 2005).

Previously, very little has been reported concerning the structures within the Pampa del Tamarugal. Several north-trending hills exposed at the center of the basin, including Cerro Longacho (20°23'00"S, 69°20'30"W) near the town of Pica and Cerro Challacollo (20°57'00"S, 69°21'30"W, Figure 2.4) have been interpreted as uplifted by west-vergent reverse faults during the Miocene (Victor *et al.*, 2004; SERNAGEOMIN, 2002). Other than the studies concerning these hills, and the interpretation of blind north-trending faults based on stream profile data along the western Andean slope (Victor *et al.*, 2004), no structures have been reported. While previous studies using subsurface data on depth to basement (Rieu, 1975) suggested that several subsurface faults trending northwest split the basin into several sub-basins, no interpretation on the timing of these subsurface faults existed prior to this study.

Observations within the forearc illustrate that deformation has regularly reactivated previous fault surfaces (Reutter *et al.*, 1996; Kuhn, 2002; Soto *et al.*, 2005), often reversing their sense of displacement (Allmendinger *et al.*, 2005, Tomlinson *et al.*, 1993, 1994; Tomlinson and Blanco, 1997a,b). While most reported structures in the forearc are west-vergent, alternating vergence on synthetic thick-skinned basement-involved faults has formed the Cordillera de Domeyko during the late Mesozoic and Cenozoic to the south of the study area under a compressive regime (Mpodozis *et al.*, 2005; Soto *et al.*, 2005). Other examples of east-vergent structures have been reported on the east side

of uplifted Mesozoic clastic and intrusive rocks at 20°10'S latitude, 30 km north of our study area (Muñoz, 2007).

The Coastal Cordillera, standing at a modern elevation of 1-2 km and running parallel to the trench (Figures 2.1 and 2.2), has been uplifted relative to sea level since the Oligocene (Hartley *et al.*, 2000). Estimates of neotectonic uplift based on studies of Pleistocene marine terraces indicate this portion of the Coastal Cordillera has risen at rates of between 0.05 to 0.3 mm/yr since approximately 125 ka (González *et al.*, 2003; Ortlieb *et al.*, 1996). The leading theory for the origin of this range is that successive underthrusting and subsequent underplating of subducted material at the trench led to a thickening at the plate margin, which resulted in the uplift of the Coastal Cordillera through isostatic adjustment (Armijo and Thiele, 1990; Delouis *et al.*, 1998).

Within the Coastal Cordillera are many different structural elements. The Atacama Fault System (AFS) (Figure 2.4), a north-south trending feature which today exhibits mostly extensional and oblique strike-slip motion (Delouis *et al.*, 1998; von Huene *et al.*, 1999; González *et al.*, 2003), is the most widely recognized and studied structural feature in the Coastal Cordillera. It has been active since the Mesozoic, initially as a left-lateral strike-slip fault (Scheuber and Andriessen, 1990). Today, it is most visible at the surface east and south of Antofagasta, where it exerts strong control on the local topography within the Coastal Cordillera and is dominated by down-to-the-east normal faults (Delouis *et al.*, 1998; González *et al.*, 2003). Scarps of up to 100 m document normal displacement which has occurred during the Cenozoic, with deformation continuing into at least the late Pleistocene (González *et al.*,

2003). Faults of the AFS trend N-S near Antofagasta, swinging to the NW at 21°30'S near the Rio Loa. In Salar Grande (Figures 2.2 and 2.4), the Salar Grande Fault (the northern extent of the AFS) exhibits predominantly dextral strike-slip motion.

Normal faulting not directly associated with the AFS also occurs in the Coastal Cordillera between 20-22°S (González *et al.*, 2003; Delouis *et al.*, 1998). Approximately 50 km to the west of the seismic grid analyzed in this study in the Salar Grande region, seismic fractures of neotectonic origin have been associated with extensional strain related to interseismic loading (Loveless *et al.*, 2005; González *et al.*, 2003).

Recently, trench-perpendicular reverse faults have been identified in the Coastal Cordillera (Figure 2.4), occurring over at least a 250 km north-south distance. East-striking fault-bend folds and fault scarps east of the town of Pisagua between 19° and 19°30'S provide a detailed record of active deformation (Caprio, 2007) which continued into at least the latest Miocene (Allmendinger *et al.*, 2005). Also in the Coastal Cordillera, immediately south and east of Salar Grande, east-striking fault scarps of the Chuculay fault system (Figure 2.4) formed by reverse motion during the Cenozoic (Allmendinger *et al.*, 2005). Some of these scarps reach 350 m height, although nearly all of this motion is interpreted to have occurred before the beginning of the Pliocene, with only several meters of reported displacement thereafter (Allmendinger *et al.*, 2005). At the latitude of 20°43'S on the western side of the Coastal Cordillera, an ENE-trending reverse fault associated with this system shows 2-3 m of offset of a 5.6 Ma reworked tuff, evidence that a minor amount of thrusting continued until at least the very latest Miocene (Allmendinger *et al.*,

2005). Cross-cutting (thereby postdating) one of these reverse fault scarps is the previously-mentioned Salar Grande Fault. It therefore appears that, within the Central Depression and Coastal Cordillera between 20 and 23°S, both reverse and normal fault displacements have continued since the end of the Miocene.

Methods

We used 14 reflection seismic lines, logs and cuttings from 4 hydrocarbon exploration boreholes, and sedimentological and chronological data from surface exposures (Figure 2.4) to help constrain the evolution of the Pampa del Tamarugal basin in relationship to structural evolution of the Andean forearc. In particular, we have documented the timing, magnitude and character of structural deformation. With those data, we compiled in maps the evidence of faulting and folding as well as the locations with growth strata. Seismic stratigraphic geometries illuminated many of the relative timing relations for the structures, and stratigraphy and ash chronology of the exposed strata and borehole data provided the age control. Seismic variations were mapped and interpreted in the context of sedimentological variations documented at the surface and in boreholes.

Paper seismic lines with stacking velocities originally obtained by Evergreen Resources and ENAP were provided by International Exploration Associates Ltd. Paper seismic lines were scanned, converted to bitmap, and eventually converted to segy format using the MATLAB programming language, the Seismic Unix program, and ProMax version 2003.3.3, and then imported into the seismic interpretation software

Kingdom Suite version 8.1 (for a detailed workflow, see Appendix A.) Once in Kingdom Suite, reflectors were tied to available well log data, located at the western edge of the seismic grid in the western portion of the basin (Figure 2.4). Since only 2 wells directly tie to seismic data, we relied extensively on surface geology along the traces of the seismic lines to tie surface stratigraphy to seismic stratigraphy, especially the locations where reflectors intersect with the land surface. Tested at the two wells, the stratigraphic matches were of moderate quality (see below, Figure 2.7).

Relevant geologic information was obtained from geologic maps, aerial photographs, Landsat TM imagery, and personal field observations. In support of the seismic interpretation, structural and stratigraphic information were collected during >50 days of field work focused on the eastern canyons, widely distributed knobs in the middle of the basin, the Loa Canyon in the southwestern sector of the basin, as well as observations of relevant geology in regions adjacent to the study area. These surface and borehole data and reflector characteristics provide sufficient data with which to map the sedimentary units that overlie the basement. The seismic data and outcrop stratigraphy are of high enough resolution to map unconformity-bounded stratigraphic sequences in the entirely nonmarine Cenozoic fill. Faults and folds as recorded based on the seismic data were mapped in tandem with features seen on Landsat TM imagery and on a 90 m resolution digital elevation model (DEM). Sedimentary facies were inferred based on correlation between seismic reflector character (amplitude, frequency,

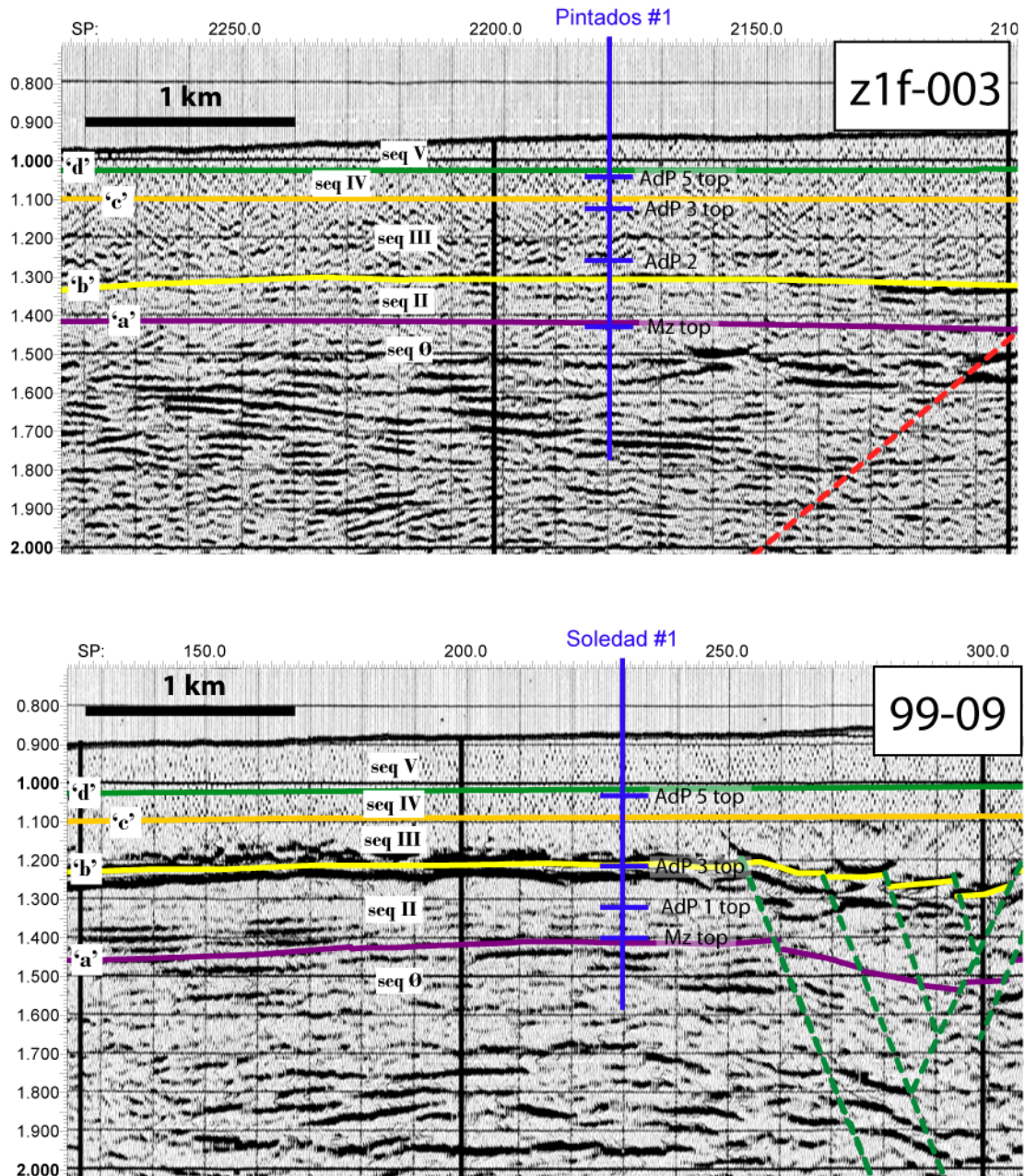


Figure 2.7: Well ties for the Pintados #1 and Soledad #1 wells, correlated with seismic lines z1f-003 and 99-09, respectively. See text and Figure 2.8 for explanation of seismic sequences. See Figure 2.4 for well and seismic line locations.

configuration and coherency; Mitchum, 1977) and sediments observed in well logs and in outcrop, allowing for the interpretation of relationships between structures and environments over the entire depositional basin.

To generate maps of the depths to sequence boundaries required conversion from TWTT to depth, calculated using the Dix Equation from stacking velocities at 2.5 km (100 shot points) spacing along each seismic line. Contour maps for each horizon were then generated using Kingdom Suite's "TKS 8.1 inverse distance to a power" gridding algorithm. A grid increment of 1,000 meters in both horizontal directions was chosen based on an iterative process, and then spot checked to chose the increment which best represented the data. Using these gridded horizons, isopach maps were then generated in a similar fashion.

Seismic mapping of some of the Cenozoic units proved challenging. This is underscored by the fact that stratigraphic units and thicknesses reported from subsurface and borehole studies did not always correlate exactly with reflections seen in the data. This made seismic mapping of units as seismic sequences all the more necessary. In particular, three key sequence boundaries are recognized in the surface stratigraphy but difficult in places to map in the subsurface: the boundaries between basement and Cenozoic fill, Altos de Pica members 3 and 5, and middle Miocene and the Arcas Unit. The sequence boundary between the middle Miocene (AdP member 5) and the Arcas Unit is poorly resolved in the seismic data due to the characteristics of the geophysical survey (shot spacing, input pulse frequency), which was conducted for a Mesozoic target. As such, the parameters of the survey were optimized for deeper reflectors (>1 second two-way travel time [TWT]), whereas the middle

Miocene to Recent horizons of interest for this study are almost entirely within the upper 500 milliseconds (TWT) of data. Therefore, this geologically key sequence boundary is generally located in the seismic mute zone. Also, because of the lithological similarities between the middle Miocene and uppermost Miocene-Pliocene units (both are dominated by unconfined, ephemeral alluvial sheetflood deposits with the same source area and therefore clast composition), uncertainty arises in defining the contact through well log interpretation. It is therefore conceivable that the seismic interpretation of the boundary between the top of the Altos de Pica as defined by Dingman and Galli (1965) and the base of the approximately 7-5.5 Ma deposits may be picked too deeply in the seismic interpretation. In general, the pick does agree with exposure of the contact in the field, but tying this boundary, seen only at the far eastern extent of the seismic lines, with the rest of the survey leads to some degree of uncertainty.

The boundary between the AdP members 3 and 5 in the seismic data is in many places indistinct, either due to the poorly-resolved reflections at shallow depth, or because rock properties in some locations are similar. At the eastern limit of the basin where most outcrops exist, it has been observed that the most effective method of identifying the contact between AdP members 3 and 5 is by recognition of an erosional surface with a slight angular unconformity. This unconformity serves as a sequence boundary that could be identified locally in seismic lines in many locations throughout the basin (most notably at eastern edges of both western and eastern sub-basins), and extended along the same

surface, or at least a very close approximation of the contact, for the entire basin.

Another horizon which is somewhat challenging to map in the subsurface is the lowest horizon mapped, the top of the Mesozoic. This surface has been tied to sparse well data at the far western limit of the data, and outcrop studies conducted in several canyons to the east. These observations seem to allow for a fairly accurate representation of the contact with the seismic data, but as illustrated in Figure 2.7, locally the identification of this boundary is in places still somewhat uncertain.

Lastly, the spacing of the seismic lines is quite large (Figure 2.4) compared to the lateral variability of the nonmarine stratigraphy and the dimensions and spacing of complicated structures within the basin. Correlation of the sequences between neighboring parallel east trending seismic lines (with ~10 km average spacing) is tied with only one north-south trending tie line, which itself crosses several faults at a highly oblique angle. Large magnitude faults and major stratigraphic packages could be best tied between seismic lines and corroborated by the independent data sets, leading us to be confident that the seismic mapping results which follow are accurate to a first order.

Results

Pampa del Tamarugal Surface Stratigraphy

In surface sections within the basin, mostly alluvial and aeolian facies were observed at the eastern limit of the basin, with lacustrine, alluvial and playa facies dominating the central and western portions of

the basin. In most sections, only the stratigraphy representing the middle Miocene to Recent deposits were observable, with the Lower Miocene strata generally concealed beneath the surface. The locations of the studied sections detailed below are indicated on Figure 2.4, and the details of the stratigraphic sections are expanded in Figure 2.5.

Quebrada Chintagua:

Quebrada Chintagua is a composite section with the upper 600 m described in the east end of the drainage (20°31'15"S, 69°18'45"W) and the lower 300 m partially observed at El Salto Chico, approximately 11 km to the west (20°30'00"S, 69°12'45"W). The most striking feature of the section described at Quebrada Chintagua is the predominance of aeolian sands. The entire section measures over 900 m thickness, and exposes AdP members 1, 2, 3, 4 and 5 very near the AdP type section (Dingman and Galli, 1965). The lowermost ~320 m consist of well sorted sandstone and conglomerate, representing aeolian and fluvial facies. Atop the ignimbrite which defines the AdP member 2 rests ~100 m of sandstone with lenses of matrix-supported conglomerate, whose clasts are dominated by welded tuffs, one of which was dated as 19.65 ± 0.2 Ma (Ar/Ar sanidine). This unit is overlain at the eastern extreme of Quebrada Chintagua by the AdP member 4 ignimbrite, but within 2 kilometers westward this pinches out and the contact between AdP member 3 and AdP member 5 is a gentle angular unconformity. The lower 200 m of AdP member 5 are dominated by sandstone with very large scale cross beds. Lenses of matrix-supported conglomerates include boulders of reworked AdP member 4, one clast of which was dated as 16.4 ± 0.5 Ma. This lower part of AdP member 5 represents an aeolian setting.

Quebrada Chacarilla:

At approximately 20°43'S, 69°12'W, the stratigraphy within Quebrada Chacarilla details 650 m of sedimentary and volcanic Cenozoic fill onlapping an angular unconformity atop the Lower Cretaceous sandstones of the Quehuita Formation (Tomlinson *et al.*, 2001). Chronostratigraphic constraints are provided by ignimbrites dated at 24.0 ± 0.8 , 23.6 ± 1.0 and 22.3 ± 1.0 Ma near the base of the AdP member 1, 20.9 ± 1.8 Ma for the ignimbrite which defines AdP member 2 (Dingman and Galli, 1965), and a disconformity thought to correspond in time to AdP member 4 further north, which has an average age of 16.3 ± 0.8 Ma (Tomlinson *et al.*, 2001). Above this disconformity rests sand and conglomerate of alluvial facies, near the top of which is an ash which dates at ~13 Ma (Ar/Ar biotite), which informs us that these are rocks of the AdP member 5. At the top of this subsequence is developed a paleosol, probably representing a long-lived exposure event. Over this ancient soil is well-sorted, crossbedded sandstones of largely aeolian facies, and finally alluvial conglomerates, all likely still within the AdP member 5.

Quebrada Guatacondo:

The stratigraphy was described along a transect between 20°58'S, 69°11'W and 20°56'S, 69°07'W. The exposed section measures roughly 250 m thickness; the lower two AdP members are not exposed. A Mesozoic basement knob separates the part of the canyon where the surface profile was described (Figure 2.5) from the Pampa del Tamarugal valley where the seismic data exist, indicating that the Guatacondo

strata may not have accumulated in the same depocenter that is imaged by the seismic data. These data indicate that ~500 m of Altos de Pica might occur near Quebrada Guatacondo. AdP member 3 is composed of 100 m of crossbedded sandstone and subordinate matrix-supported pebbly sandstone and clast-supported pebble conglomerate. These represent rare debris flows and local fluvial sandstones in an aeolian dune field. Beds of the AdP member 3 dip westward at the studied location, and this dip progressively decreases upsection. This member consists of medium-grained sandstone with increasing occurrences of coarse-grained sandstone and conglomerate resting within cut and fill features. AdP members 3 and 5 are separated by an erosional unconformity. The AdP member 5 is conglomerate with abundant cut and fill features and rounded gravels and coarse sands.

Quebrada Sipuca:

The deposits described here were studied over a transect between 21°14'00"S, 69°11'00"W and 21°12'40"S, 69°02'00"W. Approximately 225 m of vertical section of Altos de Pica Formation at this location reveal interbeds of tabular sandstone and conglomerate in nearly equal proportions, with lenses of conglomerate occurring much less frequently. About 50 m below the top of the Altos de Pica at this location is a prominent erosional surface, overlain by coarse sandstone and gravel of fluvial facies. Two ashes dated at 19.69 ± 0.03 and 17.86 ± 0.12 Ma (Ar/Ar, single crystal sanidine and Ar/Ar, biotite, respectively) underlie that erosional surface and one ash, dated at 15.83 ± 0.04 Ma (Ar/Ar, single crystal sanidine) overlies it. These dates inform us that this section is largely correlative with AdP members 3 and 5. Between the Jurassic to

Cretaceous Chacarilla Formation and the lowermost sandstones and conglomerates of the Altos de Pica Formation is a ≤ 10 m-thick, largely covered interval with an important claystone component. We do not know if this is the lowest member of the Oligo-Miocene Altos de Pica, or an older unit. At the very top are up to 50 m of poorly-sorted conglomerate of the Arcas Unit with interbedded Carcote Ignimbrite of latest Miocene age. These strata rest in angular discordance on the Altos de Pica beds.

Quebrada Tambillo

The rocks within Quebrada Tambillo were studied along a transect between approximately $21^{\circ}26'00''\text{S}$, $69^{\circ}15'00''\text{W}$ and $21^{\circ}29'00''\text{S}$, $69^{\circ}05'00''\text{W}$. An anticline within the Quebrada was associated with thickening of the lower unit on its eastern limb. Therefore, the total thickness, here reported as 130 m, may contain structural complications, and may not be representative of regional unit thickness. At the base of the measured section are poorly-sorted, moderately dipping ($\sim 15^{\circ}$) cobble conglomerate resting in an angular unconformity above Mesozoic marine strata. Resting above a planar, but strongly angular, unconformity is both matrix and clast supported coarse sandstone and conglomerate, interbedded with tabular beds of pebble to cobble conglomerate, which contains an ash dated at 19.77 ± 0.1 Ma (Ar/Ar single crystal sanidine weighted mean). Overlying this unit is a conglomerate with large-scale channel forms interbedded with tabular clast and matrix supported gravels. An ash within this unit dated at 11.62 ± 0.05 Ma (Ar/Ar biotite total gas), the youngest date obtained for Altos de Pica age-equivalent rocks within the basin. At the very top are

approximately 50 m of poorly-sorted conglomerate with an ash (likely the Carcote Ignimbrite) dated at 5.26 ± 0.02 (Ar/Ar biotite total gas). These strata rest in angular discordance on the Altos de Pica beds.

Cerrito Chipana/ east of Cerro Challacollo:

At $20^{\circ}59'23''\text{S}$, $69^{\circ}18'26''\text{W}$, rocks exposed 4 km to the southeast of Cerro Challacollo contain interbedded laminated limestone, gypsum, anhydrite and sandstone, overlying a basal conglomerate. Ash beds are interbedded with both the conglomerate (24.4 ± 0.3 Ma) and with the fine grained siliciclastics and evaporites (18.89 ± 0.24). These facies indicate that this central part of the PdT basin was a shallow-lacustrine environment during the early Miocene, and that strata which are age-equivalent to the AdP members 1 and 3 are represented within this exposure. Ten kilometers to the north ($20^{\circ}53'56''\text{S}$, $69^{\circ}20'40''\text{W}$), exposures at Cerrito Chipana reveal a continuation of this same facies. We interpret that ash layers near the base of a 65 m section of shallow lacustrine evaporites and fine-grained siliciclastic strata correlate with the late early Miocene ash layers to the east of Cerro Challacollo. It is worth noting that Parraguez (1998), in her description of sediments of the lower member of the El Diablo Formation 250 kilometers to the north along Quebrada La Higuera, detailed fine-grained carbonate-cemented sandstones containing pumice clasts beneath sandstone containing silicified plant remains, all resting atop the Oxaya Formation, which dates between ~ 23 and ~ 19 Ma. Here at the Challacollo locality, we observe a similar pattern: ashes of approximately Oxaya Formation age underlie shallow lacustrine and playa sediments which also contain small (< 2 cm diameter) silicified plant branches and pumice clasts. In the

Pintados #1 and #2 wells, limestone with silicified plant twigs is found above a zone of volcanics interpreted as AdP member 2, which dates to ~20 Ma in the region.

Lomas de Sal:

The deposits within the northernmost canyon which cuts through the Lomas de Sal are described in detail by Sáez *et al.* (1999). As observed by us in the field (21°23'45"S, 69°25'50"W), they consist of 10 meters of anhydrite with thinly laminated limestone overlain at an erosional surface by ~50 m of horizontally-bedded halite containing thin (<20 cm) interbeds of anhydrite. Sáez *et al.* (1999) report that this entire evaporite package attains a thickness of 100 m, and rests atop 2 meters of distal alluvial siltstones, sandstones and conglomerates. A thin ash layer near the very top of (but still within) the lowermost anhydrite yielded an age of 5.56 ± 0.09 Ma (Ar/Ar on biotite, A. Jensen, pers. comm., 2004). The uppermost halite is part of a sedimentary package known in the study area as the Soledad Formation.

Loa Canyon:

This outcrop is located near 21°36'S, 69°35'W, and consists of observations made from this point to ~10 km north of this location. Stratigraphy within the Loa Canyon was previously described by Sáez *et al.* (1999). Its lowermost unit consists of a variable thickness (between 0 and >100 m) of rounded gravels filling in paleotopography of the underlying Coastal Cordillera basement igneous rocks. Because at many locations along the canyon, basement rocks were not observed, the maximum thickness of this lowermost unit could not be determined.

Above an erosive contact is a ~70 m unit of anhydrite, 20 m of thinly-bedded fine-grained siltstone and sandstone, whose thickness is also variable, and an uppermost ~40 m thick unit of thinly-bedded limestone and sandstone of the Quillagua Formation. An ash dating to 5.8 ± 0.4 Ma sits at the conformable contact between the siltstone and limestone units (Sáez *et al.*, 1999).

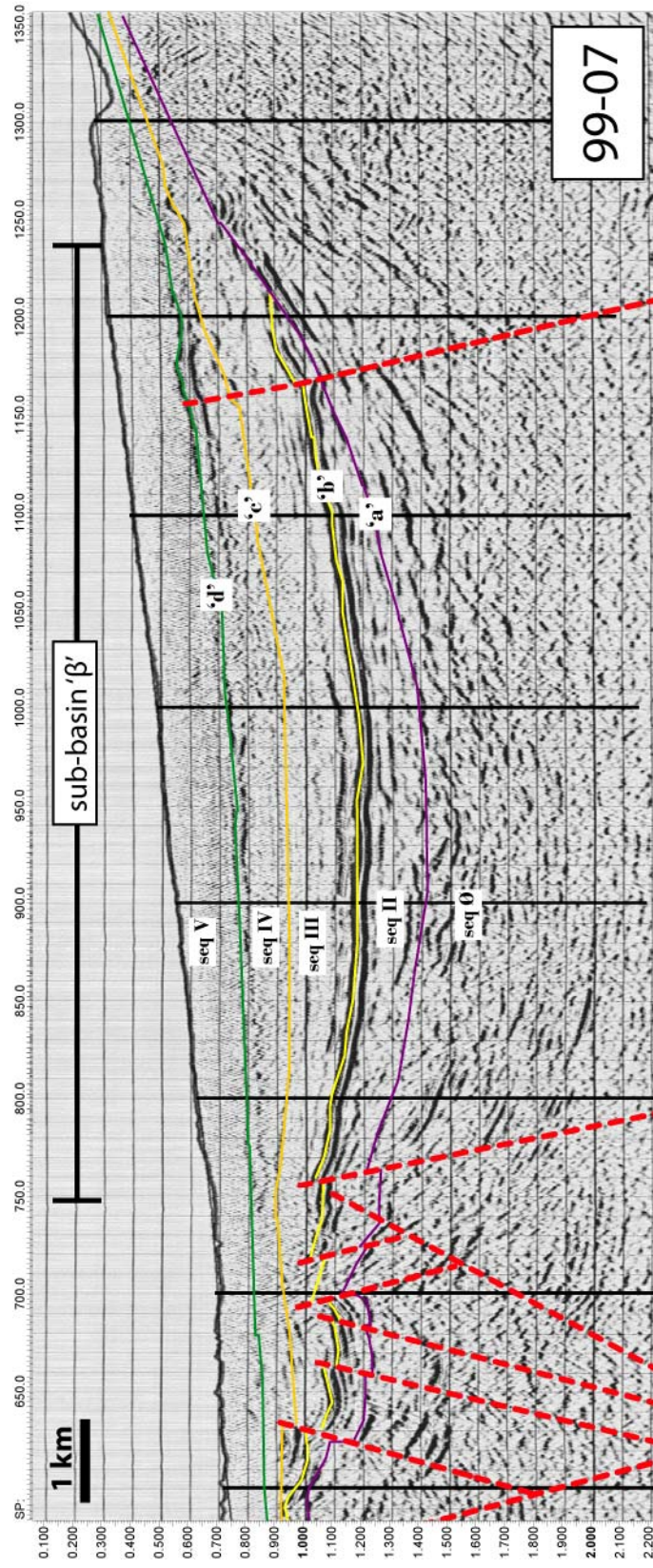
Correlating Seismic Sequences with Surface Stratigraphy

Despite the reflection heterogeneity that is expected of nonmarine strata, the seismic reflection data can generally be broken into sequences based on broad reflection character and configuration (Table 2.2; Figure 2.8). Seismic sequence \emptyset is the lowermost sequence considered here, and has a highly variable character. Near the top of this sequence, the reflections are of highly variable frequency and amplitude. However, they can be broadly characterized as medium amplitude and medium frequency, semi-continuous to continuous, and often dipping, although in many places this unit is transparent or the reflections are disrupted and chaotic. Above this sequence is sometimes found seismic sequence I, a discontinuous unit which is restricted to very localized zones. Internally, it is characterized by high-amplitude, high-frequency, discontinuous, subhorizontal reflections that often truncate one another within the sequence. Sequence boundary 'a' separates sequences \emptyset and I, and is generally a continuous, high amplitude, parabolic-shaped reflection. The upper boundary of seismic sequence I is sequence boundary 'a'. In most locations, sequence boundary 'a' and 'a1' coalesce to become the same surface. Sequence boundary 'a' is often characterized by truncation of the sequence \emptyset and sequence I (where

Table 2.2: Reflection characteristics associated with seismic sequences and sequence boundaries, and corresponding lithologic units

seismic sequence	reflection character	sequence boundary	interpreted unit	dates
V	transparent reflection with high reflectivity and continuity		late Miocene - Pliocene (?)	<7 Ma
IV	horizontal reflections with medium to high reflectivity and continuity	d	Altos de Pica member 5	16-11 Ma
III	medium to high amplitude reflection, with medium to high continuity. In many places, this reflection truncates reflections of sequence III Low to medium amplitude, semi-continuous to continuous. Reflections generally parallel sequence boundary 'b', with noticeable onlap onto 'b' at eastern limit of seismic data.	c	Altos de Pica member 3	20-16 Ma
II	High amplitude and high continuity reflection continuous reflections with medium amplitude	b	Altos de Pica member 2	~20 Ma
I	Reflection often truncates sequence I reflection, with highly variable amplitude which often appears transparent Discontinuous, high amplitude, high frequency subhorizontal reflections which truncate one another	a	Altos de Pica member 1	~26(?) - 20 Ma
∅	Continuous, high amplitude, parabolic-shaped reflection Highly variable, often medium amplitude, medium frequency, often dipping, semi-continuous to continuous reflection. Reflections often appear chaotic to transparent	a1	Mesozoic "basement"	>~40 Ma

Figure 2.8: A portion of seismic line 99-07, used to develop relationships between lithofacies and the associated seismic response. Note the broad sub-basin (β) and the overall lack of reflections within it. The location of the seismic line can be found on Figure 2.4. For a description of criteria used in defining seismic sequences and seismic sequence boundaries, see Table 2.2.



present) reflections. This boundary is a reflection of highly variable amplitude, and is often transparent. Seismic sequence II generally contains continuous reflections with medium amplitude. Sequence boundary 'b' is the most easily identifiable reflection within the basin, and is high amplitude with a high degree of lateral continuity. Due to its high reflectivity, it is this reflection on which much of the seismic correlation has been based. Seismic sequence III is highly variable, but generally characterized by low to medium reflectivity. Reflections are semi-continuous to continuous. Reflections of seismic sequence III generally parallel sequence boundary 'b', with a noticeable onlap of these reflections onto 'b' at the eastern limit of the basin. Seismic sequence III in many places displays reflections that are truncated by sequence boundary 'c'. This sequence boundary is generally a reflection of medium to high amplitude, which is semi-continuous to continuous. Above sequence boundary 'c' is seismic sequence IV. Reflections within this sequence are often observed to onlap sequence boundary 'c', and are horizontal with medium to high reflectivity and medium to high continuity. Sequence boundary 'd' is generally highly reflective with high amplitude and high continuity, but is in some places disrupted. Seismic sequence V is generally in the seismic mute zone, and is defined here as the transparent package found above sequence boundary 'd'.

Outcrops within canyons at the eastern edge of the seismic data allow for correlation between what is seen in the seismic data and surface stratigraphy in this part of the basin. An excellent opportunity exists to correlate the seismic sequences to the surface stratigraphy at Quebrada Chintagua. At the eastern end of Quebrada Chintagua (Figure

2.4), the unit exposed in the canyon wall is the ~325 m thick AdP member 5 (Figure 2.5); 2.3 km to the south, the shallowest reflection imaged by seismic line 99-03 is sequence boundary 'd', below which is revealed the ~350 m thick seismic sequence IV (Digert *et al.*, 2003). Seismic sequence III underlies sequence IV in this part of line 99-03, and this correlates to the AdP member 3, which underlies AdP member 5 in the Chintagua outcrops. In addition, sequence boundary 'b' is well imaged at this location, and the AdP member 2 ignimbrite is seen in outcrop at Quebrada Chintagua. At the western end of the basin, Pintados #1 also affords us the opportunity to connect seismic stratigraphy with known rock units within the Altos de Pica Formation. At a depth of ~350 m in the borehole is encountered the AdP member 2 (Figure 2.5), which was defined in seismic line 99-03 as seismic sequence boundary 'b'. While the well tie at this location is not exact (the predicted depth for sequence boundary 'b' based on stacking velocities is 399 m, whereas it is in fact found at 352 m in the borehole), it does give us confidence that assumptions made from the seismic sequences can be translated to an understanding of the timing of depositional events.

For the eastern ends of seismic lines 99-04, 99-05, 99-06, 99-07, 99-08, 99-09, and 99-11, the high amplitude and continuity of sequence boundary 'd' could be projected to surface exposures of the contact between the Arcas Unit alluvial deposits and underlying Altos de Pica Formation. In addition, the contact between the Mesozoic basement and Neogene fill was observed near many of these same seismic lines, both at the eastern edge of the grid of seismic data as well as at the location of basement knobs along seismic lines 99-07 and 99-08. In the seismic

data, highly dipping, medium frequency and amplitude reflections were detected associated with Jurassic-Cretaceous marine sediments in outcrop, and transparent or chaotic reflections are seen in the seismic data and can be associated with outcrops of basement rocks of mostly volcanic origin. These observations provided verification that sequence boundary 'a' is the contact of the Altos de Pica Formation over Mesozoic basement. At low elevation within the valley, <10 km from where seismic sequence II is located very near to the surface of seismic line 99-06, rare outcrop within the study area of AdP member 1 and lowermost AdP member 3 occurs and has been dated (Figure 2.4, "Cerrito Chipana and Challacollo"). The chronologic constraints confirm that seismic sequence II can be assigned to AdP member 1.

Time Stratigraphy

Observations of surface stratigraphy and well log data in conjunction with seismic units indicate that time-equivalent rocks are often represented by very different lithofacies throughout the basin, depending on the sedimentary environment in the various locations at the time of deposition. For this reason, rock type is not a favorable choice for determination of units. Additionally, ignimbrites are restricted to certain parts of the basin, providing age control in only very localized locations, and not allowing for broad chronostratigraphic correlation by geochronological methods. As a result, it is necessary to define the various members within the Altos de Pica Formation by another criterion if we are to achieve a reliable framework for correlation across the basin.

We accept the Dingman and Galli (1965) approach for subdividing the strata within the basin by chronostratigraphic, not lithostratigraphic, means. The contact between the Neogene strata which make up the majority of the basin fill and the underlying Mesozoic-Paleogene basement within the basin-center is a smooth pediment surface known as the Choja Pediplain further north (Galli, 1967; Mortimer and Saric, 1975), and corresponds to our sequence boundary 'a'. Incision into this pediment surface produced small pockets of gravels within our study area. These discontinuous deposits are here referred to as seismic sequence I. This incision surface is referred to here as sequence boundary 'a1'. An age for the base of the lowest, regionally extensive Neogene sedimentary unit, AdP member 1, is difficult to determine within the basin, as is the case with the correlative Azapa Formation to the north. The Azapa Formation is a unit of genetically related siliclastic deposits of late Oligocene age (>25 Ma) resting on Mesozoic basement, and consisting of well-rounded clasts derived from volcanic and sedimentary rocks to the east (Salas *et al.*, 1966). The AdP member 1 is here defined within the basin as those genetically-related deposits resting atop this ancient pediplain and found beneath the Altos de Pica member 2 ignimbrite (where present) which rest atop largely Mesozoic basement, and is equivalent to our seismic sequence II.

The age of the AdP member 2 can generally be determined to range from 20.90 ± 0.21 Ma and 20.61 ± 0.21 Ma (Victor *et al.*, 2004), although a date of 24.33 ± 0.26 Ma from Cerro Longacho, has also assigned by Victor *et al.* (2004) to the AdP member 2. While this appears to be inconsistent with other studies, as it would necessitate a hiatus in

sedimentation and volcanic activity of 3.5 million years between the lowermost and uppermost eruptive events, it cannot be ruled out. Because field relations imply that both dated samples are indeed from the AdP member 2 ignimbrite, we propose that the older apparent date may reflect undetected gas in the Rb/Sr system and should be approached with caution. The Altos de Pica member 3 can be defined at its base by the 20.61 ± 0.21 Ma AdP member 2, and at its top locally by the AdP member 4, which has been dated consistently between 16.4 and 16.2 Ma (Figure 2.3; Table 2.1). However, this ignimbrite only exists in the far northeastern section of the basin, and time equivalent lithofacies of the AdP member 3 range from alluvial and aeolian near the western Andean slope to lacustrine and salar facies in the center of the basin. In addition, the Altos de Pica member 2 is only proven to exist in outcrops north of and including Quebrada Chacarilla ($\sim 20^{\circ}45'S$). We therefore find it necessary to define the AdP member 3 in the subsurface as those rocks which are between 20.61 and 16.4 Ma, and which are seen in seismic stratigraphy as belonging to seismic sequence III. The Altos de Pica member 5 appears to be separated from older lithologies by a hiatus observed in outcrop as resting on an angular unconformity. The uppermost ash layer described within the AdP member 5 dates to 11.62 ± 0.05 Ma, with an indeterminate amount of time represented by thin (~ 50 m) strata above (Figure 2.3; Table 2.2). AdP member 5 is here defined as lithologies within the Pampa del Tamarugal that are younger than the youngest volcanics of the AdP member 4, dated at 16.27 ± 0.16 Ma, (Victor *et al.*, 2004), but older than the regionally extensive pediplain which formed in the Middle Miocene shortly after the eruption responsible for the 11.62 ± 0.05 Ma tuff. In our seismic dataset, AdP

member 5 is equivalent to seismic sequence IV. By process of elimination, sequence V includes the Uppermost Miocene-Pliocene (?) Arcas Unit strata that overlie an erosional unconformity and in which the Carcote Ignimbrite, ~5.4 Ma are interbedded.

Seismic facies

Among the seismic lines in the basin, the eastern half of seismic line 99-07 (Figure 2.8) displays the thickest accumulation of the Altos de Pica Formation (sub-basin 'β', ~10 km east of Cerro Challacollo [Figure 2.4]), is also the most devoid of structural complications, and is near outcrops. We select this part of seismic line 99-07 as the data with which to develop inferences concerning the sedimentary properties of certain seismic facies. The seismic character that is most striking in sub-basin 'β' on this seismic section is the relative lack of internal reflections within seismic sequences III and IV. Nearby outcrops within Quebrada Guatacondo show that sandy units dominate AdP member 3, with aeolian, alluvial and subordinate fluvial sand-rich facies (Figure 2.5). A lack of lithologic contrast is reflected in overall lack of reflections within the seismic data within seismic sequence III. In the Guatacondo outcrops, AdP member 5 grades into a coarse conglomerate near its top, with abundant cut and fill features typically on the order of 50-100 m width associated with increased fluvial activity (Figure 2.9). At the far eastern end of 99-07 (shotpoints 1150-1270), seismic sequence IV grades upward from a transparent lower half, which we interpret to be the signal of the sandstone of the lower AdP member 5 in outcrop, to a high amplitude, low frequency pair of reflections, which we interpret to mark the base and top of the conglomerate of the AdP member 5. In this part

Figure 2.9: Photograph of the southern canyon wall of Quebrada Guatacondo (~20°55'S, 69°08'W) illustrating fluvial channelization and deposition in otherwise alluvial and aeolian sediments within the Altos de Pica member 5. These sediments are immediately adjacent to exposed Mesozoic basement, possibly creating focused drainages at this location during deposition.

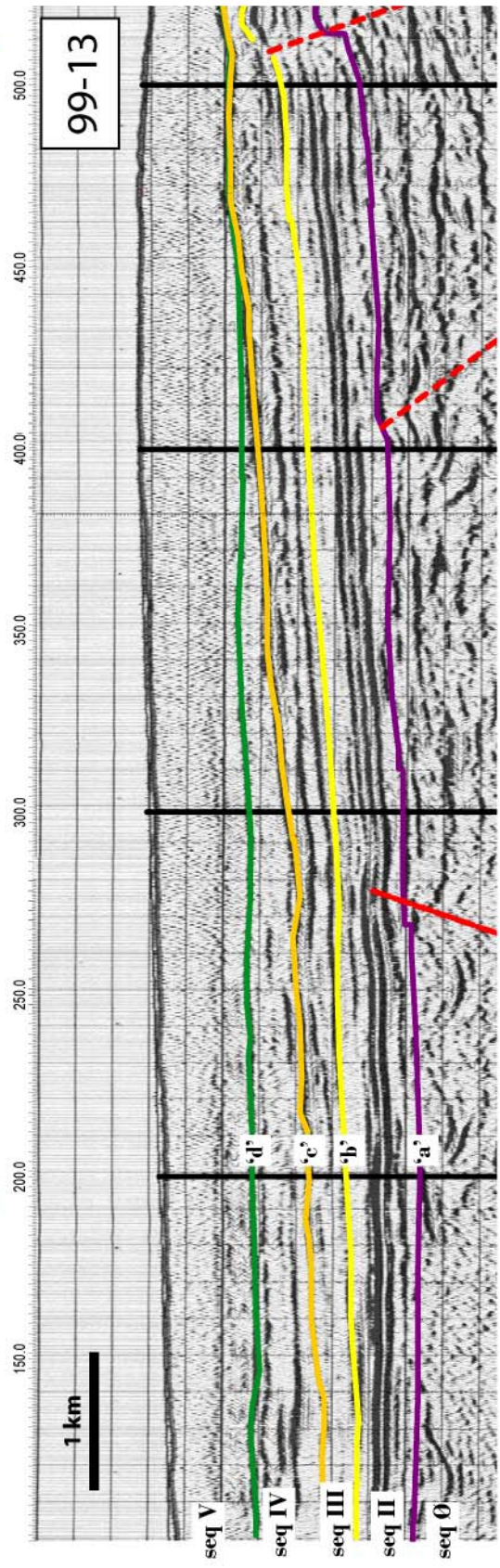
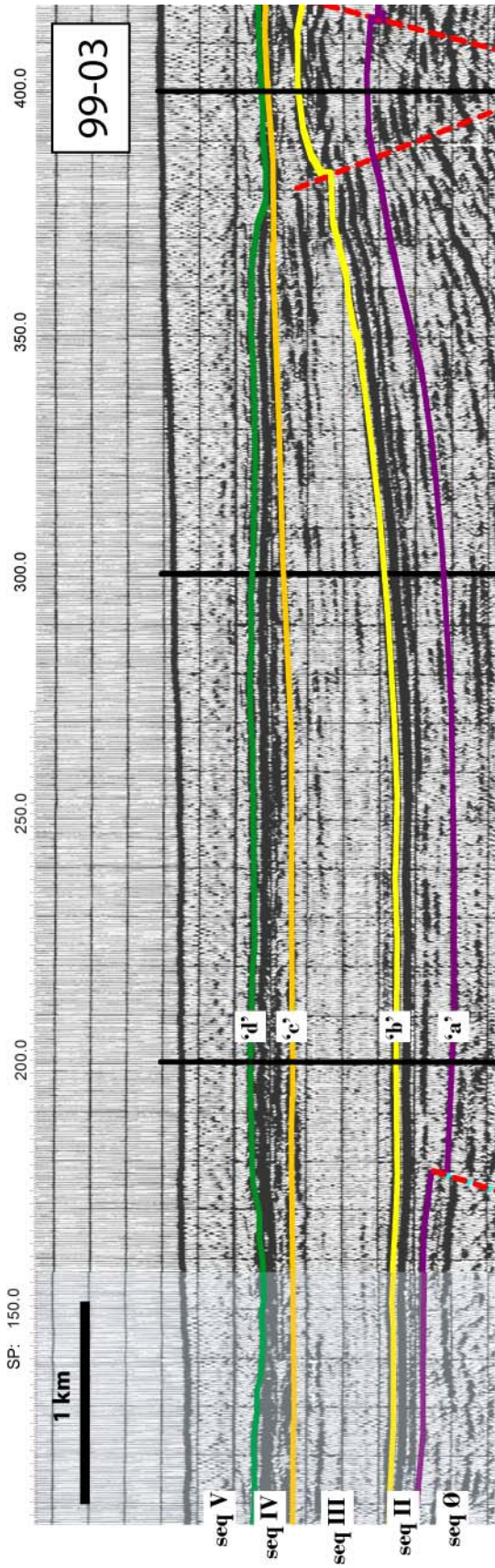


of the seismic data, we observe high amplitude, wavy reflections near the top of seismic sequence III, at sequence boundary 'c', and within sequence IV (Figure 2.8). This seismic character might be expected in a cut and fill system typical of a proximal alluvial fan (Blair and McPherson, 1994). Further to the west (Figure 2.8, shotpoints 1000-1150), the reflections in seismic sequences III and IV are slightly disrupted, though an apparently low impedance contrast produces little in the way of internal reflections (Figure 2.8). These disruptions can be expected of medial fan facies, where there is minor channelization of sands and conglomerates (Blair and McPherson, 1994). Further still to the west (shotpoints 980 – 640), the upper part of seismic sequence III and sequence IV are transparent, as is sequence boundary 'c'. Small outcrops of AdP member 3 near shotpoint 700 (~20 m of stratigraphic thickness), and 65 meters of correlative deposits 10 km to the north at Cerrito Chipana (Figure 2.5) indicate that shallow lacustrine facies exist in this portion of the basin at stratigraphic levels correlated to sequence III. However, units within this package are apparently too thinly bedded to be individually resolved by the seismic data, as indicated by the lack of reflections of seismic sequence III. In the outcrops near shotpoint 700, the lowest unit exposed is composed of a thin sheetflood conglomerate of AdP member 1. This facies corresponds to the medium amplitude, moderately continuous reflections of seismic sequence II.

Another example of seismic character tied to lithologic data is found where the Pintados #1 borehole intersects seismic line z1f-003 at shotpoint 2180 (Figure 2.7), within a sub-basin located at the northwestern end of the seismic grid. Medium frequency, low-amplitude

to transparent reflectors at the west end of z1f-003 atop an unconformity associated with sequence boundary 'a' correlate with sands and gravels possibly reflecting a mixture of alluvial and fluvial deposits at the far western end of the basin during this time. However, the seismic data quality of the reflections within seismic sequence III and shallower for this seismic line is relatively poor at the location of the well tie, so we must look to seismic lines 99-03 and 99-13 (Figure 2.10) in conjunction with the Pintados #2 borehole (8 km to the north, and ~7 km west-northwest of line 99-03; Figure 2.4) for useful comparisons. These lines are located 8 km to the northeast and southeast, respectively, of the Pintados #1 borehole (Figure 2.4). Corresponding to the western-most 150 shotpoints (equivalent to 3.75 km horizontal distance) of line 99-03, seismic sequence III displays a transparent character, similar to that seen in the transparent section described above within seismic line 99-07. However, within the same seismic sequence, line 99-13 exhibits high amplitude, high frequency reflections. On seismic line 99-13, internal reflection geometries within sequence III also reveal alternating downlap and onlap patterns. The high amplitude and high frequency character of the reflections becomes even more pronounced at the same relative position within this sub-basin for seismic line 99-04, 10 km to the south of seismic line 99-13. Pintados #2 has a high proportion of limestone at depths between 184 to 305 m (805 to 684 m above sea level), which corresponds (based on lithologies and well log curve matching between the two boreholes) to seismic sequence III, whereas the correlative section in Pintados #1 (168 to 277 m well depth, 834 to 725 m above sea level) consists largely of sandstone with thin interbeds of limestone (Figure 2.6). The depositional environment of seismic sequence III at

Figure 2.10: Side by side comparison of portions of seismic lines 99-03 and 99-13, revealing the change in seismic character interpreted to reflect a change in depositional facies. Note the relative lack of reflections within the sub-basin above seismic sequence boundary 'b' within seismic sequence III on line 99-03, and the high amplitude and frequency reflections in the same seismic sequence on seismic line 99-13. Reflections become apparent at the eastern end of the sub-basin on line 99-03. At this location, transparent reflections correspond to lacustrine facies, whereas high amplitude reflections correspond to alluvial facies. For line locations, see Figure 2.4.



Pintados #2 is interpreted to be predominantly lacustrine, whereas Pintados #1, just 8 km to the south, is interpreted as a position across which the boundary between a distal alluvial fan and lake margin shifted repeatedly. The weak horizontal reflections, where perceptible, within seismic sequence III of line 99-03, reflect these lacustrine, largely limestone, lithofacies. The high frequency, high amplitude reflections within sequence III on seismic lines 99-13 and 99-04 possess both onlap and downlap geometries, and most likely represent alluvial lithofacies with a small component of interbedded lacustrine lithofacies. Downlap and thinning of units along seismic line 99-13 and 99-04 towards lower elevations to the west is indicative of depositional topography, whereas the thickness increase at the center of the sub-basin, as well as onlap geometries at the eastern end of the sub-basin within the western section of seismic line 99-03, reflects deposits which filled paleotopography.

Given that a minimum unit thickness is required to produce an impedance contrast which is detectable in the seismic reflection data, each individual bed is not being imaged. However, thin beds of different lithologies observed in the Pintados #1 borehole (Figure 2.6), and likely present at seismic lines 99-13 and 99-04, representative of continually changing environments brought about by fluctuating water levels in this sub-basin, creates packages composed of several distinct units with similar rock properties. It appears that these packages provide enough of an impedance contrast to produce distinct reflections in the seismic data. Conversely, the Pintados #2 borehole shows slightly thicker units with similar lithologies, grading from marginal lacustrine (marly sandstone lithology) to shallow lacustrine (limestone). These relatively subtle

lithologic variations, directly correlative to an environment of deposition in which standing water was consistently present, are not sufficient to produce the impedance contrast necessary to result in internal reflections within seismic sequence III.

Horizontal variations within these seismic lines are also detectable. Between shotpoints 100 and 200 on seismic line 99-13, the reflections within seismic sequence III are more discontinuous than at similar levels in sequence III further to the east (shotpoints 200-320, Figure 2.10). The same is true of seismic line 99-03, where at the eastern edge of this sub-basin, reflections are characterized by high amplitude and high frequency reflections associated with higher energy alluvial deposition. This is most likely the result of periodic influxes of siliciclastic deposits into the margin of this sub-basin. Deposition of these alluvial/marginal lacustrine sediments at the eastern end of the sub-basin occurred with enough regularity that the physical rock properties of these interbeds were altered, resulting in impedance contrasts with the lacustrine deposits, and ultimately producing the high-frequency, high-amplitude seismic response observable in the seismic data.

In summary, seismic data at the northwestern corner of our study area, in conjunction with borehole cuttings which allow for lithofacies characterization near these seismic lines, reveal that many tens of meters of shallow lacustrine facies are likely to produce a transparent seismic facies in this basin, whereas interbedded lacustrine and alluvial siliciclastic deposits near a sub-basin margin apparently are more apt to produce high amplitude, high frequency internal reflections, which exhibit both downlap and onlap. This is consistent with our finding that

shallow lacustrine and playa facies seen at Cerrito Chipana (Figure 2.5) corresponds to the transparent zone within seismic sequence III of the central portion of seismic line 99-07.

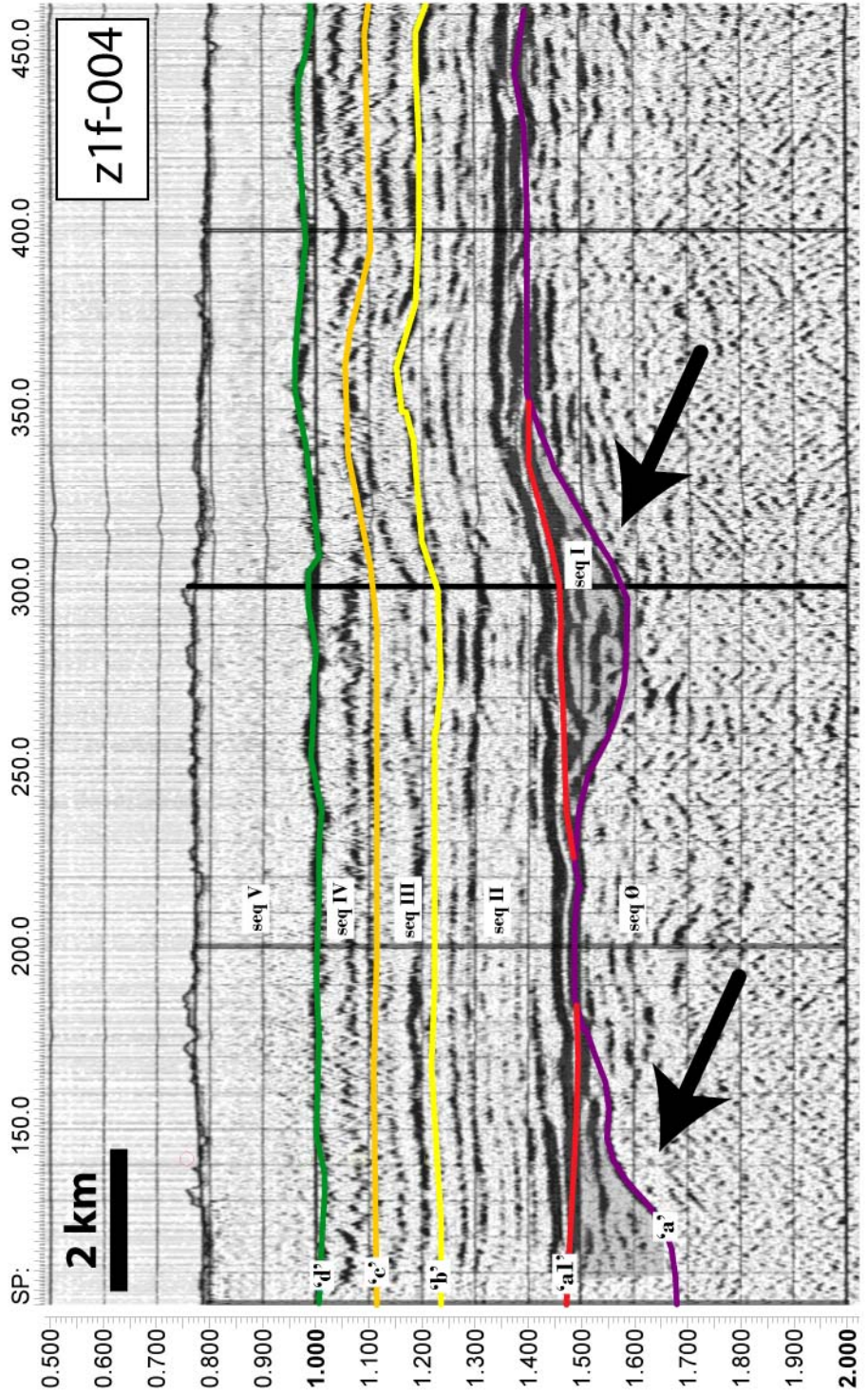
The same seismic response for similar salar and lacustrine deposits is detected at the location of the Soledad #1 borehole, at the west end of seismic line 99-09 (Figure 2.7). Here, parallel, continuous, low to medium amplitude reflections of medium frequency grades into transparent reflections above, and correlate with evaporites interbedded with mudstones. Based on the borehole cuttings from this location, the sedimentary rocks present here are interpreted to represent predominantly playa lake deposits. The continuous, high-amplitude reflection identified as sequence boundary 'b' throughout much of the basin has been correlated to the AdP member 2 ignimbrite. However the Soledad #1 borehole did not encounter this ignimbrite, and the possibility exists that this reflection has been miscorrelated at this location. If this were the case, this reflection may in fact be imaging the boundary between salar and playa lake deposits of the AdP member 3 below and alluvial deposits of the AdP member 5 above. The transition between these two units is quite abrupt (Figure 2.5) and the impedance contrast expected would likely produce a strong seismic reflection. The implication is that the reflection mapped as sequence boundary 'b' in this sector may actually be sequence boundary 'c'.

The facies significance of transparent seismic facies is non-unique, however. At Quebrada Chintagua, near the eastern end of seismic line 99-03, seismic sequences III and IV are transparent. However, the predominant lithofacies at the Quebrada Chintagua outcrop is

crossbedded aeolian sandstone, in a lithologically monotonous stack ~400 m thick. In order to interpret the environment responsible for the transparent seismic character at a given location, it is necessary to understand the paleo-topographic context of the sediments and the position of the sediments within the basin. Zones of transparent seismic facies in areas with depositional relief (identified by a number of criteria, including obvious strata thickness variations and onlap of units onto surfaces below) are likely to represent an aeolian depositional environment. However, where the transparent reflections are within seismic sequences which were deposited within topographic lows, and are thus more likely to have been within a depositional environment more favorable to ponding of water, then the facies represented by these transparent zones is more likely to be lacustrine.

At studied outcrops along the Río Loa, a pronounced paleo-relief exists at the top of the Mesozoic basement, resulting in highly variable thickness of the overlying sedimentary rocks. Above this basal relief, paleotopographic lows are filled by bedded conglomerate of an indeterminate age. In the seismic data, it is sometimes observed that an incision surface of approximately 2 km width exists beneath the regionally extensive sequence boundary 'a'. The reflections within these incisions onlap cut and fill features carved into seismic sequence Ø, are high amplitude and high frequency, and are here referred to as seismic sequence I (Figure 2.11). The top of the fill is known locally as sequence boundary 'a1'. Using the Loa Canyon outcrops (Figure 2.5) as an analogy, this seismic architecture most likely represents fluvial or alluvial conglomerates which have filled paleorelief at the top of seismic sequence

Figure 2.11: A portion of seismic line z1f-004 showing onlap of sediments within seismic sequence I, beneath sequence boundary 'a' onto reflections of sequence Ø. Sequence boundary 'a1' is found between sequences Ø and I. These cut-and-fill features are typically on the order of 1-2 km wide, and are inferred to be fluvial deposition in incised channels within a pediplanation surface. The location of the seismic line can be found on Figure 2.4.



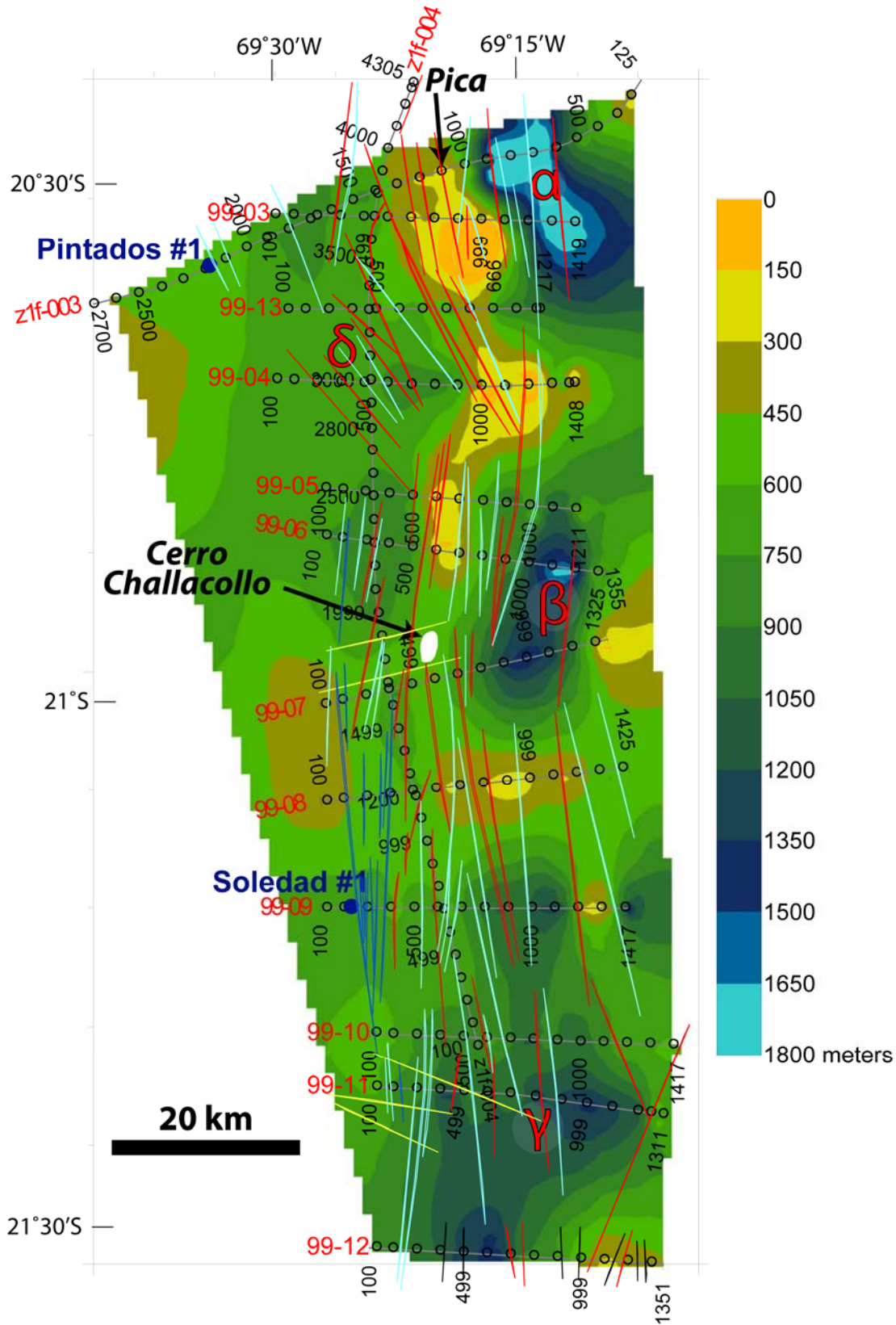
Ø. Since these features in the seismic data are most apparent on the north-trending seismic line z1f-004, this paleorelief is most likely the result of west-trending channels incised into the sequence boundary 'a' pedimentation surface. This interpretation is consistent with west-directed paleoflow indicated by imbrications of clasts in the basal conglomerate along the Loa Canyon. This highly variable thickness might be represented by the ~350 m of basal sandstones and conglomerates observed in the Hilaricos #1 well (Figure 2.5), also located in the southwestern corner of the study area.

Basin geometry

To a first order, the Cenozoic sediments of the Pampa del Tamarugal define a lens-shaped basin that is roughly symmetrical about a north-trending axis, thinning on both its east and west edges (Figure 2.2). However, much variability exists in this geometry, with the thickest sediment accumulations observed in separate depocenters in the northeastern, east-central, and southern portions of our study area (Figure 2.12). The maximum thickness of the basin fill is in general found within its eastern half. For example, an approximate thickness of 1500 m for the Altos de Pica Formation forms a localized zone trending north-northwest near the eastern edge of seismic lines 99-03 and z1f-003 (sub-basin 'α' of Figure 2.12). Farther south, the combined thickness of the Altos de Pica and Arcas Unit reaches as much as 1700 m along a 10 km-wide north-south trending zone along the eastern portions of seismic lines 99-05, 99-06 and 99-07 (sub-basin 'β' of Figure 2.12). A broader, less well-defined basin (sub-basin 'γ' of Figure 2.12) exists at the location of southern seismic lines 99-09, 99-10, 99-11, and 99-12, with thickness

Figure 2.12: Map illustrating the total Cenozoic sediment thickness and fault network within the Pampa del Tamarugal between approximately 20°30 – 21°30'S and 69°00' - 69°30'W. Greek symbols represent sub-basins referred to in the text. Seismic grid with associated shotpoint locations are in black. Well locations are shown as solid blue circles. Fault traces are mapped where they offset sequence boundary 'a'. Red lines indicate west-vergent reverse faults, light-blue lines indicate east-vergent reverse faults, dark blue lines are normal faults, and yellow lines illustrate east-striking faults.

total Cenozoic sediment thickness



of Altos de Pica to Recent age deposits reaching as much as 1400 m along portions of seismic lines 99-11 and 99-12. The west-central portion of seismic line 99-12 is the same general region in which Sáez *et al.* (1999) reported the greatest thickness of Upper Miocene to Pliocene (?) lacustrine- and salar-dominated sediments, and also immediately adjacent to the location of the Arcas Fan, where clastic sediment thickness of the Arcas Unit locally exceeds 200 m (Kiefer *et al.*, 1997). A fourth distinguishable sub-basin exists along and to the west of seismic line z1f-004, extending from the western section of seismic line 99-06 and northward to seismic lines z1f 003 and 99-03. It is a shallow, north-trending sub-basin which has filled with 600 to 1000 m of Altos de Pica to Recent aged sediments (sub-basin 'δ' of Figure 2.12). While not part of the gridded dataset due to its proximity to the edge of the survey, the western end of seismic line z1f-003 thins gradually to zero where it abuts basement rocks of the Coastal Cordillera.

Conversely, the overall geometry of the Pampa del Tamarugal basin can also be described by the disruptions caused by several observable structural highs. The general trend is for a thinning of the basin towards the north and east, with the obvious exception of sub-basin 'α' at the eastern edge of seismic lines z1f-003 and 99-03. The eastern sub-basins 'α', 'β' and the eastern flank of 'γ' are separated by two east-trending structural highs, at a distance from one another of ~40 km. These occur at the eastern edge of seismic line 99-04 and along the entire length of seismic line 99-08, where Cenozoic fill is entirely absent and basement knobs are present at the surface. Sediments thin noticeably to less than 400 m at the western ends of seismic lines 99-07 and 99-08.

Facies

Several distinct facies reflect both the climate and physical position of the sediments within the basin at the time of deposition (Figures 2.13, 2.14 and 2.15). As a generality, sediments at the eastern end of the basin are coarse grained and texturally immature. This textural immaturity is consistent with clast compositions (A. Tomlinson and N. Blanco, pers. comm., 2003) and paleocurrent indicators which signify sediment transported westward from the nearby Precordillera. These eastern sediments remain coarse-grained throughout Altos de Pica time. These siliciclastic deposits are largely aeolian in the northeastern part of our study area, becoming increasingly fluvial, then alluvial, as one moves further south. Where observed in outcrop, the alluvial deposits represent predominantly proximal and medial fan facies.

Exposures of AdP member 1 are rare in the study area, except for their type location near Pica, where they are conglomerates and sandstones of a mixed fluvial and alluvial nature. Aeolian sandstones are common within AdP members 3 and 5 in the central and northern sectors of our study area, and are rare in the south. The aeolian-dominated extreme occurs at Quebrada Chintagua, where 400 m of predominantly aeolian sandstone post-dates AdP member 2 (post-~20 Ma). Member 5 generally becomes more conglomeratic upsection in the eastern canyon exposures. Evidence of fluvial activity in the form of cut and fill features and sorting of clasts is common, and is present in both AdP members 3 and 5. Fluvial activity is especially noticeable near areas

Figure 2.13: True depth west-to-east cross-section showing generalized sediment distribution at approximately 21°S. Lithologies based on a combination of seismic facies analysis, well log interpretation, and outcrop studies. Dark lines represent time surfaces (sequence boundaries).

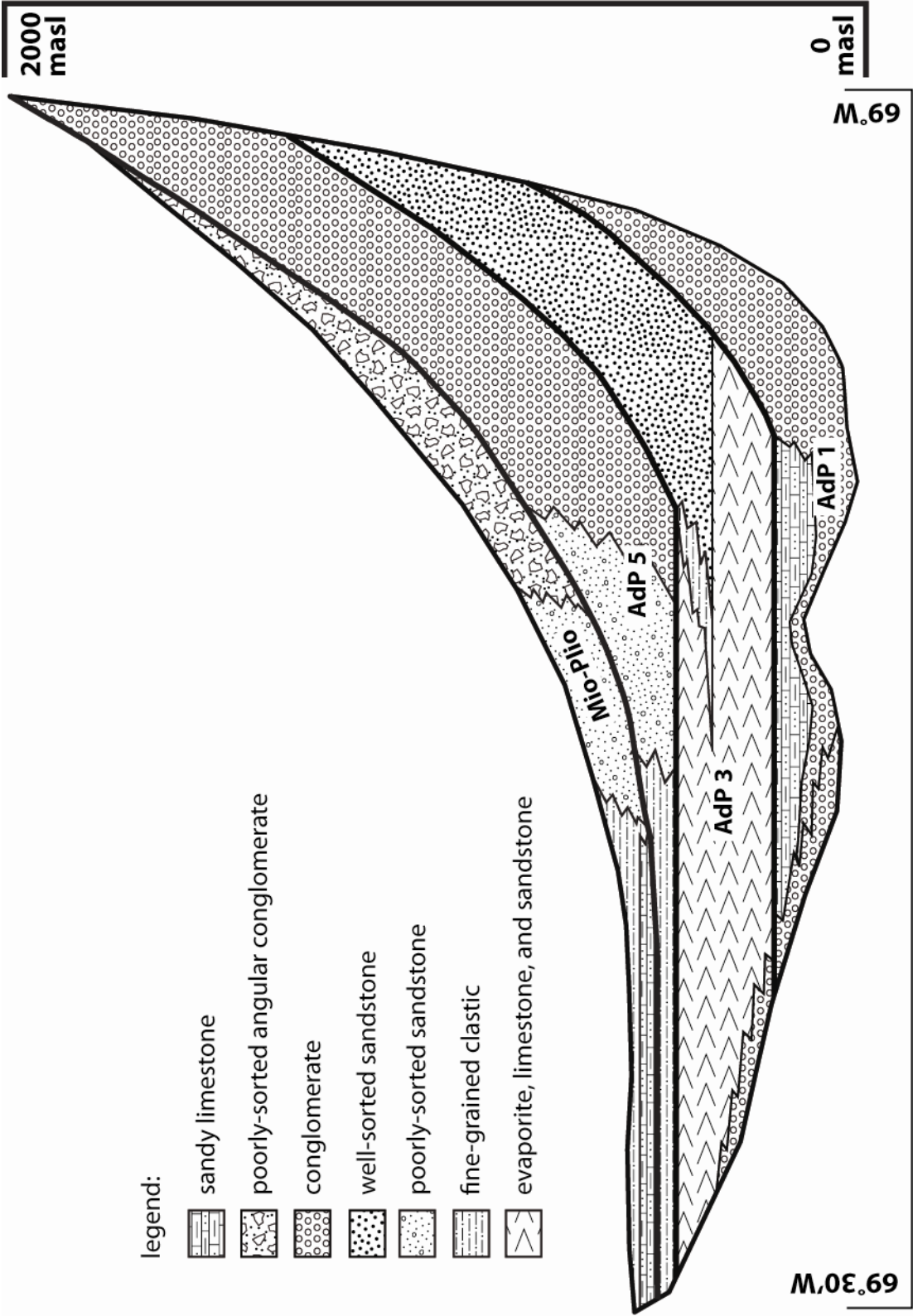


Figure 2.14: General facies interpretation at 11 surface and well sites. Facies interpretation is broken down into 4 time periods, correlating to the AdP members 1, 3, 5, and Arcas Unit. Where more than one facies is present during a time period, the time period is broken into 2 categories. A general tendency of lacustrine and salar facies is seen at the central and western sectors of the basin, whereas aeolian, alluvial and fluvial facies dominate the eastern portion.

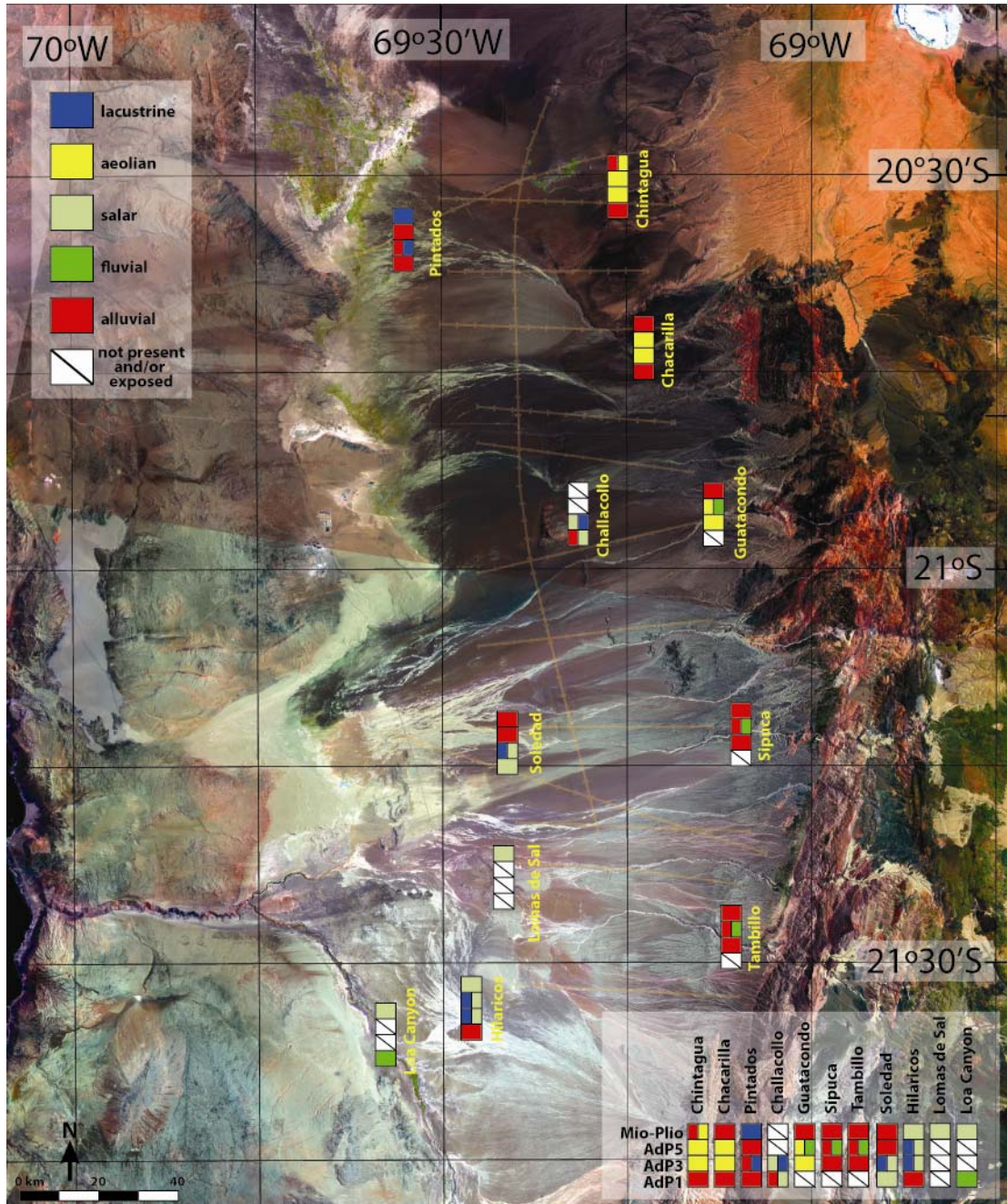
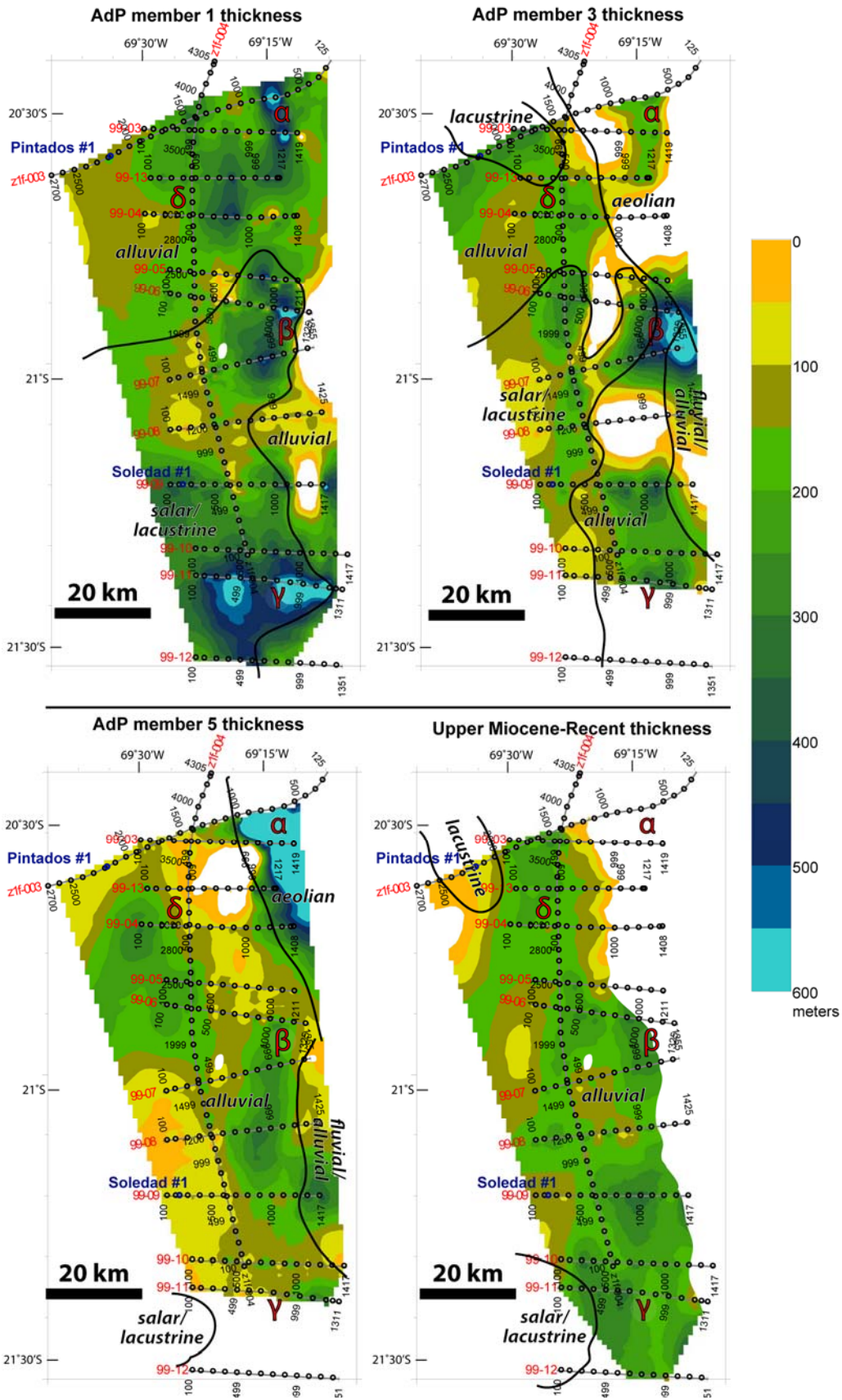


Figure 2.15: Unit thickness maps for 4 time periods considered as part of this study. Overlain on these maps are generalized interpretations of depositional environments, integrating seismic facies analyses as well as field and borehole observations. Of particular note is the expansive lacustrine and salar system during AdP members 1 and 3 time intervals, and its severe restriction by the time of AdP member 5 deposition.



where local paleorelief created a situation of focused drainages, such as in the case of the Guatacondo and Maní canyons.

In the basin center, rocks of AdP member 1 are mostly conglomerates, illustrated by the well data as well as one small exposure near Cerro Challacollo. The Altos de Pica member 3 of the basin center and southern end is lacustrine, unlike alluvial facies seen in the east. For example, well-sorted fine-grained sandstones and evaporites occur in the Soledad #1 well and the Cerrito Chipana/east of Challacollo outcrops.

In the northwestern part of the basin, both alluvial and lacustrine facies are represented in the Oligocene to middle Miocene strata. There, limestone was penetrated by the Pintados wells within AdP member 3 (Figure 2.6). The remainder of the deposits at the northern flank of our study area is dominated by distal alluvial fan facies, with only the uppermost Miocene to Lower Pliocene (?) deposits including a thin interbed (<30 m) of shallow lacustrine deposits.

At the southwestern corner of the study area, thickness is highly variable, as is sedimentary environment. Alluvial conglomerates dominated during the initial basin stages and infill the relief above basement rocks. Outcrop studies along the Rio Loa near the contact of the basin with the Coastal Cordillera reveal that the thickness of the AdP is in many places clearly less than 200 m, at these far western positions. However, lack of age constraint makes it difficult to distinguish between different members within the formation, as well as to identify the contact between the AdP and Upper Miocene-Pliocene (?) salar and lacustrine

deposits. Just to the east, however, a thick section of siliciclastics most likely representing AdP members 3 and 5 is observed in the Hilaricos #1 well (Figure 2.5). Across the southwestern area between ~7 Ma and sometime after ~5.5 Ma, shallow lacustrine/playa lake and distal alluvial fan facies interfinger. The high degree of thickness variations indicate numerous local depocenters and areas of positive relief. This playa environment produced in places 100 m of halite that postdate 5.56 ± 0.09 Ma.

Pampa del Tamarugal Structure

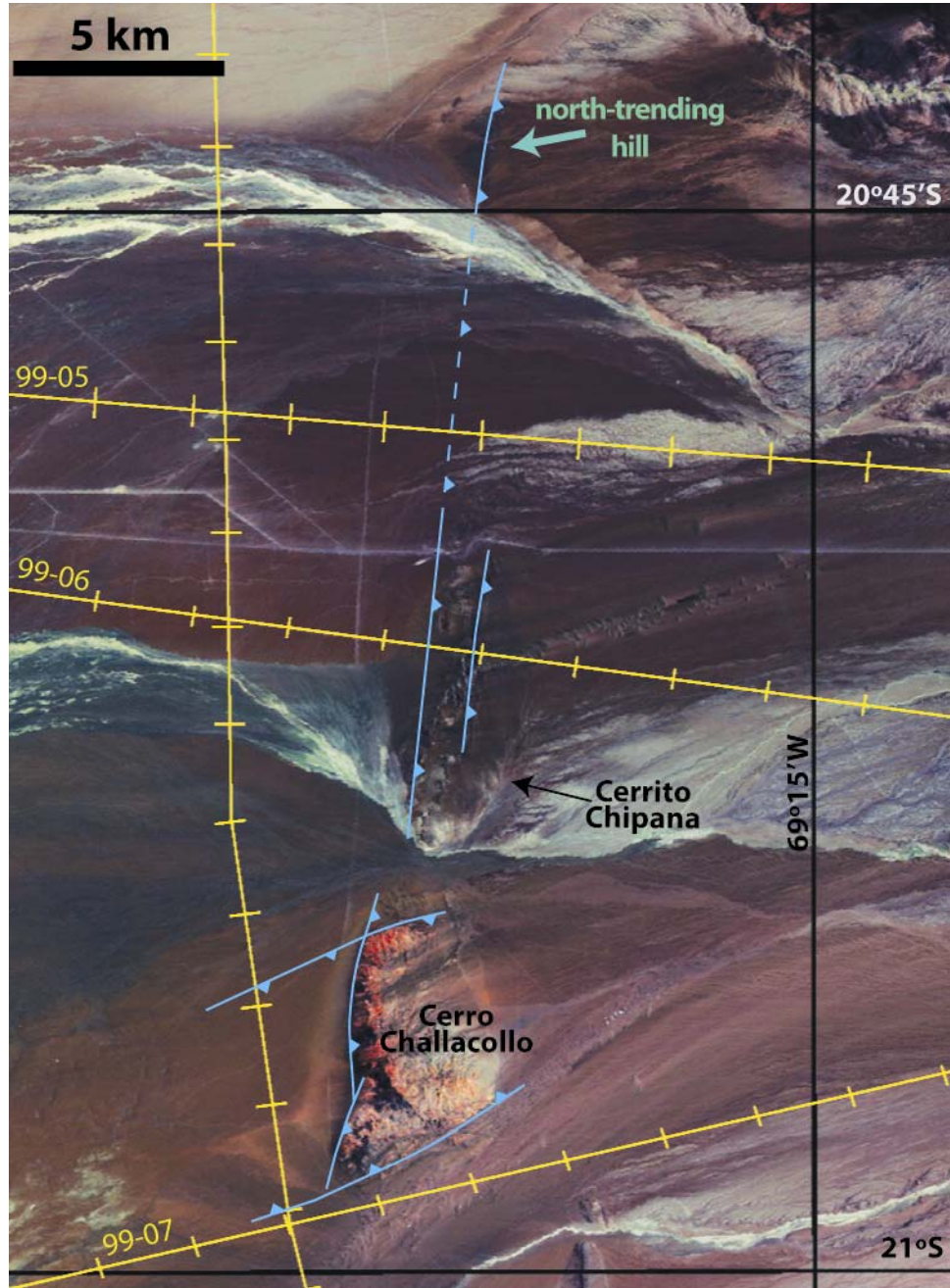
The basin has undergone a considerable amount of Neogene deformation (Figure 2.12), in contrast to the smooth appearance of the modern surface of the Pampa del Tamarugal valley (Figure 2.4). The basin is located at the intersection of structural domains recognized along the western Andean slope and the Coastal Cordillera. Because of very little outcrop in the valley, with maximum bedrock incision rarely exceeding 100 m except in the far northeastern sector of the study area, only the thinnest veneer of sediments is exposed, and geologic structures are rarely encountered in the field. Seismic evidence reveals that the region south of seismic line 99-04 is substantially more complex than the adjoining part of the basin to the north. Both eastward- and westward-dipping, mostly high angle reverse faults are present in all sectors of the basin (Figure 2.12). The general fault trace orientation of these west-vergent reverse faults is roughly north-south, parallel to the current configuration of the offshore Peru-Chile trench. In the northern third of the study area, northwest trending west-vergent reverse faults exist at a greater concentration than anywhere else in the basin (Figure 2.12). In

sharp contrast, reverse faults, striking predominantly east-west, are sporadically present in the western part of the seismic grid. In addition, high angle normal faults striking north-south exist at the western portions of the seismic grid, in the central and southern sectors, resulting in the formation of grabens of up to 10 km width. Thinning of the basin on both its eastern and western flanks, as well as an increased concentration of east-vergent faults as one approaches the Coastal Cordillera, and a predominance of west-vergent faults at the toe of the western Andean slope brings into question past assumptions about its origin as an orogenic-scale graben bounded by normal faults (Mortimer, 1973; Cabrera *et al.*, 1995; Jensen *et al.*, 1995).

Despite its overall smooth appearance, numerous surface features within the Pampa del Tamarugal match data in the subsurface, and allow for confidence in extending structural interpretations to zones beyond the locations of the seismic lines. For example, the axis of a small hill centered at 20°44'S, 69°20'W (Figure 2.16) is aligned exactly with the western edge of Cerro Challacollo and the associated Cerrito Chipana immediately to its north (Figure 2.8), allowing us to confidently deduce that faults seen in the seismic data adjacent to these hills are the same fault, or at least populations of the same fault system. Lineaments, visible on air photos and satellite images of the southwestern part of the basin, are shown to pinpoint the locations of blind faults because where they cross seismic lines, there are consistently offsets and disruptions of horizons beneath the surface (Figure 2.8).

The study area can be broadly categorized into three distinct segments: northern, central and southern. These categories are based on

Figure 2.16: Thematic mapper image from the center of the Pampa del Tamarugal showing alignment of hills which corresponds to west-vergent faults visible in the seismic data. Southern hill is Cerro Challacollo, a Mesozoic-early Tertiary volcanic complex.

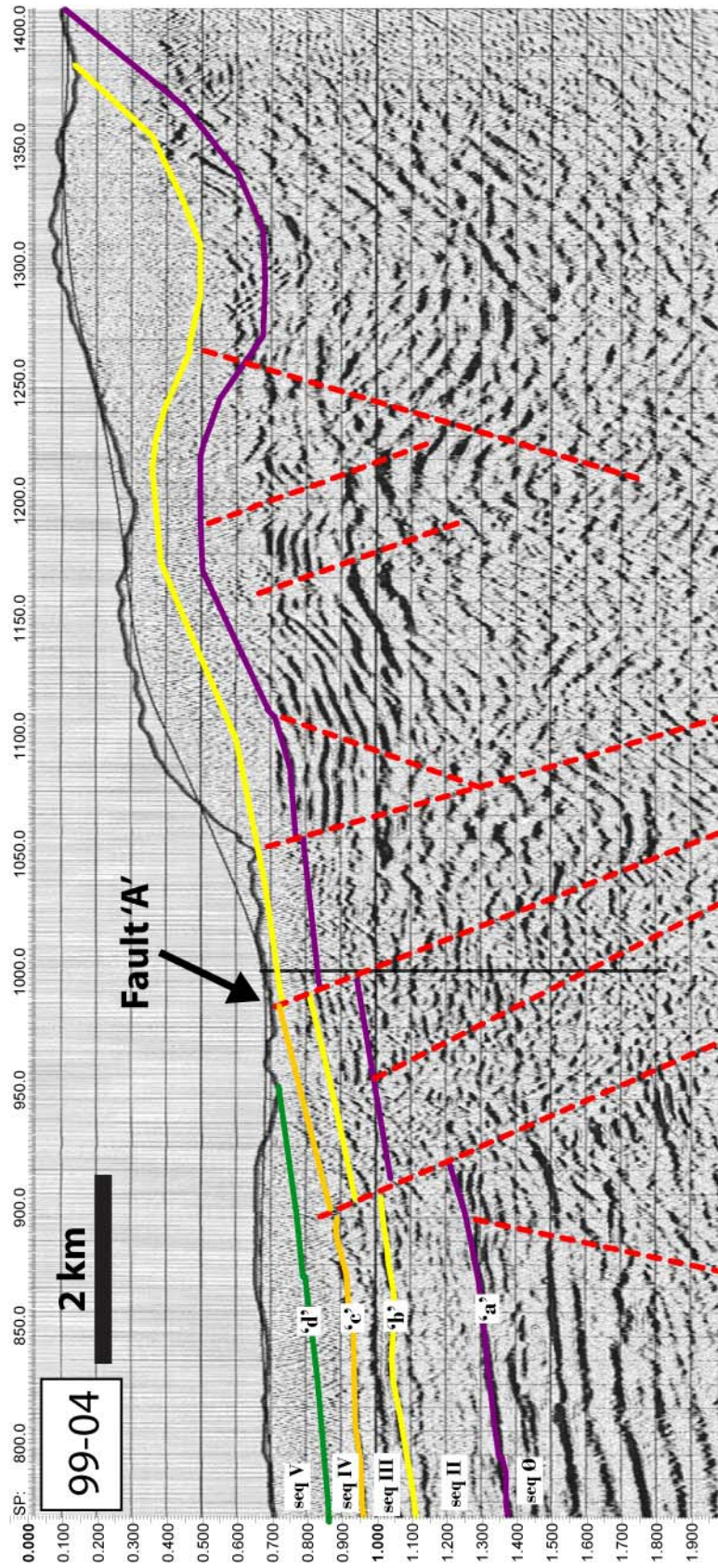


different trends, densities, and types of faults, timing of deformation events, and degree of deformation within the basin.

Northern sector

North and north-northwest trending reverse faults in the far northeastern corner of the study area (north of and including seismic line 99-04) are similar in orientation and timing to that which is seen in the study of Victor *et al.* (2004) and to the north (Farias *et al.*, 2004; Muñoz, 2007; Pinto *et al.*, 2004), and can be considered to be a part of the Western Thrust System. These reverse faults are high angle, with a shallow dipping backlimb and a more steeply dipping forelimb, as previously described by Victor *et al.* (2004). Less abundant are high-angle east-vergent reverse faults with this same trend. These faults cut seismic sequences I, II and III, but do not generally offset sequence boundary 'c' in this sector. Although nearly all of these faults are blind, one example of their surface expression is the north-northwest trending straight boundary between the fan of Quebrada Chacarilla and the bedrock of Sierra Moreno, which projects to fault 'A' of seismic line 99-04 (Figure 2.17). At this location, the course of the Chacarilla stream channel turns abruptly from a west-southwest to a northwest orientation. The spring which is the source of the oasis of Puquio de Núñez (Figure 2.4) is located along the trace of the fault, most likely due to preferential water flow along the fault surface. The same relationships are observed in Quebrada Ramada immediately to the south, where bedrock of the Altos de Pica Formation is juxtaposed against the alluvial sediments of the Arcas Unit along a northwest-trending line which also corresponds to an abrupt turn of the stream channel to the northwest

Figure 2.17: The eastern end of seismic line 99-04, showing north-trending and northwest-trending reverse faults which affected the northeastern sector of the basin. Fault 'A' corresponds to a northwest-trending fault which affects modern landforms within Quebrada Chacarilla. The location of the seismic line can be found on Figure 2.4.



(Figure 2.4). The deflection of these streams has been interpreted as a consequence of strike-slip motion within the Precordilleran Fault System (Houston, 2001; 2002). While seismic data cannot reveal pure strike-slip deformation, the seismic data clearly reveals north-northwest reverse faults at this location, and we feel that this offset is more likely the cause of this deflection. These faults at Quebrada Ramada represent the southern limit of the set of faults with this north-northwest trend (Figure 2.12).

Further west along seismic lines z1f-003, 99-03, 99-13, and 99-04, at the longitude of the town of Pica, north and northwest trending west- and east-vergent reverse faults extend to very near the modern surface (Figure 2.18). These faults are responsible for thin, north-trending hills, including Cerro Longacho (Figure 2.4), and their throw resulted in very thin sedimentary cover at several locations, such as is observed near shotpoint 950 on seismic line 99-03 (Figures 2.12 and 2.18). The north-northwest trending fault set is still present at this position in the middle of the basin, but largely affects only sequences Ø-III, with only minor deformation of sequences IV and V observed (Figure 2.18). Faulting is much less common at the western end of the seismic data, and faults which are present fold but do not cut seismic sequences III, IV and V. Fault density decreases markedly within the western 5 km of lines 99-03, 99-13 and 99-04, and only relatively minor blind east-vergent reverse faults are present at the western 25 km of line z1f-003, deforming all resolvable seismic sequences (Figure 2.19).

The eastern end of seismic line 99-04 lies at the intersection between north and north-northwest trending faults (Figure 2.12). The

Figure 2.18: A portion of seismic line 99-03, showing north-trending faults, forming hills in the northern sector of the study area. Refer to Figure 2.4 for seismic line location.

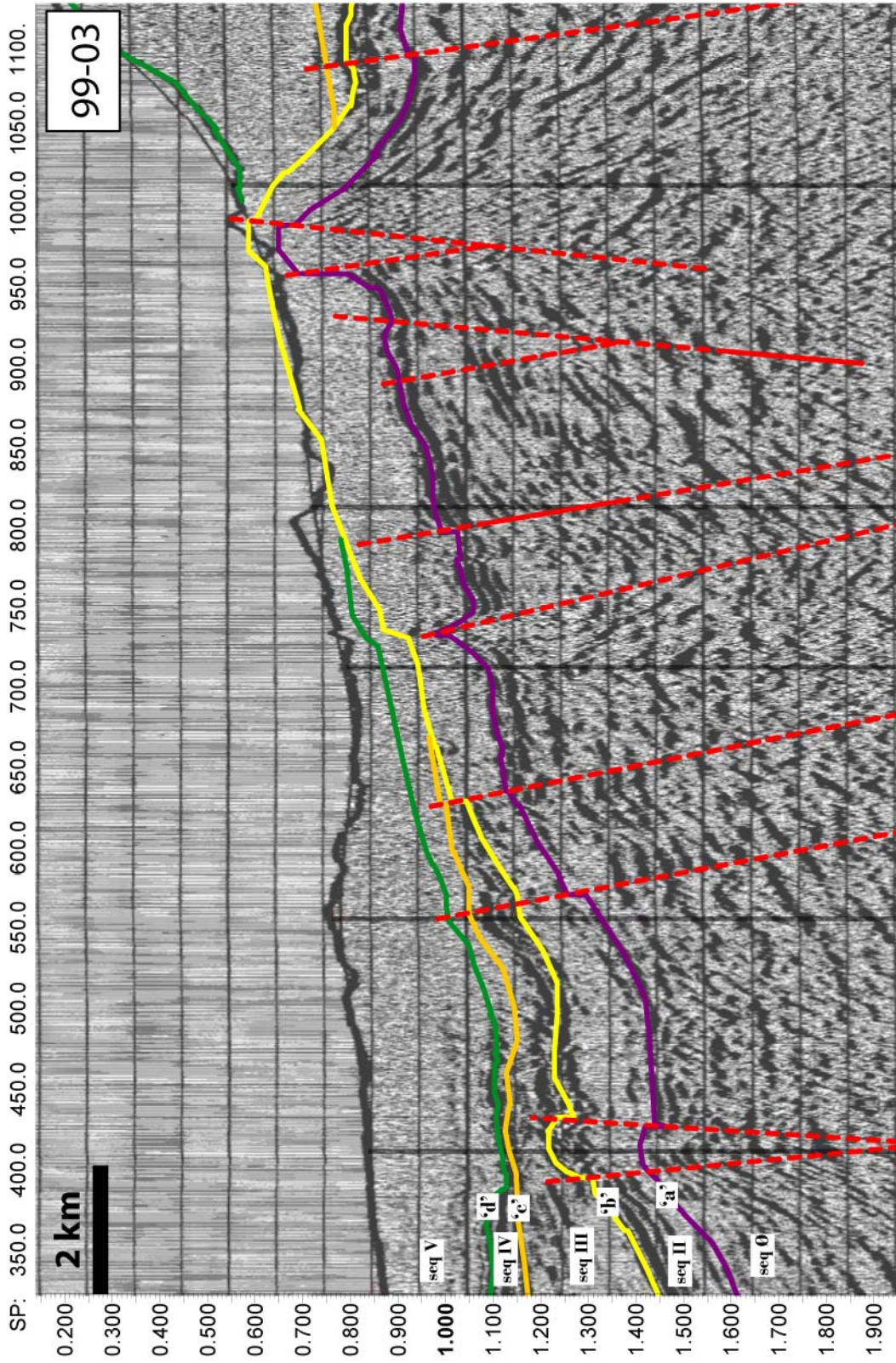
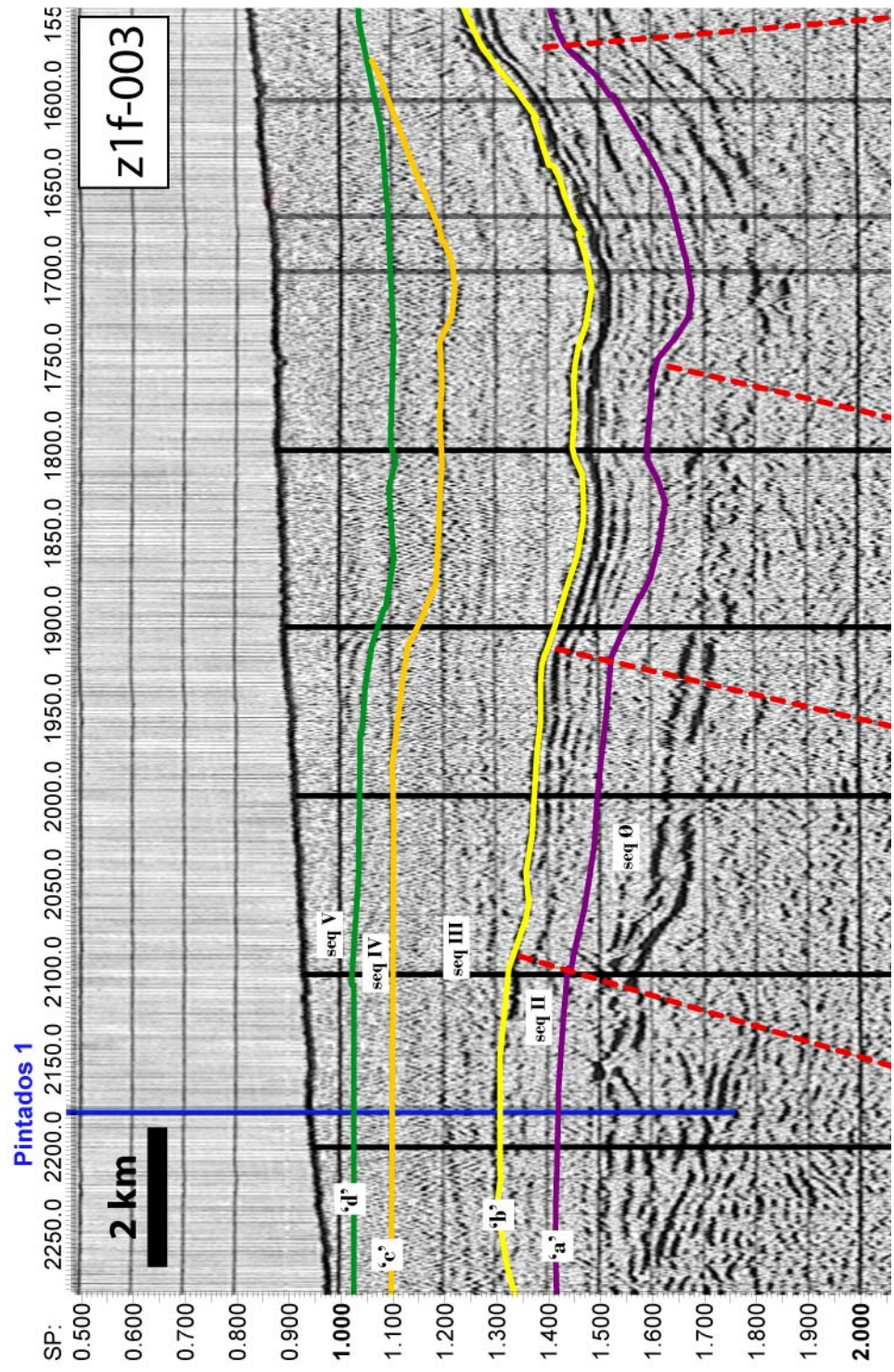


Figure 2.19: A portion of seismic line z1f-003, the only seismic line that images the far west section of the Pampa del Tamarugal basin, illustrating east-vergent reverse faults. Dramatic thinning of sediments is seen at the western edge of this line, in contrast to previous assumptions that the basin is an orogenic-scale graben. The location of the seismic line can be found on Figure 2.4.



cumulative throw from these two fault sets of ~400 m has resulted in bringing Mesozoic sedimentary rocks to within ~100 m of the surface at this location (Figure 2.17). Throw on these N-S faults diminishes from 99-04 to 99-05, and disappears altogether at seismic line 99-06.

Central sector

The central sector of the seismic grid, here defined as between and inclusive of seismic lines 99-05 and 99-08, is marked by both east- and west-vergent, high angle reverse faults, with the highest fault density along the central and western portions of the seismic data, decreasing dramatically at the eastern margin of the Pampa del Tamarugal basin (Figure 2.12). This fault set is predominantly north-trending. The reverse faults are especially dense across a 15 km wide region, with the western boundary of this zone delineated at the surface by the western edge of Cerro Challacollo. The trace of a west-vergent fault marks the western boundary of Cerrito Chipana immediately to the north. The west-vergent reverse faults associated with the western boundary of Cerro Challacollo are the most conspicuous structural features within the entire basin, with cumulative offset of sequence boundary 'b' reaching 500 m on line 99-07 (Figure 2.20). Fault density is especially high on line 99-08, where numerous small-magnitude faults occur every few hundred meters within the center and western portions of the line, giving the data a very choppy and disrupted appearance. All seismic sequences appear to be deformed within this faulted zone.

Seismic line z1f-004 reveals east-striking reverse faults which are also present in this sector of the basin (Figure 2.21). An anticline in the

Figure 2.20: A section of seismic line 99-07, which reveals a portion of the deformation history associated with the uplift of Cerro Challacollo. Rotation of reflections associated with seismic sequence III (between the yellow and orange reflections) indicates all movement on this major west-vergent fault occurred after ~16 Ma. The location of the seismic line can be found on Figure 2.4.

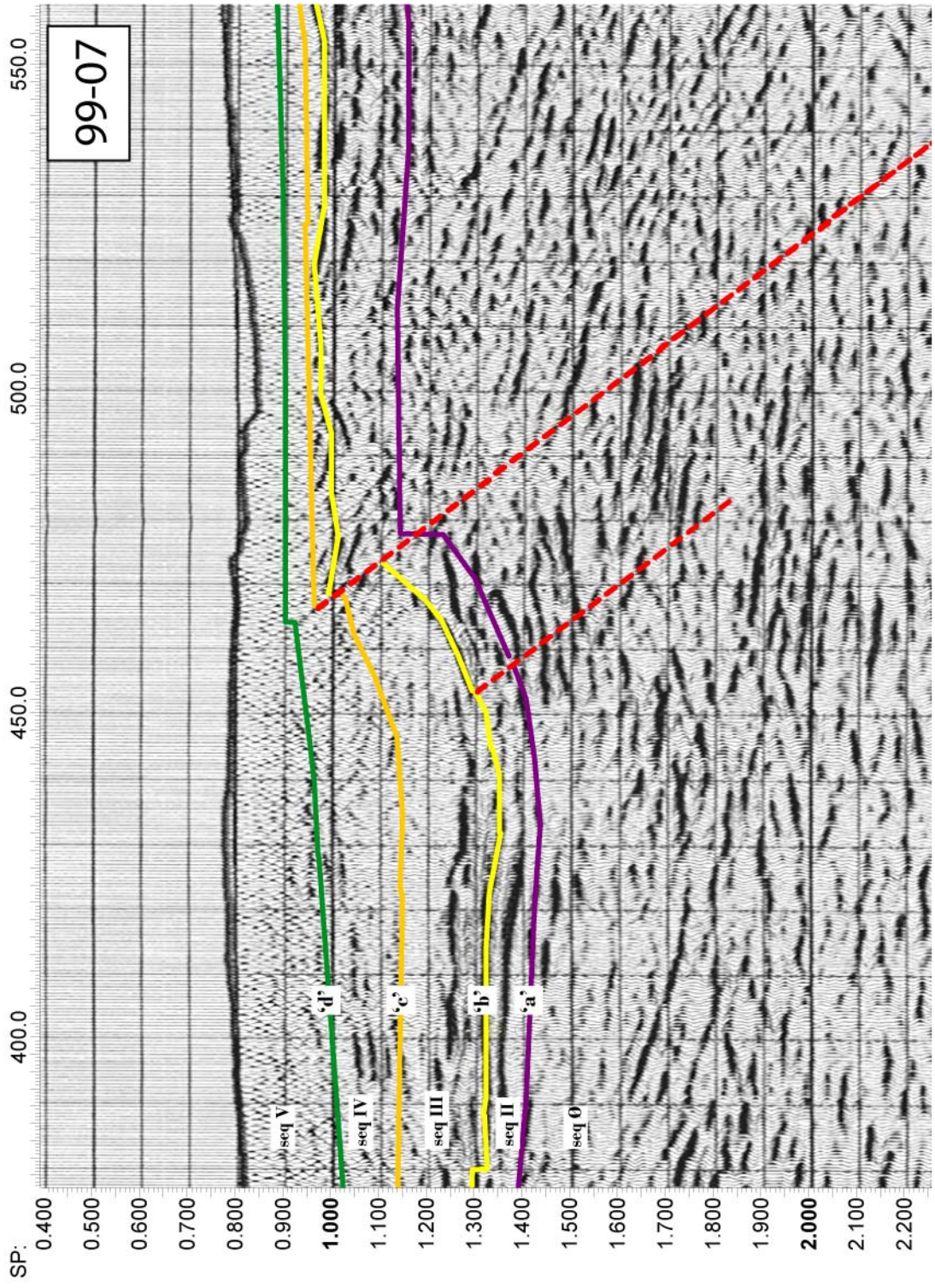
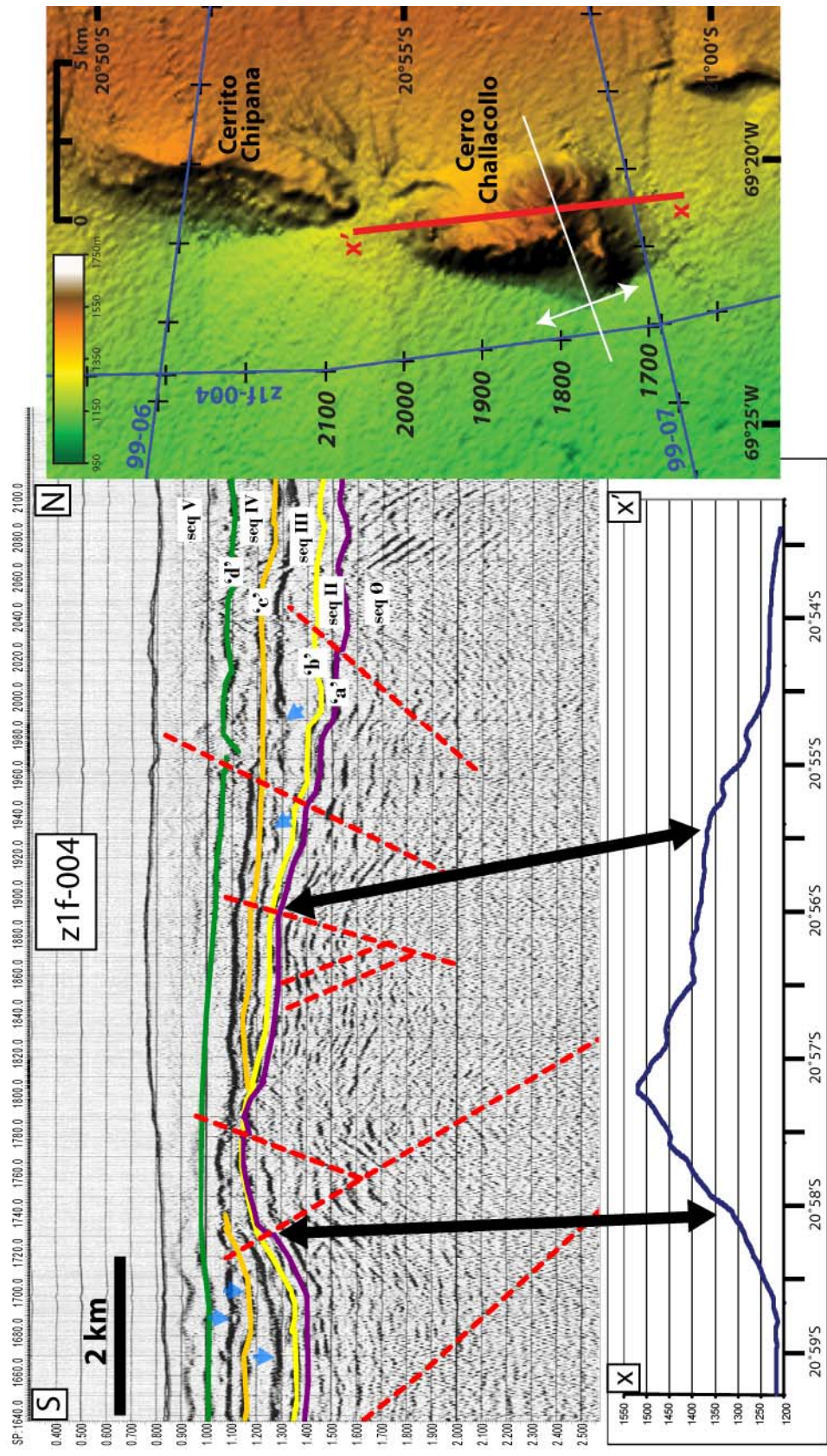


Figure 2.21: North-south topographic profile illustrating the morphological similarity between Cerro Challacollo and the accompanying portion of seismic line z1f-004. Inset topographic profile is at the same horizontal scale as the seismic line. Sequence boundary 'a' (purple reflection) is interpreted as the same surface as is seen in outcrop as "Cerro Challacollo". Black arrows indicate correlative features within the surface and seismic topography. Close correspondence between the outcrop morphology of Cerro Challacollo and seismic data of boundary 'a' indicates that an east-west structural grain is present at this location within the basin, upon which a north-trending structural trend is superimposed. Conversely, a similar correspondence is not seen between Cerrito Chipana immediately to the north and seismic line z1f-004, which is taken as evidence that the east-west trending structures illustrated in this figure isolate Cerro Challacollo from Cerrito Chipana to the north. Blue arrows are included to highlight wavy and broken reflections between and within sequences III and IV, representing surfaces which were incised by the focused drainage created as a result of the Middle Miocene uplift



seismic data between shotpoints 1700 and 2000 has a steeply-dipping southern limb, and a more gently-dipping northern limb. This anticline is the result of faults at depth, with a high-angle south-vergent reverse fault folding seismic sequence boundary 'a', and smaller amounts of folding of overlying sequences and sequence boundaries. At the northern end of this anticlinal structure, a backthrust at approximately shotpoint 1950 affects all resolvable seismic sequences. The morphology of Cerro Challacollo along a north-south transect mimics the structure that is observed in seismic line z1f-004, both in form and length (Figure 2.21). This correspondence indicates that the structures responsible for Cerro Challacollo are in fact a combination of these east-trending reverse faults in conjunction with the north-striking faults. These east-trending faults appear to die to the east of Cerro Challacollo, although the relative lack of seismic coverage perpendicular to their strike makes it difficult to discern their full east-west extent.

Both Cerro Challacollo and Cerrito Chipana to the north have aligned western boundaries, and seismic lines 99-06 and 99-07 confirm west-vergent faulting at the western boundaries of these hills. However, the modern surface of Cerrito Chipana does not show a topographic slope to the north or south, nor is any significant structure apparent adjacent to it on seismic line z1f-004. Therefore, while Cerro Challacollo appears to be due to a combination of both north- and east-striking reverse faults, Cerrito Chipana was only impacted by north-striking reverse faulting. This is also reflected in the elevations of these hills, with Cerro Challacollo reaching 1850 m, and Cerrito Chipana has a maximum elevation of only 1450 m.

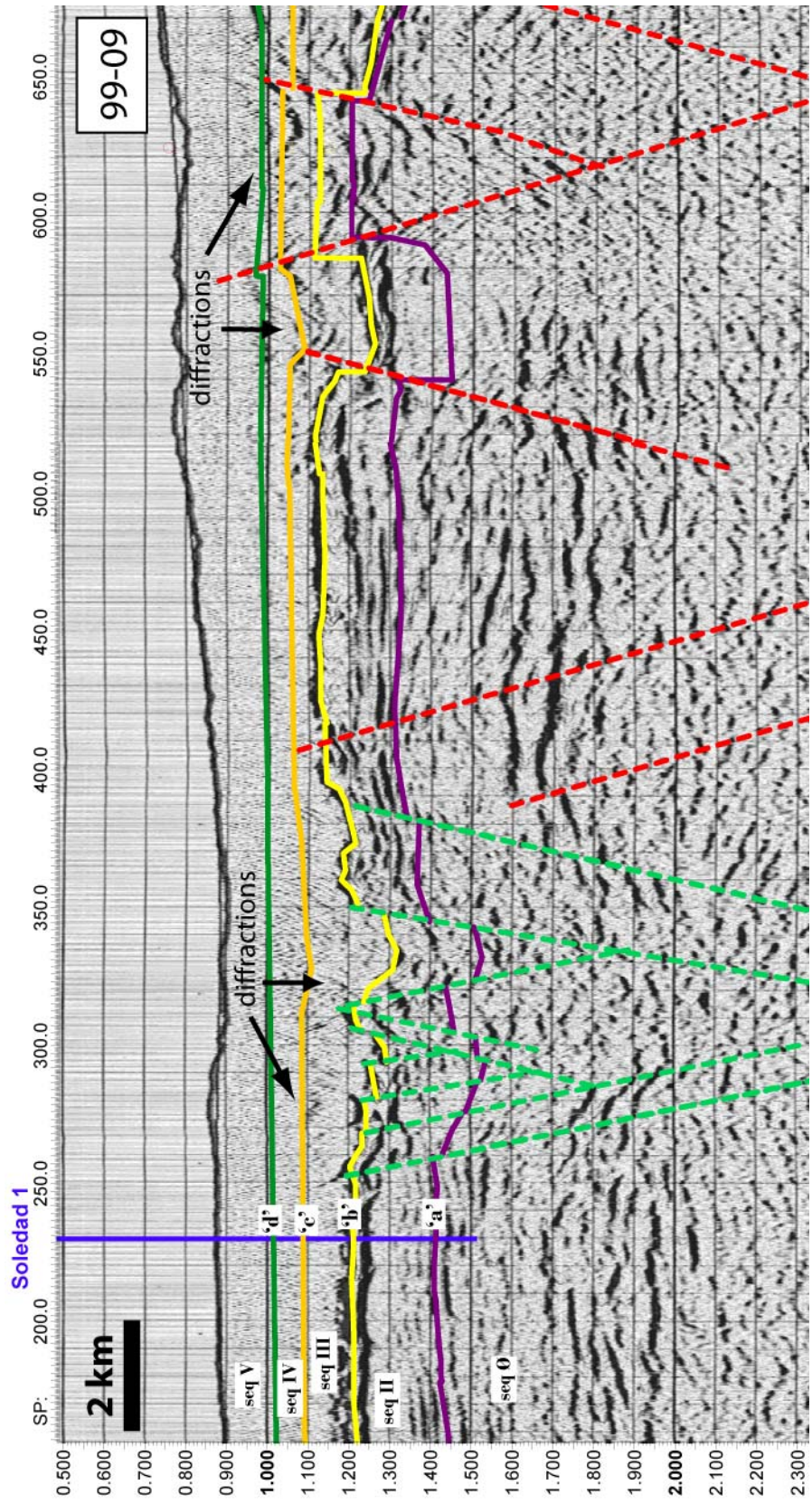
At the southwestern corner of the central sector, north-trending normal faults with both east and west dip-slip motion are observed, with high angle fault planes creating a buried graben of between 5 and 10 km width. Reverse faults become relatively less abundant in this area to the west of Cerro Challacollo, but where they are present, they tend to be east-vergent.

Southern sector

The southwestern sector of the seismic data clearly indicates that deformation in this segment of the basin is of much greater magnitude and complexity than in the northern portion of the Pampa del Tamarugal basin. Here, east-vergent faults dominate, but there are also west-vergent reverse faults. The east-vergent faults in places produce up to 200 m of vertical offset of the lowermost seismic sequences at the western end of seismic lines 99-09 and 99-10 (Figure 2.22), affecting seismic sequence III, which is the shallowest resolvable sequence at this location. These faults are high angle with horizontal back limbs, creating the appearance of a “plateau” along the western sector of the seismic grid in the southern sector. It is within this “plateau” that the graben-forming normal faults observed in the western portion of the central sector extend into the southern sector, with this graben best developed between shotpoints 250 and 400 on seismic line 99-09 (Figure 2.22). In the central and western portion of this southern sector, fault concentration is greatest in the basin. The eastern end of this sector is devoid of structural complexity, and what faults do occur only affect the lower seismic sequences.

The interpretation of structures in this sector is complicated by the

Figure 2.22: A portion of seismic line 99-09 illustrating north-trending east-vergent reverse faults (dashed red lines) and north-trending, graben-forming normal faults (dashed green lines) present within the southwest portion of the study area. Although located in the seismic mute zone, diffractions within portions of seismic sequences III and IV indicate that strata may be broken, and that deformation has continued into at least the middle Miocene. The location of the seismic line can be found on Figure 2.4.



lack of stratigraphic control and, in the case of both seismic lines 99-11 and 99-12, the lack of seismic line or well ties. Since the faulting appears to create large amounts of displacement, and since the nature of the reflectors makes it very difficult to be confident of correlation across each fault, only generalizations about magnitude and timing of offsets are possible. Deformation of the otherwise-smooth “modern” topographic surface illustrates that deformation has in some places occurred within the last 5.3 million years. Relationships among seismic reflections thought to correlate across fault zones indicate that reactivation has occurred. In some cases, this reactivation is thought to have been in the opposite direction relative to the original motion along the fault plane.

Both small scale normal and reverse faults are evident within Lomas de Sal, a small hill of halite and anhydrite with approximately 100 m of relief above the surrounding pampa. Exposure within the western 3 km of the northernmost canyon that has been cut through these evaporite deposits reveals that normal faulting has been very active in the Lomas de Sal. Eastward-dipping high angle normal faults consistently cut the strata, which consistently dip at $\sim 5^\circ$ to the west, leading to consistent repetition of stratigraphy by domino style block faulting, with displacement on individual faults generally around 1 m. Although they were not observed directly in the field due to the somewhat poor nature of the outcrop, it is assumed that on a spacing of several hundred meters, normal faults with offsets with a magnitude of approximately 50 meters are present. In one instance, a west-vergent reverse fault was also observed with approximately one meter of displacement. A fault breccia was also observed within a fault zone in a

halite mine at the extreme northwestern end of the hill, an indication that brittle deformation was active in this region, and disruption of beds was not simply the result of non-structural processes such as salt dissolution or block slumping.

Ages of Deformation Within the Basin

Seismic and outcrop studies, in conjunction with remotely sensed data, clearly indicate that the structures within the basin were likely active by the latest Oligocene, during the entire duration of the Miocene, and extending into at least the early Pliocene. The general trend is that the age of deformation becomes younger to the south and west. In the southwest part of the basin, the modern surface is offset and all seismic sequences and sequence boundaries are faulted, which indicate that minor deformation was active through the entire Miocene, and possibly into the earliest Pliocene. At these same latitudes, seismic data and outcrop indicate that faulting ceased by the mid to late Miocene at the eastern basin margin.

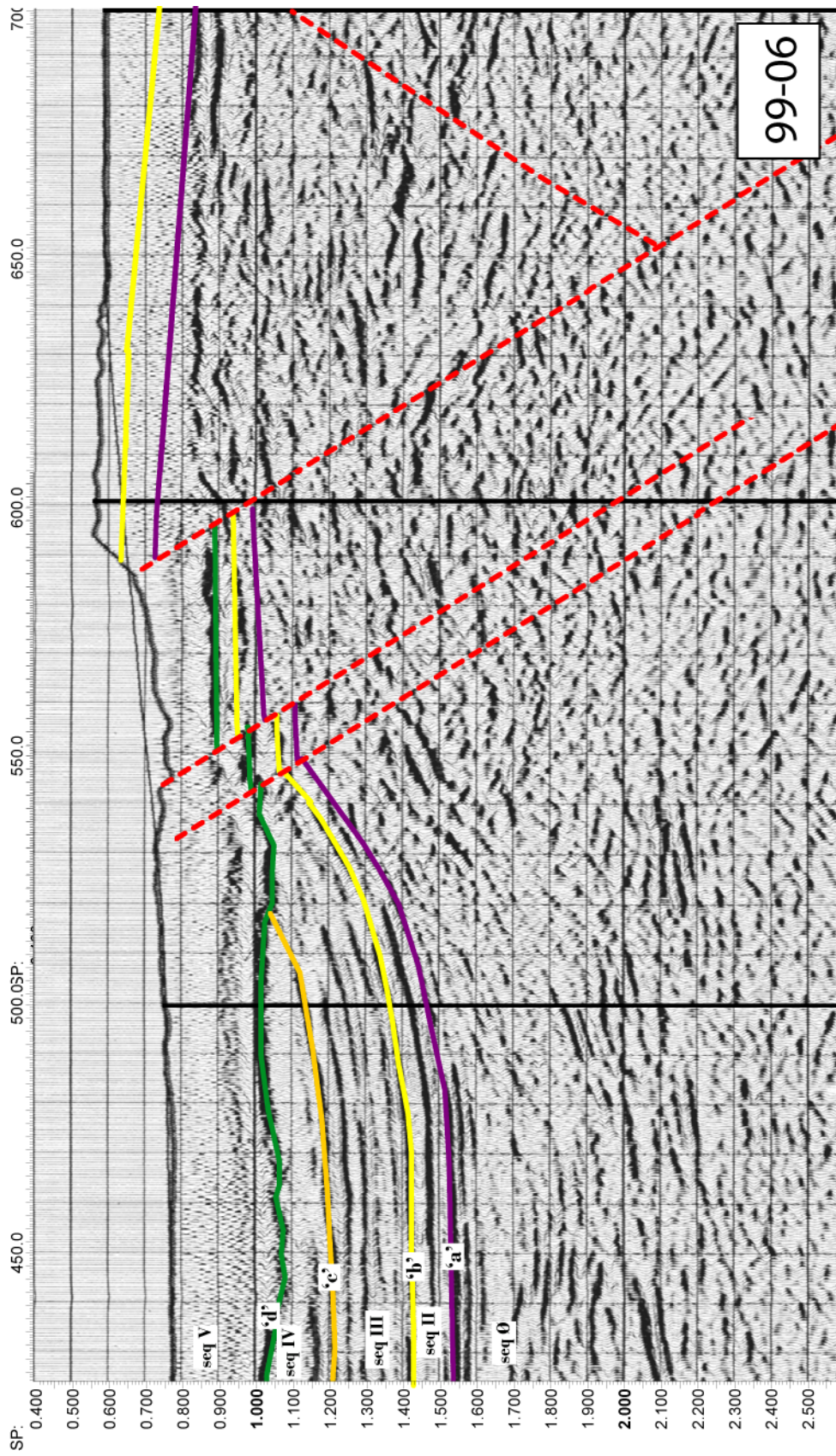
Oligocene deformation is seen in the northern sector of the seismic grid, with termination of deformation during the Middle Miocene. On seismic line 99-03 between SP's 200-400 (Figure 2.10), growth strata, illustrated by fanning of reflections within seismic sequence Ø to the west of a high angle west-vergent reverse fault, indicate that the youngest age for the initiation of this fault is late Oligocene. Reflections within seismic sequence III, as well as sequence boundary 'c' adjacent to the west-vergent reverse fault, dip gently westward, and are truncated by sequence boundary 'd'. Seismic sequence IV onlaps sequence boundary

'c', and does not reveal growth or rotation. Sequence boundary 'd' is not cut by this fault. A very small amount of growth within seismic sequence III indicates that this west-vergent fault was also active during this time interval, with continued deformation after the deposition of sequence III. Deformation ceased before deposition of sequence IV, and has not been active thereafter. Since the deposition of sequence IV is interpreted to have terminated at ~11 Ma, deformation at this location ended sometime in the Middle Miocene.

Deformation further south, in the center of the seismic grid, also indicates Early and Middle Miocene deformation. Seismic line 99-07 reveals westward rotation of seismic sequences III and IV, with no rotation of sequence boundary 'd' at SP 450 (Figure 2.20) on the eastern flank of a small sub-basin to the west of a west-vergent fault. Along strike, we see the same basic relationship on seismic line 99-06, but we can also clearly see the unconformity (sequence boundary 'd') has been faulted (Figure 2.23). This fault on seismic line 99-06 emerges at the surface at the western edge of the north-south trending Cerrito Chipana to the north of Cerro Challacollo. At its base, Cerrito Chipana contains an ash believed to correlate with an 18.89 Ma ash 8 km to the southeast, indicating that movement on this fault is at least as young as ~18 Ma. Rotation of seismic sequence III, which shows no growth, indicates that fault initiation was post-16 Ma. The faulting of sequence boundary 'd' indicates that the latest movement along this fault plane occurred after ~11 Ma.

East-west trending faults at the northern and southern flanks of the Cerro Challacollo anticline were active in the early Miocene, with

Figure 2.23: A section of seismic line 99-06, run across Cerrito Chipana, just north of Cerro Challacollo, illustrating west-vergent faulting in the center of the region of study. The location of the seismic line can be found on Figure 2.4.



minor fault movement continuing into at least the late Miocene. Onlap of ~20-16 Ma strata associated with seismic sequence III onto sequence boundary 'b' (Figure 2.21) indicate that this structure was present prior to 20 Ma. In addition, lacustrine and playa sediments of AdP member 3 are present in outcrop both to the north at Cerrito Chipana, and to the east (Figure 2.5), but are at Cerro Challacollo, only pre-Altos de Pica rocks are exposed, most likely because this hill was already standing in relief above the surrounding landscape during the Miocene lake phase. Channelization at the northern and southern fringes of the uplift (seismic line z1f-004 within seismic sequences III and IV [Figure 2.21]) is evidence that this uplift created a focused drainage network. Rotation of reflections within seismic sequence III, especially along the southern flank of the Cerro Challacollo anticline (Figure 2.21), indicate continued faulting and uplift post-16 Ma. An unconformity (sequence boundary 'c' (?)) at the crest of this anticline is onlapped and eventually buried by seismic sequence IV, indicating a decreased uplift rate after 16 Ma. However, faulting of sequence boundary 'd' at the northern end of the structure as well as short-wavelength folding on its south side indicate post-11 Ma deformation continued on these faults. This, in conjunction with post-11 Ma movement along west vergent faults which form the western edge of Cerro Challacollo (discussed previously at seismic line 99-07, Figure 2.20) indicate that Cerro Challacollo has experienced additional uplift since ~11 Ma as a result of both the north-south and east-west trending fault sets. A subtle topographic high above the buried Cerro Challacollo anticline suggests minor post 5.3 Ma fault activity. Thus, it is quite possible that the history of fault activity along east-west trending reverse faults in this region spans the entire Miocene.

Evidence for termination of deformation in the Middle Miocene is also observed at the eastern end of the basin. In outcrop at the eastern margin of the basin within Quebrada de Sama (21°22'33"S, 69°05'08"W; Figure 2.4), a west-vergent fault which strikes N40E displaces beds within the canyon by ~10 m. Units above rest atop an angular unconformity, and themselves show only slight folding above the fault tip (Figure 2.24). As stated earlier, the similarity of the sediments between AdP members 3 and 5 often necessitates a non-lithologic means for differentiation between the two members. Based on the proximity of this quebrada to dated ashes within Quebrada Tambillo (IB-18; 19.77 Ma IB-20; 11.62 Ma; Figure 2.4) we assume that the AdP member 3 is present at the bottom of Quebrada de Sama, with the AdP member 5 above. This is consistent with faulting which is active in this part of the basin in the middle Miocene (during and shortly after deposition of the AdP member 3) with only a very limited activity on these faults after deposition of AdP member 5. In fact, none of the seismic data at the eastern end of the study area shows faulting of sequence boundary 'd', correlative to the top surface of AdP member 5. Since the youngest stage of the AdP member 5 has a maximum age of 11.62 Ma, any significant faulting within the basin at its eastern margin ended by ~11.6 Ma.

On seismic line 99-10 at SP 590, a well-imaged west-vergent reverse fault with ~125 m of displacement is accompanied by growth within seismic sequence II (Figure 2.25). Sequence boundaries 'b', 'c' and 'd' are kinked, and strata thicken on the downthrown block of the east-vergent splay of this fault within sequences III and IV. A rare internal reflector within seismic sequence V also shows hanging wall uplift, and

Figure 2.24: West-vergent reverse fault located at 21°22'33"S, 69°05'08"W affecting rocks of AdP member 3 age, but leaving AdP member 5 almost completely undeformed. Planation surface above faulted unit suggests that significant time elapsed between the episode of faulting and the aggradation of sediments atop the unconformity.

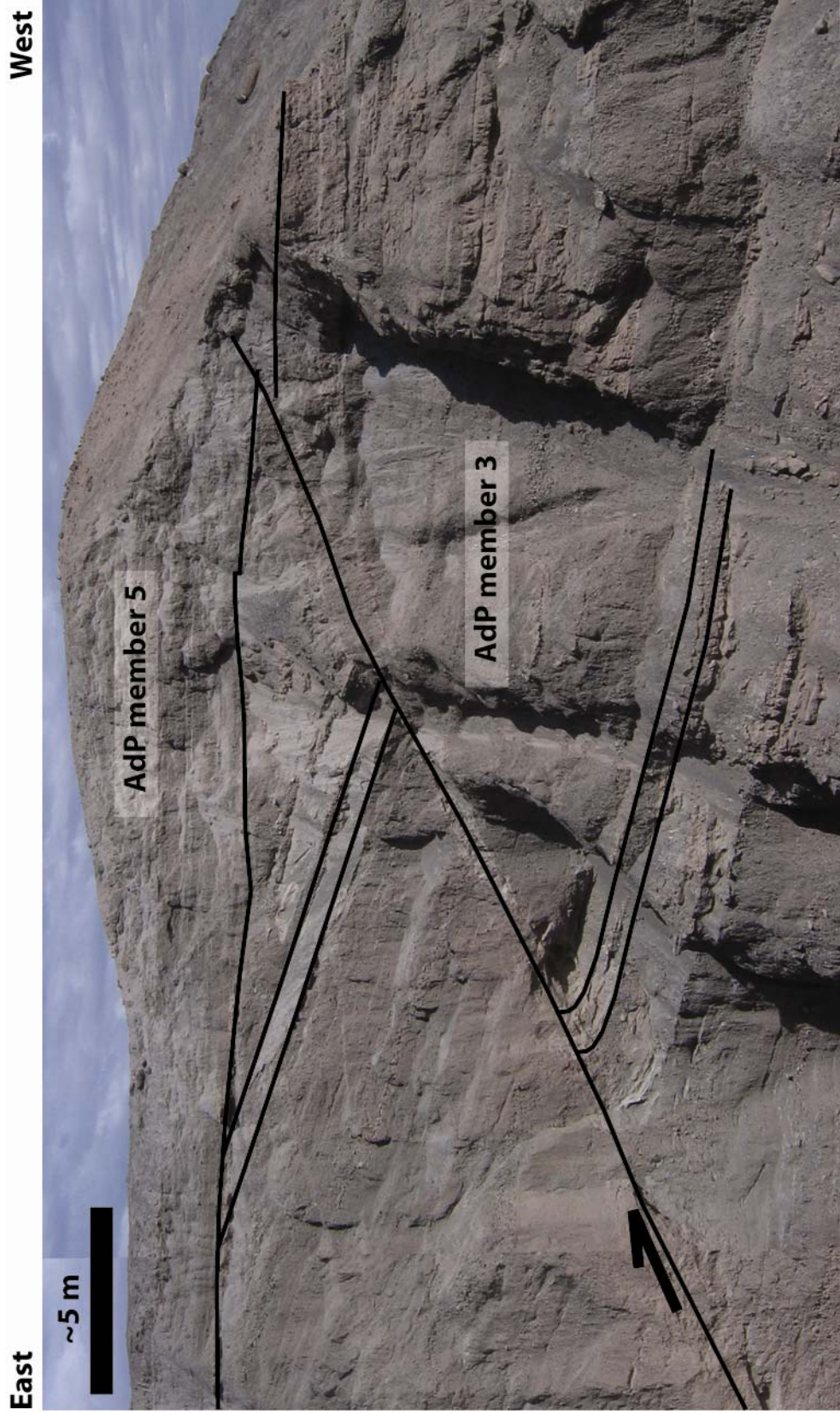
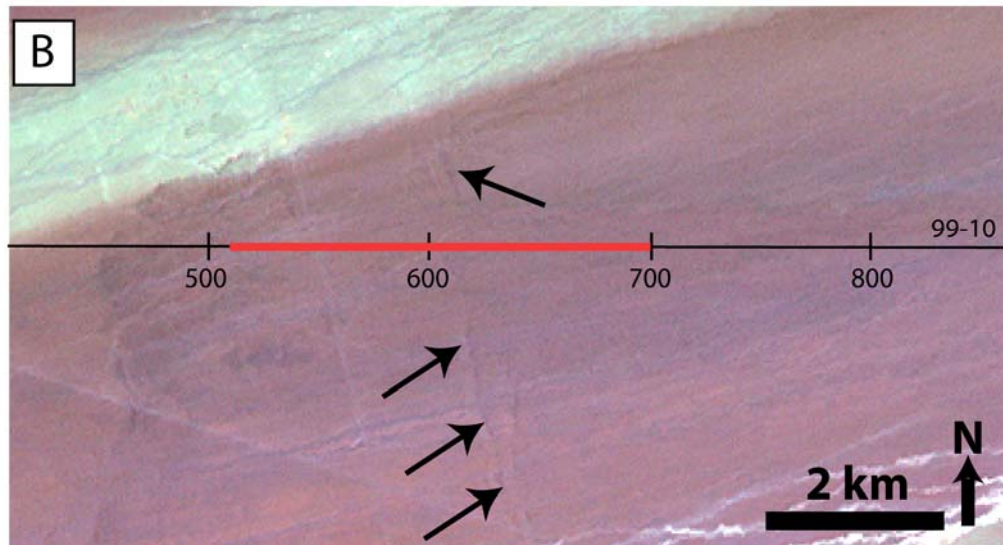
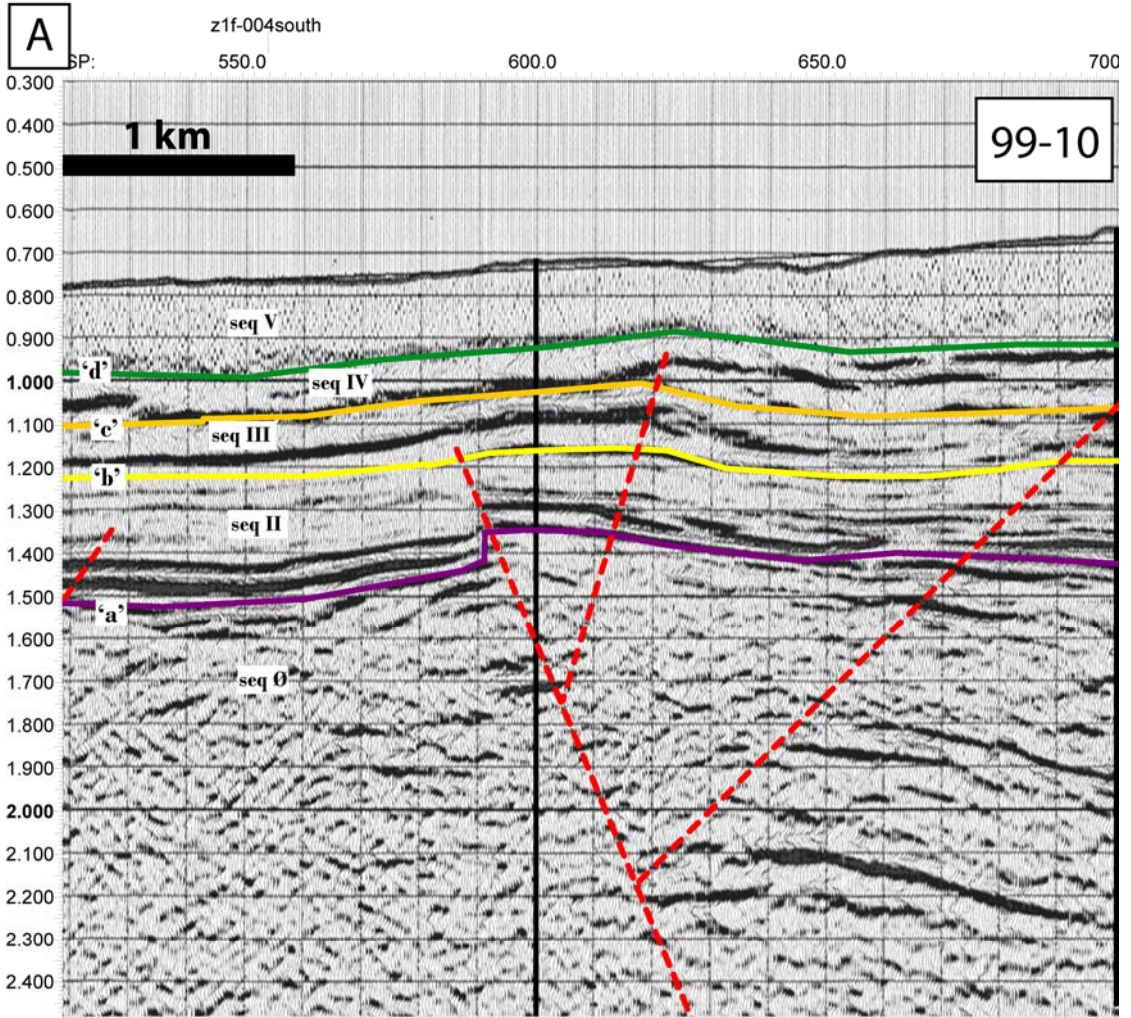


Figure 2.25: A) A portion of seismic line 99-10 and thematic mapper image revealing late Miocene deformation in the south-central portion of the study area. Sediments thicken within seismic sequence II to the west of the west-vergent fault, and east of the splay of this fault within seismic sequence IV. B) Thematic mapper scene, with faint lineations delineated by arrows, that are visible at the modern surface of the basin. Given that the modern topographic surface is ~5.3 Ma in this portion of the basin, some late Miocene – Pliocene (?) deformation has occurred at this location. Red line illustrates the section of seismic line shown in A).

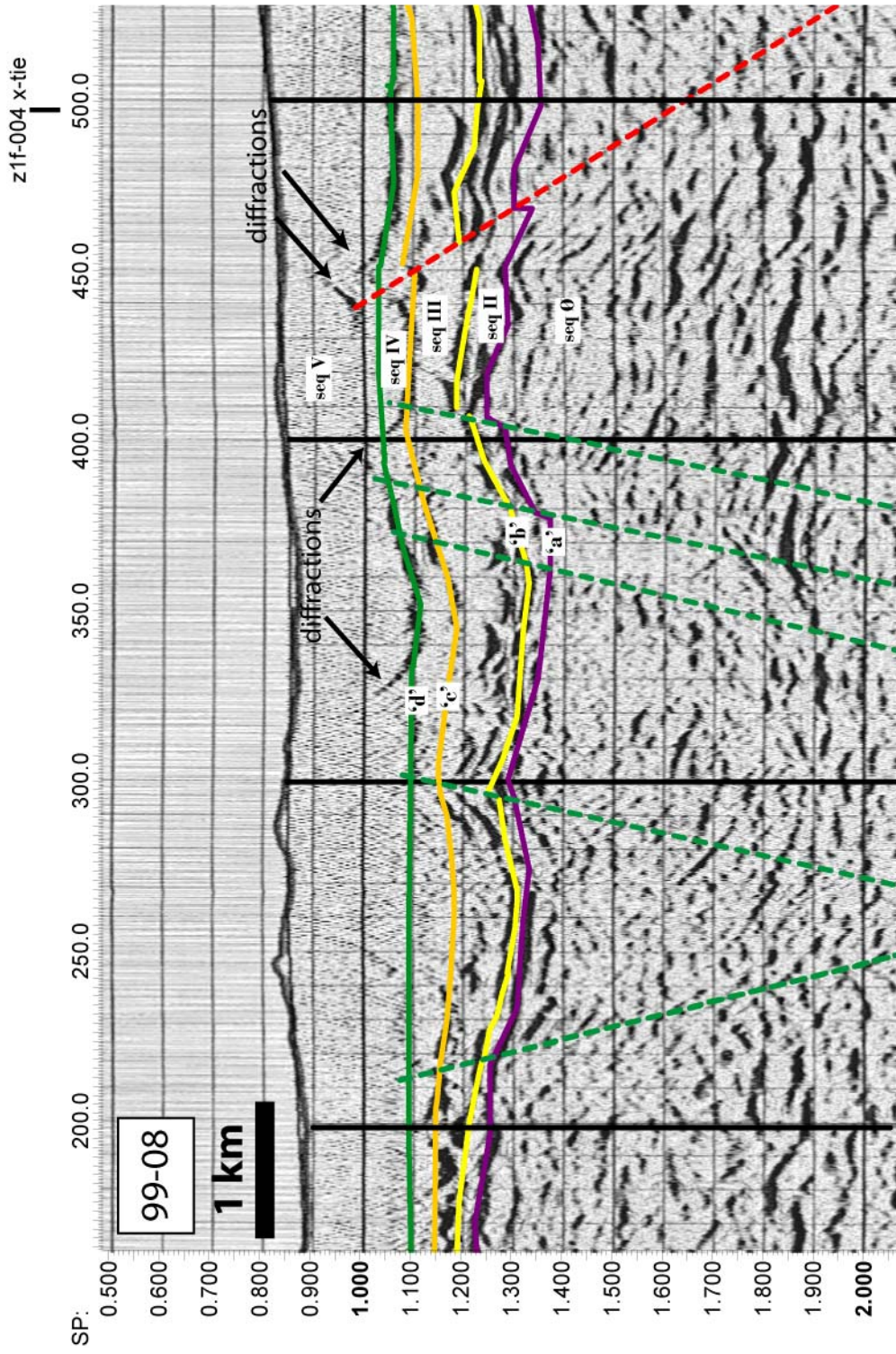


in fact, this is a location where TM imagery reveals surface lineaments, exactly in line with this fault trace (Figure 2.25). So while the majority of deformation associated with this fault occurred during deposition of sequence III, lesser amounts of motion continued at least until the end of the Neogene depositional package (post-5.56 Ma) at this location.

Within seismic lines 99-08 and 99-09, it is apparent that west-vergent faults within the eastern half of the basin at this latitude remained active into the mid Miocene, but have not been actively deforming since ~11 Ma. However, faulting is younger to the west, perhaps with activity in the early Pliocene. Near and to the west of the intersection of 99-08 and 99-09 with seismic line z1f-004, diffractions of seismic reflections along and above sequence boundary 'd' are observed (Figure 2.26), possibly resulting from disrupted strata. This is also an area that shows disruptions of the generally smooth topographic surface. Volcanic clasts indicate that the maximum age for this depositional surface is 5.6 Ma. A small amount of westward tilting of seismic sequence III on seismic line 99-08 to the east of its intersection with seismic line z1f-004 is observed, and faulting of horizons up to and including seismic sequence III, with only gentle folding of sequence boundary 'd', is present on the adjacent line 99-09. No surface deformation is associated with these faults. This indicates that deformation ceased at the eastern end of these lines before ~11 Ma, whereas deformation is younger to the west.

It is difficult to determine from the data when the initiation of normal faulting at the southwestern corner of the study area began. However, faulting has clearly been active since the Middle Miocene,

Figure 2.26: A section of seismic line 99-08 reveals late Miocene deformation in the south-central portion of the study area. Dashed red lines are interpreted reverse faults, and dashed green lines are interpreted normal faults. Diffractions here interpreted to be the result of disruptions within the strata are observed within seismic sequence V, and disturbances are clearly seen at the topographic surface less than 5 km to the south of line 99-08, indicating that some late Miocene – Pliocene (?) deformation has likely occurred at this location. For location of the seismic line, refer to Figure 2.4.



offsetting sequence boundary 'b' and creating disruptions in the overlying seismic sequences (Figure 2.22). A slight depression of the modern topographic surface suggests that this graben may have continued to develop into the late Miocene, but lack of seismic resolution above seismic sequence III makes a conclusive determination impossible.

Minor deformation that is not resolvable by seismic data can be clearly observed within structures known to be at least as young as latest Miocene. Figure 2.27 illustrates 8 m of fine-grained, poorly-sorted CaCO₃- and NaCl-cemented siltstones and sandstones of mixed alluvial and fluvial origin, located at 21°22'57"S, 69°16'31"W, in westward-tilted layers whose dip decreases upsection. Obvious onlap is detected atop two separate bedding surfaces (Figure 2.27 B), indicating progressive westward rotation. Within this outcrop are both normal and reverse faults, with both down to the east and west senses of slip, and offsets of less than 50 cm. In addition, air photos reveal that the outcrop, while perhaps aided by undercutting of an ephemeral stream, has a very well-defined WNW trend which is nearly identical to that of the northern delineation of the Lomas de Sal approximately 10 km to the west, as well as structures seen in the Coastal Cordillera 50 km to the west. Sample GH-04-01 (Ar-Ar, biotite) from a volcanic clast at the base of this section yielded an age of 5.60 ±0.3 Ma (this study), giving a maximum age of deformation at this location.

Additional evidence for minor deformation during or since the latest Miocene is observed in a region of rolling hills approximately 25 km to the north of this outcrop (Figure 2.28). Exposures here are limited,

Figure 2.27: Late Miocene – Pliocene (?) deformation observed at 21°22'57"S, 69°16'31"W, in the south-central portion of the study area. A) Photograph of the ~8 m high outcrop, viewed towards the south, of alluvial and fluvial deposits which have been uplifted and faulted. A clast of a dated tuff indicates that west-vergent faulting and associated folds are younger than 5.6 Ma. Note hammer (circled) for scale. B) A schematic of the outcrop detailing the folded strata and onlap, representing several stages of growth of the structure within the outcrop. C) Air photo of the uplifted hill, showing west-northwest fault (?) scarp (black arrows) and north-trending lineaments interpreted to be associated with west-vergent faults in the subsurface. These lineaments are small depressions at the surface which may be related to zones of dissolution along preferential groundwater pathways associated with faults zones, or may be small normal faults associated with tensile stresses at the crest of the anticline. Location of the outcrop in A) is indicated by 'X'.

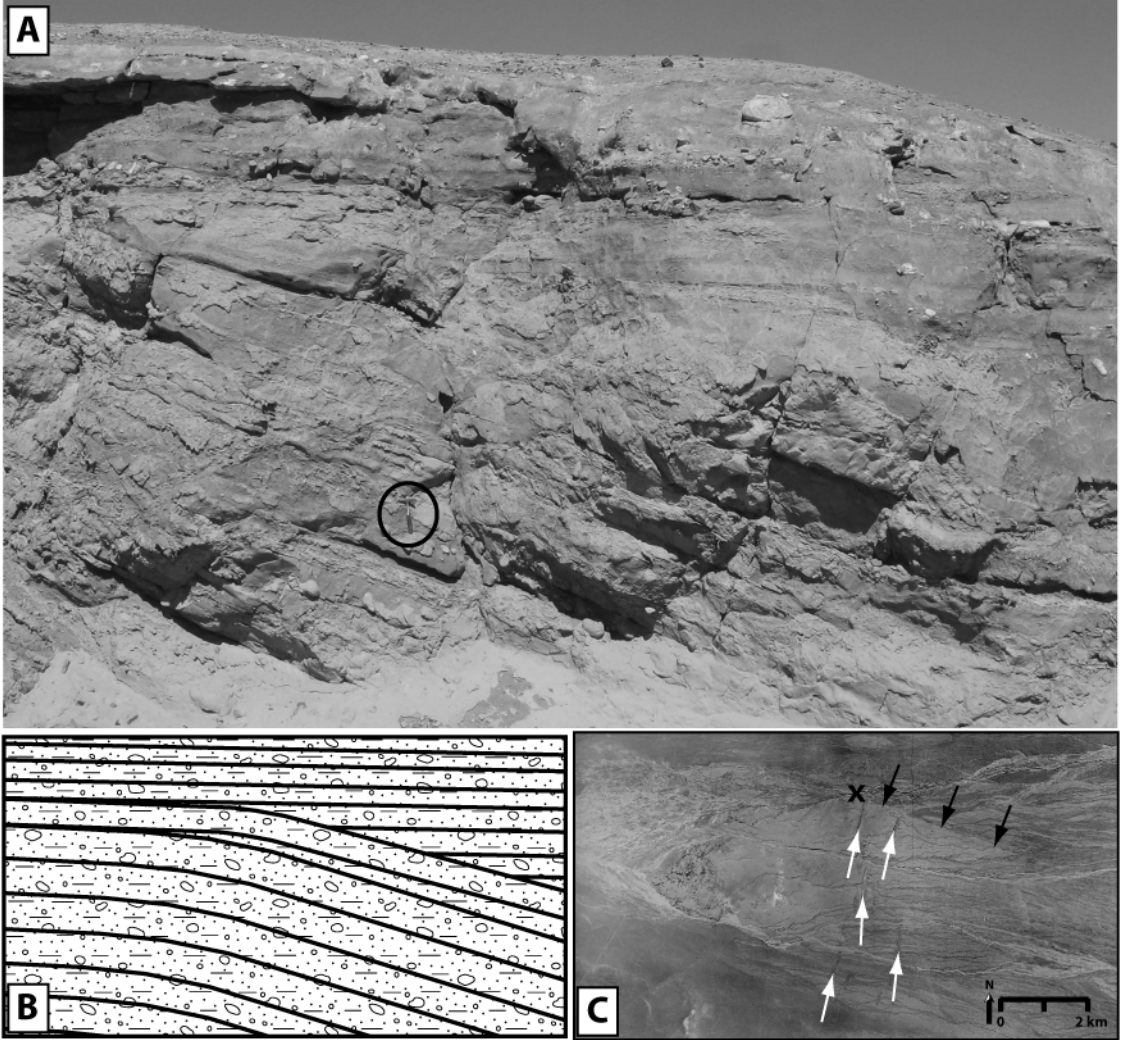
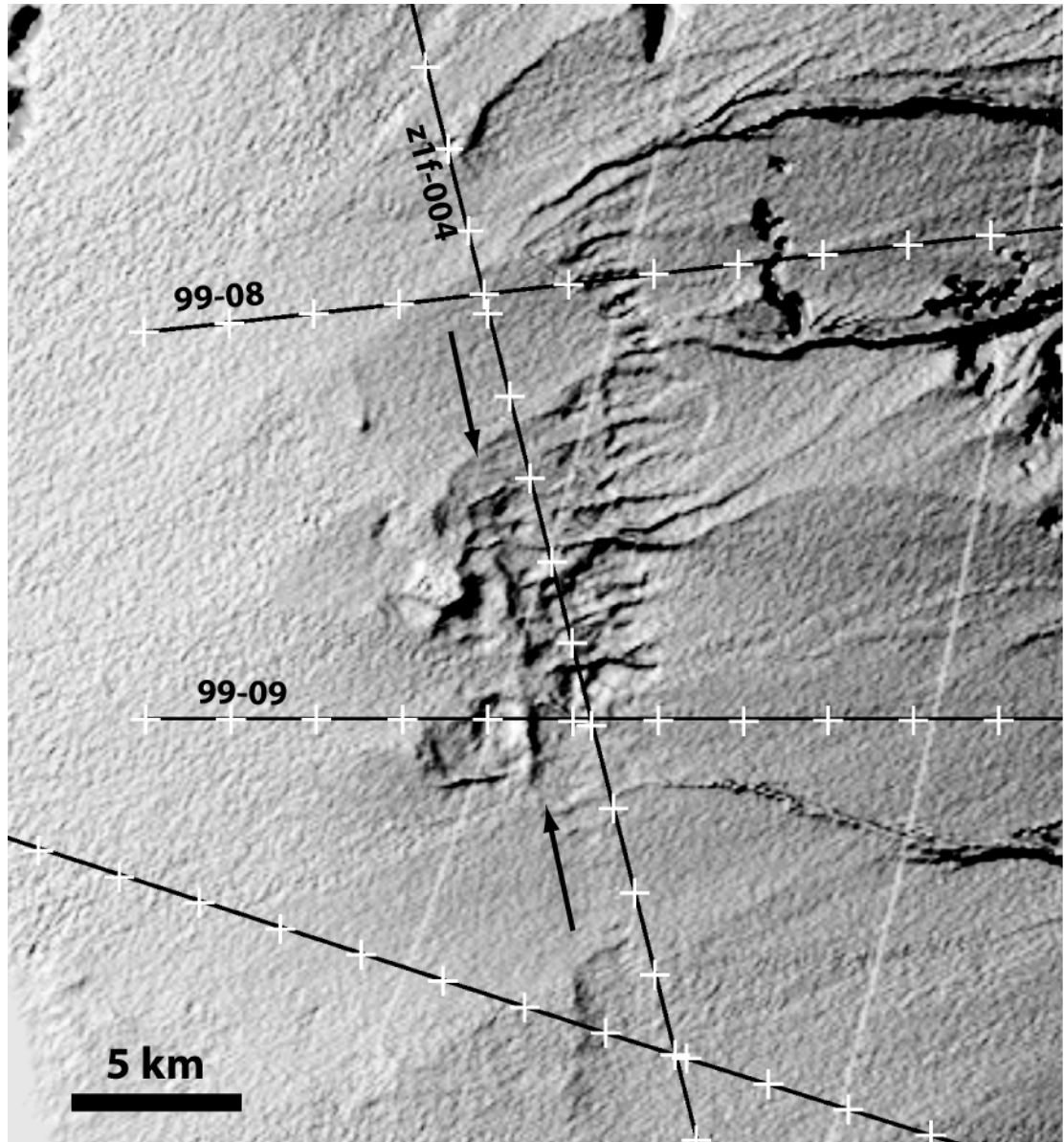


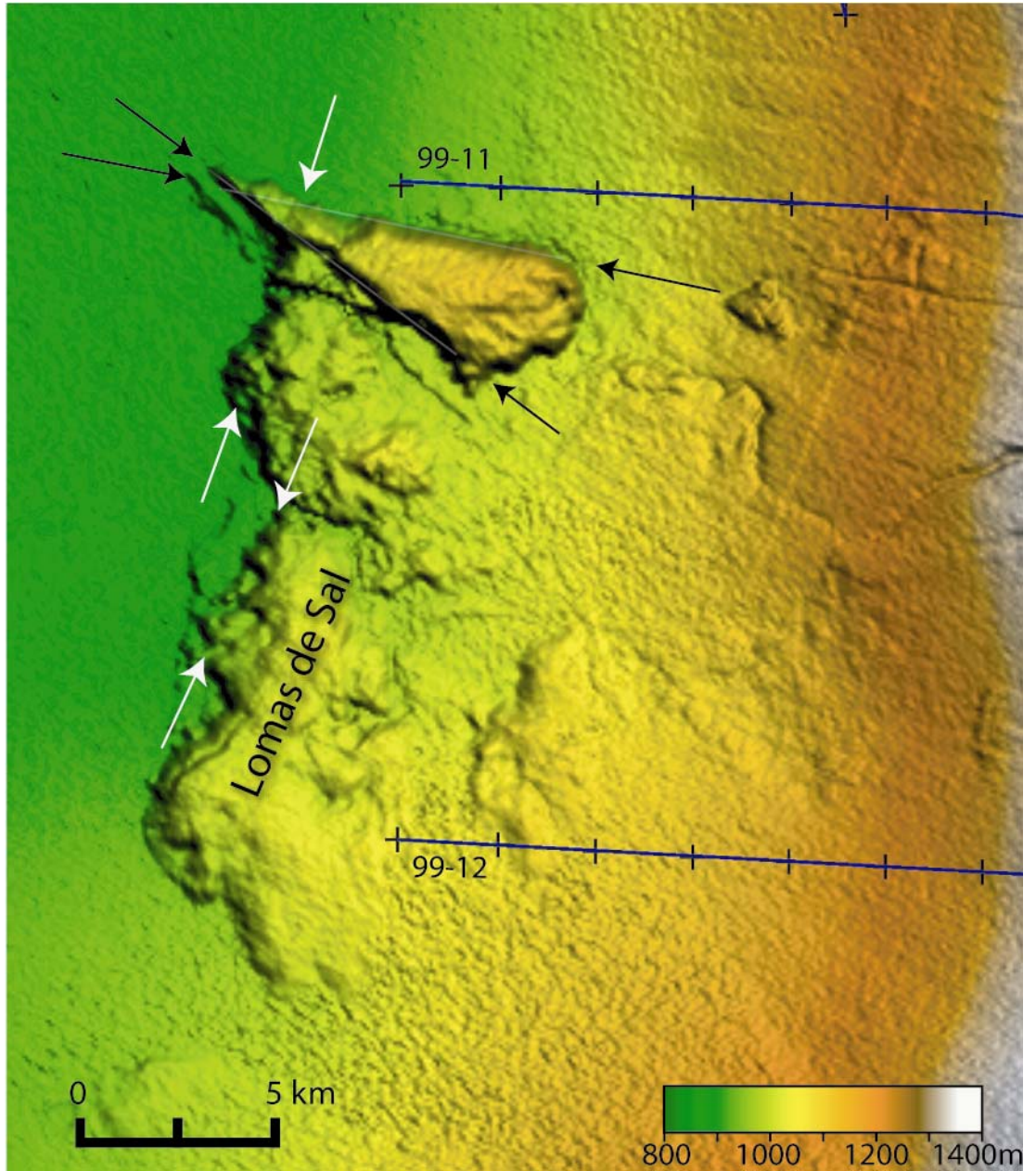
Figure 2.28: A sun-shaded 90 m-resolution DEM illustrating young deformation revealed by the general disruption of the modern topographic surface. A volcanic clast within correlative sediments 25 km to the south indicates that this surface is younger than 5.6 Ma, and an ignimbrite intercalated with correlative deposits further to the east (sample IB-09a, Hoke *et al.*, 2007) suggests the surface may be younger than ~5.38 Ma. Arrows outline a surface lineation that matches a prominent fault trend within the seismic data. The white lines running through the center of the figure are an artifact of data collection, and hold no geological significance.



but a 5 m-high outcrop reveals decimeter scale normal and reverse faults within alluvial sediments presumed to be the age equivalents of the southern rocks. Landsat imagery also hints at the possibility of an orthogonal set of small-scale scarps that trend both WNW and ENE, although the evidence for these as structurally-generated lineaments is inconclusive.

Evidence for the youngest deformation within the basin can be found at the southwestern corner of the study area. The Lomas de Sal stands approximately 100 m above the surrounding pampa, with its northern and northwestern boundaries sharply defined (Figure 2.29). These boundaries are oriented east-west and east-southeast, respectively, following roughly the same trend as reverse fault scarps observed to the west in the Coastal Cordillera (Figure 2.4; Allmendinger *et al.*, 2005). The Lomas de Sal mostly consists of ~100 meters of halite (Sáez *et al.*, 1999) that was deposited after 5.56 Ma (A. Jensen, pers comm., 2004). Since the entire thickness of halite was formed within a salar many tens of meters below its present elevation (relative to the surrounding topographic surface), the most logical explanation is that reverse faulting has uplifted these evaporites approximately 100 m since their deposition. The sharpness of the scarps at the northern and northwestern borders of the Lomas de Sal suggests that these faults have been active most recently, but well-defined eastern and western limits of this structure suggest that north-south-trending reverse faults have also been active after 5.56 Ma. The time that elapsed between the ash dated at 5.56 Ma at the base of the halite and the 100 m of halite deposits is

Figure 2.29: A sun-shaded 90 m-resolution DEM of the Lomas de Sal, showing sharp scarps which are present, especially at the northern and southern ends of the northern “nose” of the hill (indicated by arrows and light-gray lines). Possible north-northeast-trending reverse faults are illustrated by white arrows. The western and especially eastern boundaries of the hill are less well defined (although the lack of definition on the eastern side is partially a function of burial by alluvial sediments from the east). This, along with the elevation of the “nose” being higher than the portion of the hill to its south, suggests that the west/northwest-striking reverse faults may be younger than the north-northeast trending faults.



indeterminate, but it is reasonable to assume that all of this uplift has occurred since the beginning of the Pliocene.

Groundwater and structure

Mechanisms for dissolution along faults can be deduced from the following logic. In regions where lineations appear to reveal small-scale local subsidence of the land surface (Figure 2.27), seismic reveals that reverse faults often underlie these zones. The extent of these elongated depressions is ~100 meters wide by up to 1500 m in length, with generally less than 10 m of relief. Considering that much of the shallow bedrock is known to be composed of evaporites, including Neogene deposits of gypsum, anhydrite and halite (Sáez *et al.*, 1999), fresh water with relatively low electrolyte composition can cause dissolution along zones of preferential groundwater flow, such as faults.

Near the village of Quillagua, large dolines up to 200 m in diameter are present in regions near the Río Loa. These dolines are common in a cluster to the east of the village, between the high elevations of the Precordillera which is the source of waters to the east and the river, whereas they are much less common in areas containing identical bedrock to the west of the river (Sáez *et al.*, 1999). This suggests that the dissolution responsible for the dolines did not depend on water from the Río Loa, but rather that an important contribution of fresh water also originated from the east. Similarly, this is most likely the case to the northwest in Salar Grande, where sinkholes and dissolution tubes have been reported at the eastern margin of the salar (Chong *et al.*, 1999).

Although the majority of the canyons in the study area today host ephemeral streams, it is known that in this region of the Atacama Desert, high rates of freshwater discharge occurred during humid intervals in the Pleistocene, resulting in perennial streams (Nester *et al.*, 2007). The ENE fracture networks reported at the eastern edge of Salar Grande (Chong *et al.*, 1999) which have acted in the past as conduits to flow were directly downstream of these vigorous, perennial stream systems. With an increase in the elevation of the water table, fresh waters will find fault zones and preferentially dissolve evaporite bedrock, leading to small depressions regardless of the sense of fault motion. Although rates of dissolution of evaporites are somewhat poorly constrained, it is conceivable that these ancient perennial streams have resulted in local topographic expression of faults occurring just beneath the land surface. This is confirmed by the presence of small valleys observed mimicking fault traces in areas of known reverse fault motion (Figure 2.27). Since the groundwater in this portion of the Pampa del Tamarugal is today known to be extremely saline, as observed in water wells drilled by Sociedad Química y Minera de Chile (SQM), as well as springs to the west where the water table intersects the local ground surface, dissolution of bedrock more likely was the result of past increases in freshwater discharge. Since the evaporite bedrock in this sector of the basin is late Miocene – Pliocene (?) in age (Chong *et al.*, 1999; Pueyo *et al.*, 2001; Sáez *et al.*, 1999), this increase in freshwater had to have occurred since the end of the Miocene.

Summary of Basin Evolution

Taken together, the well data, geochronological dates of volcanic layers, surface exposures and seismic facies analyses allow us to reconstruct the evolution of the Pampa del Tamarugal basin. What follows is a summary of the basin evolution, divided by time periods which generally correlate with the members of the Altos de Pica Formation (~26 -~11 Ma), and pre- and post-Altos de Pica sedimentary rocks.

Pre-26 Ma

The amount and extent of sedimentation which occurred prior to the Altos de Pica Formation is somewhat difficult to gauge, but evidence exists that it may have been at least a minor component within the Pampa del Tamarugal basin. The difficulty arises from the fact that no outcrops within the basin of sedimentary rocks older than ~26 Ma have yet been found which are intercalated with datable volcanic units. However, seismic evidence in conjunction with well data and surface exposures indicate fluvial and alluvial deposits of an indeterminate age resting atop sequence boundary 'a', an unconformity with Mesozoic and Paleogene rocks below. They are found filling paleotopography at the southern sector of the basin, or as cut and fill deposits observed at the southern end of seismic line z1f-004 (Figure 2.11). These deposits may be several hundred meters thick in places, as is suggested by fluvial and alluvial deposits resting above igneous basement rocks at the location of the Hilaricos #1 borehole (Figure 2.5).

26-20 Ma

Well data indicate that clastic and evaporite sedimentary rocks of AdP member 1, deposited between ~26 and 20 Ma, rest atop a generally smooth unconformity (sequence boundary 'a'), correlative to the Choja Pediplain further to the north (Galli, 1967), although this surface has since been folded and faulted during subsequence deformation events. In the north, near Pica, well sorted sandstone and conglomerate observed in outcrop (Figure 2.5) represents a mixed fluvial and alluvial environment during the deposition of AdP member 1 (Figure 2.14), whereas a dominantly alluvial environment is observed at the western end of the basin at this latitude. Based on seismic facies analysis, alluvial deposition with a small fraction of fluvial deposition dominates along the entire eastern basin margin for this time interval (Figure 2.15). Towards the basin center, mixed shallow lacustrine/playa and alluvial environments are present, observed in outcrop to the east of Cerro Challacollo (Figure 2.5). Depocenters at the northern and eastern sectors (sub-basins 'α' and 'β', Figure 2.15) were already well developed by this time interval. Sub-basin 'β' appears to have originated to the west of a west-vergent reverse fault, whereas sub-basin 'α' was likely formed within the backlimb of a west-vergent, northwest trending reverse fault. Cerro Challacollo experienced uplift from east-west trending reverse faults during this interval, and was likely already standing in relief above the lakes present at the time.

Further south, in the center of the basin, well data indicate a dominance of salar facies at the location of the Soledad #1 borehole. These sediments often filled depressions which, as in the north, were

produced by faulting. These depressions are most typically found on the footwall side of mostly west-vergent reverse faults (seismic line 99-10 shotpoints 580, 800; also line 99-09 shotpoints 700-900 and line 99-08 shotpoint 500), but also in tandem with east-vergent faults within seismic sequence II (line 99-09 shotpoints 1000 and 550 and line 99-11 shotpoint 790). This was an area of low topography, although east-vergent faults in the central and western portions of the basin at this latitude maintained the western $\sim 1/3$ of the basin at a somewhat high depositional position relative to the main depocenter of the basin, further east within sub-basin 'γ'. The Coastal Cordillera probably existed at the time, preventing drainage from the Pampa del Tamarugal, and encouraging accumulation of evaporites. Evaporite facies can be observed in the seismic data as low to medium amplitude, high frequency parallel reflections at the west end of lines 99-09 (Figures 2.7 and 2.22), 10, 11 and 12. At the western boundary of the basin, evaporites also filled in subtle preexisting topography, much as they do today in the same area along the eastern rim of the Coastal Cordillera.

At the end of this time interval, the volcanic eruptions responsible for the Altos de Pica member 2 ignimbrite undoubtedly had a substantial impact within the basin, especially nearest to the eruptive center in the northern and central sectors of the study area. It is likely that surficial drainage patterns, sedimentation, and surface water and groundwater chemistry changed significantly at ~ 20.6 Ma following this event.

20-16 Ma

Between 20 and 16 Ma during deposition of AdP member 3, structures in the north were particularly active, and water was relatively abundant in the basin. Areas of low topography were controlled largely by west-vergent, high angle reverse faults. In the north, these faults in many cases appear to have been blind, creating flexures rather than surface ruptures. Exceptions to these north-northwest-trending faults do exist, however. The main east-striking faults cutting through the center of the study area were active during and soon after this time, with 100's of meters of relief generated. The structural depressions were occupied by semi-permanent lakes in the center of the basin (Figure 2.15). Lake deposits are represented by limestone in the Pintados #2 well, and their seismic response, as generally transparent or low-amplitude, high frequency signal, appears in many areas throughout the basin during this interval. While these lakes may have been semi-permanent, they were shallow, and subtle variations in topography brought changes in depositional environment, with alluvial facies dominant in regions above lake levels in the center of the basin. The largest lake during this time was within the east-central sector of the basin, at times occupying a zone at least 15 km wide and 25 km long between 20 and 16 Ma. The deepest portion of this sub-basin records a seismic character consistent with lacustrine facies, and evaporite facies at the western edge of this lake reveal a fluctuating lake level, and help to define its extent.

A period of relatively humid conditions is reported regionally between 20-16 Ma, based on lacustrine deposits with silicified plant remains as far north as 18°45'S within the Central Depression in the

Lower El Diablo Formation (Parraguez, 1998). Very similar deposits were sampled at the Pintados #2 well in the western section of the Pampa del Tamarugal basin at 20°30'S (this study). Shallow lacustrine and playa facies near Cerro Challacollo, and seismic facies suggestive of lacustrine conditions at the south end of the study area, in conjunction with the other evidence of lacustrine and playa deposits previously mentioned, certainly attest to both the regional significance and probably relative stability of this humid interval. Also, the increased humidity during the time interval represented by the AdP member 3 lacustrine and playa deposits (relative to the increased aridity of the late Miocene) likely played a role in weathering of the Cerro Challacollo surface, which was already exposed by 20-16 Ma, if not sooner.

A strong east-west environmental gradient existed. Because the Precordillera was already in existence at this time, it provided detritus that filled any available accommodation space at the far eastern end of the basin with clastic sediments, especially sub-basin β (Figure 2.15). In the north, winds reworked the alluvial deposits to create cross-bedded aeolian sandstone, but in the south, fine and medium grained alluvial and fluvial deposits predominate. No lacustrine deposits exist near the eastern basin margin, which suggests that the depositional surface was likely at a higher elevation near the eastern basin margin than was the surface of the western part of the PdT. Relative to the clastic sediments which came later during the time of AdP member 5 deposition, finer-grained sediments dominate during deposition of the AdP member 3, even near the mountain front. This is despite the fact that there was likely enough water available at this time to generate the stream power

required to deliver coarse sediments to the basin. At this time, the Altiplano had attained less than half of its modern elevation (see Chapter 3; Gregory-Wodzicki, 2000, 2002; Garzzone, 2006). As a result, outweighing the increased discharge brought about by an increased moisture supply may have been the still relatively small relief between the Precordillera/Altiplano and the Pampa del Tamarugal basin. This would have resulted in a lower hydraulic gradient, and a lower sediment carrying capacity. Other unknown factors, including the sizes and reorganization of paleo-stream catchments, may have also played a pivotal role in delivering finer grain-sizes to the basin during this interval.

Although the largest sub-basin (β , Figure 2.15) existed at the eastern portion of the Pampa del Tamarugal basin, there also existed relative topographic high zones at this time, especially along seismic line 99-08. Most of this area has only very thin deposits of AdP member 3, so there was little accommodation. Basement rocks at this location that today stand above the surface of the pampa likely were also exposed during this time interval, as suggested by their highly weathered surfaces. Basement rocks associated with seismic sequence \emptyset , which today can be seen very near the surface, have probably also been very near the surface since at least the mid Miocene. Medium frequency, high amplitude reflections at the east end of 99-08 attest to the alluvial sediments that are mostly observed within Quebrada Maní and which filled small amounts of accommodation space around these basement highs.

Accommodation space was available for thick clastic deposits to accumulate at the east end of seismic line 99-03, in depocenter 'α' (Figure 2.15). However, by the Middle Miocene (~16 Ma), the margin of the basin had been transformed to become uplifted as part of the Precordillera (east ends of seismic lines 99-13, 99-04 and 99-05) through motion along a combination of north- and northwest-trending high angle west vergent faults. This is substantiated by the observation that a thick accumulation of the AdP member 4 (Huasco Ignimbrite, ~16.3 Ma) is found within the sub-basin 'α' syncline, but it is absent immediately to the south where there was no accommodation space available.

Having begun during deposition of at least a portion of AdP member 1, an approximately 15 km-wide sub-basin (β) continued to develop during deposition of AdP member 3 (Figure 2.15), almost entirely uninterrupted by internal structural complications (Figure 2.8). This sub-basin was even larger than the current depression mapped using seismic data (Figure 2.12). Faulting at its western limit has dissected this sub-basin, exposing at the surface examples of the lacustrine and playa lithofacies (Cerro Challacollo and Cerrito Chipana outcrops, [Figure 2.5]) deposited within it. This sub-basin was present at the same time that the east end of seismic line 99-04 was characterized by a lack of accommodation space. This part of the basin is located at the intersection of north- and north-northwest trending fault sets. It is the combined vertical throw of the north- and northwest-trending faults prior to the deposition of the AdP member 4 (~16.3 Ma, Tomlinson *et al.*, 2001) that created increased elevation of these Mesozoic basement rocks in this area relative to their surroundings. This local structural relief generated

by early Miocene uplift is also illustrated by the change in geometry of the eastern sub-basin along strike. There was accommodation space at the eastern end of seismic line 99-13 and 99-05 during the deposition of the AdP member 3, but none available for the deposition of AdP members 3 and 4 at the eastern end of line 99-04. As the north-northwest trending fault set dies to the south, accommodation space increased at the eastern end of seismic lines 99-05, 99-06, and especially 99-07, reflected by the increased thickness of Cenozoic strata (Figure 2.12).

16-11 Ma

An increase in the proportion of coarse grained clastic sediment associated with an alluvial environment is seen in the deposits of AdP member 5 at approximately 16 to 11 Ma, with a general disappearance of lacustrine and evaporite facies across much of the basin (Figure 2.15). This shift is likely the result of a decrease in overall available moisture, with insufficient moisture to maintain lakes at the center of the basin, but with still enough precipitation and stream power available to deliver sediments to the basin via flash-floods. Sediment source also appears to be closer to the basin, with clasts in general becoming larger and less well-sorted. The AdP member 5 is also in general a thinner unit than AdP member 3 (Figure 2.15) even though they both represent approximately the same amount of time, reflecting a decreasing ability to deliver sediments further to the west into the center of the basin. A decrease of structural deformation in the northern sector of the basin may have

eliminated localized depressions, and once these systems will filled with sediments, accommodation space disappeared.

Relatively thin deposits are represented by post AdP member 3 rocks in the southwestern corner of the study area, and what is encountered is mostly distal alluvial fan deposits. This in tandem with the lack of playa and lacustrine facies in the central portion of the basin, indicates a dramatic decrease in moisture. Structural depressions were still being created, as this was a time of increased faulting in the southern sector of the study area, but these depressions were no longer able to support lakes of any significance due to the decreased water inflow into the basin.

The northern portion of the study area experienced a filling of accommodation space by the lacustrine deposits prior to ~16 Ma, and accommodation space was further limited as a result of uplift along the Western Thrust System, especially north of seismic line 99-05. The notable exception to this is in areas to the east of faults with shallow dipping backlimbs which created sub-basins, such as sub-basin 'α' (Figures 2.12 and 2.15) between lines z1f-003 and 99-03. Here, sediment either traveled short distances from the nearby mountain front to collect on the eastern side of fault blocks, in a setting similar to accumulations on the eastern side of the Oxaya Anticline (Garcia and Hérail, 2005) along strike of the Andean mountain front further north, or were blown in from the center of the valley to the west. Other than this exception, the northeastern region had largely become a sediment bypass zone, with deposition likely being transferred either to the western portion of the Pampa del Tamarugal basin (sub-basin δ), along the axis of the basin to

the south where accommodation space within sub-basin β was still in existence at this time (Figure 2.15), or perhaps to the north of our study area.

~7-5.3 Ma

After the deposition of AdP member 5, a large gap in the stratigraphic record indicates little in the way of depositional activity. During this hiatus, pediplanation was extensive and the landscape was dissected. Due to a lack of chronological control, it is not known what conditions were like in the center of the basin itself. Since much of this region may have been fed by groundwater responsible for evaporites, it is possible that the continued deformation observed in the central and southern portions of the seismic grid could have allowed for continued creation of local depocenters that were fed by groundwater, producing evaporites (*e.g.*, Hilaricos Anhydrites of Sáez *et al.*, 1999, an undated formation of evaporites beneath ~6 Ma limestones and sulphate evaporites.) But it is also quite possible that conditions were dry enough that even the groundwater source vanished. A pulse of deposition occurred during the latest Miocene-Pliocene (?) (Figure 2.3), manifested in alluvial fans mostly in the central and southern portions of the study area, which in many places are observable as the surface cover within the central axis of the basin. Accumulations of evaporites and lacustrine marls interfingered with fluvial deposits, and are found in the southwestern portion of the basin during this wet episode. By the early Pliocene, these deposits largely ceased, reflecting another decrease in moisture during this time.

Discrete sub-basins and sediment bypass zones have been reported at the western limit of the sedimentary basin during the late Miocene (Chong *et al.*, 1999; Pueyo *et al.*, 2001; Sáez *et al.*, 1999). Taken together, studies which detail reactivation of faults in the Coastal Cordillera, and the new recognition that structures within the Coastal Cordillera also extend into the Central Depression, allow for fault reactivation as a mechanism for the creation of the Lomas de Sal. It seems reasonable to speculate that a basin with a surface area and trend similar to basins which have developed at the southwestern corner of the study area at various times during the Neogene as a result of normal fault activity (*e.g.* western end of lines 99-08 and 99-09 between ~21-16 Ma, Figure 2.15) or a combination of normal and reverse faulting (*e.g.*, at the west-central portion of line 99-11 after ~7 Ma, Figure 2.15) developed during the late Miocene at the current location of the Lomas de Sal. Such a basin could have originally received freshwater sourced from ephemeral streams to the east, creating a saline lake, and depositing the limestone, gypsum and anhydrite as detailed by Pueyo *et al.* (2001) and Sáez *et al.* (1999). Subsequently, the area near the Lomas de Sal was downdropped during latest Miocene-Pliocene (?) normal faulting. This same normal faulting could have produced the conduits for flow of very saline groundwater, since thick halite deposits in this region are generally the result of highly concentrated and evolved waters having accumulated appreciable Na and Cl while migrating through the subsurface (Chong *et al.*, 1999). Given the high degree of late Miocene – Pliocene (?) structural activity at precisely the location of the thickest accumulation of evaporites at the southwestern sector of our study area, a large proportion of the water may have traveled long distances underground. A

plausible scenario is that the water traveled through groundwater seepage from the Altiplano to the east, ascending from deep aquifer systems through fault networks at this basin center location. After accumulation of the ~100 m of halite, these faults may have become reactivated in a reverse sense, uplifting the entire structure. The W-E trend of the northern portion of the Lomas de Sal is consistent with trends of reverse faults seen to the west in the coastal Cordillera, as well as only 40 km to the north as the southern-bounding fault of Cerro Challacollo. One hundred meters of structural inversion since 5.56 Ma of the Lomas de Sal is of greater magnitude than what has thus far been documented in the Coastal Cordillera. However, the seismic data adjacent to the Lomas de Sal confirm this possibility by indicating a disruption of reflectors to the degree necessary to produce this amount of uplift. We have also documented small-scale normal and reverse faults in outcrop to the northeast of the Lomas de Sal, and within the incised canyons in the Lomas de Sal itself, so we know that faulting of both of these styles have been active in the region since 5.56 Ma.

Based on the comparison of stratigraphy between outcrop, borehole and seismic data, there is clearly a high degree of lateral variability within the Miocene-Pliocene sedimentary system. However, this should come as no surprise given the variability observed in the modern landscape. For example, evaporitic basins such as Salar de Llamara containing modern brines saturated in calcite and gypsum lie adjacent to alluvial fans and emergent basement rocks within and immediately adjacent to the Coastal Cordillera.

Conclusions

We conclude that temporal changes within the basin during the Neogene were related to climatic forcing. Sediment delivery to a basin in a hyperarid environment is not only a function of sediment supply related to relief at the basin margin, but also the availability of mechanisms for weathering and sediment delivery. Stream power must be sufficient in order for sediment to be transported from high elevation locations to the basin.

The nonmarine depositional sequences, and their associated sequence boundaries, within the Pampa del Tamarugal appear to be primarily controlled by climate. Deformation within the basin is not of sufficient magnitude to modify regional depositional patterns sufficiently to drive sequence generation, nor is the timing of deformation clustered in correspondence with the timing of the sequences or sequence boundaries to suggest a causal relationship.

Observations in arid environments illustrate that dune field preservation and growth is assisted by groundwater (Swezey, 2001; Chen *et al.*, 2004). This water anchors the dune in place by filling pore spaces through capillary action. Today, the largest dune field in the study area is observed near the village of Pica, where perennial streams and oases provide the stability necessary for their support. This realization helps to explain the fact that the greatest dominance of dune fields was during a period of greater moisture, during the time of AdP member 3 deposition from ~20 to 16 Ma. At that time the evaporites in the center of the basin

(Soledad #1 borehole and Cerrito Chipana) attest to arid conditions, while simultaneously there was enough water present to maintain standing lakes and support plant growth, as well as to support growth and subsequent preservation of extensive dune fields.

Lacustrine facies were replaced by largely alluvial facies during and near the end of the deposition of AdP member 5 time basin-wide. Intensification of aridity along the western Andean slope after ~15 Ma, illustrated by numerous studies of proxy evidence (Alpers and Brimhall, 1988; Hoke *et al.*, 2004; Kober *et al.*, 2006, Rech *et al.*, 2006) resulted in lack of *in situ* weathering of many of the landforms created by previous deformation episodes. Sedimentation ceased entirely sometime soon after 11.62 Ma in the Pampa del Tamarugal. This is near the time of reported long-wavelength uplift of the Altiplano (see Chapter 3). Global aridity associated with the development and growth of the Antarctic ice cap in the Middle Miocene (Woodruff *et al.*, 1981; Zachos *et al.*, 2001) is nearly coincident with the end of supergene enrichment of porphyry copper deposits at 14 Ma, an oft-cited proxy for the onset of hyper-aridity in the Atacama Desert (Alpers and Brimhall, 1988). This global desiccation may have been enough of a forcing mechanism to change the environment within the study area from predominantly lacustrine to alluvial. Uplift of the Altiplano apparently accelerated at ~10 Ma (see Chapter 3; Gregory Wodzicki, 2000; 2002; Garziona *et al.*, 2006), perhaps attaining elevations close to its modern altitude by 6.8 Ma (Garziona *et al.*, 2006), intensifying regional aridity through orographic blocking of moisture derived from the east. This, combined with the Middle Miocene climatic deterioration, may have crossed an important threshold along the

western Andean slope, lowering discharge to the point where stream power was no longer sufficient to carry sediment downslope. This corroborates other findings that the end of sediment transport and deposition coincided with a shift to more arid conditions at ~10 Ma between 18 and 20.5°S (Hoke *et al.*, 2004). With no transport mechanism, sediment delivery into the basin ceased.

The apparently diachronous surface for the top of the El Diablo/Altos de Pica member 5 surface is interpreted as less an indicator of diachroneity of the onset of hyperaridity but rather variations within headwaters of the different regions. In the north, sediment delivery to the forearc basin allowed for continued aggradation until perhaps ~7.5 Ma, at least 3 million years longer than in our study area of the Pampa del Tamarugal. The difference in time of onset may be a function of catchment basin size at elevations, with larger and higher catchments north of ~20°S. Since precipitation, sourced from the east, is today primarily a function of elevation along the western Andean slope at this latitude (Houston and Hartley, 2003), catchments which extend to higher elevations will have increased discharge, and therefore, increased sediment carrying capacity. This is borne out by studies of late Miocene to Recent sediment transport further north along the western slope near Arica (Kober *et al.*, 2006). In areas south of ~20°S, the Andean Precordillera separates surface catchments from higher elevations further east, which places a severe limit on the potential amount of surface runoff, and thus, carrying capacity. The higher elevation within catchments and larger catchment size north of 20°S likely persisted to provide stream power above the threshold value for a longer period,

prolonging sediment transport and deposition into the basin. Even in that way, eventually desiccation along the western Andean Slope due to continued uplift and blockage of water-bearing airmasses from eastern sources won the battle.

At ~7 Ma, a rejuvenation of moisture into the Pampa del Tamarugal basin occurred. Since in all likelihood the Altiplano was already within several hundred meters of its modern elevation by this time (see Chapter 3; Garzzone *et al.*, 2006), oscillations in the degree of aridity related to global climate change, rather than orographic patterns, was the likely cause of this increased water supply to the basin. For several hundred thousand years, precipitation was enough to once again create lacustrine and playa environments (either via direct runoff or groundwater input) in the center of the basin (Sáez *et al.*, 1999; Pueyo *et al.*, 2001). There was also sufficient stream power to transport sediment by alluvial processes downslope from the Precordillera into the basin. This humid interval was relatively short lived, and except for sporadic intervals of sediment transport in the time-span from the Pliocene to Recent, sedimentation into the basin once again ceased. While the supposed breakthrough of the Río Loa through the Coastal Cordillera (Pueyo *et al.*, 2001; Sáez *et al.*, 1999) may have drained shallow lakes present in the latest Miocene at 21°30'S along the western edge of the basin, the Río Loa history does not explain the termination of alluvial deposition throughout the basin. Instead, climate was the primary driver for sediment transport during the brief late Miocene pluvial phase.

The recognition of widespread lacustrine deposits during much of the Middle Miocene also allows us to draw conclusions concerning the

history of the Coastal Cordillera and its topographic position relative to the adjacent Pampa del Tamarugal valley. The existence of long-lived lakes within the intramassif forearc basin as early as ~20 Ma indicates that these deposits collected within a topographically closed valley since at least the latter part of the early Miocene. Contemporaneous lacustrine strata 100's of kilometers to the north (Parraguez, 1998) indicate that a proto-Coastal Cordillera was present over a distance of at least 300 km between 19° and 22°S. While studies of the evolution of the modern canyons indicate that the modern Coastal Cordillera existed by the latest Miocene or early Pliocene (Hoke *et al.*, 2007; Sáez *et al.*, 1999), our results significantly extend back in time the origin of the Coastal Cordillera as a topographic barrier.

REFERENCES

- Allmendinger, R. W., Gonzalez, G., Yu, J., Hoke, G., and Isacks, B., 2005, Trench-parallel shortening in the Northern Chilean Forearc: Tectonic and climatic implications: *Geological Society of America Bulletin*, v. 117, no. 1-2, p. 89-104.
- Allmendinger, R. W., and Gubbels, T., 1996, Pure and simple shear plateau uplift, Altiplano-Puna, Argentina and Bolivia: *Tectonophysics*, v. 259, no. 1-3, p. 1-14.
- Allmendinger, R. W., Isacks, B. L., Jordan, T. E., and Kay, S. M., 1997, The evolution of the Altiplano-Puna plateau of the Central Andes: *Annual Reviews of Earth Science*, v. 25, p. 139-174.
- Alpers, C. N., and Brimhall, G. H., 1988, Middle Miocene climatic change in the Atacama Desert, northern Chile: Evidence from supergene mineralization at La Escondida: *Geological Society of America Bulletin*, v. 100, p. 1640-1656.
- Armijo, R., and Thiele, R., 1990, Active faulting in northern Chile; ramp stacking and lateral decoupling along a subduction plate boundary?: *Earth and Planetary Science Letters*, v. 98, no. 1, p. 40-61.
- Blair, T. C., and McPherson, J. G., 1994, Alluvial Fans and Their Natural Distinction from Rivers Based on Morphology, Hydraulic Processes, Sedimentary Processes, and Facies Assemblages: *Journal of Sedimentary Research Section a-Sedimentary Petrology and Processes*, v. 64, no. 3, p. 450-489.
- Caprio, 2007, A relative growth history of the Atajana Fault System, northern Chile, 19 deg S [Master thesis]: Cornell University, 327 p.
- Chen, J. S., Li, L., Wang, J. Y., Barry, D. A., Sheng, X. F., Gu, W. Z., Zhao, X., and Chen, L., 2004, Water resources - Groundwater maintains dune landscape: *Nature*, v. 432, no. 7016, p. 459-460.
- Chong, G., Mendoza, M., García-Veigas, J., Pueyo, J. J., and Turner, P., 1999, Evolution and geochemical signatures in a Neogene forearc evaporitic basin: the Salar Grande (Central Andes of Chile): *Palaeogeography, Palaeoclimatology, Palaeoecology*, v. 151, p. 39-54.
- Delouis, B., Philip, H., Dorbath, L., and Cisternas, A., 1998, Recent

crustal deformation in the Antofagasta region (northern Chile) and the subduction process: *Geophysical Journal International*, v. 132, no. 2, p. 302-338.

Dickinson, W. R., 1995, Forearc basins, *in* Busby, C. J., and Ingersoll, R. V., eds., *Tectonics of sedimentary basins*: Oxford, Blackwell Science, p. 221-261.

Dickinson, W. R., and Seely, D. R., 1979, Structure and Stratigraphy of Forearc Regions: *Aapg Bulletin-American Association of Petroleum Geologists*, v. 63, no. 1, p. 2-31.

Digert, F., Hoke, G., Jordan, T., and Isacks, B., 2003, Subsurface stratigraphy of the neogene Pampa del Tamarugal basin, northern Chile, *in* X Congreso Geológico Chileno, Concepción, Chile, p. 8.

Dingman, R. J., and Galli O, C., 1965, Geology and ground-water resources of the Pica area, Tarapaca Province, Chile, U. S. Geological Survey Bulletin: Reston, VA, USGS, 1-113 p.

Ewing, S. A., Sutter, B., Owen, J., Nishiizumi, K., Sharp, W., Cliff, S. S., Perry, K., Dietrich, W., McKay, C. P., and Amundson, R., 2006, A threshold in soil formation at Earth's arid-hyperarid transition: *Geochimica Et Cosmochimica Acta*, v. 70, no. 21, p. 5293-5322.

-, 2006, A threshold in soil formation at Earth's arid-hyperarid transition: *Geochimica Et Cosmochimica Acta*, v. 70, no. 21, p. 5293-5322.

Farias, M., Charrier, R., Comte, D., Martinod, J., and Herail, G., 2005, Late Cenozoic deformation and uplift of the western flank of the Altiplano: Evidence from the depositional, tectonic, and geomorphologic evolution and shallow seismic activity (northern Chile at 19 degrees 30 ' S): *Tectonics*, v. 24, no. 4.

Flint, S., Turner, P., Hartley, A., and Jolley, E., 1991, From Foreland Rift to Fore-Arc Basin - Tectonothermal Controls on Subsidence and Stratigraphic Development in the Mesozoic-Recent Salar-De-Atacama Basin, Chilean Andes: *Aapg Bulletin-American Association of Petroleum Geologists*, v. 75, no. 3, p. 575-575.

Galli-Olivier, C., 1967, Pediplain in Northern Chile and the Andean uplift: *Science*, v. 158, no. 3801, p. 653-655.

Garcia, M., and Herail, G., 2005, Fault-related folding, drainage network evolution and valley incision during the Neogene in the Andean

- Precordillera of Northern Chile: *Geomorphology*, v. 65, no. 3-4, p. 279-300.
- Garzione, C. N., Molnar, P., Libarkin, J. C., and MacFadden, B. J., 2006, Rapid late Miocene rise of the Bolivian Altiplano: Evidence for removal of mantle lithosphere: *Earth and Planetary Science Letters*, v. 241, no. 3-4, p. 543-556.
- González, G., Cembrano, J., Carrizo, D., Macci, A., and Schneider, H., 2003, The link between forearc tectonics and Pliocene-Quaternary deformation of the Coastal Cordillera, northern Chile: *Journal of South American Earth Sciences*, v. 16, p. 321-342.
- Gregory-Wodzicki, K. M., 2000, Uplift history of the Central and Northern Andes: A review: *Geological Society of America Bulletin*, v. 112, no. 7, p. 1091-1105.
- , 2002, A late Miocene subtropical-dry flora from the northern Altiplano, Bolivia: *Palaeogeography Palaeoclimatology Palaeoecology*, v. 180, no. 4, p. 331-348.
- Hartley, A. J., May, G., Chong, G., Turner, P., Kape, S. J., and Jolley, E. J., 2000, Development of a continental forearc: A Cenozoic example from the Central Andes, northern Chile: *Geology*, v. 28, no. 4, p. 321-324.
- Hoke, G. D., 2006, The influence of climate and tectonics on the geomorphology of the western slope of the Central Andes, Chile and Peru [Doctoral thesis]: Cornell University, 296 p.
- Hoke, G. D., Isacks, B. L., Jordan, T. E., Blanco, N., Tomlinson, A. J., and Ramezani, J., 2007, Geomorphic evidence for post-10 Ma uplift of the western flank of the central Andes 18 degrees 30'-22 degrees S: *Tectonics*, v. 26, no. 5.
- Hoke, G. D., Isacks, B. L., Jordan, T. E., and Yu, J. S., 2004, Groundwater-sapping origin for the giant quebradas of northern Chile: *Geology*, v. 32, no. 7, p. 605-608.
- Houston, J., 2001, The year 2000 storm event in the Quebrada Chacarilla and calculation of recharge to the Pampa Tamarugal aquifer: *Revista Geologica De Chile*, v. 28, no. 2, p. 163-177.
- , 2002, Groundwater recharge through an alluvial fan in the Atacama Desert, northern Chile: mechanisms, magnitudes and causes: *Hydrological Processes*, v. 16, no. 15, p. 3019-3035.

- Houston, J., and Hartley, A. J., 2003, The central andean west-slope rainshadow and its potential contribution to the origin of HYPER-ARIDITY in the Atacama desert: *International Journal of Climatology*, v. 23, no. 12, p. 1453-1464.
- Isacks, B. L., 1988, Uplift of the central Andean plateau and bending of the Bolivian orocline: *Journal of Geophysical Research*, v. 93, p. 3211-3231.
- Jensen, A., Dörr, M., Götze, H.-J., Kiefer, E., Ibbeken, H., and Wilke, H., 1995, Subsidence and sedimentation of forearc-hosted, continental pull-apart basin: the Quillagua trough between 21degs30 and 21degs45'S, Northern Chile, *in* Recent and ancient systems in lacustrine margins, abstracts, Antofagasta, Chile, p. 5-6.
- Kiefer, E., Dorr, M. J., Ibbeken, H., and Gotze, H. J., 1997, Gravity-based mass balance of an alluvial fan giant: the Arcas Fan, Pampa del Tamarugal, Northern Chile: *Revista Geologica De Chile*, v. 24, no. 2, p. 165-185.
- Kober, F., Schlunegger, F., Zeilinger, G., Schneider, H., Willett, S. D., Hovius, N., Brandon, M. T., and Fisher, D. M., 2006, Surface uplift and climate change; the geomorphic evolution of the western escarpment of the Andes of northern Chile between the Miocene and present, *Geological Society of America (GSA)*, Boulder, CO, p. 75-86.
- Kuhn, D., 2002, Fold and thrust belt structures and strike-slip faulting at the SE margin of the Salar de Atacama basin, Chilean Andes: *Tectonics*, v. 21, no. 4.
- Lamb, S., and Hoke, L., 1997, Origin of the high plateau in the Central Andes, Bolivia, South America: *Tectonics*, v. 16, no. 4, p. 623-649.
- Loveless, J. P., Hoke, G. D., Allmendinger, R. W., Gonzalez, G., Isacks, B. L., and Carrizo, D. A., 2005, Pervasive cracking of the northern Chilean Coastal Cordillera: New evidence for forearc extension: *Geology*, v. 33, no. 12, p. 973-976.
- Michalski, G., Bohlke, J. K., and Thiemens, M., 2004, Long term atmospheric deposition as the source of nitrate and other salts in the Atacama Desert, Chile: New evidence from mass-independent oxygen isotopic compositions: *Geochimica Et Cosmochimica Acta*, v. 68, no. 20, p. 4023-4038.

- Mitchum, R. M., 1977, Seismic stratigraphy and global changes of sea level. Part XI. Glossary of terms used in sequence stratigraphy, *in* Payton, C. E., ed., *Memoir of the American Association of Petroleum Geologists*: Tulsa, OK, American Association of Petroleum Geologists, p. 205-212.
- Mortimer, C., 1973, The Cenozoic history of the southern Atacama Desert, Chile: *Journal of the Geological Society of London*, v. 129, p. 505-526.
- Mortimer, C., and Saric Rendic, N., 1975, Cenozoic studies in northernmost Chile: *Geologische Rundschau*, v. 64, no. 2, p. 395-420.
- Mpodozis, C., Arriagada, C., Basso, M., Roperch, P., Cobbold, P., and Reich, M., 2005, Late mesozoic to paleogene stratigraphy of the Salar de Atacama Basin, Antofagasta, Northern Chile: Implications for the tectonic evolution of the Central Andes: *Tectonophysics*, v. 399, no. 1-4, p. 125-154.
- Muñoz, N., and Charrier, R., 1996, Uplift of the western border of the Altiplano on a west vergent thrust system, Northern Chile: *Journal of South American Earth Sciences*, v. 9, no. 3/4, p. 171-181.
- Munoz, N., and Sepulveda, P., 1992, Estructuras compresivas con vergencia al oeste en el borde oriental de la Depresion Central, norte de Chile (19 degrees 15'S): *Revista Geologica de Chile*, v. 19, no. 2, p. 241-247.
- Muñoz, V. A., 2007, Evolución morfoestructural del piedemonte Altiplánico Chileno durante el Cenozoico Superior entre La Quebrada de Tarapacá y La Quebrada de Sagasca (19deg45 - 21deg15'S) [PhD thesis]: Universidad de Chile, 118 p.
- Naranjo, J. A., and Paskoff, R., 1985, Evolucion Cenozoica del Piedemonte Andino en la Pampa del Tamarugal, norte de Chile (18 degrees - 21 degrees S): *Actas - IV Congreso Geologico Chileno*, v. 4, p. 5.149-5.165.
- Nester, P. L., Gayo, E., Latorre, C., Jordan, T. E., and Blanco, N., 2007, Perennial stream discharge in the hyperarid Atacama Desert of northern Chile during the latest Pleistocene: *Proceedings of the National Academy of Sciences of the United States of America*, v. 104, no. 50, p. 19724-19729.

- Ortlieb, L., Zazo, C., Goy, J. L., HillaireMarcel, C., Ghaleb, B., and Cournoyer, L., 1996, Coastal deformation and sea-level changes in the northern Chile subduction area (23 degrees S) during the last 330 ky: *Quaternary Science Reviews*, v. 15, no. 8-9, p. 819-831.
- Parraguez, G., 1998, Sedimentología y geomorfología producto de la tectónica cenozoica, en la Depresión Central, I Región de Tarapacá, Chile [Memoria de Título thesis]: Universidad de Chile, 108 p.
- Pinto, L., Herail, G., and Charrier, R., 2004, Sedimentación sintectónica asociada a las estructuras neógenas en la Precordillera de la zona de Moquella, Tarapacá (19° 15'S, norte de Chile): *Revista Geologica de Chile*, v. 31, no. 1, p. 19-44.
- Rech, J. A., Currie, B. S., Michalski, G., and Cowan, A. M., 2006, Neogene climate change and uplift in the Atacama Desert, Chile: *Geology*, v. 34, no. 9, p. 761-764.
- Rech, J. A., Quade, J., and Hart, W. S., 2003, Isotopic evidence for the source of Ca and S in soil gypsum, anhydrite and calcite in the Atacama Desert, Chile: *Geochimica et Cosmochimica Acta*, v. 67, no. 4, p. 575-586.
- Reutter, K. J., Scheuber, E., and Chong, G., 1996, The Precordilleran fault system of Chuquicamata, Northern Chile: Evidence for reversals along arc-parallel strike-slip faults: *Tectonophysics*, v. 259, no. 1-3, p. 213-228.
- Rieu, M., 1975, Les formations sedimentaires de la Pampa del Tamarugal et le rio Loa ("Norte Grande" du Chili): *Cahiers - ORSTOM, Serie Geologie*, v. 7, no. 2, p. 145-164.
- Sáez, A., Cabrera, L., Jensen, A., and Chong, G., 1999, Late Neogene lacustrine record and palaeogeography in the Quillagua-Llamara basin, Central Andean fore-arc (northern Chile): *Palaeogeography Palaeoclimatology Palaeoecology*, v. 151, no. 1-3, p. 5-37.
- Salas, R., Kast, R. F., Montecinos, F., and Salas, I., 1966, Geología y recursos minerales del departamento de Arica: Instituto de Investigaciones Geológicas, *Boletín*, v. 21, p. 1-114.
- Scheuber, E., and Andriessen, P. A. M., 1990, The kinematic and geodynamic significance of the Atacama fault zone, northern Chile: *Journal of Structural Geology*, v. 12, p. 243-257.
- SERNAGEOMIN, 2002, Mapa geológico de Chile, 3 sheets, Santiago,

Chile.

- Somoza, R., 1998, Updated Nazca (Farallon)—South America relative motions during the last 40 My: implications for mountain building in the central Andean region: *Journal of South American Earth Sciences*, v. 11, no. 3, p. 211-215.
- Soto, R., Martinod, J., Riquelme, R., Herail, G., and Audin, L., 2005, Using geomorphological markers to discriminate Neogene tectonic activity in the Precordillera of North Chilean forearc (24-25 degrees S): *Tectonophysics*, v. 411, no. 1-4, p. 41-55.
- Swezey, C., 2001, Eolian sediment responses to late Quaternary climate changes: temporal and spatial patterns in the Sahara: *Palaeogeography Palaeoclimatology Palaeoecology*, v. 167, no. 1-2, p. 119-155.
- Tomlinson, A. J., and Blanco, N., 1997, Structural evolution and displacement history of the West Fault System, Precordillera, Chile: Part 1. Synmineral history, *in VIII Congreso Geológico Chileno III*, p. 1873-1877.
- , 1997, Structural evolution and displacement history of the West Fault System, Precordillera, Chile: Part 2. Postmineral history, *in VIII Congreso Geológico Chileno III*, p. 1878-1882.
- Tomlinson, A. J., Blanco, N., Makshev, V., Dilles, J. H., Grunder, A. L., and Ladino, M., 2001, Geología de la Precordillera Andina de Quebrada Blanca-Chuquicamata, Regiones I y II (20degs30'-22degs30'S): Servicio Nacional de Geología y Minería, IR-01-20.
- Tomlinson, A. J., Mpodozis, C., Cornejo, P. C., and Ramirez, C. F., 1993, Structural geology of the Sierra Castillo-Agua Amarga Fault System, Precordillera of Chile, El Salvador-Potrerrillos, *in Second ISAG*, Oxford, p. 259-262.
- Tomlinson, A. J., Mpodozis, C., Cornejo, P. C., Ramirez, C. F., and Dimitru, T., 1994, El sistema de fallas Sierra Castillo-Agua Amarga: transpresión sinistral eocena en la Precordillera de Potrerillos-El Salvador, *in VII Congreso Geológico Chileno*, p. 1459-1463.
- Victor, P., Oncken, O., and Glodny, J., 2004, Uplift of the western Altiplano plateau: Evidence from the Precordillera between 20 degrees and 21 degrees S (northern Chile): *Tectonics*, v. 23, no. 4.

- von Huene, R., Weinrebe, W., and Heeren, F., 1999, Subduction erosion along the North Chile margin: *Journal of Geodynamics*, v. 27, p. 234-247.
- von Rotz, R., Schlunegger, F., Heller, F., and Villa, I., 2005, Assessing the age of relief growth in the Andes of northern Chile: Magneto-polarity chronologies from Neogene continental sections: *Terra Nova*, v. 17, no. 5, p. 462-471.
- Woodruff, F., Savin, S. M., and Douglas, R. G., 1981, Miocene Stable Isotope Record - a Detailed Deep Pacific-Ocean Study and Its Paleoclimatic Implications: *Science*, v. 212, no. 4495, p. 665-668.
- Wörner, G., Hammerschmidt, K., Henjes-Kunst, F., Lezaun, J., and Wilke, H., 2000, Geochronology (Ar-40/Ar-39, K-Ar and He-exposure ages) of Cenozoic magmatic rocks from Northern Chile (18-22 degrees S): implications for magmatism and tectonic evolution of the central Andes: *Revista Geologica De Chile*, v. 27, no. 2, p. 205-240.
- Wörner, G., Uhlig, D., Kohler, I., and Seyfried, H., 2002, Evolution of the West Andean Escarpment at 18 degrees S (N. Chile) during the last 25 Ma: uplift, erosion and collapse through time: *Tectonophysics*, v. 345, no. 1-4, p. 183-198.
- Zachos, J., Pagani, M., Sloan, L., Thomas, E., and Billups, K., 2001, Trends, rhythms, and aberrations in global climate 65 Ma to present: *Science*, v. 292, no. 5517, p. 686-693.

CHAPTER 3

EVIDENCE FOR LONG-WAVELENGTH WESTWARD ROTATION OF THE WESTERN ANDEAN SLOPE (20°45' - 21°45'S) FROM MIOCENE TO RECENT²

Introduction

A major thrust of current Andean research is to understand the timing and magnitude of the rise of the Altiplano-Puna plateau. Studies of this plateau, the second highest on Earth, are intended to improve understanding of the large-scale processes involved in mountain-building at this convergent, non-collisional boundary between the oceanic Nazca Plate and the continental South American Plate. Many factors appear to be involved in post-Mesozoic plateau uplift, and many are most likely inter-related. These include (but are not limited to) changes in the angle of the subducting Nazca Plate through time (James and Sacks, 1999), relative rates and directions of relevant plate motions (Pardo-Casas and Molnar, 1987; Somoza *et al.*, 1998), changes in intensity and location of arc magmatism (Kay *et al.*, 1994; Lamb and Hoke, 1997), climate and its role in delivering sediment to the oceanic trench, thus altering shear stresses along the plate interface at the subduction zone (Lamb and Davis, 2003), lower crustal delamination (Kay and Kay, 1993; Kay *et al.*, 1994; Molnar and Garzzone, 2007),

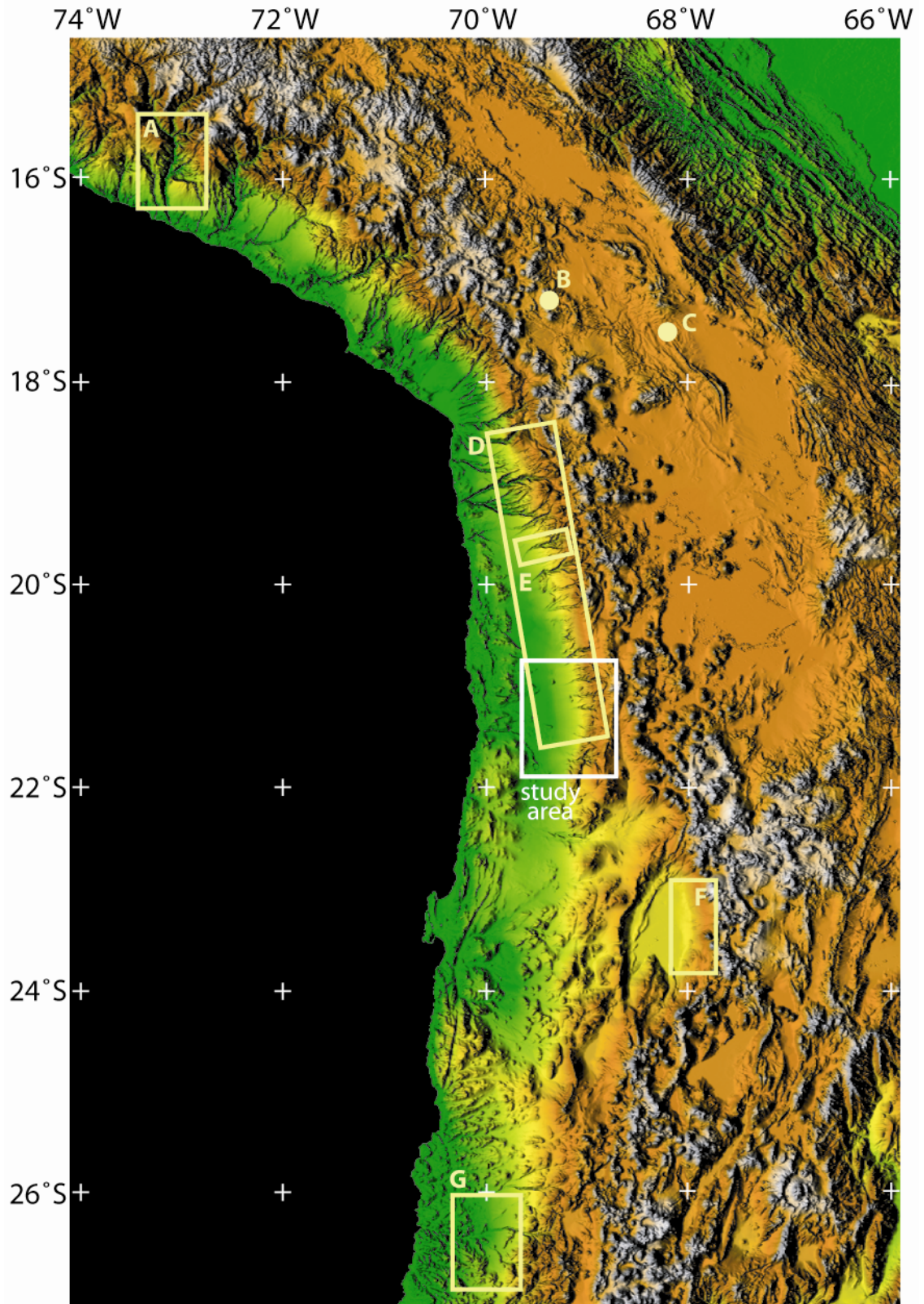
²Portions of the following chapter to be published with collaborators Blanco, N., Jordan, T., Hoke, G., and Tomlinson, A.

underplating of the lithosphere as a consequence of tectonic erosion (Baby *et al.*, 1997), middle- to lower-crustal flow (Barke and Lamb, 2006; Gubbels *et al.*, 1993; Isacks, 1988; Kley and Monaldi, 1998), heating and weakening of the crust due to various processes such as increased heat flow or flat slab subduction hydration of the lithosphere (James and Sacks, 1999), and deformation on the plateau and at its margins leading to crustal shortening and thickening (Beck and Zandt, 2002; Elger *et al.*, 2005; McQuarrie *et al.*, 2005).

Several methods have been employed at various locations of the Central Andes in an effort to ascertain the elevation history of the Altiplano-Puna plateau and of the surface which connects this morphotectonic province with the Central Depression (Figure 3.1). In recent years, the most often quoted evidence for Altiplano uplift has been the Gregory-Wodzicki (2000, 2002) paleoaltimetry studies based on analysis of leaf morphology of paleoflora. These estimates compare leaf morphologies with modern floral assemblages in order to derive paleotemperature at the site. The resulting estimation of mean annual temperature is then assumed to vary as a function of altitude, to which a terrestrial lapse rate is applied in order to derive a paleoelevation. Another method used in an attempt to quantify uplift is measuring oxygen isotopes from carbonates as a proxy for paleoprecipitation, and then inferring elevation based on modern changes in $\delta^{18}\text{O}$ values of stream waters with altitude (Garzzone *et al.*, 2006; Ghosh *et al.*, 2006).

Researchers have also used the vertical component of fault and fold offsets as a measure of progressive change of surface relief of the study area (Farías *et al.*, 2005; Muñoz and Charrier, 1996; Victor *et al.*,

Figure 3.1: Digital elevation model derived from 1 km resolution shuttle radar topography mission (SRTM) data illustrating other studies relevant to this study, with labeled morphotectonic provinces. Our study area is delineated by the white box. A = Schildgen *et al.*, 2007; Thouret *et al.*, 2007; B = Gregory-Wodzicki, 2000, 2002; C = Garziona *et al.*, 2006; Ghosh *et al.*, 2006; D = Hoke *et al.*, 2007; E = Farias *et al.*, 2005; F = Jordan *et al.*, 2006; G = Riquelme *et al.*, 2003. Inset cross section A-A' illustrates topography and, within the Pampa del Tamarugal valley, the base of Cenozoic strata.

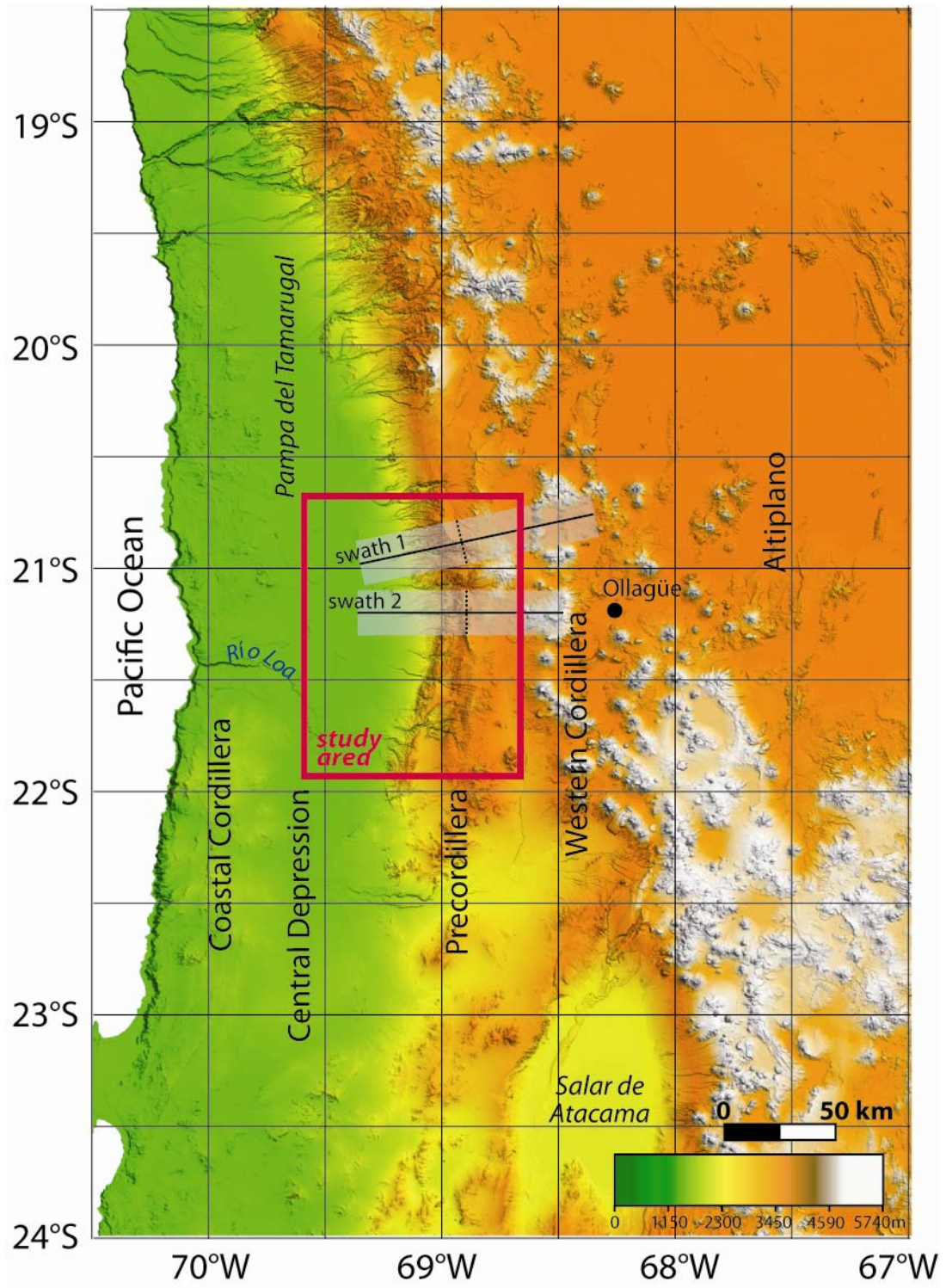


2004). Another method employed is the use of geomorphological indicators, which include measuring changes in surface tilts (Muñoz and Charrier, 1996) and stream incision (Fariás *et al.*, 2005; Hoke, 2006; Kober *et al.*, 2006; Muñoz and Charrier, 2005).

Many of these methods arrive at slightly different estimates for absolute elevation change or rates of plateau uplift. In addition, many of the previously mentioned methods are in fact proxies for different aspects of the evolution of the Cenozoic central Andean orogeny. For example, incision may or may not be a direct result of uplift, but could instead be measuring, among other things, climate change or drainage reorganization. Surface relief brought about by folds or faults measures relative changes in elevation, but is not a direct measure of surface uplift (Garzzone *et al.*, 2007; Holmes, 1965). However, each new study brings the evolution of the central Andes into a sharper focus.

The Western Andean Slope is a remarkably simple plane inclined 3-5° to the west (Hoke, 2006; Hoke *et al.*, 2007) which connects the forearc basins of northern Chile and southern Peru to the Altiplano plateau. The Western Andean Slope is about 50 km wide and 3000 m in relief, from the ~1000 m elevation of the forearc basins at its western side to the ~4000 m elevation of the Altiplano plateau on its east (Figure 3.2). At several latitudes, the dipping surface has been shown not to be shaped by surface-breaking discrete tectonic faults but rather to have been rotated by a long-wavelength folding process, hence to form a monocline (Hoke *et al.*, 2007; Isacks, 1988; Schildgen *et al.*, 2007).

Figure 3.2: Digital elevation model based on changes 90 m resolution shuttle radar topography mission (SRTM) data of the Central Andes with labeled morphotectonic provinces. Our study area is delineated by the red box. Location of the 20 km-wide swath profiles are shown, with the break-in-slope (or “rollover” of topography) along these swaths illustrated as a dashed line. Here, the western Andean slope rises at an angle of between approximately 3 and 5°, with minimal evidence for surface-breaking faults. The western Andean slope connects the Pampa del Tamarugal with the Precordillera and Altiplano, which has an average elevation at the latitude of this study of approximately 3700 m.



As pointed out by England and Molnar (1990), it is important to distinguish between surface uplift, rock uplift, and exhumation. Our objective is to measure surface uplift. Because erosion of the regional land surface is extraordinarily slow in the hyperarid Atacama Desert (values below 1 meter per million years have been measured by a variety of techniques; Dunai *et al.*, 2005; Ewing *et al.*, 2006; Hoke, 2006; Kober *et al.*, 2006), exhumation has been almost nil during the late Miocene to Recent except in the canyons of southern Peru and northernmost Chile (García and Hérail, 2005; Schilgen *et al.*, 2007; Schlunegger *et al.*, 2006; Thouret *et al.*, 2007). Consequently, for the area between 20 and 22°S that lacks deep canyons, we can focus on rock and surface uplift. Our objective is to apply the new chronologic and geometric description of the evolution of the Pampa del Tamarugal forearc basin (see Chapter 2) to quantification of the progressive increase in relief of the western Andean slope (Figure 3.3). The desired measure, of the creation during specific time intervals of structural relief between the forearc basin and Altiplano plateau, can be thought of as the increase of topographic relief through time of the catchment area of the basin. For most major sedimentary basins, there may have been some degree of tectonic subsidence of the basement of the basin which accommodated the accumulation of strata. If so, the structural relief that today exists between the west end and east end of a given relict landscape preserved in the basin and exposed on the Western Slope is a sum of absolute subsidence of the basin and absolute uplift of the Altiplano plateau. We

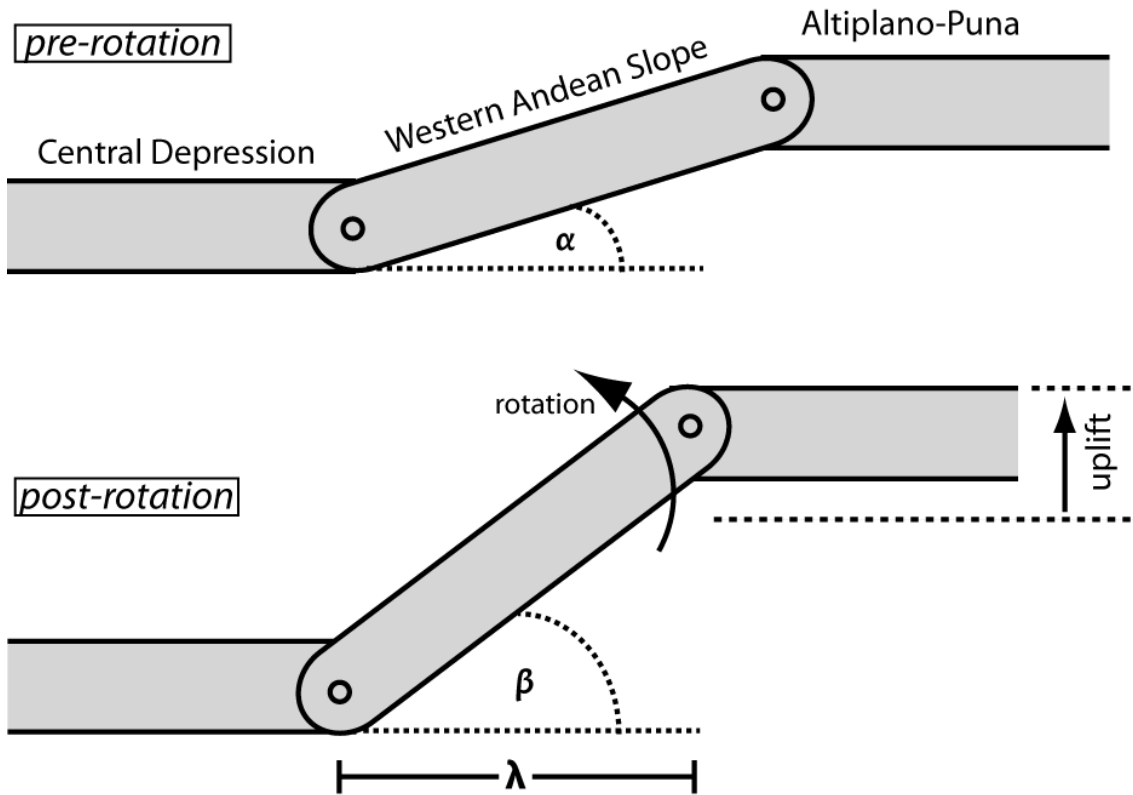


Figure 3.3: A schematic diagram illustrating proposed long-wavelength rotation which generated uplift of the Altiplano-Puna plateau. The difference between angles “ α ” (original depositional slope) and “ β ” is the degree of long-wavelength rotation of the western Andean slope. This rotation angle, in conjunction with the wavelength (λ) of rotation, is the basis for our uplift estimates. Modified from Lamb and Hoke, 1997.

reason (below) that the Pampa del Tamarugal experienced little or no tectonic subsidence, and therefore propose that the relief generated between these two landscape features was determined solely by the absolute elevation change of the feature which has varied (Figure 3.3).

Forearc sedimentary basins have no standard for tectonic subsidence: some subside by thousands of meters, others do not subside at all (Dickinson, 1995). The northern Chilean forearc is constructed on continental lithosphere and did not develop major sedimentary basins. Within the Central Depression, the Pampa del Tamarugal basin, the primary focus of this work, is an intramassif forearc basin in the sense of Dickinson and Seely (1979). The maximum thickness of Cenozoic strata is 1700 m, but at least 80% of the basin contains less than 1000 m of fill (see Chapter 2). If compensated isostatically this represents only ~300 m maximum of tectonic subsidence, and would be less if the elevation of the depositional surface increased while deposition progressed. By the standards of sedimentary basins, this is a small magnitude of tectonic subsidence. For a nonmarine basin, the best clues to the existence of tectonic subsidence contemporaneous with sedimentation are in the geometry of the subsurface strata. Large-offset faults commonly bound and subdivide basins that suffer tectonic subsidence; folds and inclined strata are evidence of those structures. Using those criteria, the sub-horizontal strata across the width of the Pampa del Tamarugal basin, a lack of faulted margins, and a lack of large-offset faults within the basin are good indications that there was no basin-scale tectonic subsidence. In contrast, these criteria and the facies patterns (see Chapter 3) support the interpretation that sediment ponded in a topographically closed

valley, whose depositional surface rose in elevation as strata accumulated.

Our approach to estimating a rise of the Altiplano plateau is to track through time the increase in topographic relief of the Western Andean Slope (Hoke *et al.*, 2007) through the recognition of planar surfaces which have undergone long-wavelength rotation (Figure 3.3). What we can measure is the magnitude of newly created structural relief from an unperturbed position within the forearc basin to a position part way to the crestline of its catchment basin. While our data only directly measure the monocline evolution for the lower part of the Western Andean Slope (elevations below 3500 m), the simplicity of the monoclinical form allows us to extrapolate the result to the lip of the plateau near 4000 m. We are then able to compare our results with those of the other studies along the western Andean slope which measure either absolute or relative elevation changes through time of various segments of the forearc (Table 3.1).

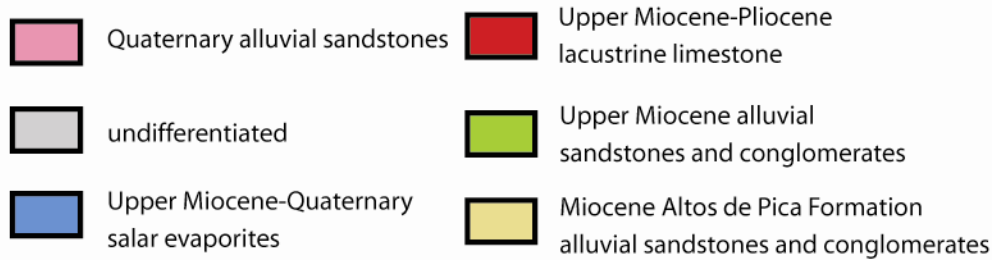
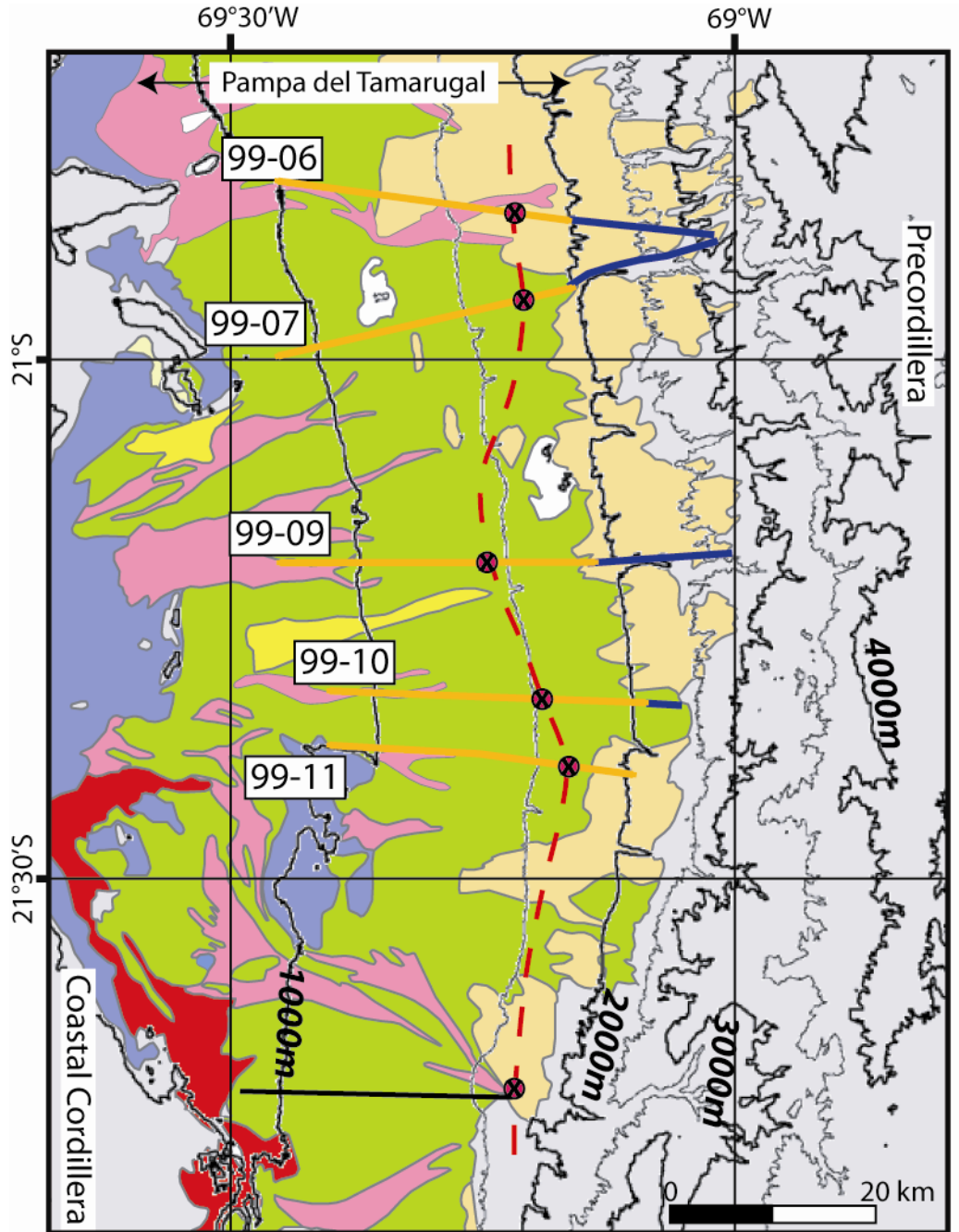
Stratigraphy

The Oligocene and Neogene stratigraphy of the Pampa del Tamarugal is largely dominated by nonmarine sediments consisting of a combination of alluvial, lacustrine and salar sediments (Figure 3.4), and primary and reworked extrusive volcanic material (ignimbrites and tuffs). The Oligocene and lower Miocene rocks are not observable at most locations in outcrop, but their relative positions and thicknesses have been determined from boreholes (Victor *et al.*, 2004; see Chapter 2) and

Table 3.1: Summary of uplift estimates of late Miocene to Recent Altiplano-Puna plateau. See Figure 3.1 for region that corresponds to each study

uplift estimate	time period	location (lat)	method	reference
2.4 km	since 9 Ma	~16° S	incision history	Schildgen <i>et al.</i> , 2007
2.78 ± 0.6 km	since ~10.7 Ma	17°17' S	leaf morphologies	Gregory-Wodzicki, 2002
2.5-3.5 km	10.3-6.8 Ma	~17°30' S	oxygen isotopes	Garzzone <i>et al.</i> , 2006
0.6-1.5 km	since 8 Ma	~19°40' S	structural back-calculation	Fariás <i>et al.</i> , 2005
1.08 ± 0.23 km	since 9 Ma	~18°30' - ~21°40' S	stream channel profiles	Hoke <i>et al.</i> , 2007
1.16 ± 0.48 km	since ~11 Ma	~20°45' - ~21°15' S	long-λ surface rotation	this study
1.9 ± 0.6 km	since ~10 Ma	~23°20' S	long-λ surface rotation	Jordan <i>et al.</i> , 2006

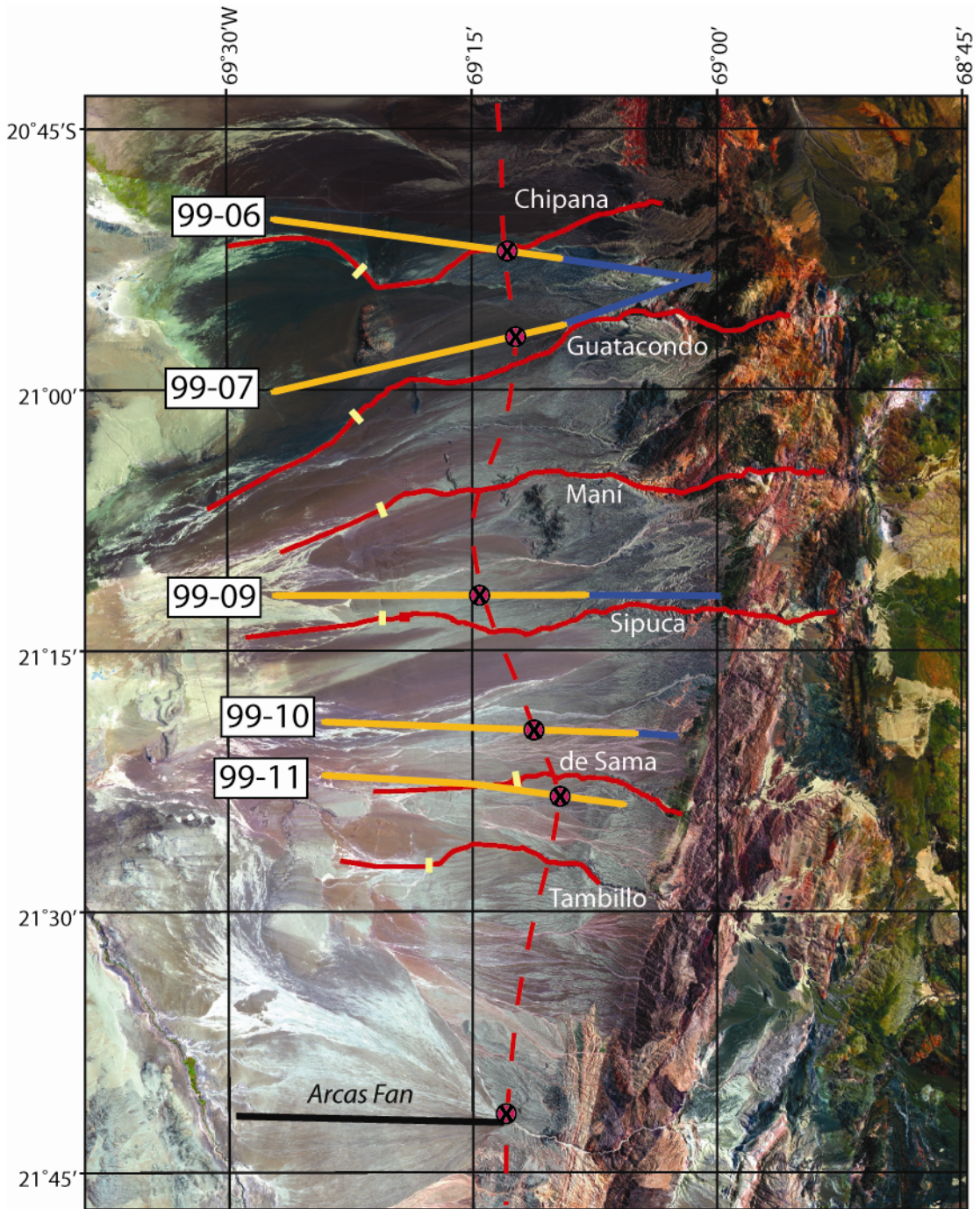
Figure 3.4: Geologic map with superimposed topographic contours (CI = 500 m). The map has been simplified to include only the units within the Pampa del Tamarugal that are relevant to this study. Orange lines represent seismic lines, and blue lines extending to the east represent topographic transects where they extend from the seismic data. 'X's represent locations of monoclinical fold axes based on these transects, and dashed red line indicates approximate location of monoclinical fold axis. Black line in the southern section of the map illustrates the location of topographic cross section in Figure 3.11



their spatial extent is known from seismic mapping (see Chapter 2). The Upper Oligocene to Middle-Upper Miocene deposits are known in the study area as the Altos de Pica (AdP) Formation, and are subdivided into members 1-5 based on lithologic variations observed in outcrop at ~20°30'S at the toe of the western Andean slope (Dingman and Galli, 1965). Close to the sedimentary source area of the Precordillera and Altiplano, the eastern limit of the Pampa del Tamarugal sedimentary basin is the AdP pinch out atop the pre-Neogene basement at elevations ranging from 2500 – 3500 m (Victor *et al.*, 2004; Figure 3.4). Overlying the AdP are poorly-consolidated Upper Miocene alluvial deposits. These have been best described at 21°40'S, where they comprise the Arcas Fan in the eastern basin (Kiefer *et al.*, 1997), and are intercalated in the western sector of the basin with the lower units of a sequence of Upper Miocene – Lower Pliocene (?) lacustrine limestone and evaporite deposits (Sáez *et al.*, 1999). These deposits are defined in this work as the Arcas Unit.

In the Pampa del Tamarugal basin, late Miocene sedimentation derived from higher elevations to the east occurred during two discrete time intervals. One period occurred at the end of the deposition of the Altos de Pica Formation. At an exposure within Quebrada Tambillo (Figure 3.5), a tuff near the top of the AdP member 5 dates to 11.62 ± 0.05 Ma (Ar/Ar biotite total gas). Above this tuff, an additional ~50 m of conglomerate was deposited, after which this depositional surface was abandoned. We assign an age of ~11 Ma as the end of deposition of the AdP member 5 in this region. Depositional abandonment formed a regional pediplain throughout our study area above these first Upper

Figure 3.5: Landsat TM image of the study area, illustrating the locations of channels (red lines) and seismic lines (orange lines) used in the study. Red lines indicate the locations of channel profiles detailed in Figure 3.8, and the yellow tick marks along their course indicate the point at which the channels transition from confined (upstream) to unconfined (downstream). Blue lines represent an extension eastward from the seismic data used for the surface profiles illustrated in Figure 3.8. Black line within the southern sector indicates the location of the Arcas Fan profile illustrated in Figure 3.11. Black 'X's show the approximate position of the monoclinial fold axis based on the seismic data (for lines 99-06, 99-07, 99-09, and 99-10), horizontal strata (line 99-11), and lack of rotation of the Arcas Fan. The dashed red line represents the approximate western limit of the rotated surfaces, and thus approximates the downdip hinge of the monoclinial fold.



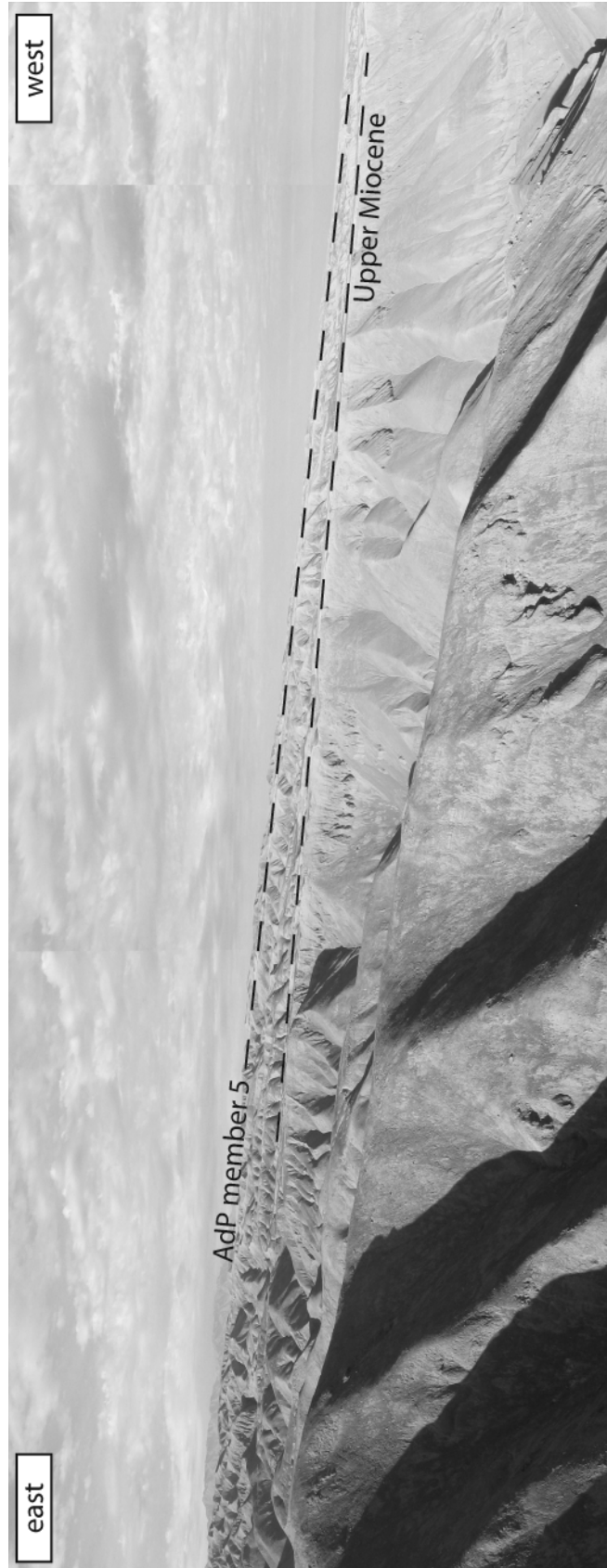
Miocene deposits. This pediplain is observable today as a moderately dissected surface whose interfluves, when connected, form a nearly planar surface (Figure 3.6).

This westward-dipping plane can be extended into the subsurface, where seismic data reveal that it continues beneath onlapping deposits. An ash within the Arcas Unit, the Carcote Ignimbrite, dates at 5.38 ± 0.09 Ma (Hoke *et al.*, 2007). Atop this ash at the latitudes of this study are typically another 10-20 meters of alluvial deposits. After the deposition of this unit, the primary aggradational phase within the basin ceased. Based on the age of the Carcote Ignimbrite, we assign an age of 5.3 Ma for the cessation of deposition for this latter phase of late Miocene deposition.

The Arcas alluvial fan is the result of the second late Miocene depositional phase, and is centered at $21^{\circ}40'S$. At its thickest point, the Arcas Fan attains a thickness of 200 m (Kiefer *et al.*, 1997), and is a spectacular example of a fossilized megafan, with a depositional surface that has experienced only minor reworking since its abandonment at the end of the Miocene. The fossilized nature of its surface is illustrated both by preservation of its symmetric cone-shaped morphology and the onlapping of the principally lacustrine, Uppermost Miocene –Lowermost Pliocene Quillagua Formation sediments above the fan apron along the Río Loa (Sáez *et al.*, 1999).

For this study, the most important attribute of the Miocene depositional environment is the primary depositional dip, which set the original geometry of the strata. Modern deposits are similar to those of

Figure 3.6: Photograph taken at ~2500 m elevation of the upper Quebrada de Sama catchment, looking south, which illustrated the relationships of dips of the pediplain surfaces (superimposed as dashed lines) atop the Arcas Unit and the Altos de Pica member 5. Note that even though dissection of the pediplain atop the AdP member 5 is quite extensive, a planar surface can still be defined. Also note that the dip of the AdP member 5 pediplain surface is greater than the dip of the pediplain atop the Arcas Unit.



the AdP member 5 and Arcas Unit, and thus inform us that environments during these three time intervals were most likely similar. The modern hyperarid environment produces infrequent sheetflood deposits at a periodicity of approximately 5 years (Houston, 2002), which fan out at the location where channels become unconfined, at elevations between 1000 and 1500 m. These sheetfloods produce poorly-sorted, tabular, matrix-supported conglomerates.

The geomorphology of alluvial fans is well described, and provides a guideline for our assumption about the geometry of the alluvial deposits of the AdP member 5 and Arcas unit prior to their burial and possible tectonic rotation. Blair and McPherson (1994), Calvache *et al.* (1997) and de Chant *et al.* (1999) illustrated that radial elevation profiles from the fan apex have a nearly planar to slightly concave form. Whipple *et al.* (1998) pointed out that radial profiles that transition from gently convex near the fan apex to gently concave in the medial and distal fan are expected of fans whose sediment transport is dominated by suspension, like those of the Pampa del Tamarugal.

While fluvial activity during the Quaternary resulted in terraced sediments of fluvial origin, has been reported in some of these same channels (Nester *et al.*, 2007), these unconsolidated deposits have all been abandoned and incised. Since this brief humid interval, channel gradients have readjusted to the infrequent flood events which construct the modern alluvial fans under the current hyperarid environment.

Methods

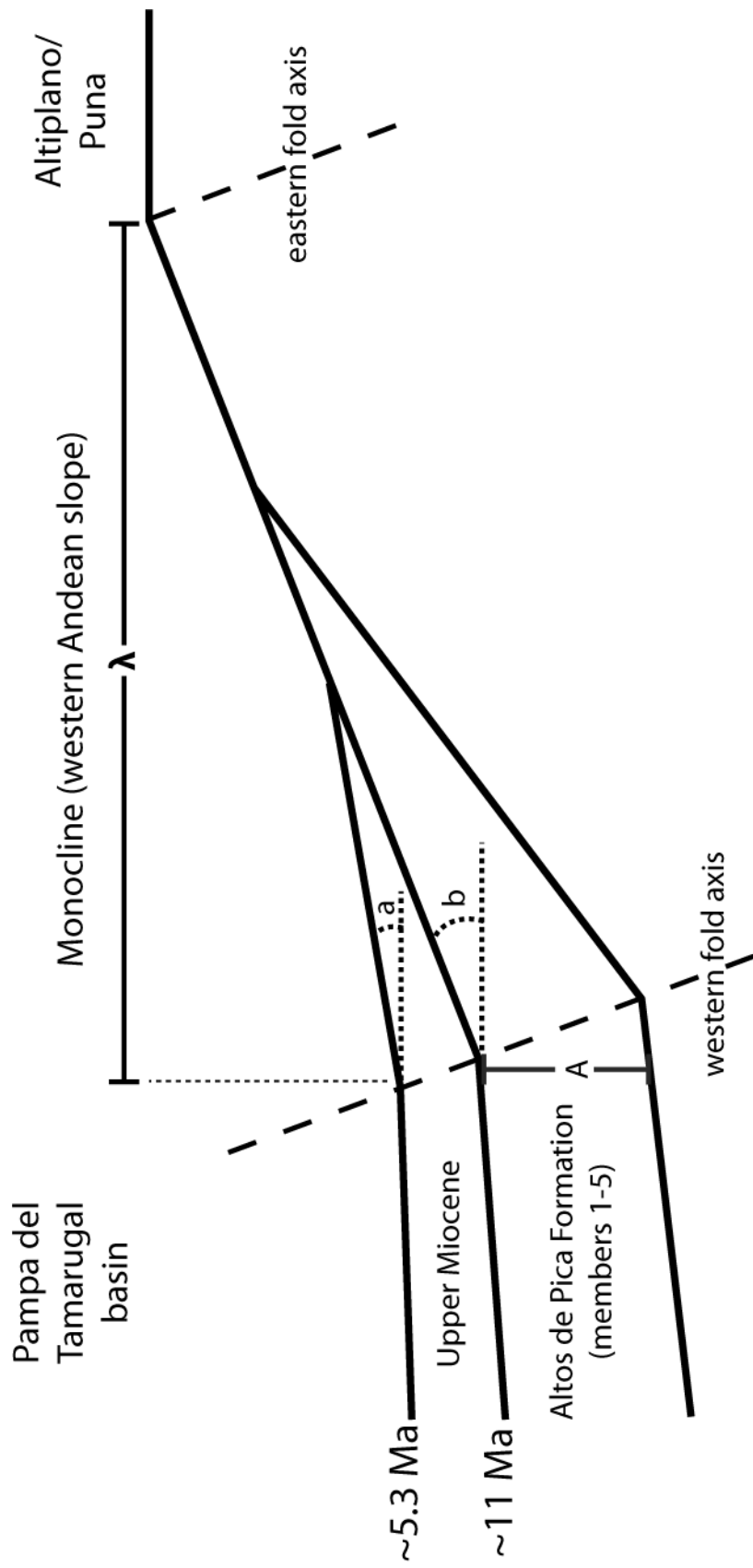
For this study, rotation angles of abandoned late Miocene depositional surfaces along the western Andean slope were measured from a baseline of the original depositional angle of alluvial fan surfaces. Therefore, in order to calculate modifications in slope through time for the Pampa del Tamarugal, a geometrical starting condition for the depositional surfaces needed to be defined. This was accomplished by the recognition of the depositional angles of modern and currently aggrading alluvial fan surfaces. Modern fan apices were located by close visual inspection of Landsat TM images and DEMs (90 m shuttle radar topography mission [SRTM] data) of ephemeral stream channels (Figure 3.5).

To be sure that the depositional angle is primarily the result of alluvial depositional processes, only stream channels which lack obvious recent tectonic perturbations near their transition from erosional to aggradational at the canyon mouths were considered. Six channels, Quebradas Chipana, Guatacondo, Maní, Sipuca, de Sama and Tambillo, were considered here as meeting the above criteria (Figure 3.5). (Although Guatacondo is considered a perennial stream along much of its course, it, too, becomes ephemeral at its distal, western end, and its sediments also fan out into an alluvial fan). Longitudinal channel profiles were created using the 90 m SRTM data, and depositional slopes were determined for a distance of 3 km downslope from the point of unconfined flow. This distance was used because it was both short enough to be useful as an original depositional angle, while long enough to smooth any artificial bumps which may have been produced owing to

the relatively coarse 90 m data resolution, which also has a vertical resolution of a few meters (B. Isacks, pers. comm., 2007). As such, this starting condition is considered to be the greatest depositional slope for the alluvial fan system within the Pampa del Tamarugal during the time intervals of interest for this study. Any difference between this reference slope and a slope observed for the ancient surfaces will therefore be a minimum estimate of change, and uplift calculated using this criterion can be considered a conservative estimate.

The modern dips of ancient surfaces were calculated using the paleosurfaces associated with sediments representing the end of AdP member 5 deposition and the end of the late Miocene depositional episode (Figure 3.7). Profiles from surface data were augmented by extending the slope of the AdP member 5 into the subsurface where it is buried beneath the onlapping Arcas Unit deposits. Based on geochronological constraints for the cessation of deposition for these two units, an age of 11 Ma for the abandonment of the AdP member 5 surface and of 5.3 Ma for the surface of the Arcas Unit has been assigned. The differential between the current angles from horizontal of these surfaces and the angles calculated for the modern alluvial system is considered to be the degree of post-depositional rotation of these surfaces. In addition, no surface-breaking faults were observed in the study area along the east to west transects considered here, and surfaces appear smooth and continuous over distances of 10's of kilometers. Therefore, any observed tilting of these surfaces is likely the result of long-wavelength rotation, rather than small-scale features which would only be of local structural interest.

Figure 3.7: Schematic diagram illustrating the various geometric relationships between the sedimentary units and surfaces described in this study. “a” and “b” are the angles of rotation which the surfaces which were abandoned at ~5.3 and ~11 Ma, respectively, have experienced. “ λ ” is the wavelength over which the rotation has occurred. “A” is the total current (compacted) thickness of the Altos de Pica Formation at the western monoclinial fold axis which is detailed for 3 locations in Table 3.3.



Along each seismic profile, we needed to identify the AdP member 5 and Arcas Unit and measure the positions of the unconfined surfaces above and below the Arcas Unit. Identification of surface stratigraphy was obtained from a combination of geologic maps, TM imagery, and field observations (see Chapter 2). Regional surfaces beneath the Pampa del Tamarugal basin floor from a 2D grid of seismic reflection data have been mapped using Kingdom Suite software. Seismic travel time to depth conversion using interval velocities at every 100 shotpoints (2.5 km horizontal distance) resulted in depths to the reflectors. We utilized our knowledge of the surface geology from field observations along the traces of the seismic lines to tie surface stratigraphy to reflections, especially the locations where reflectors intersect with the land surface. This allowed for the extension of surface dip angle observations into the subsurface further to the west. The angles of the two stratigraphic horizons of interest were calculated along seismic lines 99-07, 99-09 and 99-10, and to the east of these seismic lines to the up-dip limit of the surface of the AdP member 5 deposits (Figures 3.4 and 3.5). Conversion of time to depth for selected locations of these seismic lines at the shortest possible horizontal intervals allowed by the data (*i.e.*, at each shot point for which stacking velocities are reported) was carried out to test the magnitude of errors owing to lateral variability of stacking velocities could be detected.

It was also necessary to determine if within the Pampa del Tamarugal basin there is a western limit of the long-wavelength rotation (lower hinge, Figure 3.3). This was accomplished by analyzing the geometry of stratigraphic surfaces in order to identify whether westward

decreases in slopes were present which outpaced decreases in original depositional angles. Breaks in slope of subsurface seismic reflections corresponding to the upper surface of the AdP member 5 were compared with observations of changes in slope of the upper surface of the Arcas Unit at the modern land surface. These observations were combined with the identification of paleohorizontal subsurface reflections, and determinations as to whether or not these reflections had undergone post-depositional rotation.

The eastern rotation limit (upper hinge in Figure 3.3) was defined by the break in slope of the broad and continuous topographic surface of the western Andean slope. This low relief pediplain surface extends to the east of the position of onlap of the Altos de Pica into the Precordillera. In its eastern part, it is underlain by Mesozoic sedimentary rocks (Figure 3.4). To determine location of the break-in-slope (or “rollover” of topography) from the western Andean slope to the Altiplano, two west-to-east swath profiles were constructed using the 90 m SRTM digital topography, calculating mean elevations along the paths of the seismic lines considered for this study (Figure 3.2; northern swath brackets spans seismic line 99-07; southern swath spans between 99-09 and 99-10). These two swaths are each 20 km wide, and were calculated at 500 m intervals along the paths, thus providing an average topography covering a total of 40 km north-south distance parallel to the mountain front on which the position of the rollover between the Altiplano and the western Andean slope was identified and transferred to a basemap.

Potential compaction of the strata related to burial was addressed for the AdP in order to determine possible contributions to the apparent

angles of rotation. The three transects that were studied, 99-07, 99-09 and 99-10, have maximum thicknesses of between ~950 and ~1200 m (see Chapter 2) of Cenozoic sediments within the segment which has undergone rotation. Sediments within local depocenters at the west end of the transects will compact more than the relatively thin sedimentary deposits to the east. This differential compaction must be recognized and removed from the modern measure of westward inclination in order to isolate the effect of tectonic rotation, which we want to quantify. Decompaction calculations were accomplished using the OSXBackstrip software (Cardozo, 2003) based on 35% depositional porosity.

Results

Calculations of depositional angles for modern unconfined alluvial sediments within the Pampa del Tamarugal for six channels (Figure 3.5) reveal an average angle of $1.8 \pm 0.2^\circ$, with a range between 1.6 and 2.0° (Figure 3.8, Table 3.2). This is near the lower limit of, but still within, the global data set for angles of deposition for alluvial sediments (Blair and McPherson, 1994). This angle of 1.8° is taken as the original depositional angle for all alluvial sediments considered as part of this study.

Ancient abandoned surfaces at the eastern limit of the Pampa del Tamarugal Basin reveal a progressive decrease in dip through time, from a mean of $4.3 \pm 0.8^\circ$ for the top of the AdP member 5, to $2.6 \pm 0.2^\circ$ for the top of the Arcas Unit. These alluvial deposits are compositionally and texturally similar, and thus are assumed to have had similar original angles at their times of deposition. The difference between the primary depositional dip ($1.8 \pm 0.2^\circ$) and the current dip of these surfaces ($4.3 \pm$

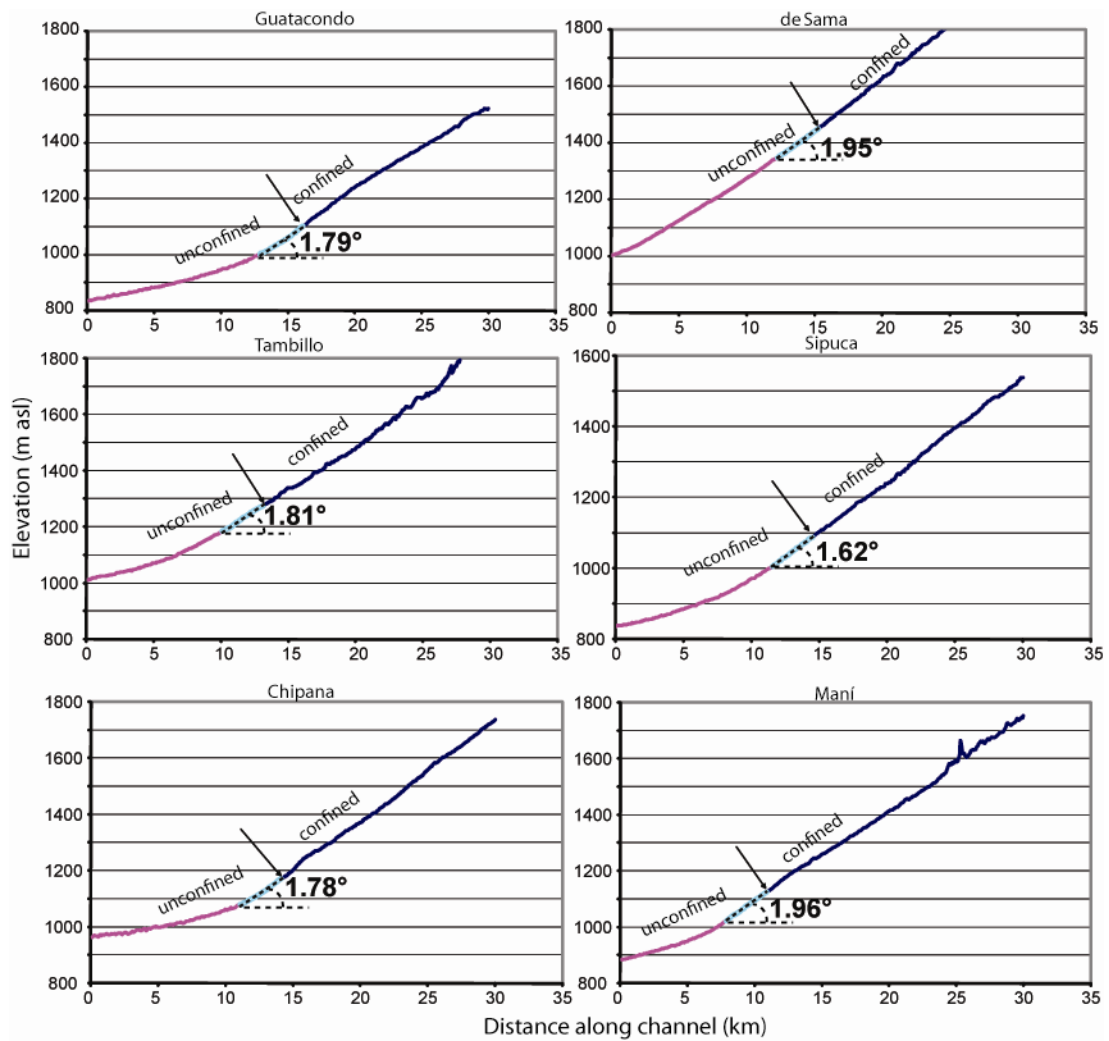


Figure 3.8: Longitudinal channel profiles for the six catchments used to determine the depositional angle for the modern alluvial system. The arrow indicates the point at which the channel becomes unconfined downstream. For the depositional angle, a linear best-fit line (dashed black line) was generated for the first 3 km (light blue line) of the unconfined segment of the channel. The angle this line makes with the horizontal is included for each channel.

Table 3.2: Modern depositional angles for 6 stream channels in the study area. “Distance” refers to length from the apex of the fan over which the measurement was calculated

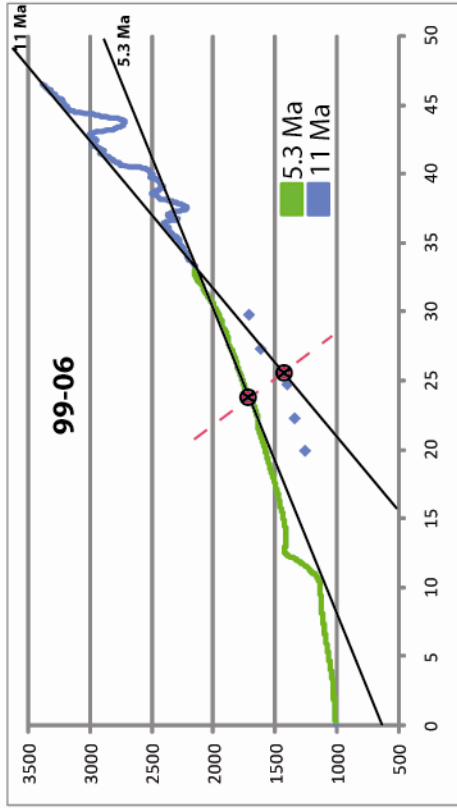
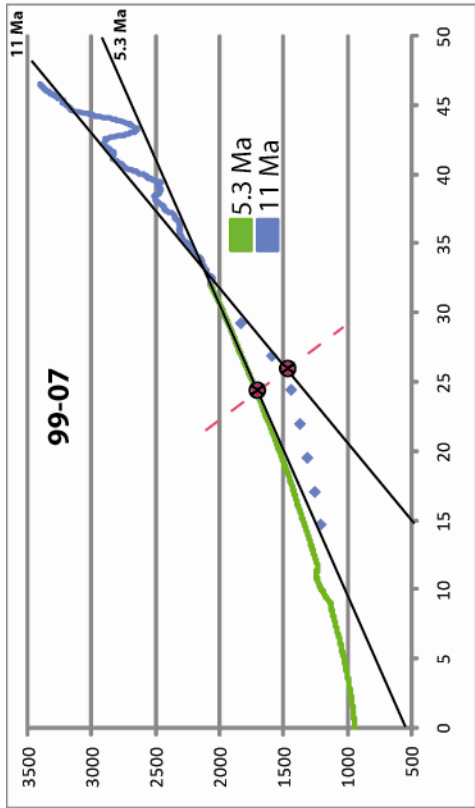
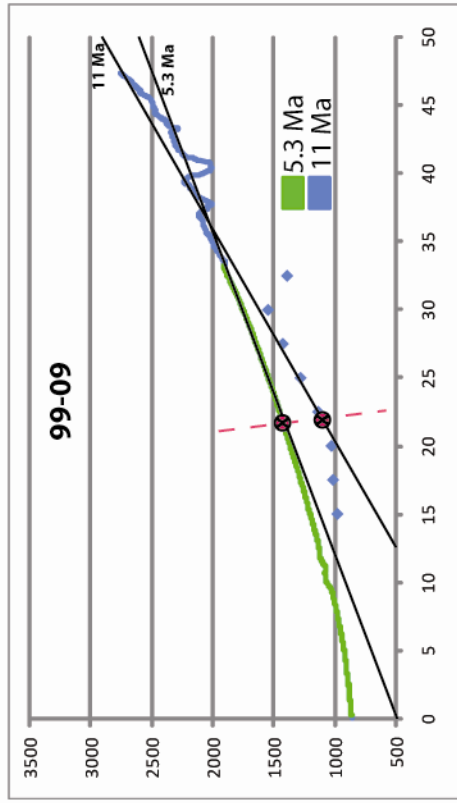
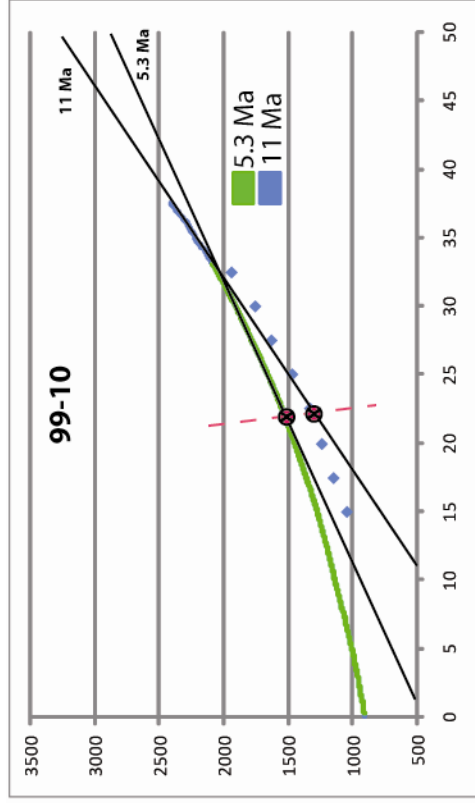
channel	distance (km)	modern angle (°)
Chipana	3	1.8
Guatacondo	3	1.8
Maní	3	2.0
Sipuca	3	1.6
de Sama	3	2.0
Tambillo	3	1.8
		mean: 1.8
		±0.2

0.8° and $2.6 \pm 0.2^\circ$) represents the post-depositional rotation, which is a combination of compaction and tectonic rotation. (Figures 3.8 and 3.9). After subtraction of the compaction rotation of the Altos de Pica Formation, the average slope along three roughly parallel profiles that are perpendicular to the regional topographic slope atop AdP member 5 deposits is $4.0 \pm 0.7^\circ$ (Figure 3.9, Table 3.3). The slope along these same transects atop the Arcas Unit averages $2.6 \pm 0.2^\circ$ (Figure 3.9, Table 3.3). No clear north-south trend is detected for either surface. Uncertainties on the angles include the accuracy of the conversion of seismic travel time to depth, and several assumptions needed to calculate burial compaction (depositional porosity, current porosity, diagenetic history).

Post depositional rotation of these Miocene surfaces is summarized in Figure 3.10. Assuming an original depositional angle of 1.8° of the AdP member 5 surface, rotation of 1.4° occurred between ~11 Ma and ~5.3 Ma. Onlap of the Arcas Unit thus took place atop an AdP member 5 which was inclined at an average angle of 3.2° . Since ~5.3 Ma, an additional rotation of 0.8° affected the 11 Ma AdP member 5 surface in addition to the Arcas Unit deposits, bringing the angles to the modern values of 4.0° and 2.6° , respectively.

Locations were identified where breaks in surface topographic slopes coincide with changes in slopes of the 11 Ma AdP member 5 surface along the seismic transects. These locations are interpreted as representing a west-vergent monoclinial fold axis (Figures 3.4 and 3.5).

Figure 3.9: Calculated angles of surfaces used to determine angles of rotation for 11 Ma and 5.3 Ma time periods along and to the east of seismic lines 99-06, 99-07, 99-09 and 99-10. Line 99-06 was not used for the calculation of surface uplift for statistical reasons due to its close proximity with line 99-07, but it is useful for helping to identify the western limit of rotation along the western Andean slope. Green line represents the upper surface of the Arcas Unit, and blue line represents the upper surface of the Altos de Pica Formation. Blue diamonds represent the surface of the Altos de Pica member 5 in the subsurface, converted from time to depth using interval velocities at 2.5 km intervals (100 shotpoints). Black lines represent the interpreted surface of the sediments that have been dissected (in the case of the Altos de Pica Formation) and rotated. 'X's represent change in angle of the surfaces, and the red dashed line indicates the interpreted location of the western limit of rotation.



distance from west end of seismic line (km)

elevation (m asl)

Table 3.3: Illustration of modern slopes of ancient surfaces for the three seismic lines used in this study. “a” and “b” show slopes of the surfaces abandoned at ~5.3 Ma and ~11 Ma, respectively. “A” and “A’” are the current thicknesses and decompacted thicknesses, respectively of the entire Altos de Pica Formation at the location of the western monoclinial fold axis. Compaction was calculated based on Sclater and Christie (1980) and Allen and Allen (1990) using N. Cardozo’s freeware OSXBackstrip, with initial porosity of 35% and a “c” value of 0.4. “ Δ ” represents the change in angle of the top surface of the AdP member 5 caused by compaction of the AdP unit. “b’” illustrates the angle of the top of the AdP derived by subtracting the compaction rotation value from the observed modern surface slope. ‘ λ ’ is the wavelength over which uplift estimates were applied.

seismic line	~5.3 Ma		AdP 1-5 thickness		~11 Ma			
	a (°)		A	A'	b(°)	Δ °	b' (°)	λ (km)
99-07	2.7		874	915	5.1	0.4	4.7	30
99-09	2.4		799	826	3.6	0.2	3.4	30.5
99-10	2.8		744	770	4.1	0.1	4.0	27.5
mean:	2.6				4.3		4.0	29.3
±	0.2				0.8		0.7	1.6

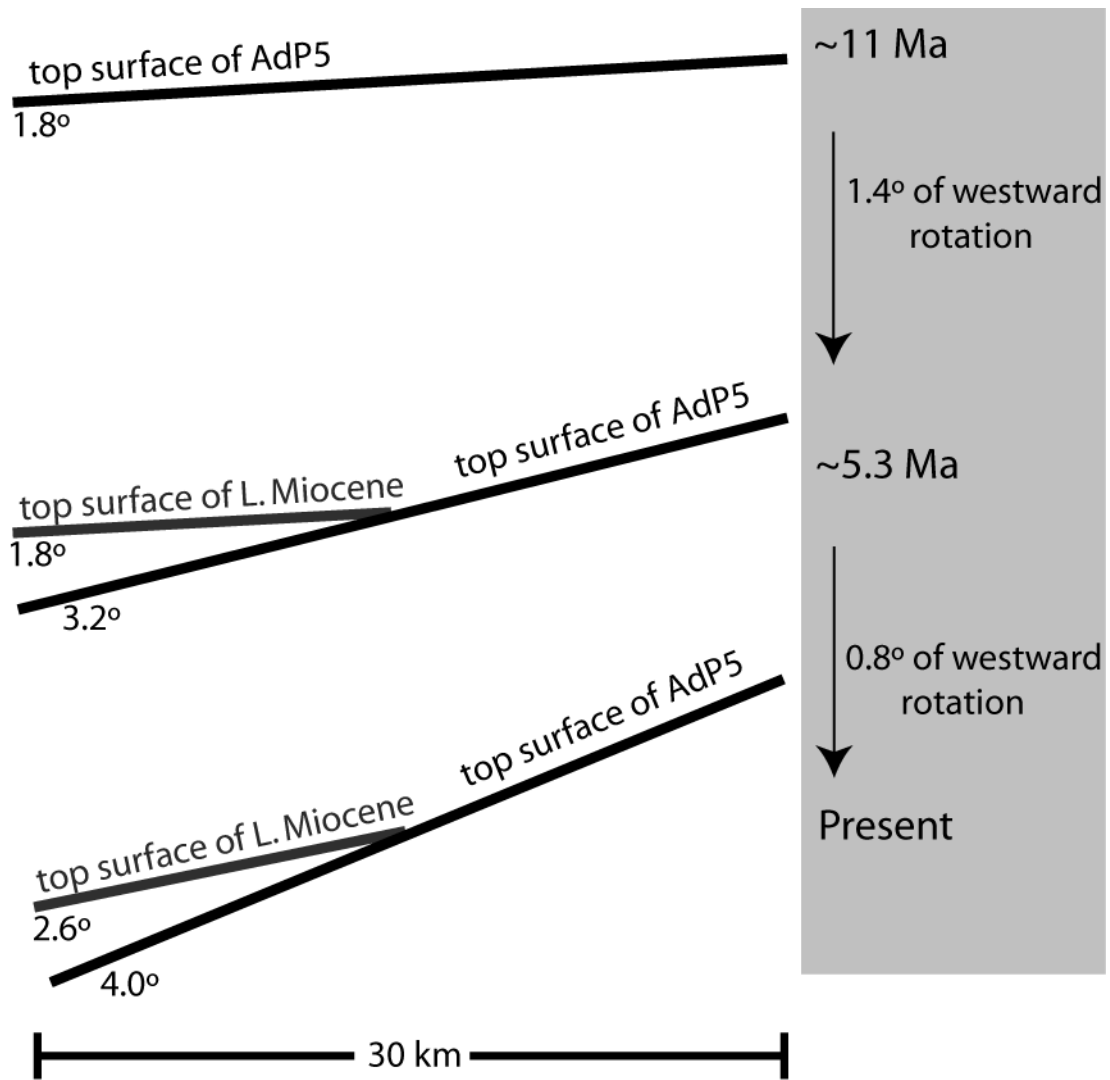


Figure 3.10: Schematic diagram of Late Miocene and Altos de Pica member 5 surfaces, and their calculated westward rotations through time, assuming an initial angle of deposition of 1.8° .

Just as revealing are profiles which do not show such evidence for post-late Miocene rotation. The modern slope of the Upper Miocene Arcas Fan provides an independent test for the western limit of surface rotation. A longitudinal profile from the apex of the fan to the fan apron (Figures 3.4 and 3.5) reveals a concave form (Figure 3.11). The maximum angle of this relict surface is at the fan head where, using the same constraints as were employed to calculate modern depositional angles, the first 3 kilometers yield a slope of $\sim 2.0^\circ$. This angle is at the upper limit within our measure of error for the modern depositional angles of the alluvial deposits (Figure 3.8; Table 3.2). This also informs us that if the tectonic rotations occurred after ~ 5.3 Ma at the latitude of $21^\circ 40'S$, they have not affected the Arcas Fan, since the calculated surface angle is within the range of the modern alluvial depositional system (modern range = $1.6^\circ - 2.0^\circ$, Arcas Fan = 2.0°). By inference, the western limit of surface rotation lies east of the apex of the Arcas Fan. It could even be argued that, because the surface dip of the most proximal part of the Arcas Fan is equal to the high end of the range, the fan head is almost exactly at the western limit of rotation, and has, as a result, experienced little or no rotation.

We obtain an additional constraint on the western limit of slope rotation from data near the eastern end of seismic line 99-11 (Figure 3.12). The seismic data reveal that Middle Miocene AdP member 3 is characterized by a transparent seismic facies that is interpreted as a lacustrine deposit (see Chapter 2), and that the sequence boundary above this member is horizontal near the east end of line 99-11. For this reflection representing the sequence boundary today to be horizontal

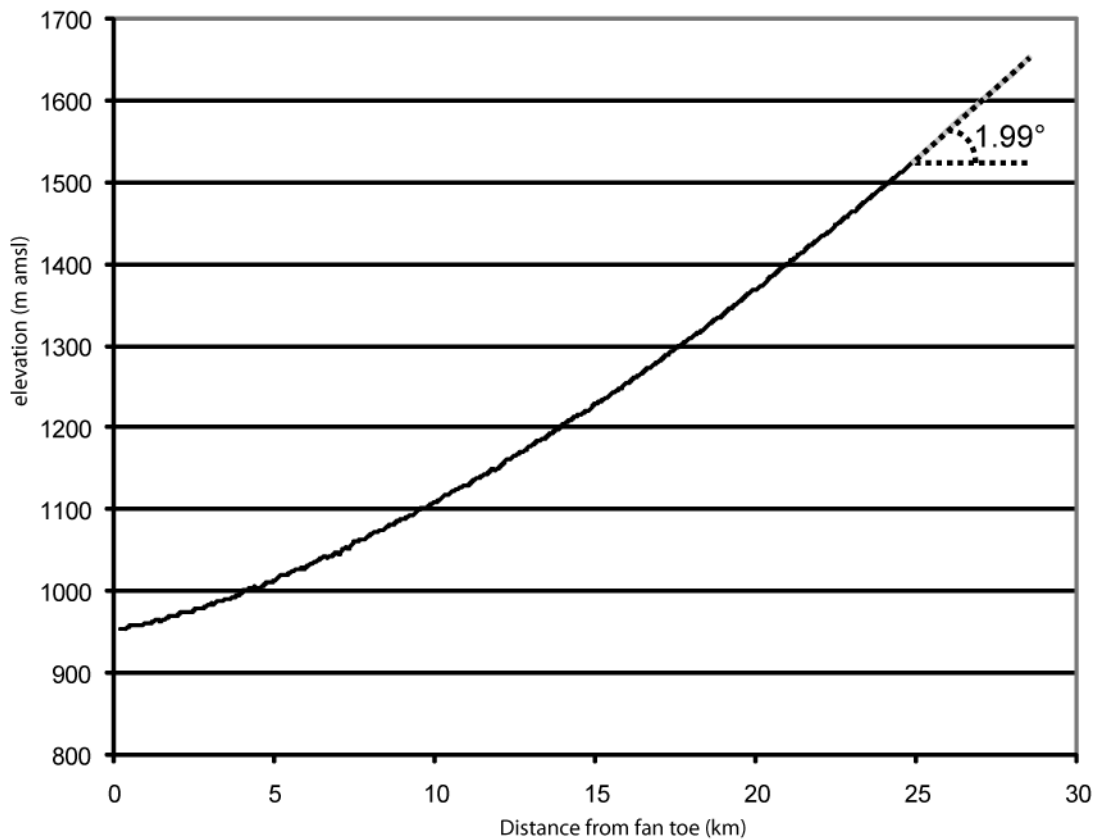
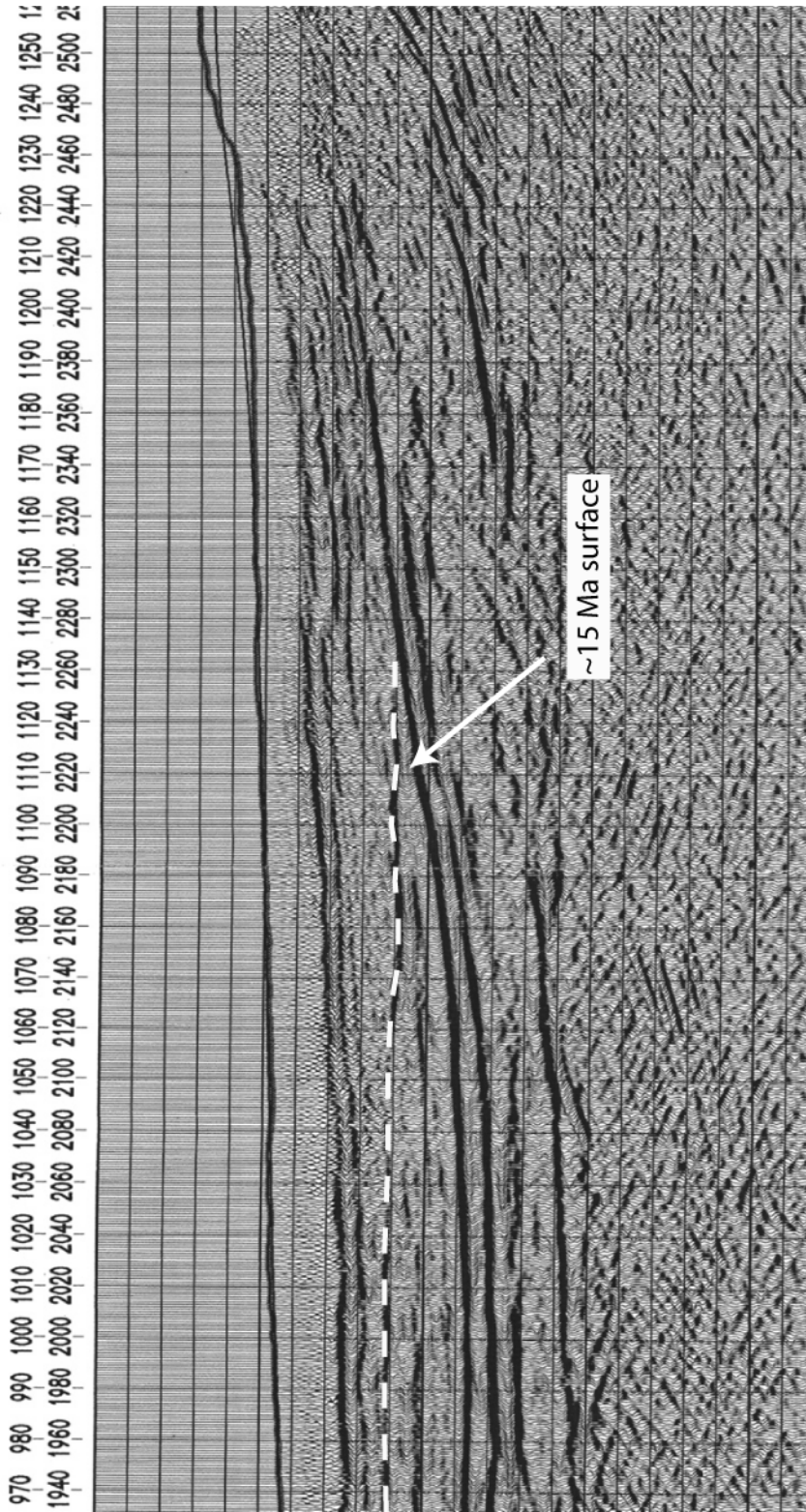


Figure 3.11: Longitudinal profile across the modern surface of the Arcas Fan (location of transect shown in Figures 3.4 and 3.5). The angle of 1.99°, calculated for the most proximal 3 km of the alluvial fan (gray line), is assumed to be very near the original angle of deposition, and has likely been unaffected by Pliocene-Recent rotation. A linear best-fit line was generated for the most proximal 3 km (black dashed line). The angle this line makes with the horizontal is included. This surface was abandoned at approximately 5.3 Ma.

Figure 3.12: Seismic line 99-11 with interpreted upper surface of the Altos de Pica member 3 illustrated as a dashed white line. The horizontal nature of the reflection indicates that no westward rotation has occurred at this location since the beginning of the Altos de Pica member 5, approximately 15 Ma. For the location of this seismic line, please see Figures 3.4 and 3.5



requires that no tilting of this horizon has occurred since the initiation of deposition of the overlying AdP member 5, approximately 15 Ma.

Therefore, any rotation of the western Andean slope since the Middle Miocene at this latitude has to have occurred to the east of $69^{\circ}10'W$, the eastern limit of the AdP member 3 portrayed on seismic line 99-11.

Summarized on a topographic map, these observations indicate that the lower, or western, monoclinial fold axis intersects the topographic surface throughout the study area at an elevation between approximately 1500 – 1750 m (Figure 3.4). To the east of this fold axis, the rotations calculated above describe the uplift of the western Andean slope. We define the eastern limit of the rotation as the point where swath profiles indicate topographic rollover, from a western zone where the slope of the low-relief landscape surface comprised of the top of AdP member 5 and the beveled Mesozoic strata within the western Precordillera averages $\sim 4.0^{\circ}$, to an eastern sub-horizontal and more irregular surface (Figure 3.13). This occurs at an elevation of approximately 4300 m within the study area, yielding a minimum rotational wavelength of ~ 30 km from the western monoclinial fold axis to the eastern rollover.

Geometric relationships using this 30 km wavelength and the calculated rotation angles of $1.4 \pm 0.7^{\circ}$ between 11 Ma and 5.3 Ma and $0.8 \pm 0.2^{\circ}$ between 5.3 Ma and the present yield 735 ± 370 m and 420 ± 105 m of topographic uplift, respectively, during these periods, with total uplift of 1155 ± 475 m since ~ 11 Ma (Table 3.4). This translates to a rate of uplift of the eastern margin of the AdP outcrop belt of $\sim 130 \pm 65$ m/Myr between 11 and 5.3 Ma and 80 ± 20 m/Myr between 5.3 Ma and

Figure 3.13: 20-km wide swath profiles created using data from the 90 m resolution shuttle radar topography mission (SRTM). The “rollover” was determined by visual inspection, and is the location where the abrupt break in the smooth west-facing slope of the western Andean slope occurs. Locations illustrated in Figure 3.2

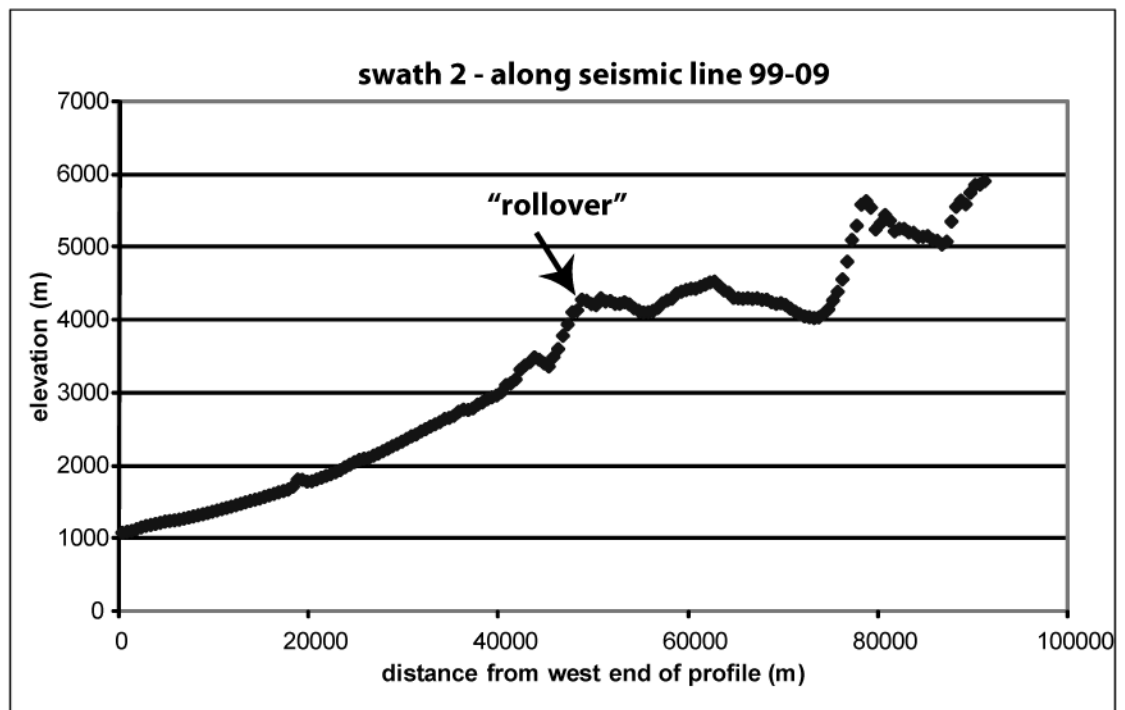
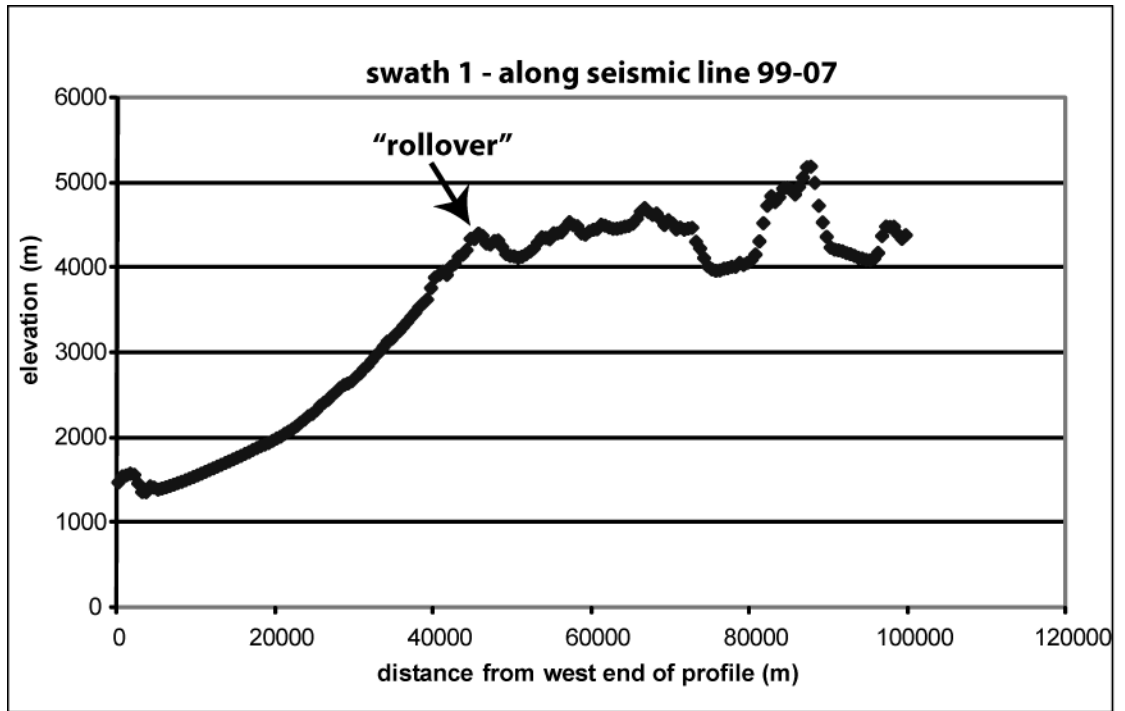


Table 3.4: Magnitudes and rates of uplift based on geometric relationships of time surfaces along the western Andean slope. “% relief generation” is based on the modern relief between the Altiplano and Central Depression at 21°S, which is ~2700 m.

time interval	uplift (m)	rate (m/Myr)	% relief generation
5.3 -0 Ma	420 ± 105	80 ± 20	16 ± 4%
11 - 5.3 Ma	735 ± 370	130 ± 65	27 ± 14%
total	1155 ± 475		43 ± 17%

the present. Uncertainties on the amounts of uplift during the two intervals include the accuracy of conversion of seismic travel time to depth, several assumptions needed to calculate burial compaction, and the estimation of the position of the eastern rollover of the monocline. Conversion of seismic travel time to depth to the base of the Neogene deposits reveals variability of less than 0.1% at a horizontal distance of 0.625 km to either side of the interpreted western limit of rotation for the three seismic lines considered here. This variability is minor, and is to be expected within a system where minor lateral variability of rock properties occurs within nonmarine facies over this distance. This result gives us confidence that the stacking velocities for the seismic data used in the determination of AdP member 5 surface slopes have not introduced significant error into these calculations. The compaction quantity is poorly constrained because the depositional porosity, final porosity, and diagenetic history are all unknown. Because the position of the upper rollover of the monocline is chosen based on relief even though it occurs at high elevations where the climate is wetter and more suited to denudation of the monoclinical surface, there is the possibility that we underestimated the width of the monocline. Our estimate represents a minimum estimate of surface uplift of the western margin of the Altiplano.

Today, the Pampa del Tamarugal has an average elevation of approximately 1000 m (Figure 3.2). At the latitude of the PdT but to its east, where it is not covered in stratovolcanoes or lava flows, the Altiplano has an average elevation of ~3700 m, with the extensive surface of Salar de Uyuni resting at an elevation of ~3660 m, and the village of

Ollagüe located at 3700 m, at the western edge of the broad, internally-drained Altiplano plateau (Figure 3.2). As discussed earlier, exhumation of the ancient surfaces during the time interval considered here has been practically nil. Therefore, any increases in topographic uplift calculated by the geometric relationship between rotation angle of ancient surfaces and wavelength of rotation can be directly transferred to rock uplift. Comparing the mean topographic uplift of 1155 m calculated for the last 11 million years, to the relief between the Altiplano and Pampa del Tamarugal of 2700 m, we arrive at ~43% of relief between the Pampa del Tamarugal and Altiplano generated entirely along the ~30 km distance of the western Andean slope during this interval. Conservative assumptions were used in the determination of this estimate. These include a minimum wavelength distance for rotation of 30 km and the highest observed original angle of deposition based on the modern alluvial system. Therefore, this number could be reasonably considered a lower limit. If we instead consider the high end of our ranges of uplift, we conclude that 1630 m of uplift, corresponding to ~60% of total relief, could have been generated during the last 11 million years (Table 3.4).

Regional Uplift Estimates

Using a wide variety of methods, a growing body of evidence indicates that significant uplift of the Altiplano has occurred since ~10 Ma (Table 3.1). By putting the results of this study into the context of these other estimates of timing and magnitude of uplift along the western Andean slope and Altiplano of the Central Andes, a clear signal takes shape. To the north (~16°S), along the western Andean slope of southern Peru, independent studies determine 2.4 km of Altiplano uplift since 9

Ma (Schildgen *et al.*, 2007) and at this same location, 2-2.5 km of stream incision between ~13 and 3.8 Ma, with the majority occurring after 9 Ma (Thouret *et al.*, 2007). For a site within the Bolivian Altiplano at 17°17'S, Gregory-Wodzicki (2000, 2002) compares leaf morphologies with modern floral assemblages in order to derive paleotemperature, and thus, paleoaltimetry for this site. These studies suggest 2780 ± 600 m of uplift since ~10.7 Ma. Using isotopic data from lacustrine carbonates at ~17°30'S as paleoaltimeters, Garzzone *et al.* (2006) and Ghosh *et al.* (2006) (date later revised by Garzzone *et al.*, 2007 and Quade *et al.*, 2007) document $\sim 2500 \pm 1000$ m of uplift of the Altiplano between 10.3 and 6.8 Ma. Approximately 300 km to the east, in a study which straddles 20°S within the Eastern Cordillera, encompassing ~500 km north-south distance parallel to the axis of the Andes, Barke and Lamb (2006) document $\sim 1700 \pm 700$ m of rock uplift with no evidence of surface-breaking faults or surface rotation since ~12-9 Ma. This last study suggests that wholesale uplift has not been restricted to the Altiplano-Puna plateau at these latitudes, but also extends a significant distance to the east.

Closer to our study area, Farías *et al.* (2005) estimates between 600 and 1500 m of post-8 Ma uplift of the western Altiplano at ~19°40'S in Quebrada Aroma caused by long-wavelength westward tilting. Using knickpoint bounded segments of modern stream profiles to reconstruct paleo-profiles as a proxy for tectonic uplift, Hoke *et al.* (2007) estimate 1080 ± 230 m of topographic relief generation since 9 Ma along the courses of channels from 18°30' and 21°40'S, including channels considered as a part of this study. At about 23°20'S, Jordan *et al.* (2006)

used a method analogous to this study to illustrate that at least 1900 ± 600 m of tectonic uplift of the Puna plateau relative to the forearc Salar de Atacama Basin occurred since ~ 10 Ma (data revised by T. Jordan, pers. comm., 2008). Earlier in the Miocene, tectonic rotation created $\sim 3000 \text{ m} \pm 2400 \text{ m}$ of rock relief.

Qualitatively, Riquelme *et al.* (2003) report late Miocene uplift at the eastern edge of the Central Depression between 26 and 27°S as evidenced by incision of the Atacama Gravels, which they attribute to wholesale westward tilting of the central Andean forearc. Similarly, in a broad study of the Central Andes inclusive of northern Chile between 16 and 23°S , Lamb and Hoke, (1997) describe a series of nested alluvial fans, growing progressively younger basinward within the Central Depression. These fans rest atop middle Miocene ignimbrites, which have a regional dip slope of up to $\sim 5^\circ$ to the west (Hoke, 2006; Lamb and Hoke., 1997).

Conclusions

While other studies drew conclusions about the magnitude of surface uplift, an important component to this study is that it also constrains the style of deformation. Alternate interpretations of the styles of deformation include large-scale surface rotation on a monocline that includes the full upper crust, uplift across a series of west-vergent surface breaking faults, wholesale uplift of the forearc and plateau as a single unit, or a combination of the styles. Schildgen *et al.* (2007) discovered no evidence of surface-breaking faults while also observing patterns of thermochronological data that are consistent with broad warping after 9 Ma of the western Andean slope. That study was at a

latitude of $\sim 16^{\circ}\text{S}$, a region which has no morphological forearc basin, and the rotation includes the full width of the forearc. The lack of surface-breaking faults post-dating 11 Ma in our study area between the forearc basin and the western Andean slope (or within the western Andean slope), in conjunction with other findings that the majority of faulting along the western Andean slope ceased by ~ 10 Ma (Charrier *et al.*, 2005; Elger *et al.*, 2005; Fariás *et al.*, 2005; García and Hérail, 2005; Pinto *et al.*, 2004; Victor *et al.*, 2004; Chapter 2), largely rules out upper crustal shortening in the Western Cordillera or Precordillera as the primary uplift mechanism during this period. Paleo-stream profiles of Hoke *et al.* (2007) reveal that, in our study area, uplift rates since ~ 10 Ma decreased from east to west, from the western Andean slope to within the Central Depression. This is consistent with our findings for a component of surface uplift at the western flank of the Altiplano generated by monoclinical rotation. However, neither the findings by Hoke *et al.* (2007) nor our study rule out the possibility that an additional component of surface uplift of the Altiplano was also in response to wholesale uplift of the forearc and Altiplano *en masse*.

Studies within 100 km to the north of our study area reveal that significant uplift, prior to ~ 10 Ma, was accommodated by a series of high angle faults known as the Western Thrust System (WTS, Fariás *et al.*, 2005; Victor *et al.*, 2004). At ~ 10 Ma, activity along the WTS north of the study area largely ceased. In the study area, west-facing asymmetric folds over blind reverse faults, like those of the WTS, also occur in the canyons immediately east of the seismic grid described in this paper. These folds largely predate AdP member 5 (see Chapter 2), and are therefore consistent with the middle Miocene timing of WTS-related uplift

better documented to the north. The WTS was active during the same time as contractional deformation was occurring on the Altiplano (Elger *et al.*, 2005). While the WTS may have accommodated uplift prior to 10 Ma (Fariás *et al.*, 2005; Victor *et al.*, 2004), our study and the study by Schildgen *et al.* (2007) at 16°S indicate that Middle Miocene upper crustal deformation cannot be solely responsible for the relief generated between the Central Depression and Altiplano since the beginning of the Miocene. In addition, as has been recently pointed out in reference to the central Andean orogeny (Garzzone *et al.*, 2007) structural uplift does not equate directly to surface uplift, with increased crustal thickness associated with generated structural relief translating into only a small percentage of surface uplift.

The demonstration that conservative estimates illustrate that relief across the western Andean slope increased $\sim 1155 \text{ m} \pm 475$ since $\sim 11 \text{ Ma}$ leads to an appreciation that the other $\sim 1545 \text{ m} \pm 475$ of the current 2700 m relief between the PdT and the Altiplano plateau pre-dated 11 Ma. We cannot specify the times of creation of this pre-late Miocene relief. Some part of it probably was created by the WTS during the early and middle Miocene. Some of this uplift was likely also relict from pre-Neogene tectonic activity (Haschke and Günther, 2003).

This study joins a set of other studies which reveal that largely synchronous uplift, on a 1-2 km scale, occurred over a distance of greater than 1000 km ($\sim 16^\circ$ - 26° S) along the western border of the Altiplano-Puna plateau since $\sim 10 \text{ Ma}$, (Fariás *et al.*, 2005; Garzzone *et al.*, 2006; Ghosh *et al.*, 2006; Gregory-Wodzicki, 2002; Hoke *et al.*, 2007; Jordan *et al.*, 2006; Thouret *et al.*, 2007), and may have extended as far

to the east as the Eastern Cordillera at these same latitudes (Barke and Lamb, 2006). This surface uplift began approximately the same time as 1) the end of deformation along the western Andean slope, at ~10 Ma (Farías *et al.*, 2005; Victor *et al.*, 2004; Chapter 2), 2) the end of significant deformation within the Altiplano, at ~10 Ma (Elger *et al.*, 2005), and 3) a shift in deformation from the Eastern Cordillera to the Subandean thrust and fold belt, at ~9 Ma (Gubbels *et al.*, 1993; Echavarría *et al.*, 2003). This coincidence in timing suggests that a fundamental change in mountain building style for the Central Andes occurred at this time, as suggested by other researchers (Gubbels *et al.*, 1993; Hoke *et al.*, 2007).

Two processes appear to be likely candidates for wholesale monoclinical warping over such a regional extent. Delamination of the eclogitic lower crust is believed to have occurred beneath the Altiplano-Puna plateau (Kay and Kay., 1993; Kay *et al.*, 1994; Schurr *et al.*, 2006), and has been presented as a possible mechanism for rapid uplift during the late Miocene (Garzzone *et al.*, 2006; Molnar and Garzzone, 2007). In addition, rapid uplift could occur as weakened lower- to middle-crust was displaced in response to underthrusting of the Brazilian Shield, in accord with the second stage of the Isacks (1988) model of deformation for the Altiplano. Both could theoretically occur over the ~1000 km along-strike distance.

The time span of uplift may provide a means to differentiate between these two mechanisms. Garzzone *et al.* (2006) and Molnar and Garzzone (2007) illustrated the plausibility of uplift of the Altiplano by >1500 m in less than 4 million years for the delamination mechanism.

Ghosh *et al.* (2006) and Garzione *et al.* (2006) propose Altiplano delamination between 10 and 6 Ma, whereas Puna delamination is better documented to have occurred since 5 Ma (Kay and Kay, 1993; Kay *et al.*, 1994). At the eastern edge of the Salar de Atacama adjacent to the Puna at $\sim 22^{\circ}40'S$, it is suggested that plateau uplift was greater during an earlier (pre 10-5 Ma) phase, but continued through to very recent times, as indicated by progressive fanning geometries of originally-horizontal surfaces (Jordan *et al.*, 2006). Progressive uplift from Middle Miocene to Recent at this location is not consistent with the delamination hypothesis, unless delamination occurred repeatedly.

If uplift is instead driven by lower crustal thickening as the Brazilian Shield was thrust under the Andes, it stands to reason that the time(s) of uplift should closely match the times of thrusting and the magnitude of uplift should scale to the amount of thrust shortening. Echavarría *et al.* (2003) provided two end-member options for the history of thin-skinned shortening in the Subandean belt to the east of the Altiplano and Eastern Cordillera, each compatible with chronologic and geometric constraints. The model that identified an early and a late pulse of thrusting attributed 55% of the shortening to the time since ~ 5.3 Ma. The alternative model implies that 70% of total shortening occurred since 5.3 Ma. Unfortunately, the Echavarría *et al.* (2003) study does not fully account for shortening at the western limit of the Subandean belt, where a large quantity of deformation prior to 5.3 Ma may have been focused. Until this limitation in the data for the eastern thrust belt is fully resolved, it is not possible to state definitively whether or not a direct

correlation exists between shortening in the Subandean thrust and fold belt and rates of plateau uplift measured on the western flank.

Recognition of the mechanism for late Miocene to Recent plateau uplift remains unclear while our understanding of timing and magnitudes of deformation across the central Andean mountain belt continues to improve. The style of deformation suggested by our study is consistent with both delamination and thickening of the lithosphere by underthrusting of the Brazilian Shield. Observations strictly related to timing and magnitudes of deformation within the Central Andes at least leave open the possibility that uplift since ~10 Ma was driven by ductile thickening of the lower to middle crust by the underthrusting Brazilian Shield. However, the timing of proposed delamination events does not fully fit the data for uplift history. With available data, we conclude that crustal thickening brought about by underthrusting of rigid continental crust beneath the Altiplano-Puna plateau is the most likely cause for late Miocene to Recent plateau uplift.

REFERENCES

- Allen, P. A., and Allen, J. R., 1990, Basin Analysis: Principles and Applications: Cambridge, Blackwell Scientific Publications, 451 p.
- Baby, P., Rochat, P., Mascle, G., and Hérail, G., 1997, Neogene shortening contribution to crustal thickening in the back arc of the Central Andes: *Geology*, v. 25, no. 10, p. 883-886.
- Barke, R., and Lamb, S., 2006, Late Cenozoic uplift of the Eastern Cordillera, Bolivian Andes: *Earth and Planetary Science Letters*, v. 249, no. 3-4, p. 350-367.
- Beck, S. L., and Zandt, G., 2002, The nature of orogenic crust in the central Andes: *Journal of Geophysical Research-Solid Earth*, v. 107, no. B10.
- Blair, T. C., and McPherson, J. G., 1994, Alluvial Fans and Their Natural Distinction from Rivers Based on Morphology, Hydraulic Processes, Sedimentary Processes, and Facies Assemblages: *Journal of Sedimentary Research Section a-Sedimentary Petrology and Processes*, v. 64, no. 3, p. 450-489.
- , 1994, Alluvial fan processes and forms., *in* Abrahams, A. D. a. P., A., ed., *Geomorphology of Desert Environments*: London, Chapman Hall, p. 354-402.
- Calvache, M. L., Viseras, C., and Fernández, J., 1997, Controls on fan development - evidence from fan morphometry and sedimentology; Sierra Nevada, SE Spain: *Geomorphology*, v. 21, p. 69-84.
- Cardozo, N., 2003, Mechanical and Kinematic Investigations of Fault Propagation Folding and Foreland Subsidence [Ph.D. thesis]: Cornell University, 211 p.
- Charrier, R., Chavez, A. N., Elgueta, S., Herail, G., Flynn, J. J., Croft, D. A., Wyss, A. R., Riquelme, R., and Garcia, M., 2005, Rapid tectonic and paleogeographic evolution associated with the development of the Chucal anticline and the Chucal-Lauca Basin in the Altiplano of Arica, northern Chile: *Journal of South American Earth Sciences*, v. 19, no. 1, p. 35-54.
- de Chant, L., Pease, P. P., and Tchakerian, V. P., 1999, Modelling alluvial fan morphology: *Earth Surface Processes and Landforms*, v. 24, p. 641-652.

- Dickinson, W. R., 1995, Forearc basins, *in* Busby, C. J., and Ingersoll, R. V., eds., *Tectonics of sedimentary basins*: Oxford, Blackwell Science, p. 221-261.
- Dickinson, W. R., and Seely, D. R., 1979, Structure and Stratigraphy of Forearc Regions: *Aapg Bulletin-American Association of Petroleum Geologists*, v. 63, no. 1, p. 2-31.
- Dingman, R. J., and Galli O, C., 1965, Geology and ground-water resources of the Pica area, Tarapaca Province, Chile, U. S. Geological Survey Bulletin: Reston, VA, USGS, 1-113 p.
- Dunai, T. J., Lopez, G. A. G., and Juez-Larre, J., 2005, Oligocene-Miocene age of aridity in the Atacama Desert revealed by exposure dating of erosion-sensitive landforms: *Geology*, v. 33, no. 4, p. 321-324.
- Echavarría, L., Hernández, R., Allmendinger, R. W., and Reynolds, J., 2003, Subandean thrust and fold belt of northwestern Argentina: Geometry and timing of the Andean evolution: *AAPG Bulletin*, v. 87, no. 6, p. 965-985.
- Elger, K., Oncken, O., and Glodny, J., 2005, Plateau-style accumulation of deformation: Southern Altiplano: *Tectonics*, v. 24, no. 4.
- England, P., and Molnar, P., 1990, Surface Uplift, Uplift of Rocks, and Exhumation of Rocks: *Geology*, v. 18, no. 12, p. 1173-1177.
- Ewing, S. A., Sutter, B., Owen, J., Nishiizumi, K., Sharp, W., Cliff, S. S., Perry, K., Dietrich, W., McKay, C. P., and Amundson, R., 2006, A threshold in soil formation at Earth's arid-hyperarid transition: *Geochimica Et Cosmochimica Acta*, v. 70, no. 21, p. 5293-5322.
- Farias, M., Charrier, R., Comte, D., Martinod, J., and Hérail, G., 2005, Late Cenozoic deformation and uplift of the western flank of the Altiplano: Evidence from the depositional, tectonic, and geomorphologic evolution and shallow seismic activity (northern Chile at 19 degrees 30 ' S): *Tectonics*, v. 24, no. 4.
- Garcia, M., and Hérail, G., 2005, Fault-related folding, drainage network evolution and valley incision during the Neogene in the Andean Precordillera of Northern Chile: *Geomorphology*, v. 65, no. 3-4, p. 279-300.
- Garzzone, C. N., Molnar, P., Libarkin, J. C., and MacFadden, B. J., 2006,

Rapid late Miocene rise of the Bolivian Altiplano: Evidence for removal of mantle lithosphere: *Earth and Planetary Science Letters*, v. 241, no. 3-4, p. 543-556.

-, 2007, Reply to Comment on "Rapid late Miocene rise of the Bolivian Altiplano: Evidence for removal of mantle lithosphere" by Garzzone et al. (2006), *Earth Planet. Sci. Lett.* 241 (2006) 543-556: *Earth and Planetary Science Letters*, v. 259, no. 3-4, p. 630-633.

Ghosh, P., Garzzone, C. N., and Eiler, J. M., 2006, Rapid uplift of the Altiplano revealed through C-13-O-18 bonds in paleosol carbonates: *Science*, v. 311, no. 5760, p. 511-515.

Gregory-Wodzicki, K. M., 2000, Uplift history of the Central and Northern Andes: A review: *Geological Society of America Bulletin*, v. 112, no. 7, p. 1091-1105.

-, 2002, A late Miocene subtropical-dry flora from the northern Altiplano, Bolivia: *Palaeogeography Palaeoclimatology Palaeoecology*, v. 180, no. 4, p. 331-348.

Gubbels, T., Isacks, B., and Farrar, E., 1993, High-level surfaces, plateau uplift, and foreland development, Bolivian central Andes: *Geology*, v. 21, p. 695-698.

Haschke, M., and Günther, A., 2003, Balancing crustal thickening in arcs by tectonic vs. magmatic means: *Geology*, v. 31, no. 11, p. 933-936.

Hoke, G. D., 2006, The influence of climate and tectonics on the geomorphology of the western slope of the Central Andes, Chile and Peru [Doctoral thesis]: Cornell University, 296 p.

Hoke, G. D., Isacks, B. L., Jordan, T. E., Blanco, N., Tomlinson, A. J., and Ramezani, J., 2007, Geomorphic evidence for post-10 Ma uplift of the western flank of the central Andes 18 degrees 30'-22 degrees S: *Tectonics*, v. 26, no. 5.

Holmes, A., 1965, *Principles of physical geology*: New York, Ronald Press, 1288 p.

Houston, J., 2002, Groundwater recharge through an alluvial fan in the Atacama Desert, northern Chile: mechanisms, magnitudes and causes: *Hydrological Processes*, v. 16, no. 15, p. 3019-3035.

Isacks, B. L., 1988, Uplift of the central Andean plateau and bending of the Bolivian orocline: *Journal of Geophysical Research*, v. 93, p. 3211-3231.

- James, D. E., and Sacks, I. S., 1999, Cenozoic formation of the Central Andes: A geophysical perspective, *in* Skinner, B. J., ed., *Geology and ore deposits of the Central Andes*, Society of Economic Geologists, p. 1-25.
- Jordan, T. E., Blanco, N., Davila, F., Hoke, G., Mpodozis, C., Nester, P. L., and Tomlinson, A. J., 2006, Evolution of the landforms across which the Atacama Desert is draped, 20°-24°S latitude: *Geological Society of America Abstracts with Programs*, v. 38, no. 7, p. 456.
- Kay, R. W., and Kay, S. M., 1993, Delamination and delamination magmatism: *Tectonophysics*, v. 219, p. 177-189.
- Kay, S. M., Coira, B., and Viramonte, J., 1994, Young mafic back-arc volcanic rocks as indicators of continental lithospheric delamination beneath the Argentine Puna plateau, Central Andes: *Journal of Geophysical Research*, v. 99, no. B12, p. 24323-24339.
- Kiefer, E., Dörr, M. J., Ibbeken, H., and Gotze, H. J., 1997, Gravity-based mass balance of an alluvial fan giant: the Arcas Fan, Pampa del Tamarugal, Northern Chile: *Revista Geologica De Chile*, v. 24, no. 2, p. 165-185.
- Kley, J., and Monaldi, C. R., 1998, Tectonic shortening and crustal thickness in the Central Andes; how good is the correlation?: *Geology*, v. 26, no. 8, p. 723-726.
- Kober, F., Schlunegger, F., Zeilinger, G., Schneider, H., Willett, S. D., Hovius, N., Brandon, M. T., and Fisher, D. M., 2006, Surface uplift and climate change; the geomorphic evolution of the western escarpment of the Andes of northern Chile between the Miocene and present, *Geological Society of America (GSA)*, Boulder, CO, p. 75-86.
- Lamb, S., and Davis, P., 2003, Cenozoic climate change as a possible cause for the rise of the Andes: *Nature*, v. 425, p. 792-797.
- Lamb, S., and Hoke, L., 1997, Origin of the high plateau in the Central Andes, Bolivia, South America: *Tectonics*, v. 16, no. 4, p. 623-649.
- McQuarrie, N., Horton, B. K., Zandt, G., Beck, S., and DeCelles, P. G., 2005, Lithospheric evolution of the Andean fold-thrust belt, Bolivia, and the origin of the central Andean plateau: *Tectonophysics*, v. 399, no. 1-4, p. 15-37.

- Molnar, P., and Garzzone, C. N., 2007, Bounds on the viscosity coefficient of continental lithosphere from removal of mantle lithosphere beneath the Altiplano and Eastern Cordillera: *Tectonics*, v. 26, no. 2.
- Muñoz, N., and Charrier, R., 1996, Uplift of the western border of the Altiplano on a west vergent thrust system, Northern Chile: *Journal of South American Earth Sciences*, v. 9, no. 3/4, p. 171-181.
- Nester, P. L., Gayo, E., Latorre, C., Jordan, T. E., and Blanco, N., 2007, Perennial stream discharge in the hyperarid Atacama Desert of northern Chile during the latest Pleistocene: *Proceedings of the National Academy of Sciences of the United States of America*, v. 104, no. 50, p. 19724-19729.
- Pardo-Casas, F., and Molnar, P., 1987, Relative motion of the Nazca (Farallon) and South American plates since Late Cretaceous time: *Tectonics*, v. 6, p. 233-248.
- Pinto, L., Hérail, G., and Charrier, R., 2004, Sedimentación sintectónica asociada a las estructuras neógenas en la Precordillera de la zona de Moquella, Tarapacá (19°15'S, norte de Chile): *Revista Geologica de Chile*, v. 31, no. 1, p. 19-44.
- Quade, J., Garzzone, C., and Eiler, J., 2007, Paleoelevation reconstruction using pedogenic carbonates, *Paleoaltimetry: Geochemical and Thermodynamic Approaches: Reviews in Mineralogy & Geochemistry: Chantilly, MINERALOGICAL SOCIETY OF AMERICA*, p. 53-87.
- Riquelme, R., Martinod, J., Hérail, G., Darrozes, J., and Charrier, R., 2003, A geomorphological approach to determining the Neogene to Recent tectonic deformation in the Coastal Cordillera of northern Chile (Atacama): *Tectonophysics*, v. 361, no. 3-4, p. 255-275.
- Sáez, A., Cabrera, L., Jensen, A., and Chong, G., 1999, Late Neogene lacustrine record and palaeogeography in the Quillagua-Llamara basin, Central Andean fore-arc (northern Chile): *Palaeogeography Palaeoclimatology Palaeoecology*, v. 151, no. 1-3, p. 5-37.
- Schildgen, T. F., Hodges, K. V., Whipple, K. X., Reiners, P. W., and Pringle, M. S., 2007, Uplift of the western margin of the Andean Plateau revealed from canyon incision history, southern Peru: *Geology (Boulder)*, v. 35, no. 6, p. 523-526.
- Schlunegger, F., Zeilinger, G., Kounov, A., Kober, F., and Husser, B.,

- 2006, Scale of relief growth in the forearc of the Andes of Northern Chile (Arica latitude, 18 degrees S): *Terra Nova*, v. 18, no. 3, p. 217-223.
- Schurr, B., Rietbrock, A., Asch, G., Kind, R., and Oncken, O., 2006, Evidence for lithospheric detachment in the central Andes from local earthquake tomography: *Tectonophysics*, v. 415, no. 1-4, p. 203-223.
- Sclater, J. G., and Christie, P. A. F., 1980, Continental stretching: An explanation of the post mid-Cretaceous subsidence of the central North Sea basin: *Journal of Geophysical Research*, v. 85, p. 3711-3739.
- Somoza, R., 1998, Updated Nazca (Farallon)—South America relative motions during the last 40 My: implications for mountain building in the central Andean region: *Journal of South American Earth Sciences*, v. 11, no. 3, p. 211-215.
- Thouret, J. C., Worner, G., Gunnell, Y., Singer, B., Zhang, X., and Souriot, T., 2007, Geochronologic and stratigraphic constraints on canyon incision and Miocene uplift of the Central Andes in Peru: *Earth and Planetary Science Letters*, v. 263, p. 151-166.
- Victor, P., Oncken, O., and Glodny, J., 2004, Uplift of the western Altiplano plateau: Evidence from the Precordillera between 20 degrees and 21 degrees S (northern Chile): *Tectonics*, v. 23, no. 4.
- Whipple, K. X., Parker, G., Paola, C., and Mohrig, D., 1998, Channel dynamics, sediment transport, and the slope of alluvial fans: Experimental study.: *Journal of Geology*, v. 106, no. 6, p. 677-693.

CHAPTER 4

PERENNIAL STREAM DISCHARGE IN THE HYPERARID DESERT OF NORTHERN CHILE DURING THE LATEST PLEISTOCENE³

Abstract

A large fraction of the vital groundwater in the Atacama Desert of northern Chile is likely composed of 'fossil' or 'ancient' reserves that receive little or no recharge in today's hyperarid climate. Here we present evidence for latest Pleistocene perennial streamflow in canyons from the hyperarid core of the Atacama Desert in northern Chile. Fluvial terraces in the Pampa del Tamarugal (PdT) basin (21°S) contain widespread fossil wood, *in situ* roots, and well-preserved leaf litter deposits indicative of perennial surface flow currently absent in these channels. Nineteen radiocarbon dates on these deposits from four separate drainages within this endorheic basin indicate ages from 16,380 to 13,740 cal yr BP, synchronous with paleolake Tauca on the Bolivian Altiplano and other regional evidence for wetter conditions during the latest Pleistocene. Groundwater-fed riparian ecosystems and associated fluvial deposits abound today in the absence of direct rainfall in northern Atacama

³Previously published in slightly modified form as: Nester, P.L., Gayó, E., Latorre, C., Jordan, T.E., and Blanco, N., 2007, Perennial stream discharge in the hyperarid Atacama Desert of northern Chile during the latest Pleistocene: Proceedings of the National Academy of Sciences of the United States of America, v. 104, no. 50, p. 19724-19729.

canyons with perennial discharge. Our relict riparian ecosystems from the PdT basin are indicative of conditions similar to these northern canyons. Given that discharge was higher than present during this time, we propose that these deposits represent the most important groundwater recharge events of the last 18,000 years. A lesser recharge event occurred during the Holocene, when phreatophytic trees also grew in these drainages between 1070-700 cal yr BP, during the Medieval Climatic Anomaly. Taken together, our evidence lends further support for gradient changes in the equatorial Pacific as a major driver of hydrologic change in the Atacama on both centennial and millennial timescales.

Introduction

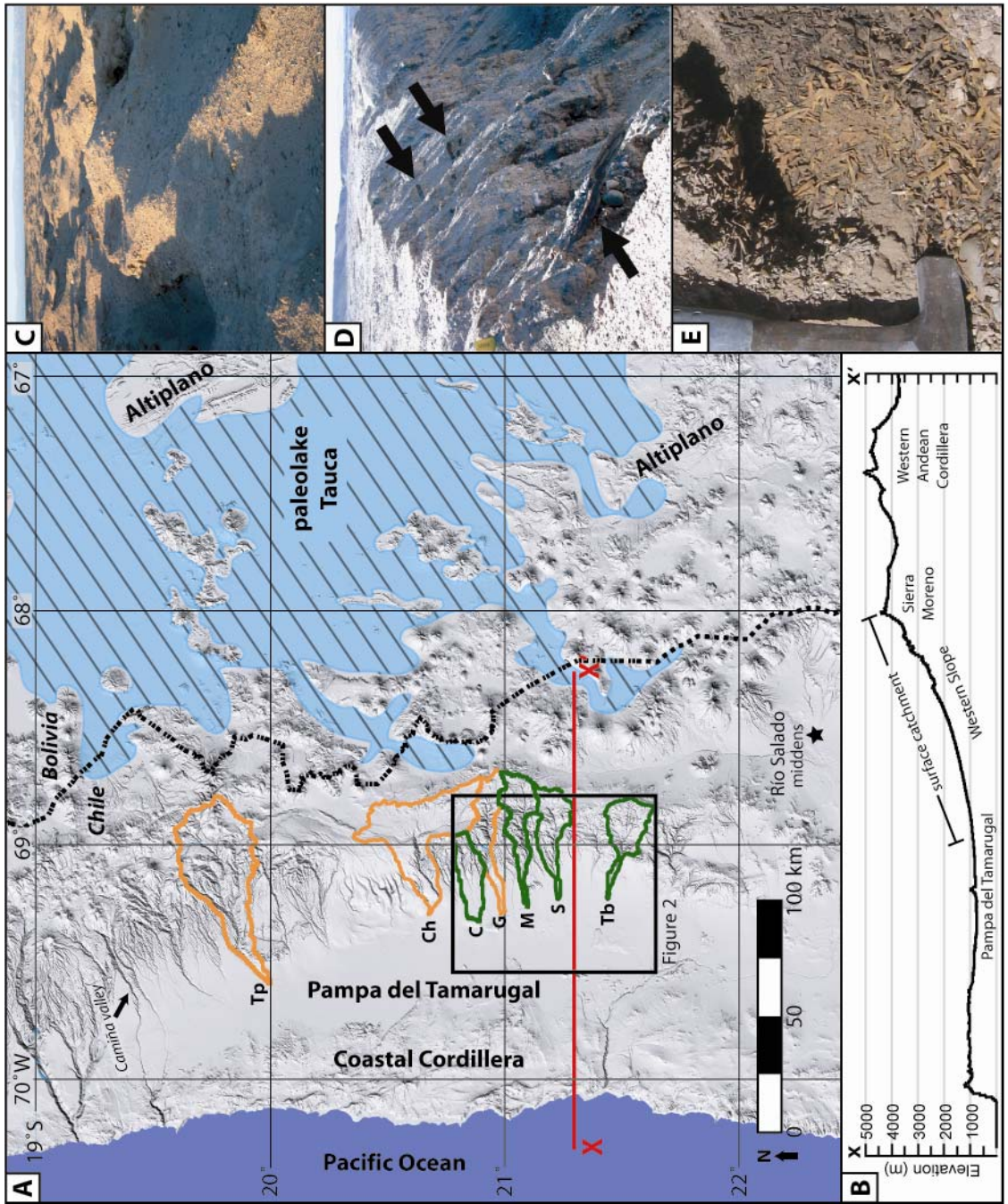
The hyperarid Atacama Desert drapes across the western flank of the Andes Mountains, at the western extreme of central South America, including much of northern Chile. The extreme lack of precipitation is a feature that has remained stable over millions of years owing to major coupled atmospheric and tectonic feedbacks (Alpers and Brimhall, 1988; Lamb and Davis, 2003; Houston and Hartley, 2003; Dunai *et al.*, 2005; Rech *et al.*, 2006). But short-lived times of increased precipitation exist in paleo-hydrological records at elevations above 2000 m, reflecting millennial-scale variations in global climate. In particular, two major periods of increased precipitation are known to have affected groundwater tables and plant species distributions during the late Quaternary (Betancourt *et al.*, 2000; Rech *et al.*, 2002; Latorre *et al.*, 2003; Latorre *et al.*, 2006; Lowenstein *et al.*, 2003). The impacts of these wet phases in the lower elevation desert, expressed either as increased

precipitation or as variations in surface runoff and local groundwater table, have largely remained unstudied, although attempts have been made to understand current climate and the hydrologic system feedbacks (Fritz *et al.*, 1981; Aravena *et al.*, 1999; Houston, 2002). Increased surface flow over this region during predominantly late Pleistocene humid intervals may have modified the landscape, and contributed to groundwater recharge.

Groundwater is a precious resource throughout the hyperarid and arid Atacama Desert for life (both that of native vegetation and of humans) and industry. In particular, all aspects of copper production and the people which serve the industry rely on groundwater. Today, over 23% of global copper is produced in the Atacama Desert (COCHILCO, 2006) and in the year 2000, 16% of Chile's GDP was derived from copper exports (COCHILCO, 2006). Consequently, recognition of inputs and outputs to groundwater supplies is a vital part of Chile's economic planning. Nevertheless, few studies have assessed connections between water balances and past climates.

Here, we report on new evidence for latest Pleistocene recharge of major aquifers in the Atacama Desert, through the proxies of fluvial deposits and associated riparian ecosystems. This study is specific to the Pampa del Tamarugal (PdT), a low elevation endorheic basin located 19°30'–22°S latitude at the base of the Western Andean Cordillera (WAC) in the hyperarid core of the Atacama Desert (Figure 4.1). These fluvial sediments were deposited during humid climate “windows”, in stark contrast to the Mio-Pliocene arid-hyperarid climates that preceded their deposition (Rech *et al.*, 2002; Sáez *et al.*, 1999) and the hyperarid conditions present today. Multiple terraced deposits inset into Neogene

Figure 4.1: A) Regional map of northern Chile showing study area in relation to the approximate maximum extent of paleolake Tauca. Green and orange lines enclose surface water catchments mentioned in text (green where the trunk stream is ephemeral and bordered by late Pleistocene wood-bearing sediments; orange where the trunk stream is perennial) (Tp=Tarapacá; Ch=Chacarilla; C=Chipana; G=Guatacondo; M=Maní; S=Sipuca; Tb=Tambillo). B) Topographic cross section (located along X-X' in A). C) Photograph of T2 surface at Tb. Note numerous excavated “mounds” dotting the landscape, indicating the vast expanse of organic Pleistocene deposits. D) Black arrows indicate logs transported within late Pleistocene aggradational fill. (Notebook at left for scale.) E) A *Schinus molle* leaf litter deposit at Tb.



sediments along the eastern portion of the southern PdT display several aggradation and incision cycles along canyon walls, and connected surfaces of fans associated with the fluvial activity spread out from these canyons into the basin center. Although plantless today, these terraces and fans literally abound with Pleistocene fossil wood and leaf beds (Figure 4.1c,d,e), all of which are found *in situ* or have been transported only very short distances.

We use ^{14}C -dating (Table 4.1), sedimentological evidence and macrofossil analyses to infer the latest Pleistocene drainage basin environment and paleoclimate by analogy to current climatic conditions and riparian ecosystems in the region. Our chronology establishes regional-scale connections between documented humid intervals to the east on the Altiplano, Western- and Pre-Cordillera of the central Andes and our low elevation fluvial record. We discuss the implications of our results for past freshwater recharge of the PdT basin, where groundwater is a major economic resource.

Modern Environment and Groundwater

Intense aridity of the Atacama Desert is brought about by a combination of long-term stable climatic factors. These include blocking of the mid-latitude Westerlies by the stable subtropical high-pressure belt, an orographic rainshadow generated by the Altiplano and WAC, and a strong coastal thermal inversion created, largely, by the cold, north-flowing Humboldt Current (Houston and Hartley, 2003; Miller, 1976). Austral summer rainfall between 18 - 24°S occurs in the highlands (>2000 m) when the intensified Bolivian High advects moisture-laden

Table 4.1. Sample locations and conventional or AMS ^{14}C dates of organic material

Spl. #	Lab code	Loc. ($^{\circ}\text{S}/^{\circ}\text{W}$)	Spl. ID	^{14}C yr BP	cal yr BP (2σ)	$\delta^{13}\text{C}$ (‰)
Chipana canyon drainage						
1	UCIAMS-29216	20.90 69.34	N05-21	13,055±25	15,740-15,160	-22.7
2	UCIAMS-29221	20.90 69.34	N05-22	12,160±130	14,590-13,740	no data
Mani canyon drainage						
3	CAMS-129007	21.09 69.30	QM-2a	870±30	910-700	-10.4
4	CAMS-129008	21.09 69.28	QM-2e	960±30	930-800	-22.7
5	CAMS-129009	21.09 69.30	QM-3a	1,110±30	1,070-940	-24.3
6	CAMS-131272	21.09 69.32	QM-4	13,190±35	15,960-15,300	-24.3
Sipuca canyon drainage						
7	GX-32394	21.23 69.19	QS-1a*	13,330±80	16,250-15,420	-24.3
8	GX-32395	21.23 69.20	QS-3†	13,400±70	16,340-15,530	-24.4
9	UCIAMS-29222	21.23 69.20	N05-10	14,470±70	17,840-16,940	no data

Spl., sample; Loc., location; cal, calibrated; yr BP, years before present

Samples associated with levels of terraced deposits (explained in text):

*, T2; †, T2.5; ‡, T2.7

Table 4.1. (cont.)

Spl. #	Lab code	Loc. (°S/°W)	Spl. ID	¹⁴ C yr BP	cal yr BP (2σ)	δ ¹³ C (‰)
Tambillo canyon drainage						
10	GX-32396	21.43 69.25	QT-1*	13,290±80	16,180-15,370	-23.9
11	GX-32397	21.43 69.25	QT-5†	12,940±150	15,840-14,870	-24.8
12	GX-32398	21.43 69.25	QT-6‡	13,310±180	16,380-15,220	-24.5
13	CAMS-129367	21.44 69.26	QT-8	13,280±70	16,140-15,360	-24.0
14	CAMS-131273	21.44 69.31	QT-9	13,220±35	16,010-15,340	-27.1
15	UCIAMS-29220	21.44 69.25	N05-11	13,080±30	15,780-15,180	-20.5
16	AA62290	21.40 69.42	N04-14a	12,244±96	14,630-13,850	-28.1
17	UCIAMS-29218	21.40 69.42	N05-12a	12,735±30	15,250-14,840	-20.2
18	UCIAMS-29219	21.40 69.43	N05-18	12,435±30	14,820-14,190	-20.7
19	UCIAMS-29217	21.43 69.46	N06-11a	10,170±20	11,970-11,420	-21.7

Spl., sample; Loc., location; cal, calibrated; yr BP, years before present

Samples associated with levels of terraced deposits (explained in text):

*, T2; †, T2.5; ‡, T2.7

Amazonian air masses over the Andes (Garreaud *et al.*, 2003), occasionally as far west as the WAC and Sierra Moreno (SM). Westward transport of moisture is particularly strong during La Niña years, when the Bolivian High intensifies and migrates south over the Altiplano (Vuille, 1999; Vuille and Keimig, 2004), and, for the southern Altiplano, during years of anomalously high moisture delivery to the continent inboard of the South Atlantic (Vuille and Keimig, 2004). At these latitudes, annual precipitation amounts are a function of elevation on the Pacific facing western Andean slope. From 1975-1991, annual rainfall below 2000 m was <10 mm/yr, increasing to 120 mm/yr at 4000 m elevation (Houston, 2002).

With a mean elevation of ~1000 m, the PdT is flanked to the west by the Coastal Cordillera and to the east by the Precordillera and SM, which rise to >4000m (Figure 4.1). The westerly-flowing surface drainages in the SM are completely disconnected from the Altiplano and WAC, which lie to the east (Figure 4.1b). Baseflow originates from springs at high elevations within the surface water catchments (Houston, 2002; Magaritz *et al.*, 1989) and flows westward in widely spaced canyons. The eastern limits of groundwater catchments are not well defined (Fritz *et al.*, 1981; Magaritz *et al.*, 1989). As today's rivers and groundwater display similar stable isotopic trends with altitude, both are likely derived from the same source (Fritz *et al.*, 1981).

A latitudinal change at ~21°S from predominantly perennial (north) to ephemeral (south) streams correlates with a southward decrease in the area of the catchment basins (Table 4.1) rather than with a latitudinal

climate gradient. Given that most of the western Andean slope drainage basins are located in the high elevation WAC and SM (Figure 4.1, 4.2), and that a strong correlation of mean annual precipitation with elevation is known to exist (Houston and Hartley, 2003), larger catchment areas correlate with greater discharge delivered to the trunk streams in this region (Table 4.2). For reference, the perennial Tarapacá River (~150 km to the north of our study area, Figure 4.1) had an average discharge of $0.303 \text{ m}^3/\text{s}$ for the period 1984-1990, fluctuating between monthly averages of $0.159 \text{ m}^3/\text{s}$ (November) and $0.438 \text{ m}^3/\text{s}$ (February) (JICA, 1995). The Chacarilla perennial stream, (~20 km north of our northernmost site, Figure 4.1) had a discharge of $0.015 \text{ m}^3/\text{s}$ at the end of the 1999 dry season (Houston, 2002).

The drainages that enter the southern PdT in our study area have almost no surface flow in their trunk streams. Surface water that reaches the PdT through the canyons during a ~5 year frequency storm event quickly infiltrates the unconsolidated streambeds (Fritz *et al.*, 1981; Houston, 2002). These convective storms in the SM and WAC can produce ~10-40 mm of rainfall/day at higher elevations (Houston, 2002; Houston, 2006). Rough estimates determine that 5-10% of the precipitation that falls today within this drainage basin recharges underlying aquifers, with 90-95% being lost to evaporation (Houston, 2002; JICA, 1995). The proportion of water infiltration to evaporation has been modeled to be much higher during extreme storm events (Houston, 2002).

Groundwater aquifers in the northern PdT and similar intermontane valleys of the Atacama Desert host many wellfields whose

Figure 4.2: Locations whose organic remains are reported here (X's) in the lower sectors of ephemeral drainages (Figure 4.1) where latest Pleistocene fluvial terraces line the canyons, and on alluvial fans spread westward from the mouths of the canyons across the floor of the PdT (contour interval = 500 m). Sample numbers correspond to Table 4.1. Gray shading indicates fans which also likely contain organic-rich deposits contemporaneous with dated material.

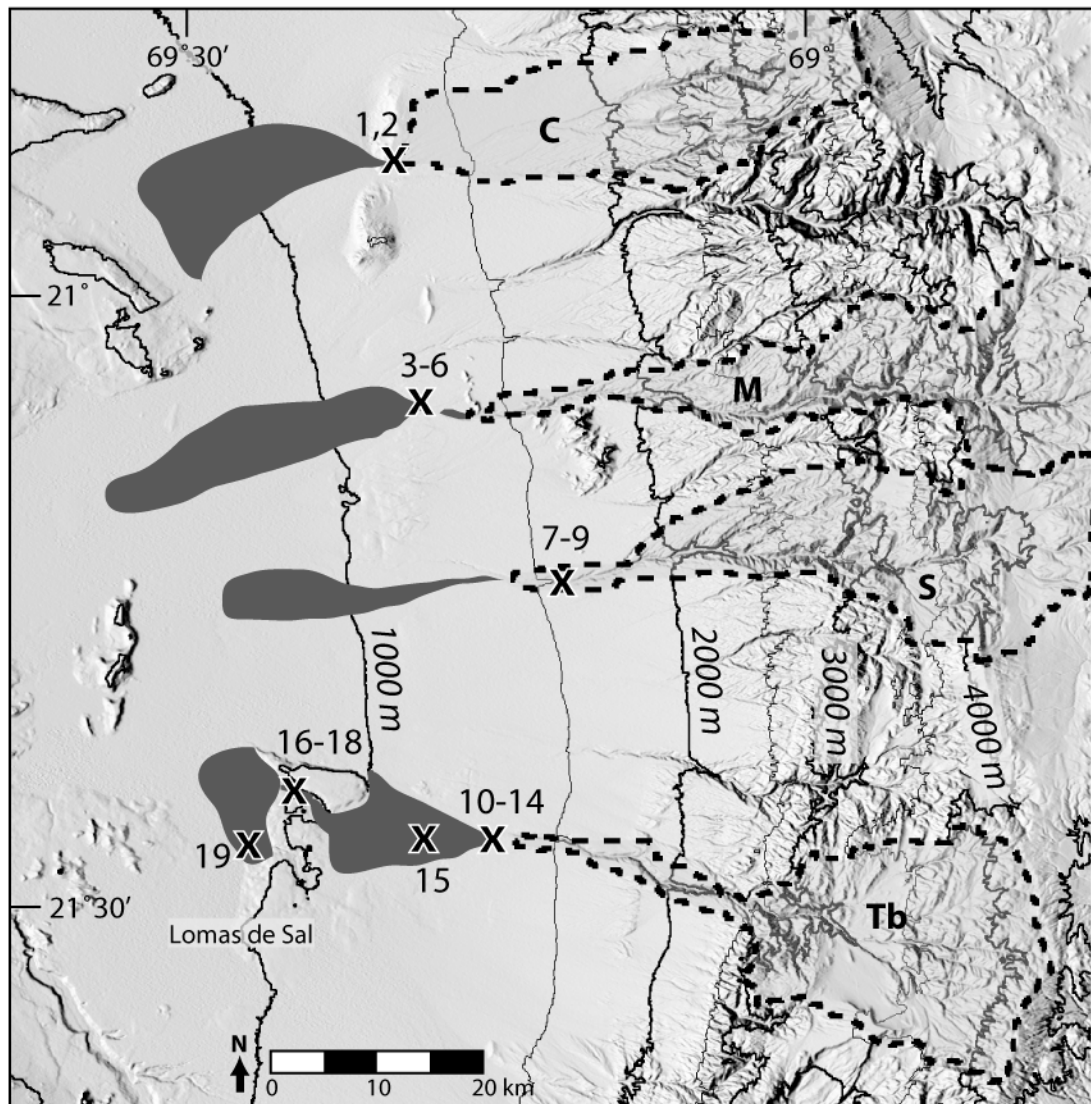


Table 4.2. North-south relationships between catchment area and stream type

Catchment	Mean latitude (°S)	CDA (km ²)	MAP (m ³)*	Stream Type
Tarapacá	19.84	1786	195.2 x10 ⁶	perennial
Chacarilla	20.66	1440	137.4 x10 ⁶	perennial
Guatacondo	20.85	495	53.2 x10 ⁶	perennial
Chipana	20.98	370	7.6 x10 ⁶	ephemeral
Maní	21.05	488	56.6 x10 ⁶	ephemeral
Sipuca	21.20	481	37.4 x10 ⁶	ephemeral
Tambillo	21.50	438	28.6 x10 ⁶	ephemeral

CDA, cumulative drainage area; MAP, mean annual precipitation

* 0-2300 m: $MAP=0.03e^{0.002*altitude}$; 2300-4300 m: $MAP=e^{0.0012*altitude}$
(Houston and Hartley, 2003)

water is piped long distances to mines and municipalities. Some shallow (<50m) PdT aquifers recharge locally (Houston, 2002; Houston, 2006), but sparse ^{14}C data from the deeper aquifers (100 to 300 m depth), in conjunction with other evidence, suggest that some of the groundwater was recharged >10,000 years ago (Fritz *et al.*, 1981; Magaritz *et al.*, 1989; JICA, 1995). Too few data exist to estimate what portion of the produced groundwater is fossil. For the southern PdT, only saline water aquifers are recognized.

Sediments deposited in the modern PdT reflect the asymmetry of its modern hydrologic environment. In the eastern canyons and on their alluvial fans, unsorted mudflow and debris flow deposits are widespread, emplaced by mass wasting triggered by the rare convective storms at high elevations (Houston, 2002; Houston, 2006). In the western part of the valley where the water table nearly intersects with the land surface, its evaporation leads to precipitation of salts, forming salt pans (*salars*) (Aravena *et al.*, 1999; Houston, 2002; Magaritz *et al.*, 1999; Houston, 2006).

Direct rainfall in the PdT is negligible (absent for decades in some places) and the interfluvies in the study area below ~2500 m elevation are entirely devoid of macroscopic life. In fact, large expanses of this “Absolute Desert” (Arroyo *et al.*, 1988) are covered by highly soluble nitrate deposits (Ericksen, 1981; Michalski *et al.*, 2004). Plant life only occurs today in perennial or intermittent channels and oases. Natural and planted forests of the phreatophyte *Prosopis tamarugo* (Mimosaceae) are extensive in the distal portion of the northern PdT where groundwater is within ~10 meters of the land surface. Occasional storm runoff supports sparse patches of halophytes in intermittent washes

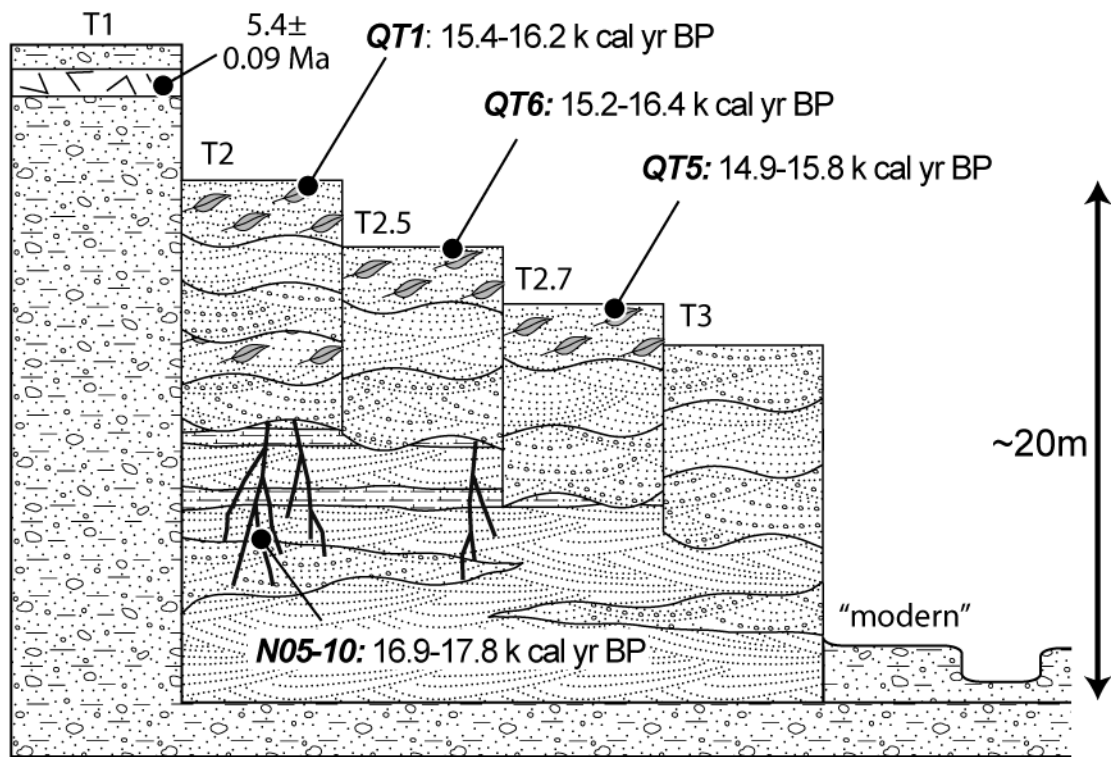
such as *Distichlis spicata* (Poaceae), *Cressa cretica* (Convolvulaceae), *Atriplex atacamensis* (Chenopodiaceae), *Loasa fruticosa* (Loasaceae) and *Tessaria absinthioides* (Asteraceae) (Luebert and Pliscoff, 2006).

Perennial watercourses are commonplace in major canyons with outlets to the Pacific Ocean north of 19°30'S (Figure 4.1). These fertile oases support abundant riparian vegetation from their headwaters in the WAC and Precordillera through the low elevation hyperarid core of the Atacama Desert (Luebert and Pliscoff, 2006; Caviedes, 1973; Gajardo, 1994; Villagrán *et al.*, 1999; Luebert, 2004). Below 2600 m, canyon floodplains are dominated by *Escallonia angustifolia* (Escalloniaceae), *Schinus molle* (Anacardiaceae), *Myrica pavonis* (Myricaceae), *Geoffroea decorticans* (Fabaceae), *Baccharis* spp, *Tessaria absinthioides* (Asteraceae), *Cortaderia atacamensis* and *Phragmites australis* (Poaceae) (Gajardo, 1994; Villagrán *et al.*, 1999; Luebert, 2004).

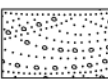
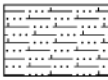

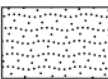
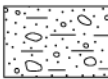

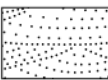

Stratigraphy and Chronology of Latest Pleistocene Fluvial Terraces

Within the PdT, the canyons are incised into debris-flow dominated alluvial latest Miocene relict terraced deposits (T1 in Figure 4.3) that have seen negligible denudation during the past 5 Myr (Kiefer *et al.*, 1997; Hoke *et al.*, 2007). Late Pleistocene inset fill terraces are preserved between 1200 and 1550 m elevation in every major canyon connected to the SM from 20°30 to 21°30'S. We describe terraces and organic-rich deposits from the Chipana (C), Maní (M), Tambillo (Tb) and Sipuca (S) drainages (Figure 4.2), each of which today hosts an ephemeral stream. While well-preserved late Pleistocene plant macrofossils were identified within multiple stages of terraced deposits at each location, the relationships of these deposits within and between Tb and S were

Figure 4.3: Generalized stratigraphy of fluvial sediments inset within Upper Miocene alluvial deposits, combining observations from the Tambillo and Sipuca canyons. All dated organic material was discovered *in situ* and taken from root material or leaf litter. Sample IDs are explained in Table 4.1. Ages listed are for single samples and denote the 2σ uncertainty. Horizontal distances are not to scale.



Legend:

- | | | | | | |
|---|-----------------------------------|---|--|---|---------------|
|  | cross-laminated sands and gravels |  | parallel-laminated CaCO ₃ -cemented sands |  | unwelded tuff |
|  | wavy-laminated silts and sands |  | well-laminated, poorly-sorted sand and gravel |  | roots |
|  | cross-laminated well-sorted sands |  | leaves, twigs and logs | | |

specifically described for this study. In the perennial Chacarilla (Ch) and Guatacondo (G) canyons (Figure 4.1), fluvial terraces occur in the same geomorphological positions as in C, M, S, and Tb, but lack associated organic-rich deposits.

In descending order (to the modern channel) the different terraces recognized at Tb and S are T1, T2, T2.5, T2.7, T3 and “modern” (Figure 4.3). At Tb, fluvial aggradational fill associated with terraces T2, T2.5, T2.7, and T3 reaches a thickness of 20m. T2 is inclined more steeply than T1, intersecting at ~1200m, west of which the fluvial fill spreads beyond the canyons to form alluvial fans. The modern channel (inset by 1-3 m into its floodplain) near 1250m elevation rests >10 meters below T3 and continues as a confined channel for 10’s of km’s downstream.

The oldest Pleistocene aggradational unit contains several horizons of a highly-eroded, carbonate-bearing incipient paleosol. It consists of crossbedded, well-sorted, rounded to subrounded, medium- to coarse-grained sands, interbedded with weakly- to prominently-bedded pebble conglomerates containing Mesozoic to Neogene volcanic and sedimentary clasts. Interbedded horizontal carbonate hardpan layers reach Stage II development. Unaltered roots (up to 20 cm diameter) and rootlets are often preserved within CaCO₃ rhizoliths. A ¹⁴C AMS calibrated date of 17,840 to 16,940 cal yr BP (all dates at 2 sigma, calibrations according to Stuiver *et al.*, 2005) on these roots gives the oldest age for the entire sequence (Table 4.1).

Aggradational fluvial deposits associated with the T2, T2.5 and T2.7 terraces are inset into either these oldest Pleistocene deposits or within the Miocene alluvial sediments. Practically indistinguishable from one another based on sediment and sedimentary structures, the terraces

can only be recognized by the relative elevations of their upper surfaces and the sequence of fill deposits subdivided based on associated erosional bases and dated organic material. Reaching a thickness of ~5 m, these aggradational fluvial deposits are very to moderately well sorted, well-rounded to subangular, cross-bedded fine to coarse sands and pebbles. The topmost surfaces of these constructional terraces are dotted with mounds of extraordinarily well-preserved organic matter which are surrounded by a small degree of rilling. These mounds contain abundant identifiable and datable organic material, and exhibit signs of extensive human wood “mining” activities since the early 1800’s (Billingham, 1893).

Apart from abundant wood and bark, these mounds abound with *in situ* leaf litter deposits. Leaves and fruits of the trees *E. angustifolia* and *S. molle* prevail. Pollen from Asteraceae, *Prosopis* sp. and Poaceae were also recovered (from Tb) as well as *Baccharis scandens* leaves and flowers, and seeds of the xerophytic annual *Cistanthe*. Poaceae and *Prosopis* pollen were detected in samples from S. AMS dates of these organic remains within the upper meter of deposits associated with the fluvial terraces range from 16,340 - 15,421 cal yr BP at S, to between 16,380 - 14,870 cal yr BP at Tb. Dates on organic deposits at M range between 15,960 and 15,302 cal yr BP.

Our ¹⁴C-chronology of *in situ* organic remains (Table 4.1) present during each aggradational phase termination illustrates a systematic decrease in ages obtained from progressively lower terrace levels. At least three relatively rapid cycles of aggradation, abandonment and incision are preserved. Terrace formation of T2.5 and T2.7 was short-

lived, and 3 separate events (T2, T2.5, T2.7) span from ~16,000 to ~15,000 cal yr BP (Figure 4.3).

The deposits associated with the T3 terrace, inset beneath the T2.7 terrace, are also fluvial in origin, with moderately well-sorted, well-rounded to subangular, cross-bedded coarse sands and pebbles. They are indistinguishable in composition from the other deposits considered here, except that they are noticeably devoid of *in situ* organic material. As such, an upper age constraint does not yet exist for these deposits.

Fluvial deposits occur also ~20 km west of the canyon T terraces within an incised ephemeral stream channel in Lomas de Sal (Figure 4.2), a 50 m high knoll of Mio-Pliocene evaporites (Sáez *et al.*, 1999). The sediments contain fine- to coarse-grained, cross-bedded gravels and sands with abundant *E. angustifolia* leaves and logs of *S. molle* up to 40 cm in diameter. The organic material dates from between 15,253 and 13,850 cal yr BP (Samples 16-18, Table 4.1). These are a flood deposit and not *in situ*. Even more distant are fan deposits containing well-sorted cross-bedded fine- to medium-grained sands with abundant *in situ* and transported organic material. Sample 19 of *in situ* roots yields a ^{14}C AMS date of 11,974-11,415 cal yr BP, indicating a vegetative cover younger than the dated terraces located upstream.

Additionally, a late Holocene constructional terrace with organic mounds is also present along small side canyons that branch off from the M main drainage. Dated to between 1,070-700 cal yr BP (samples 4-6), these mounds contain almost pure *Prosopis* sp. remains, including seeds, pods, leaves, inflorescences, and wood. Archaeological remains (charcoal, bone fragments, flakes and pottery) abound on the surface of this terrace. The most recent (“modern” in Figure 4.3) deposits are

debris-flow dominated alluvial sediments, similar to those associated with the T1 late Miocene sediments.

Paleoenvironmental Interpretation and Regional Paleoclimate

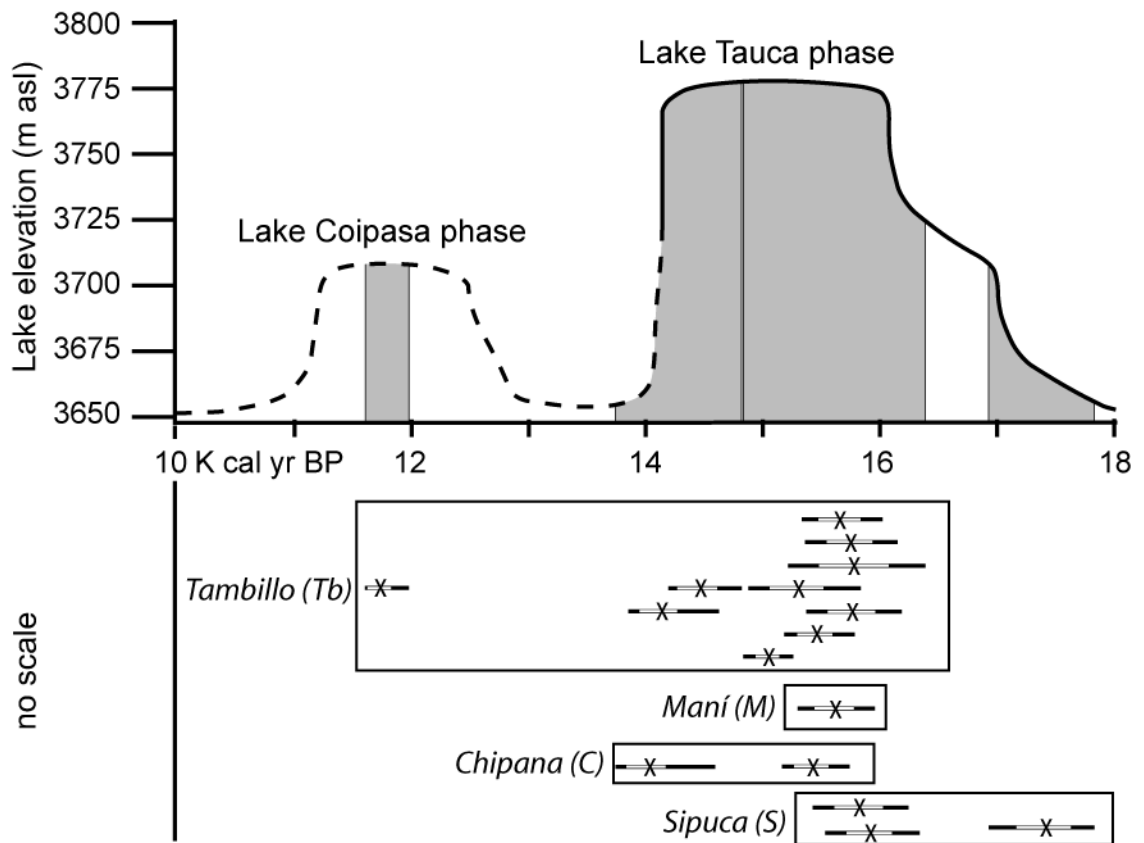
At ~1250 m elevation, the latest Pleistocene section at Tb is the best preserved and used here for overall interpretation (Figure 4.2, 4.3). The array of species present at Tb reveals a blend of facultative phreatophytes and hygrophytic taxa analogous to riparian plant communities found in canyons with perennial rivers further north (i.e. Camiña Valley, 19°20'S, Figure 4.1). *S. molle* is a xerophytic tree when local precipitation exceeds 200 mm/yr, becoming a facultative phreatophyte if precipitation drops below this threshold (Barkley, 1944). Modern *Prosopis* trees are obligate phreatophytes that can pump water from depths < 10 m (Mooney *et al.*, 1980; Aravena and Acevedo, 1985; Ehleringer *et al.*, 1992). The occurrence in these same deposits of the hygrophytes *E. angustifolia*, *C. atacamensis* and *B. scandens* indicates perennial or seasonal surface riverflow. Today, these species are restricted to the bottom of perennial river canyons (Villagrán *et al.*, 1999; Costas-Lippmann, 1979), growing just a few meters from permanent watercourses. To re-establish any of the fossil species identified would not require an increase in local precipitation but rather the introduction of stream water or an outcropping water table. Hillslope (or zonal) taxa are notoriously absent from these deposits (except for a single seed of *Cistanthe* sp., a xerophytic annual). Taken together with the preservation of both a highly soluble surficial soil layer (or “chusca” [Rech *et al.*, 2003]). and Miocene landforms (Hoke *et al.*, 2004), this lack of hillslope

taxa implies that latest Pleistocene increased groundwater levels were not caused by enhanced local precipitation. Rather, enhanced water inflow to the PdT occurred through the canyons or by groundwater flow, from increased precipitation in the highlands further east, analogous to modern altitudinal variations in mean annual precipitation.

Preserved but undated fluvial terrace flights at similar heights above the modern floors of canyons Ch and G (Figure 4.1) imply that the same wet intervals increased discharge into the PdT north of the dated deposits presented in this study. The lack of fossil organic debris on those terraces may indicate that stream power was greater or decomposition was more active, a situation with less potential to preserve plant debris.

Paleoshorelines on the Bolivian Altiplano attest to the former presence of large freshwater lakes during the late Pleistocene (Servant and Fontes, 1978; Sylvestre *et al.*, 1999; Placzek *et al.*, 2006). Recent U-Th and ^{14}C dates for shoreline tufa deposits of paleolake Tauca (Placzek *et al.*, 2006), lying between 70-300 km east of PdT (Figure 4.1), indicate enhanced precipitation (Grove *et al.*, 2003) between approximately 18,100 and 14,100 cal yr BP. PdT fluvial terrace deposits at low elevation are almost synchronous with these shoreline dates (Placzek *et al.*, 2006) for paleolake Tauca (Figure 4.4). A second lake cycle “Coipasa”, existed 13,000-11,000 cal yr BP (Placzek *et al.*, 2006) and corresponds with our most distal alluvial fan deposit. Deep groundwater at the western margin of former paleolake Tauca, dated between 17,500 and 11,000 cal yr BP (Mardones-Perez, 1998), demonstrates the importance of recharge from these highstands.

Figure 4.4: Comparison of the Tauca and Coipasa lake cycles (Placzek *et al.*, 2006) with dated organic material from fluvial deposits of the Pampa del Tamarugal from four separate drainages as part of this study. “X”s indicate median probability calibrated age. White and black bars represent 95% and 67% confidence intervals, respectively. The gray shading illustrates the 95% ¹⁴C confidence intervals from our 16 Pleistocene dates. The dashed line indicates the portion of this lake level curve considered to be slightly less well constrained by the original authors (Placzek *et al.*, 2006).



Climate change is also recorded in regions that are now geographically and climatically analogous to the headwater regions of the PdT drainage basins. Plant species found in rodent middens from 3,000 m elevation, 130 km southeast of our study area near Río Salado (Figure 4.1), are indicative of twofold precipitation increase at 17,520-16,270 cal yr BP with mean annual temperatures similar to modern (Latorre *et al.*, 2006). These ^{14}C -dates are coeval with both paleolake Tauca and with our PdT *in situ* riparian and phreatophytic vegetation. Middens formed 11,770-9,550 cal yr BP document another period of higher precipitation relative to today, correlative to the latter half of paleolake Coipasa and to the most distal PdT root-bearing fan deposit. Between 170 and 300 km SSE of our study area, middens collected from 2,400- 3,200 m are interpreted to signify 200-500% more precipitation between 16,200 and 10,500 cal yr BP than today (Betancourt *et al.*, 2000). Across the same area, paleowetland deposits signify higher groundwater tables from >15,400 to 9,000 cal yr BP at altitudes above 2500 m (Rech *et al.*, 2002).

Discussion and conclusions

Consequences of increased precipitation during the latest Pleistocene at higher altitudes not only included the increased discharge through low altitude streams of the PdT, but also major paleoecological shifts at high altitude midden sites, and of Altiplano lake highstands. Our new data demonstrate that there was enhanced stream discharge into the PdT during the time intervals of ~17,750-13,750, ~11,750, and ~1,100-700 cal yr BP. Discharges were greatest between 16,500-13,750 cal yr BP, coeval with the Tauca lake phase on the Bolivian Altiplano,

which has been related to ENSO-modulated amplification of westward drift of Bolivian High moisture during several millennia of pronounced equatorial sea surface temperature gradients (*i.e.*, La Niña-like conditions [Latorre *et al.*, 2006; Placzek *et al.*, 2006]).

Further evidence for the prominent role of the tropical Pacific in bringing about climate change comes from the younger terrace event at M, when groundwater must have been near the surface (<10 m) for *Prosopis* stands to have lived between ~1100-700 cal yr BP. This Medieval Climatic Anomaly (MCA) is of opposite hydrological impact (wet) to that of coastal Peru (dry), where lithic concentrations in a marine core document diminished strength of El Niño events during the MCA (Rein *et al.*, 2004). Other proxies throughout the tropical Pacific (Herweijer *et al.*, 2007; Cobb *et al.*, 2003; Cook *et al.*, 2004; Cook *et al.*, 2007; Mohtadi *et al.*, 2007) likewise are consistent with La Niña dominance during the MCA. Thus a similar mechanism (a sustained SST gradient across the equatorial Pacific) operating at both centennial (MCA) and millennial (late Pleistocene) timescales may be responsible for increased precipitation in the central Andes and greater groundwater recharge.

The PdT terrace flights are interpreted to have been caused by multiple changes of climate-controlled stream power. Today's surface streams carry less water than the stream power needed for either the late Pleistocene aggradation of sorted gravel bars or the intervening stages of fluvial incision (Hoke *et al.*, 2007; Bull, 1979). The near-total lack of water in the Holocene PdT led to the perfect state of preservation of latest Pleistocene and rare late Holocene organic debris.

Precipitation at high elevations brings to the PdT water that can recharge aquifers (Fritz *et al.*, 1981; Houston, 2002; Magaritz *et al.*,

1989). The evidence in the PdT indicates only two major episodes of groundwater recharge during the last 18,000 years, millennial-scale pluvial events along the western portion of the central Andes. The smaller magnitude MCA recharge event indicates a century scale oscillation of the groundwater table during the latest Holocene.

Even in the absence of incontrovertible direct dating of the groundwater stores, the physical and biological records reveal latest Pleistocene flow of water into the PdT, where it could recharge aquifers at a scale that has no match during the Holocene. Given the regional climatic consistency suggested by proxy evidence, latest Pleistocene fossil water may also be the dominant water resource in many other Atacama Desert basins. Whereas water managers might appropriately predict that decadal or century climate variation might return the region to conditions similar to those present during the MCA with modest increases in rainfall, there are no grounds to anticipate a return to latest Pleistocene levels of groundwater recharge possibly until the next global ice age returns.

REFERENCES

- Alpers, C. N., and Brimhall, G. H., 1988, Middle Miocene climatic change in the Atacama Desert, northern Chile: Evidence from supergene mineralization at La Escondida: Geological Society of America Bulletin, v. 100, p. 1640-1656.
- Aravena, R., and Acevedo, E., 1985, The use of environmental isotopes oxygen-18 and deuterium in the study of water relations of *Prosopis tamarugo* phil., in Habit, M. A., ed., The Current State of Knowledge on *Prosopis tamarugo*: Santiago, Chile, FAO, p. 251-256.
- Aravena, R., Suzuki, O., Pena, H., Pollastri, A., Fuenzalida, H., and Grilli, A., 1999, Isotopic composition and origin of the precipitation in Northern Chile: Applied Geochemistry, v. 14, no. 4, p. 411-422.
- Arroyo, M. T. K., Squeo, F. A., Armesto, J. J., and Villagran, C., 1988, Effects of Aridity on Plant Diversity in the Northern Chilean Andes - Results of a Natural Experiment: Annals of the Missouri Botanical Garden, v. 75, no. 1, p. 55-78.
- Barkley, F. A., 1944, *Schinus* L: Brittonia, v. 5, no. 2, p. 160-198.
- Betancourt, J. L., Latorre, C., Rech, J. A., Quade, J., and Rylander, K. A., 2000, A 22,000-year record of monsoonal precipitation from Northern Chile's Atacama Desert: Science, v. 289, no. 5484, p. 1542-1546.
- Billinghurst, A. G., 1893, *La Irrigación en Tarapacá*: Santiago, Chile, Imprenta y Librería Ercilla, 193 p.
- Bull, W. B., 1979, Threshold of Critical Power in Streams: Geological Society of America Bulletin, v. 90, no. 5, p. 453-464.
- Caviedes, C., 1973, A climatic profile of the North Chilean Desert at latitude 20° South, in Amiran, D. H. K., and Wilson, A. W., eds., *Coastal Deserts: Their Natural and Human Environments*: Tucson, University of Arizona Press, p. 115-121.
- Cobb, K. M., Charles, C. D., Cheng, H., and Edwards, R. L., 2003, El Niño/Southern Oscillation and tropical Pacific climate during the last millennium: Nature, v. 424, no. 6946, p. 271-276.
- COCHILCO, 2006, Anuario, Estadísticas del Cobre y Otros Minerales 1986-2005: Comisión Chilena del Cobre.

- Cook, E. R., Seager, R., Cane, M. A., and Stahle, D. W., 2007, North American drought: Reconstructions, causes, and consequences: *Earth-Science Reviews*, v. 81, no. 1-2, p. 93-134.
- Cook, E. R., Woodhouse, C. A., Eakin, C. M., Meko, D. M., and Stahle, D. W., 2004, Long-term aridity changes in the western United States: *Science*, v. 306, no. 5698, p. 1015-1018.
- Costas-Lippmann, M., 1979, Embryogeny of *Cortale- ria selloana* and *C. jubata* (Gramineae): *Botanical Gazette*, v. 140, no. 4, p. 393-397.
- Dunai, T. J., Lopez, G. A. G., and Juez-Larre, J., 2005, Oligocene-Miocene age of aridity in the Atacama Desert revealed by exposure dating of erosion-sensitive landforms: *Geology*, v. 33, no. 4, p. 321-324.
- Ehleringer, J. R., Mooney, H. A., Rundel, P. W., Evans, R. D., Palma, B., and Delatorre, J., 1992, Lack of Nitrogen Cycling in the Atacama Desert: *Nature*, v. 359, no. 6393, p. 316-318.
- Ericksen, G. E., 1981, Geology and origin of the Chilean nitrate deposits: U. S. Geological Survey Professional Paper, v. 1188, no. 37, p. 1-37.
- Fritz, P., Suzuki, O., Silva, C., and Salati, E., 1981, Isotope Hydrology of Groundwaters in the Pampa Del Tamarugal, Chile: *Journal of Hydrology*, v. 53, no. 1-2, p. 161-184.
- Gajardo, R., 1994, La vegetación natural de Chile, clasificación y distribución geográfica: Santiago, Chile, Editorial Universitaria, 165 p.
- Garreaud, R., Vuille, M., and Clement, A. C., 2003, The climate of the Altiplano: observed current conditions and mechanisms of past changes: *Palaeogeography Palaeoclimatology Palaeoecology*, v. 194, no. 1-3, p. 5-22.
- Grove, M. J., Baker, P. A., Cross, S. L., Rigsby, C. A., and Seltzer, G. O., 2003, Application of strontium isotopes to understanding the hydrology and paleohydrology of the Altiplano, Bolivia-Peru: *Palaeogeography Palaeoclimatology Palaeoecology*, v. 194, no. 1-3, p. 281-297.
- Herweijer, C., Seager, R., Cook, E. R., and Emile-Geay, J., 2007, North American droughts of the last millennium from a gridded network

- of tree-ring data: *Journal of Climate*, v. 20, no. 7, p. 1353-1376.
- Hoke, G. D., Isacks, B. L., Jordan, T. E., Blanco, N., Tomlinson, A. J., and Ramezani, J., 2007, Geomorphic evidence for post-10 Ma uplift of the western flank of the central Andes 18 degrees 30'-22 degrees S: *Tectonics*, v. 26, no. 5.
- Hoke, G. D., Isacks, B. L., Jordan, T. E., and Yu, J. S., 2004, Groundwater-sapping origin for the giant quebradas of northern Chile: *Geology*, v. 32, no. 7, p. 605-608.
- Houston, J., 2006, The great Atacama flood of 2001 and its implications for Andean hydrology: *Hydrological Processes*, v. 20, no. 3, p. 591-610.
- Houston, J., and Hartley, A. J., 2003, The central andean west-slope rainshadow and its potential contribution to the origin of HYPER-ARIDITY in the Atacama desert: *International Journal of Climatology*, v. 23, no. 12, p. 1453-1464.
- JICA, 1995, *The Study on the Development of Water Resources in Northern Chile: Division General de Agua - Ministerio de Obras Públicas*.
- Kiefer, E., Dorr, M. J., Ibbeken, H., and Gotze, H. J., 1997, Gravity-based mass balance of an alluvial fan giant: the Arcas Fan, Pampa del Tamarugal, Northern Chile: *Revista Geologica De Chile*, v. 24, no. 2, p. 165-185.
- Lamb, S., and Davis, P., 2003, Cenozoic climate change as a possible cause for the rise of the Andes: *Nature*, v. 425, p. 792-797.
- Latorre, C., Betancourt, J. L., and Arroyo, M. T. K., 2006, Late Quaternary vegetation and climate history of a perennial river canyon in the Rio Salado basin (22 degrees S) of Northern Chile: *Quaternary Research*, v. 65, no. 3, p. 450-466.
- Latorre, C. L., Betancourt, J. L., Rech, J. A., Quade, J., Holmgren, C., Placzek, C. P., Vuille, M., and Rylander, K. A., 2005, Late Quaternary history of the Atacama Desert, in Smith, M., and Hesse, P., eds., *23 Degrees South: Archaeology and Environmental History of the Southern Deserts*: Canberra, Australia, National Museum of Australia, p. 73-90.
- Lowenstein, T. K., Hein, M. C., Bobst, A. L., Jordan, T. E., Ku, T. L., and Luo, S., 2003, An assessment of stratigraphic completeness in

- climate-sensitive closed-basin lake sediments: Salar de Atacama, Chile: *Journal of Sedimentary Research*, v. 73, no. 1, p. 91-104.
- Luebert, F., 2004, Apuntes sobre la vegetación de bosque y matorral del desierto precordillerano de Tarapacá (Chile): *Chloris Chilensis*, v. 7, no. 1. <http://www.chlorischile.cl>.
- Luebert, F., and Pliscoff, P., 2006, *Sinopsis Bioclimatica Y Vegetacional De Chile*: Santiago, Chile, Editorial Universitaria, 316 p.
- Magaritz, M., Aravena, R., Pena, H., Suzuki, O., and Grilli, A., 1989, Water Chemistry and Isotope Study of Streams and Springs in Northern Chile: *Journal of Hydrology*, v. 108, no. 1-4, p. 323-341.
- Mardones-Perez, L., 1998: Université Paris, 163 p.
- Michalski, G., Bohlke, J. K., and Thiemens, M., 2004, Long term atmospheric deposition as the source of nitrate and other salts in the Atacama Desert, Chile: New evidence from mass-independent oxygen isotopic compositions: *Geochimica Et Cosmochimica Acta*, v. 68, no. 20, p. 4023-4038.
- Miller, A., 1976, The climate of Chile, *in* Schwerdtfeger, W., ed., *Climates of Central and South America: World Survey of Climatology*, p. 113-130.
- Mohtadi, M., Romero, O. E., Kaiser, J., and Hebbeln, D., 2007, Cooling of the southern high latitudes during the Medieval Period and its effect on ENSO: *Quaternary Science Reviews*, v. 26, no. 7-8, p. 1055-1066.
- Mooney, H. A., Gulmon, S. L., Rundel, P. W., and Ehleringer, J., 1980, Further Observations on the Water Relations of *Prosopis-Tamarugo* of the Northern Atacama Desert: *Oecologia*, v. 44, no. 2, p. 177-180.
- Placzek, C., Quade, J., and Patchett, P. J., 2006, Geochronology and stratigraphy of late Pleistocene lake cycles on the southern Bolivian Altiplano: Implications for causes of tropical climate change: *Geological Society of America Bulletin*, v. 118, no. 5-6, p. 515-532.
- Rech, J. A., Currie, B. S., Michalski, G., and Cowan, A. M., 2006, Neogene climate change and uplift in the Atacama Desert, Chile: *Geology*, v. 34, no. 9, p. 761-764.

- Rech, J. A., Pigati, J. S., Quade, J., and Betancourt, J. L., 2003, Re-evaluation of mid-Holocene deposits at Quebrada Puripica, northern Chile: *Palaeogeography Palaeoclimatology Palaeoecology*, v. 194, no. 1-3, p. 207-222.
- Rech, J. A., Quade, J., and Betancourt, J. L., 2002, Late Quaternary paleohydrology of the central Atacama Desert (lat 22 degrees-24 degrees S), Chile: *Geological Society of America Bulletin*, v. 114, no. 3, p. 334-348.
- Rein, B., Luckge, A., and Sirocko, F., 2004, A major Holocene ENSO anomaly during the Medieval period: *Geophysical Research Letters*, v. 31, no. 17.
- Sáez, A., Cabrera, L., Jensen, A., and Chong, G., 1999, Late Neogene lacustrine record and palaeogeography in the Quillagua-Llamara basin, Central Andean fore-arc (northern Chile): *Palaeogeography Palaeoclimatology Palaeoecology*, v. 151, no. 1-3, p. 5-37.
- Servant, M., and Fontes, J. C., 1978, Les lacs quaternaires des hauts plateaux des Andes boliviennes. Premières interprétations paléoclimatiques: *Cahiers ORSTOM*, v. 10, p. 9-23.
- Stuiver, M., Reimer, P. J., and Reimer, R., 2005, CALIB Radiocarbon Calibration, <http://calib.qub.ac.uk/calib>.
- Sylvestre, F., Servant, M., Servant-Vildary, S., Causse, C., Fournier, M., and Ybert, J. P., 1999, Lake-level chronology on the southern Bolivian Altiplano (18 degrees-23 degrees S) during late-glacial time and the early Holocene: *Quaternary Research*, v. 51, no. 1, p. 54-66.
- Villagrán, C., Castro, V., Sánchez, G., Hinojosa, F., and Latorre, C., 1999, Etnobotánica y manejo ganadero de las vegas, bofedales y quebradas en el Loa superior, Andes de Antofagasta, Segunda Región, Chile.: *Chungará*, v. 29, p. 275-304.
- Vuille, M., 1999, Atmospheric circulation over the Bolivian Altiplano during dry and wet periods and extreme phases of the Southern Oscillation: *International Journal of Climatology*, v. 19, no. 14, p. 1579-1600.
- Vuille, M., and Keimig, F., 2004, Interannual variability of summertime convective cloudiness and precipitation in the central Andes derived from ISCCP-B3 data: *Journal of Climate*, v. 17, no. 17, p. 3334-3348.

APPENDIX
DIRECTIONS FOR CONVERTING A DIGITAL IMAGE TO SEG-Y
FILE⁴

The following will allow the user to convert data from paper to digital (bitmap) and then, eventually, seg-y format, required for use with seismic interpretation software. The steps are somewhat tedious, but will allow for map-cases full of data to be once again valuable. The process involves several steps, which are: scanning of the seismic line, converting the line to a .dat file in matlab, converting this file to a seg-y file in seismic unix (shareware), creating a seg-y header, and then transferring this data to Reflexw and, in this case, Kingdom Suites. It is important to note that the seg-y file which is created is really just a seg-y file in name only, and will not give the user the capability to process or manipulate the geophysical data in any way.

First, if you are starting with a paper file, scan in seismic data. 150 dpi is sufficient, as 300 dpi for lines which have >1800 SP's tends to create files >200 MB, which Adobe Photoshop may or may not be able to parse.

Since the scans often distort the image, one has to be sure that they are straightened. This can be done in photoshop by selecting portions of the image which need to be straightened, doing a "free transform" and then a "skew" to warp the image back into horizontal.

At this point, be careful that the distortion that you have applied to the image to make it horizontal has not also now horizontally stretched the image. (This is especially a danger if you are dealing with a very long

⁴The following was modified from directions provided by David Mohrig and graduate student Kyle Straub

line.) If you suspect this to be the case, take it into Illustrator or Canvas where you can actually measure the distance between the SP's to make sure they are consistent. Crop the image so that only the seismic data is part of the image. Do this at the uppermost TWT horizon (commonly 0.0, but can be variable, sometimes -0.5, for instance). Be sure not to crop the topography, because you'll certainly need that surface. Then, convert to a grayscale bitmap (.bmp).

```
Using matlab input the following lines (example is for line z1f-005)
A=imread('z1f-005.bmp');
B=double(A);
B=B';
save z1f-005.dat B -ascii
```

Write down the number of columns and rows of the matrix that you save. This can be seen in matlab, or can be read under "dimensions" column in the details of the file window directory. Transfer the file to a directory from which you can access the program "seismic unix" (This is shareware which can be downloaded from the Colorado School of Mines website). In our lab, seismic unix is loaded onto the machine "Yukon", which is a Linux box.

Next, calculate the vertical thickness of each pixel in the image. To do this, take the total TWT of the section and divide it by the number of rows. This will be entered as "dt" in the next section. As an example, if the value is 2 msec, you will enter "2000". More likely, the value will be 2 seconds, which will be 2000000/1200 (2 seconds divided by the number of rows). This number is generally on the order of between 2000 and 5000.

It should probably be rounded to the nearest whole number, though I'm not sure this is completely necessary.

Enter the following commands to convert the file from .dat (ascii) to segy (example is for file z1f-005.dat):

```
a2b<z1f-005.dat n1='number of rows' >b.bin
suaddhead<b.bin ns='number of rows'>b.su
sushw<b.su key=dt a='vertical dt spacing' >b2.su
segyhdrs<b2.su
segypwrite tape=z1f-005.segy verbose=1 endian=1<b2.su
```

('.b', '.b2' and '.su' are just placeholder files- these can be named 'z1f-005.bin' or 'z1f-005.su' just as well.)

You now have a segy file. Unfortunately, Kingdom Suites often has trouble reading this segy file, so you will have to run through some steps in the program "Reflexw", which will amount to outputting another segy file. In Reflexw, create a project (this only means specifying a folder). The second time you run the process, you will simply "confirm project", and then select the folder:

1. Go to "modules" and select "2D data analysis"
2. Go to "File→ import"
3. select the segy file

There are some settings you should be sure are correct:

- specification: original name (otherwise, it will auto-generate a name which has no meaning to you).
- check the box next to “read start time”
- click on “plot options” in the lower right.
- Select “point mode” (wiggle mode may be the default)
- Select “new 16 bit integer”
- Export:
 - segy
 - scaling factor = 1
 - ps time incr. → box **unchecked**
 - filefilter → box **unchecked**
 - -filepath → rawdata

This will export the file into the ascii folder within the project folder which you are working. Next, open Kingdom Suites, and go to “survey management.” Select “create”, and type in the name you wish to call your seismic line. Select 2D or 3D data, and when it asks you to load the world coordinates, say “no”

Next, go to “survey→import world coordinates → 2D by dialog. At this point, click “add” and then type in the appropriate shotpoints and x/y coordinates. You can also wholesale copy and paste from Excel (you’ll need to do ctrl-v). In my case, I used UTM, which makes things much easier due to their direct conversion in meters, since my shot intervals are also in meters (25m).

Next, go to “surveys→import seg y” and select survey from the drop-down menu. Then select the proper segy file by browsing from disc

(this is the file which was output by reflexw). You can probably just say “next” for the rest of the menus here.

When you are finished, Kingdom Suites may be confused at this point, because the number of traces (equal to the number of columns of your bitmap) do not equal the number of shotpoints. Therefore, you may need to divide the number of columns by the number of shotpoints in the seismic line, and input this in the box “traces per shotpoint” (the default is ‘2’. in my case, I entered a number between 8 and 10).